Nonlinear Distortion Mechanisms and Efficiency of Balanced-Armature Loudspeakers

Jensen, Joe

Publication date:
2014

Document Version
Publisher's PDF, also known as Version of record

Technical University of Denmark

Joe Jensen

Nonlinear Distortion Mechanisms and Efficiency of Miniature Balanced-Armature Loudspeakers

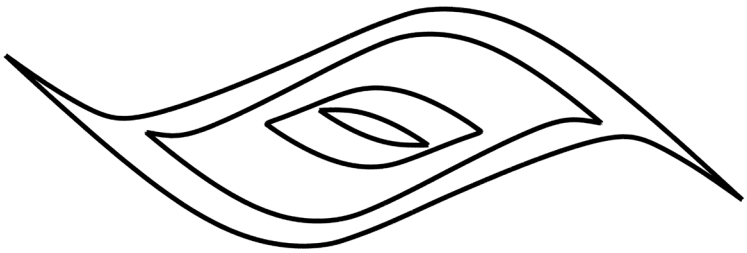

PhD thesis, March 2014

DTU Electrical Engineering
Department of Electrical Engineering

This thesis was submitted to the Technical University of Denmark (DTU) as partial fulfillment of the requirements for the degree of Doctor of Philosophy (Ph.D.) in Electronics and Communication. The work presented in this thesis was completed between July 1, 2010 and March 31, 2014 at Acoustic Technology, Department of Electrical Engineering, DTU, under the supervision of Associate Professors Finn T. Agerkvist and James M. Harte. The project was funded by Sonion A/S that also provided supervision by Aart van Halteren and Ad Lafort.

Cover illustration:
Hysteresis curves measured at 10 Hz on a ring sample of magnetic steel at different excitation levels. The curves are rotated 45° clockwise.

Department of Electrical Engineering
Technical University of Denmark
ISBN 978-87-92465-48-1 DK-2800 KONGENS LYNGBY, Denmark

Printed in Denmark by Rosendahls - Schultz Grafisk a/s

Abstract

Nonlinear distortion added by the loudspeaker (often referred to as a receiver) in a hearing aid reduces the signal-to-noise ratio in the acoustic output and may degrade the user's ability to understand speech. The balanced-armature-type loudspeakers predominantly used in hearing aids are inherently nonlinear devices, since any displacement of the loudspeaker diaphragm inevitably changes the magnetic and electrical characteristics of the loudspeaker. Additionally, for the balanced-armature loudspeaker the signal has to be transmitted through the magnetic domain (as a magnetic B-field) and the linearity of the magnetic material is therefore of great importance.

This thesis describes the inherent nonlinear parameters of the balanced-armature loudspeaker and demonstrates how the nonlinearity of these parameters may be reduced by design. A simple technique for incorporating magnetic leakage effects is introduced and it is shown how the leakage affects the linearity of the loudspeaker. Magnetic hysteresis, saturation and eddy current losses and how these effects might affect the performance of the loudspeaker are also discussed. FEM simulation software is used to investigate magnetic effects and to validate simpler equivalent circuit models. A large scale model of a balanced-armature loudspeaker has been developed and its inherent nonlinear parameters have been measured and compared to the theoretically predicted values. A measurement setup for determining the magnetic properties of soft magnetic materials has also been developed, since it is of great importance to understand what kind of linear and nonlinear transformations the magnetic materials impose on the signal.

In hearing aid applications the power efficiency of the loudspeaker is important because every reduction in power consumption will help prolong battery life and thereby reduce the frequency of necessary service checks. A great deal of the power consumed in a hearing aid goes into the amplifier that drives the loudspeaker. If the efficiency of the balanced-armature loudspeaker can be improved, the operation time of the hearing aid may be extended or the size of the hearing aid could be reduced using a smaller battery, or new features and more advanced algorithms could be embedded without compromising the operation time of the hearing aid. A new loudspeaker efficiency performance metric is proposed and it is shown how the balanced-armature loudspeaker may be optimized in terms of this.

The maximum level of the acoustic output of a balanced-armature loudspeaker is an important performance parameter since these miniature loudspeakers sometimes need to be capable of compensating for substantial hearing losses. It is demonstrated that magnetic saturation of the loudspeaker armature is likely to be the most significant cause of compression in the balanced-armature loudspeaker. It is furthermore shown which conditions should be fulfilled in order to reduce the risk of armature saturation and thereby increase the maximum output and reduce distortion.

Resumé

Ulineær forvrængning, som opstår i højttaleren i et høreapparat, reducerer signal-støj-forholdet i det akustiske signal, og dette kan medføre en degradering af brugerens evne til at forstå tale. I høreapparater anvendes balanceret-armatur højttalere, som er ulineære af design, eftersom selv den mindste forskydning af højttalerens membran vil ændre højttalerens magnetiske og elektriske egenskaber. I en balanceret-armatur højttaler bliver det elektriske signal konverteret til et magnetisk signal, inden det bliver konverteret til det mekaniske og akustiske domæne. Dette stiller store krav til de magnetiske egenskaber for materialet, som anvendes i det magnetiske kredsløb. Dette såkaldt bløde magnetiske materiale skal være så lineært som muligt og helst ikke gå i mætning.

Denne afhandling beskriver balanceret-armatur højttalerens ulineære parametre, og det demonstreres, hvordan ulinearitetet af disse kan minimeres ved korrekt design. Der introduceres en simpel metode, som kan inkorporere virkningen af magnetisk lækage flux mellem nord- og sydpolen på hver af de to permanente magneter. Magnetisk hysterese, mætning og hvirvelstrømstab, og hvorledes disse fænomener påvirker højttalerens ydelse, bliver også diskuteret. Finite Element Modeleringsprogrammet COMSOL er blevet brugt til at undersøge magnetiske virkninger og til at validere langt simplere modeller, som gør brug af ækvivalente kredsløb. En stor skalamodel af en balanceret-armatur højttaler er blevet konstrueret, og dens ulineære parametre er blevet målt og sammenlignet med forudsigelserne fra en simpel model, som gør brug af ækvivalente elektriske kredsløb. Der er også blevet udviklet et måle setup, som kan bestemme de magnetiske egenskaber for bløde magnetiske materialer. Dette setup er af stor betydning, da det kan bruges til at undersøge, hvilke ulineære transformationer det originale signal udsættes for, og hvordan dette afhænger af signalets frekvens og amplitude.

I et høreapparat er højttalerens effektivitet af højeste vigtighed, da enhver reduktion i høreapparatets effektforbrug vil hjælpe til med at forlænge dets batterilevetid og dermed reducere hyppigheden af nødvendige eftersyn. En stor del, af den effekt som forbruges i et høreapparat, flyder ind i den forstærker, som driver højttaleren. Hvis højttalerens effektivitet kan forbedres, kan høreapparatet anvendes i længere tid, eller dets størrelse kan måske reduceres ved brug af et mindre batteri, eller nye funktioner og mere avancerede algoritmer kan implementeres uden at gå på kompromis med apparatets batterilevetid. Et nyt mål for højttaler effektivitet bliver foreslået, og der redegøres for, hvordan den balanceret-armatur højttaler kan optimeres i forhold til dette mål.

Det maksimale lydtryk, som en balanceret-armatur højttaler kan producere, er en vigtig parameter, da disse miniature højttalere nogen gange skal være i stand til at kompensere for betydelige høretab. Det demonstreres, at magnetisk mætning i højttalerens armatur typisk vil være den vigtigste årsag til komprimering i balanceret-armatur højttalere. Det vises desuden, hvilke betingelser der skal opfyldes for at reducere risikoen for mætning af armaturet og dermed øge det maksimale output og reducere forvrængningen.

Acknowledgments

I would like to express my deepest appreciation to Sonion A/S and in particular to Aart van Halteren and Ad Lafort from the Dutch division of Sonion and also to Martin Bondo from Sonion, Roskilde - who is unfortunately no longer with us - for choosing to sponsor this work and to entrust me with the job.
A big thanks to my DTU supervisors Finn Agerkvist and James Harte for helping to make this Industrial Ph.D. project a reality, for supervision, discussions and cool behavior.
Another thanks to Ad Lafort for lots of help, patience, great discussions, nice dinners and fun company during my visits to Sonion in the Netherlands and also thanks to the rest of the guys in Advanced Development for great company and sometimes great table tennis matches.
Thanks to Paul van Hal for helping me out with the construction of experimental magnetic circuits and all the guys and girls at Sonion (Roskilde, DK and the Netherlands) who were involved in the development and construction of the balanced-armature loudspeaker scale model which has been of great use and still holds a lot of potential for further investigations into the balanced-armature loudspeaker design.
Thanks to Nico Stoffels from Sonion, Netherlands for helping out with the Labview programming that made it possible to get the measurement system for soft magnetic materials up and running.
Thanks to Tom Arent Petersen, Jørgen Rasmussen and Aage Sonesson for technical assistance and for helping out with the construction of various devices.
Thanks to my favorite Catalan couple Elisabet Tiana Roig and Antoni “Toni” Torras Rosell for making my days in the office at DTU much more enjoyable.
A big thanks to all my friends and colleagues at DTU, Acoustic Technology (you know who you are) for making building 352 a very special place to work, study, eat cake and drink coffee.
Thanks to the great guys at Sonion, Roskilde making my work days there a pleasant alternative to DTU.
A very special thanks to my former Sonion colleagues Andreas Tiefenau and Anne-Marie Sänger who were so extremely kind as to let me live together with them in their house and make feel very much as part of “the family” during my extended summer visits to Sonion in the Netherlands. This amazing hospitality made my stays in the Netherlands really enjoyable, so thanks again for your awesome and open way of being and I wish you and your little daughter all the best in the future!

List of publications

List of publications in the work

Paper A Joe Jensen, Finn Agerkvist, and James Harte. Nonlinear time-domain modeling of balanced-armature receivers. *Journal of Audio Engineering Society*, 59(3):91-101, March 2011.

Paper B Joe Jensen. A new method for evaluating loudspeaker efficiency in the frequency domain. In *Audio Engineering Society Convention 131*, New York, USA, October 2011.

Contents

List of symbols and abbreviations

Abbreviations

B-A loudspeaker	Balanced-Armature loudspeaker also known as a balanced-armature receiver
FEM	Finite Element Method
NdFeB	Neodymium Ferrum Boron

Latin symbols

A	Cross-sectional area of permanent magnet and air gap when they are assumed to be the same [m^2].
A_g	Cross-sectional area of air gap [m^2].
A_M	Cross-sectional area of permanent magnet [m^2].
B_a	Magnetic B-field in the armature [T].
$B_{a,0}\,(x)$	Magnetic B-field in the armature due to permanent magnets only [T].
B_r	Effective magnetic remanence i.e. the intersection between the recoil line and the ordinate (B-field) axis [T].
B_s	Armature B-field strength at magnetic saturation [T].
c	Speed of sound in dry air at 20 °C. $c = 343.2$ m/s.
C_{AB}	Acoustic compliance of back volume [m^5/N].
C_{AF}	Acoustic compliance of front volume [m^5/N].
C_{eff}	$C_{eff} = 1/k_{eff}$. Effective mechanical compliance of armature taking the magnetic stiffness compensation, back volume stiffness and suspension into account [m/N].
D	Length of one air gap when the armature is in its resting position [m].
D_{eff}	Effective air gap length that loads the magnetomotive force set up by the permanent magnet [m].
D_M	$D_M = l_M/\mu_r$. Equivalent air gap length of permanent magnet [m].

$D_{M,Th}$	$D_{M,Th} = l_M/\mu_{r,Th}$. Thévenin equivalent air gap length of permanent magnet when the leakage reluctance is taken into account [m].
D_w	Diameter of coil wire [m].
E	Young's modulus [Pa].
E_{in}	Voltage across loudspeaker terminals [V].
$f_{CIP}(\omega)$	Constant Input Power normalization function [V].
f_{n1}	First natural (resonance) frequency of armature including all relevant masses and stiffnesses [Hz].
F_f	Fill (or filling) factor. Relates the cross sectional area of the actual conducting material in the coil to the total cross sectional area occupied by the coil (no dim.).
F_{cl}	$l_c = F_{cl} l_a$. Coil-length factor. Relates the coil length to the armature length (no dim.).
F_a	Armature force due to its own mechanical stiffness [N].
$F_{a,tot}$	Total armature force due to its own mechanical stiffness and the magnetic stiffness compensation [N].
F_Φ	Armature input force generated by magnetic flux in air gaps [N].
$F_{\Phi 1}$	Displacement-dependent armature input force due to the magnetic stiffness compensation [N].
$F_{\Phi 2}$	Displacement and current-dependent armature input force due to the force factor and the coil current [N].
$F_{\Phi 3}$	Displacement and current-dependent distortion armature input force generated by the distortion force factor and the coil current [N].
$\mathcal{F}_M$	(Internal) magnetomotive force of a permanent magnet [A].
$\mathcal{F}_{M,ext}$	External magnetomotive force of a permanent magnet where the magnetomotive potential drop across the internal reluctance is subtracted [A].
$\mathcal{F}_{M,Th}$	Thévenin equivalent (internal) magnetomotive force of a permanent magnet when the leakage reluctance is taken into account [A].
$\mathcal{F}_{Mi}$	Magnetomotive force set up by current carrying coil [A].
h_a	Height or thickness of armature [m].
h_c	Inner height of a square coil [m].
h_{case}	Case height of a balanced-armature loudspeaker [m].
$H_u(j\omega)$	Voltage driven armature velocity response [m/(sV)].
i	Coil current [A].

I_a	Area moment of inertia of armature [m^4].
k_a	Mechanical stiffness of armature alone [N/m].
$k_{a,tot}(x)$	$k_{a,tot}(x) = k_a(x) - k_\Phi(x)$. Displacement-dependent armature stiffness when the mechanical armature stiffness and the magnetic stiffness compensation are taken into account [N/m].
k_A	Acoustic stiffness of back volume [N/m^5].
k_{eff}	Effective stiffness of armature when the magnetic stiffness compensation, back volume stiffness and suspension are taken into account [N/m].
k_{ma}	Combined mechanical stiffness due to armature, back volume and diaphragm suspension [N/m].
$k_{ma,st}$	Combined mechanical stiffness due to armature, back volume and diaphragm suspension which ensures a critically stable loudspeaker [N/m].
k_{mA}	Mechanical stiffness due to back volume [N/m].
k_r	$k_r = k_\Phi/k_a$. Ratio between the mechanical armature stiffness and the magnetic stiffness compensation (no dim.).
k_s	Mechanical stiffness of the diaphragm suspension [N/m].
k_Φ	Magnetic stiffness compensation [N/m].
$k_\Phi(x)$	Nonlinear (displacement-dependent) magnetic stiffness compensation [N/m].
l_a	Armature length [m].
l_c	Coil length [m].
l_{case}	Case length of a balanced-armature loudspeaker [m].
l_M	Length of permanent magnet [m].
L	Linearized electrical inductance [Wb/A] or [H].
$L(x)$	Nonlinear (displacement-dependent) electrical inductance [Wb/A] or [H].
M_{AF}	Acoustic mass of the air in the loudspeaker spout [kg/m^4].
m_a	Resting mass of armature [kg].
m_{eq}	Equivalent mass of armature [kg].
m_{tot}	Total moving mass including equivalent armature mass, mass of drive pin, diaphragm and the acoustic mass [kg].
N	Number of coil windings (no dim.).
N_c	Number of coil windings for coil with circular aperture (no dim.).

N_s	Number of coil windings for coil with square aperture (no dim.).
p_0	Standard pressure at 20 °C. $p_0 = 101.325$ kPa.
P_A	Perimeter of air gap [m].
P_c	Inner perimeter of the square coil [m].
$P_{c,c}$	$P_{c,c} = 2\pi R_{c,i}$. Inner perimeter of the circular coil [m].
$P_{c,s}$	$P_{c,s} = 2\left(w_c + h_c\right)$. Inner perimeter of the square coil [m].
$\mathcal{P}_g$	Magnetic permeance of air gap [Wb/A].
r	Mechanical resistance [kg/s] or [Ns/m].
$R_{c,i}$	Inner radius of circular coil [m].
$R_{c,o}$	Outer radius of circular coil [m].
R_L	Electrical DC resistance of a coil [Ω].
$R_{L,c}$	Electrical DC resistance of a circular coil [Ω].
$R_{L,s}$	Electrical DC resistance of a square coil [Ω].
$\mathcal{R}_g$	Magnetic reluctance of air gap [A/Wb].
$\mathcal{R}_l$	Leakage reluctance [A/Wb].
$\mathcal{R}_M$	Internal magnetic Reluctance of permanent magnet [A/Wb].
S_D	Surface area of loudspeaker diaphragm [m^2].
sat (subscript)	Denotes the value of a parameter which will ensure that the armature is exactly saturated with magnetic flux for $x = D$.
st (subscript)	Denotes the value of a parameter which will ensure that the loudspeaker is critically stable.
t_c	Thickness of square coil [m].
$t_{c,c}$	Thickness of circular coil i.e. $R_{c,o} - R_{c,i}$ [m].
$t_{c,s}$	Thickness of square coil [m].
$T = T_{me} = T_{em}$	Linearized electromechanical transduction coefficient (aka force factor) [N/A] or [Vs/m].
$T\left(x\right) = T_{me}\left(x\right) = T_{em}\left(x\right)$	Nonlinear (displacement-dependent) electromechanical transduction coefficient (aka force factor) [N/A] or [Vs/m].
$T_{me,d}\left(x, i\right)$	Distortion transduction coefficient (aka force factor) from the electrical to the mechanical domain [N/A].
$T_{em,d}\left(x, i\right)$	Distortion transduction coefficient (aka force factor) from the mechanical to the electrical domain [Vs/m].
Th (subscript)	Denotes the Thévenin equivalent of any parameter where the leakage reluctance has been taken into account using the Thévenin equivalent recoil permeability

U_{back}	Back-EMF voltage includes the voltage across the inductance and the voltage due to armature velocity [V].
$u_{CIP}(\omega)$	Constant Input Power armature velocity response [m/s].
u_D	Diaphragm velocity [m/s].
U_D	Diaphragm volume velocity [m^3/s].
V_a	Armature volume [m^3].
V_A	Acoustic back volume (behind diaphragm) [m^3].
V_c	Volume of a coil [m^3].
$V_{c,c}$	Volume of a circular coil [m^3].
$V_{c,s}$	Volume of a square coil [m^3].
V_T	Total volume i.e. the volume which is available for coil and acoustic back volume [m^3].
V_w	Volume occupied by the coil wire i.e. not the coil volume [m^3].
$V_{c,c}$	Volume occupied by the coil with circular aperture [m^3].
$V_{c,s}$	Volume occupied by the coil with rectangular aperture [m^3].
w_a	Width of armature [m].
w_c	Inner width of a square coil [m].
w_{case}	Case width of a balanced-armature loudspeaker [m].
x	Armature displacement relative to resting position [m].
x_{max}	Maximum armature displacement limited by magnetic saturation in the armature [m].
Y_m	Mechanical mobility [m/(Ns)] or [s/kg].
Z_A	Acoustic impedance [Pas/m^3].
Z_{AB}	Acoustic impedance on the back of the diaphragm [Pas/m^3].
Z_{AF}	Acoustic impedance on the front of the diaphragm [Pas/m^3].
Z_{AL}	Acoustic impedance seen from tip of the spout [Pas/m^3].
Z_E	Electrical impedance [Ω].
Z_m	Mechanical impedance [Ns/m] or [kg/s].
Z_{mA}	$Z_{mA} = S_D^2 Z_A$. The acoustic impedance reflected back to the mechanical domain [Ns/m] or [kg/s].

Greek symbols

α	$\alpha = D_M/D$. Ratio between the equivalent air gap length of the magnet and the air gap length. This parameter is sometimes known as the normalized magnet length (no dim.).
α_{Th}	$\alpha_{Th} = l_M/(\mu_{r,Th}D)$. Thévenin equivalent α or effective α when leakage reluctance is taken into account (no dim.).
α_2	$\frac{A_g}{A_M}\alpha$. α scaled by the ratio between the cross sectional areas of the air gap and the permanent magnets. This is relevant when $A_g \neq A_M$ (no dim.).
$\alpha_{2,Th}$	$\alpha_{2,Th} = \frac{A_g}{A_M}\alpha_{Th}$. Thévenin equivalent α or effective α when leakage reluctance is taken into account and $A_g \neq A_M$ (no dim.).
δ	Skin depth [m].
μ_0	Permeability of free space (4π x 10^{-7} N/A^2).
μ_r	Relative recoil permeability (no dim.).
$\mu_{r,Th}$	Thévenin equivalent relative recoil permeability when leakage reluctance is taken into account (no dim.).
Φ_g	Magnetic flux in air gap [Wb].
Φ_a	Magnetic flux in armature [Wb].
$\Phi_{a,0}$	Magnetic flux in armature due to permanent magnets [Wb].
$\Phi_{a,i}$	Magnetic flux in armature due to coil current [Wb].
Φ_{coil}	Effective flux through the coil taking both armature flux and leakage flux into account [Wb].
ρ_0	Mass density of dry air at 20 °C. $\rho_0 = 1.2041$ kg/m^3.
ρ_a	Mass density of armature [kg/m^3].
ρ_w	Electrical resistivity of wire material used in coil [Ω m].
$\omega_{e,cut}$	$\omega_{e,cut} = R_L/L$. The electrical angular cut-off frequency where the current for the blocked impedance is reduced by 3 dB [rad/s].
$\omega_{r,eff}$	Effective angular resonance frequency taking the magnetic stiffness compensation and the acoustic stiffness into account [rad/s].
$\omega_{r,a}$	Fundamental angular resonance frequency of the armature alone [rad/s].

Chapter 1

Introduction

Nonlinear distortion added by the miniature loudspeaker in a hearing aid lowers the acoustic signal-to-noise ratio and may degrade the hearing aid user's ability to understand speech. In modern hearing aids nonlinear signal processing schemes are often intentionally applied in order to compensate for hearing losses. Such nonlinear signal processing may not have the exact intended outcome since the electrical signal has to be converted into an acoustic one by a miniature balanced-armature (B-A) loudspeaker which is not perfectly linear.

The major nonlinear parameters of the common electrodynamic, moving-coil loudspeaker have been described extensively over the course of the last century [1, 2, 3] and systems for measuring these parameters have been commercialized. The balanced-armature loudspeaker (often known as a receiver) never received the same kind of attention in modern literature. One obvious reason for this is the fact that almost all modern large sized loudspeakers for professional or home-use utilize moving-coil loudspeakers. However, the balanced-armature loudspeaker is the preferred choice for hearing aid applications and the hearing aid developers rely on the linearity of these loudspeakers for correct reproduction of the intended acoustic signal. Balanced-armature loudspeakers are also becoming increasingly popular for in-ear headphones and even multi-way in-ear headphone systems. There is thus very good reason to increase our understanding of the nonlinear distortion mechanisms of the balanced-armature loudspeaker. Fig. 1.1 is an example of how a typical balanced-armature loudspeaker is constructed.

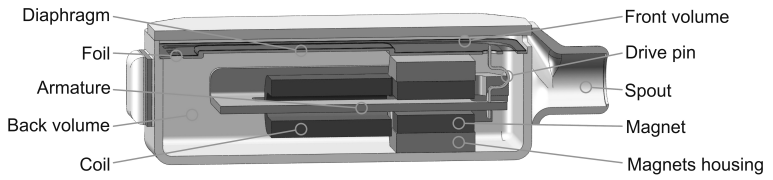

Figure 1.1: Cross-sectional view of typical balanced-armature loudspeaker. (Courtesy of Sonion A/S.)

The basic working principle of the B-A loudspeaker is depicted in Fig. 1.2. When no current is running in the coil the armature is balanced between two permanent magnets (Fig. 1.2(a)). The top magnet is trying to pull the armature up and the bottom magnet is trying to pull the armature down with equal forces leaving the armature balanced right in the middle. When the coil is excited by a positive current (indicated by the direction of the arrow) a magnetizing field is set up around the coil which magnetizes the armature in the direction to the left and this causes an increase in the magnetic flux in the upper branch of the magnetic circuit and a reduction of the

flux in the lower branch (Fig. 1.2(b)). As the flux in the upper gap is increased the force between the top magnet and the armature is also increased and as the flux in the lower air gap is reduced the force between the bottom magnet and the armature is reduced causing a net upward-directed force on the armature. The loudspeaker diaphragm is not shown in Fig. 1.2 but this would usually be connected to the tip of the armature via a thin drive pin. Looking at the working principle of the balanced-armature loudspeaker one can immediately see the inherent nonlinear nature of this design principle: Any displacement of the armature will inevitably cause the magnetic circuit to change and this causes a change in the electrical inductance which is the product of the squared number of coil windings and the permeance of the magnetic core. This distortion can be attributed to simple geometrical changes in the loudspeaker geometry caused by the movement of the armature, but there are other important sources of nonlinear distortion. These include the nonlinear acoustic capacitance of small volumes and the nonlinear relationship between the excitation and response of a magnetic material described by a hysteresis loop. The working principle of the balanced-armature loudspeaker will be discussed in much greater detail throughout this thesis and the basic working principles are derived in Chapter 5.

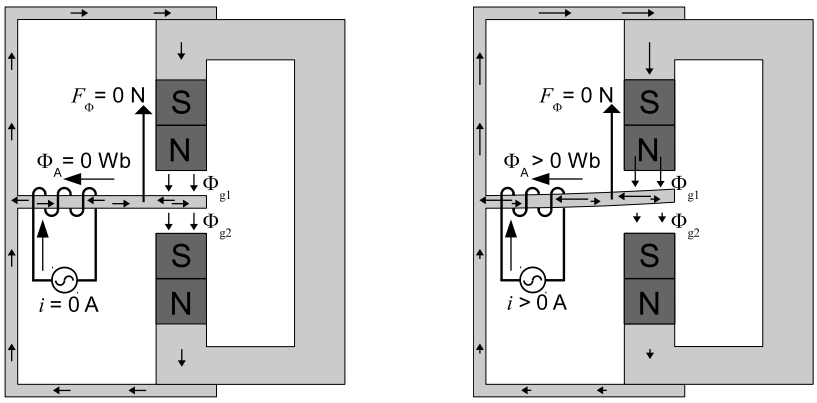

(a) No coil excitation.

(b) Loudspeaker is excited by electric current in the coil.

Figure 1.2: Simplified illustration of the balanced-armature mechanism found in hearing aid receivers. The diaphragm is not depicted.

Fig. 1.3 shows measurements of the electrical impedance and the pressure response of three different commercial miniature balanced-armature loudspeakers produced by Sonion A/S. One of the loudspeakers (type 38AM007M/8a) is a so-called dual receiver construction where two loudspeakers are placed back-to-back in such a way that the armatures are vibrating out of phase but the acoustic output adds up in phase. This configuration helps reduce the external vibrations of the dual receiver, thus reducing the amount of mechanical vibration feedback to the microphone. The dual receiver can be driven with the two individual loudspeakers connected either in parallel or in series and measurements results are shown for both cases.

In hearing aid applications the power efficiency of every single component is optimized in order to prolong battery life and thereby reduce the frequency of necessary service checks. Much of the power consumed in a hearing aid goes into the amplifier that drives the loudspeaker. If the efficiency of the balanced-armature loudspeaker can be improved, the operation time of the hearing

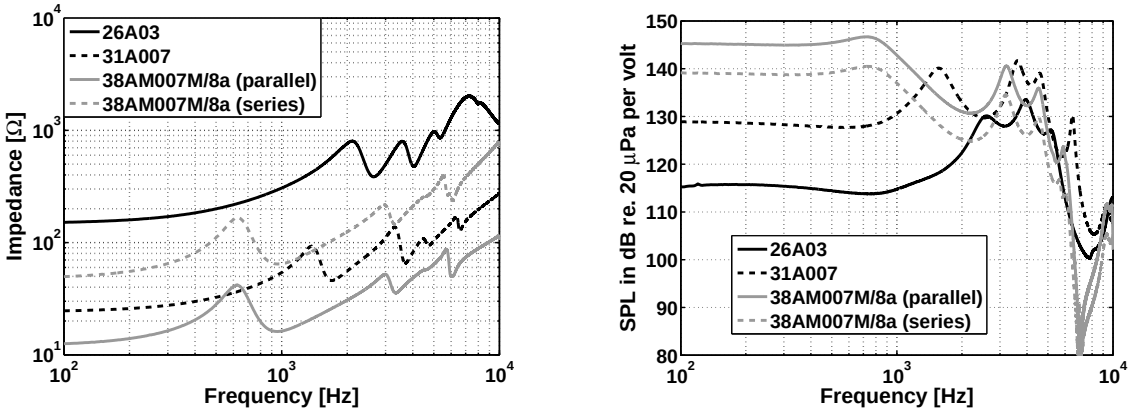

(a) Electrical impedance (magnitude).

(b) Pressure response re. 20 μPa at 1 V drive level.

Figure 1.3: Measurements of electrical impedance and pressure response for 3 different commercial balanced-armature loudspeakers produced by Sonion A/S. The loudspeakers were connected to a Brüel & Kjær Ear Simulator Type 4157 through a 20 mm rubber tube with an inner diameter of 1 mm. The Ear Simulator uses a Brüel & Kjær Type 4134 microphone. The effective volume of the coupler is specified to 1.26 cm^3 at 500 Hz. The measurements were performed using a broadband (10 Hz to 12.8 kHz) noise signal where the voltage drive level was adjusted to produce 90 dB of rms sound pressure level in the ear simulator.

aid may be extended or the size of the hearing aid could be reduced using a smaller battery, or new features and more advanced advanced algorithms could be embedded without compromising the operation time of the hearing aid.

The maximum level of the acoustic output of a balanced-armature loudspeaker is another important performance parameter since these miniature loudspeakers sometimes need to be capable of compensating for substantial hearing losses. It is therefore of great interest to understand what the limiting factors are with regard to the maximum output.

The work presented in this thesis focuses on three main areas:

- The nonlinear parameters of the balanced-armature loudspeaker.
- The power efficiency of the balanced-armature loudspeaker.
- The maximum output of the balanced-armature loudspeaker.

Since the balanced-armature loudspeaker is not very well-described in the literature this work aims broad in order to provide an overview. This also means that there is room for improvement and more concise conclusions in many areas of investigation. However, it is the author's hope that other researchers will find inspiration in this work to continue more thorough investigations in the various topics that are discussed here.

1.1 Overview of the Thesis

In this section, the structure of the thesis is briefly explained.

Chapter 1 introduces the project and explains the philosophy behind the work carried out in this thesis. **Chapter 2** introduces the concepts of electroacoustics, distortion and nonlinear

loudspeaker parameters and loudspeaker efficiency. **Chapter 3** discusses the challenges involved in the simulation of magnetic circuits and **Chapter 4** discusses the unwanted effects of eddy currents and magnetic hysteresis and saturation. In **Chapter 5**, all the key equations governing the balanced-armature loudspeaker, are derived and the mechanical properties of a simple shaped armature is presented. The performance of the coil is also discussed in this chapter. In **Chapter 6**, a graphical representation of the balanced-armature loudspeaker is presented. The time domain state space representation of the nonlinear loudspeaker is formulated and a linearized frequency-domain model is also presented. **Chapter 7** extends the loudspeaker description by analyzing the various nonlinear parameters in greater detail also demonstrating that the small acoustic back volume may exhibit nonlinear behavior. The following two chapters (**Chapters 8 and 9**) show how magnetic leakage may be accounted for in the simple circuit model, and which criteria should be fulfilled in order for the balanced-armature loudspeaker to be stable. In **Chapter 10**, the potential risk of magnetic saturation of the armature is demonstrated and this is related to the maximum output of the loudspeaker. The efficiency of the balanced-armature loudspeaker is discussed in **Chapter 11** where the efficiency analysis is carried out in the low and the high frequency regions with and without a dominating acoustic stiffness caused by the small back volume. **Chapter 12** discusses the effect of oversized permanent magnets i.e. for magnets where the cross-sectional area is larger than the area of the armature tip. **Chapter 13** introduces a large scale model of a balanced armature loudspeaker and the measurements of its nonlinear parameters are presented and discussed. Before finishing the thesis with concluding remarks, a chapter discusses the various findings and future research is proposed.

Two papers and a technical report can be found in the appendix: Paper A is concerned with the fundamental description of the nonlinear balanced-armature loudspeaker and Paper B suggests a new method for measuring loudspeaker efficiency. The technical report describes a measurement setup for characterization of soft magnetic materials. This system was designed and set up as part of the work for this Ph.D. project.

1.2 Research Approach

In this section I will try to explain the philosophy behind the work presented in this thesis. Obviously, it's not possible to do everything in the course of 3 years so compromises have to be made and one has to decide where to focus ones efforts. For instance, 3 years could easily be spent developing a generic physical model which can perfectly model the effects of magnetic hysteresis in soft magnetic materials. It is, without a doubt, extremely important to include the effects of both magnetic hysteresis and saturation in any realistic nonlinear balanced-armature loudspeaker model. However, after some consideration it was decided that it would be more beneficial to design a measurement setup capable of measuring the effective magnetic permeability and the hysteresis loops of soft magnetic ring samples. With such a test setup it is possible to make more informed choices about which soft magnetic materials should be chosen for various parts of the balanced-armature receiver, presuming that it is understood how the various magnetic properties affect the loudspeaker. Such a test setup was something that could be developed within a rea-

sonable amount of time leaving time for investigation of other aspects of the balanced-armature loudspeaker design.

It has already been mentioned that the balanced-armature loudspeaker is not very well-described in the literature so this work tries to provide an overview of the various loudspeaker properties as well as the modeling challenges. Simple lumped element modeling is used to describe the loudspeaker so that simple analytical expressions for various loudspeaker parameters, such as the electrical inductance, may be derived. When the loudspeaker parameters are put in a relatively simple form it becomes easier to interpret how these parameters are affected by various design choices such as the permanent magnet material or the air gap height. Much effort has gone into interpreting the the equations by putting them into a physically meaningful form. The importance of having meaningful physical interpretations of mathematical formulas cannot be underestimated as this will often determine whether the formulas will be found practical and whether they will find widespread use in design processes in the future.

1.2.1 Black Box Modeling

Obviously, if one have a perfect generic physical model of a balanced-armature loudspeaker at hand, it is possible to model both the linear and nonlinear effects of any balanced-armature loudspeaker. In reality, it may be difficult to capture the details of the hysteresis loop and eddy current losses depend on excitation frequency, material characteristics and loudspeaker geometry. It is the author's belief that these effects can only be modeled if the physical loudspeaker model is supplemented with some element of black box modeling and system identification techniques. It is a challenge of its own to set up a complete adaptive model structure which is capable of capturing the behavior of the balanced-armature loudspeaker, and in that process, one can easily get lost in numerical methods, error correction and model tweaking. In the end, the result may be a model which is capable of modeling the balanced-armature loudspeakers with a high degree of accuracy, but it may be difficult or almost impossible to interpret the various parameters of the model.

Such a black box model may be good enough to derive an inverse model which may be used to add distortion to the signal before it enters the loudspeakers in such a way that the acoustic signal comes out undistorted [4, 5]. However, it does not necessarily teach us how to design a loudspeaker which has low distortion or high efficiency. In order to gain this kind of insight, it is often necessary to simplify the model as much as possible while maintaining the basic functionality of the loudspeaker. A simple model is easier to interpret than a very complex model and if the simple model captures the basic behavior of the loudspeaker, it may be possible to derive analytical expressions that show us how to optimize various properties of the balanced-armature loudspeaker.

1.2.2 FEM Modeling

If a Finite Element Model is set up correctly, it may capture the physical behavior of the loudspeaker with great accuracy. However, it can be very difficult to learn which parameters significantly influence the nonlinearity and the efficiency of the loudspeaker. Blindly using the trial and

error approach adjusting a large amount of parameters in a very complex FEM model is usually not a fruitful approach. FEM simulations may however be great for capturing the last details of the behavior which cannot be captured using e.g. simple lumped-element models. FEM may also be an excellent tool for modeling sub-elements of a loudspeaker: Diaphragm breakup modes, characteristic frequencies of an armature which does not have a simple geometry, eddy current effects, magnetic leakage and so on. Setting up a complete model of a loudspeaker includes many types of physical phenomena which all interact: A current is injected in the coil which sets up a B-field in the armature and if this B-field is alternating it will induce eddy currents in the electrically conducting armature material and this will in turn set up a magnetic field in the armature which tries to oppose any change in the original B-field. The injected current will cause the coil to heat up due to its resistance which in turn will increase the electrical resistance of the coil. The magnetic field set up in the circuit will create a magnetic force that causes the mechanical armature to bend which in turn changes the magnetic flux in the armature and this induces an electrical voltage in the coil and so forth. It is a big challenge in itself to set up a good complete FEM loudspeaker model which is also capable of running without a super computer. However, if a good, complete FEM model is successfully set up it will be an excellent tool to test various loudspeaker designs that are derived using a simpler modeling approach. Thus, for the author it is considered very important to understand how to design towards specific loudspeaker properties such as a high electrical cut-off frequency, stability, large force factor, high efficiency and so forth. This is not the same as being able to set up a model which can produce the same output as some loudspeaker.

FEM simulations can be very helpful trying to reach this goal as they may help setting up more accurate lumped element models. For instance, a FEM simulation of a coil in a magnetic circuit may help understand how a much simpler lumped element model may be set up and tweaked to produce similar results.

1.2.3 Comments on Paper A

An introduction to the balanced-armature loudspeaker may be found in Paper A in the appendix. Unfortunately there was an error in the original paper shown in appendix A. An erratum has been submitted but this has not been published yet so it was not possible to include the erratum in this thesis. However, this error is not present in the work of this thesis - only in the attached paper. In sec. 5.3 it is shown how the electrical back-EMF can be written as a sum of 3 terms. In the paper, the distortion term

$$T_{em,d}\left(x,i\right)\frac{dx}{dt} = \frac{dL(x)}{dx}i\frac{dx}{dt}$$

is unfortunately missing from the derivations.

There are two major differences between the model presented in Paper A and the model presented in this thesis: The internal reluctance of the permanent magnet is added to the model presented in the thesis and it is shown how magnetic leakage may be taken into account using a simple transformation of the relative recoil permeability of the permanent magnets.

Chapter 2

Electroacoustics

The discipline of electroacoustics is concerned with the transduction of signals between the electrical and the acoustic domain. A loudspeaker may be considered as a transducer that converts (or transducts) an electrical signal into an acoustic signal. For most linear electroacoustic transducers, the transducer can be considered as two separate but coupled systems for the purpose of analysis: The electromechanical system comprising the electrical interface and some moving mechanical part, and the mechano-acoustical system usually comprising a mechanical diaphragm and the acoustic radiation impedances on both sides of the diaphragm. In this thesis, the focus is mainly on the electromechanical coupling and it is simply presumed that the acoustic load of the loudspeaker diaphragm can be represented by an appropriate impedance in the mechanical domain.

2.1 Distortion

Distortion of a signal can be defined as the alteration of some (original) signal waveform. One may talk about linear distortion where the relationship between the original signal and the distorted signal is a linear transformation which may be described in the frequency domain using a frequency response. The addition of random noise to some signal may also be considered as a type of distortion of the original signal but is usually considered simply as noise in the field of audio engineering. In electronic equipment, it is very common that circuits get contaminated by electromagnetic radiation from the electricity distribution grid. As the grid runs at some fixed frequency this frequency and its harmonics can often be measured in the output of the equipment.

When a pure tone passes through a nonlinear system the output of the nonlinear system will, generally speaking, be a sum of harmonically related tones i.e. the fundamental excitation frequency and so-called overtones that are integer multiplies of the fundamental frequency. As these overtones were not part of the original signal they are usually unwanted as they tend to smear out the information in the acoustic signal. When the input signal to a nonlinear system is sum of pure tones, so-called intermodulation distortion occurs: The frequency content of the output will be integer linear combinations of the frequencies present at the input of the nonlinear system. These output distortion patterns of a nonlinear system are signal-dependent but the system itself is usually well-defined. This means that it is much more convenient to describe the nonlinear behavior of a system from a system point of view, if it is possible to gain this kind of insight into the system.

As the focus of this work is on the efficiency and the nonlinear behavior of the balanced-

armature loudspeaker, the linear frequency response gets very little attention. The presumption is that it is possible to reduce any major flaws in the frequency response using the signal processing capabilities present in the hearing aid.

2.2 Nonlinear Loudspeaker Parameters

Nobody has managed to put such big focus on the nonlinear parameters of the moving-coil loudspeaker as Klippel (see e.g. [3, 4]). Klippel's approach is to describe the common loudspeaker parameters; the electrical inductance, the force factor and the mechanical stiffness as functions of the diaphragm displacement. A similar approach will be used throughout this thesis for the analysis of the balanced-armature loudspeaker. It turns out that there are 3 characteristic nonlinear loudspeaker parameters associated with the balanced-armature loudspeaker, namely the force factor (or transduction coefficient), the electrical inductance and the magnetic stiffness compensation. It may be argued that the mechanical suspension (or stiffness) of the diaphragm should be included as a fourth nonlinear parameter.

2.3 Loudspeaker Efficiency

In order to evaluate the efficiency of a loudspeaker one must first establish a convenient measure of the efficiency. The Constant Input Power (CIP) response is suggested as one such measure in Paper B in the appendix. In Chapter. 11 this technique is applied to the balanced-armature loudspeaker and it is demonstrated how various parameters affect the efficiency of the B-A loudspeaker design.

Chapter 3

Magnetic Circuit Analysis

A common approach for analyzing magnetic circuits, is to use so-called equivalent (electric) circuits. The idea is that magnetic properties such as magnetomotive force, magnetic reluctance and magnetic flux all have equivalent electric circuit representations. The most basic principles are described in e.g. [6], [7] or [8]. Fig. 3.1 shows the very simple and well-established way of modeling a magnetic circuit containing a permanent magnet, soft magnetic pole pieces, an air gap and an excitation coil. For this model it is assumed that the magnetic flux is confined to run in the magnetic circuit defined by the magnet, pole pieces and the small air gap. This implies the assumption that the magnetic flux remains constant throughout the circuit.

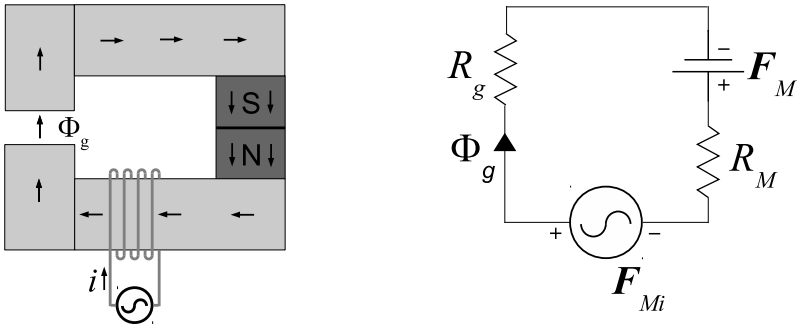

(a) Magnetic circuit. (b) Equivalent circuit.

Figure 3.1: Magnetic circuit and the equivalent circuit using resistors to model magnetic reluctances.

The magnetomotive force of the permanent magnet is

$$\mathcal{F}_M = \frac{B_r l_M}{\mu_0 \mu_r} = \frac{B_r D_M}{\mu_0}, \tag{3.1}$$

where B_r is the magnetic remanence of the permanent magnet, l_M is the magnet length, μ_0 is the vacuum permeability and μ_r is the relative recoil permeability. It turns out to be useful to introduce the equivalent air gap length of the permanent magnet:

$$D_M \equiv \frac{l_M}{\mu_r}. \tag{3.2}$$

The internal magnetic reluctance of the permanent magnet is

$$\mathcal{R}_M = \frac{l_M}{\mu_0 \mu_r A_M} = \frac{D_M}{\mu_0 A_M}, \tag{3.3}$$

where A_M is the cross sectional area of the permanent magnet. The reluctance of the air gap is

$$\mathcal{R}_g = \frac{D}{\mu_0 A_g}, \tag{3.4}$$

where A_g is the cross sectional area of the air gap and D is the height of the air gap. The magnetomotive force set up by the coil is given as

$$\mathcal{F}_{Mi}(i) = Ni, \tag{3.5}$$

where N is the number of coil windings and i is the electrical current in the coil. One weakness of this type of equivalent circuit is the fact that power and energy is not faithfully modeled when resistors model magnetic reluctances. From electrical circuit theory it follows that power is dissipated whenever an electric current runs in a resistor. However, this is not the case when there is a magnetic flux through a magnetic reluctance such as an air gap. In fact, no power is dissipated in the air gap but energy is stored. This led Hamill [9, 10] to introduce the Gyrator-Capacitor approach where the equivalent (electric) circuit element of a magnetic reluctance is a capacitor and the flow-variable is the time derivative of the magnetic flux sometimes known as the flux rate. A magnetic circuit such as this will correctly model the energy stored in the various reluctances and resistors can be employed to model losses due to magnetic hysteresis and/or electric eddy currents. The magnetic circuit is coupled to the electric circuit via a so-called gyrator in order for the magnetic circuit to be reflected correctly in the electrical domain. The gyrator inverts the impedance such that a capacitance in the magnetic circuit becomes an inductance in the electric circuit. The Gyrator-Capacitor approach is particularly useful for gaining insight in the internals of a complicated magnetic circuit which may have different losses in different branches. However, if the purpose of the equivalent circuit is to only model the magnetic flux and the stored magnetic energy and power losses are not of interest, then the simple approach with magnetic reluctances will suffice. In the frequency domain losses in the permanent magnet and/or in the soft magnetic pole pieces may be introduced using a complex relative permeability (see e.g. [11]).

3.1 Leakage

In magnetic circuits there tend to be magnetic flux leaking between regions of different magnetic potential. Consider the magnetic circuit shown in Fig. 3.2(a) which consists of a 4 mm tall permanent Ferrite magnet, soft pole pieces with an extremely high relative permeability of $1 \cdot 10^{15}$ and an air gap with a height of 1 mm. The FEM simulations shown in Figures 3.2(b) shows the magnetic B-field in a plane that cuts through the middle of the circuit (i.e. not on the surface of

the circuit). The color represents the magnitude of the B-field and the arrows show the direction in the considered plane.

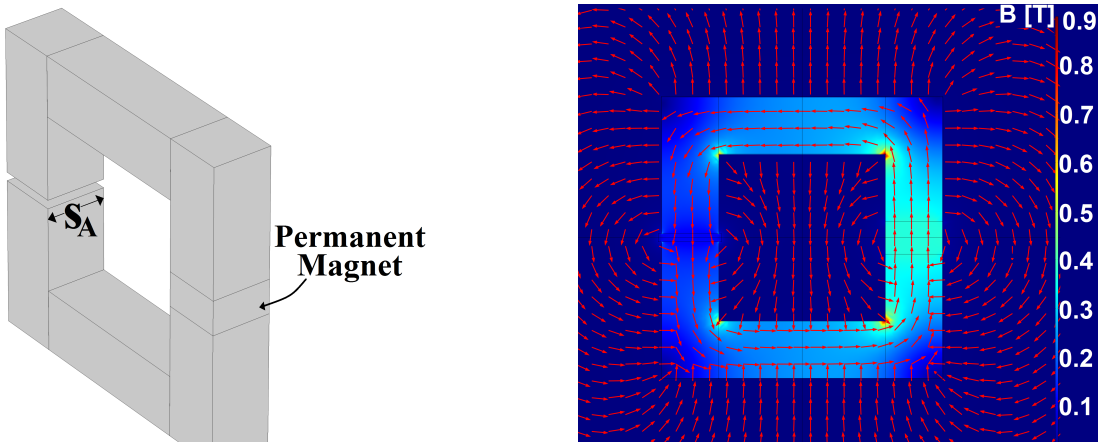

(a) 3D model of magnetic circuit.

(b) COMSOL simulation of the B-field magnitude.

Figure 3.2: COMSOL simulation of the magnetic field around a simple magnetic circuit with a permanent magnet. The soft magnetic pole pieces have a relative permeability of $1 \cdot 10^{15}$ and the permanent magnet has a remanence of 0.4 T and a relative recoil permeability of 1.15. The little red arrows indicate the direction of the B-field in the considered plane. The length of the arrows has been normalized and therefore does not reflect the magnitude of the field.

The important lesson to learn from this simulation is that magnetic flux leaks between the soft pole pieces with different magnetic potential. Thus, even though the permeability of air is very low compared to that of the soft magnetic material, the large area still makes the permeance of all these unwanted flux paths considerable compared to that of the air gap. Had the circuit been entirely closed (with no air gap) the permeance of the path defined by the pole pieces would be huge compared to the permeances of the different unwanted flux paths and the magnetic field in the pole pieces could easily be calculated disregarding these flux paths. However, whenever an air gap is introduced inside a magnetic circuit, considerable amounts of magnetic flux tend to leak into the air between surfaces of different magnetic potential rendering the simple representation in Fig. 3.1(b) obsolete. The FEM simulation clearly shows that the magnetic flux is not maintained throughout the circuit as the B-field in the air gap is much smaller than the B-field inside the permanent magnet despite the fact that the cross-sectional area is constant throughout the circuit. Roters [12] shows how to estimate the permeances of the various flux paths in magnetic circuits and using these types of equivalent circuits - taking the various leakage reluctances into account - it is usually possible to make much more accurate predictions of the (useful) B-field in the air gap. Roters observes that magnetic flux tends to leak between surfaces, edges and corners of different magnetic potential and that only the space in close vicinity to the magnetic structure should be included in the calculation of the leakage reluctances since the magnetic field quickly vanishes as the distance to the magnetic structure increases. From the shape of the magnetic flux lines which can be visualized using e.g. iron filings, it is possible to estimate the average length l of the flux lines between two surfaces, edges or corners. It is usually a trivial task to estimate the volume V occupied by the flux lines and when this is done the average cross-sectional area A can be calculated using the simple relationship $V = Al$. Using the average length and area it is possible

to estimate the permeance $\mathcal{P}_g$ using the simple formula for the permeance of an air gap between two parallel surfaces with the same cross sectional area:

$$\mathcal{P}_g = \frac{\mu_0 A}{l}. \tag{3.6}$$

Roters's approach may seem cumbersome at first - but with the aid of a numerical calculation program or even a spreadsheet the various relevant permeances can be calculated extremely fast for many geometries and good estimates can still be made for more complicated shapes. Roters's method makes it possible to make much better estimates of e.g. the useful magnetic flux in an air gap compared to the very simple magnetic circuit approach where the magnetic flux is assumed to be confined to a well-defined magnetic circuit. This is without the need for expensive, more or less complicated and time consuming FEM simulations. For the considered magnetic circuit Roters's method will result in a large amount of leakage permeances that may all be added to form one leakage reluctance $\mathcal{R}_l$ in parallel with the air gap reluctance $\mathcal{R}_g$ as illustrated in Fig. 3.3(a).

(a) Equivalent circuit. (b) Thévenin equivalent circuit.

Figure 3.3: Equivalent circuit and Thévenin equivalent circuit of the magnetic circuit shown in Fig. 3.2(a) when magnetic leakage is taken into account.

One can now see that all the (unwanted) leakage paths cause a drop in the external magnetomotive force $F_{M,ext}$ and thus also a drop in the useful flux Φ_g that goes into the air gap. Had the external loads of the permanent magnet been either very small or very large compared to the internal magnetic reluctance $\mathcal{R}_M$ then the magnet would have served as either a source of constant magnetic flux or as a source of constant magnetomotive force, respectively. The latter would usually be much preferred as the air gap flux would then be completely independent of the leakage reluctance. However, the relative permeability of modern magnetic materials is often in the range 1.05-2.5 which is very close to that of air. As the magnet length is often in the same order of magnitude as the air gap length, it turns out that the internal magnet reluctance $\mathcal{R}_M$ and the load and leakage reluctances are quite similar in size and this makes it impossible to ignore any of them for most magnetic circuits.

Fortunately, it is possible to easily make a Thévenin equivalent circuit which is depicted in Fig. 3.3(b). This circuit correctly models the magnetic potential across the load and hence the magnetic flux through the load which is the air gap in this case. The Thévenin equivalent magnetomotive force is

$$\mathcal{F}_{M,Th} = \frac{\mathcal{R}_l}{\mathcal{R}_M + \mathcal{R}_l}\mathcal{F}_M, \tag{3.7}$$

and the Thévenin equivalent magnetic reluctance is

$$\mathcal{R}_{M,Th} = \frac{\mathcal{R}_l}{\mathcal{R}_M + \mathcal{R}_l}\mathcal{R}_M. \tag{3.8}$$

The definitions of the magnetomotive force and the internal reluctance of a permanent magnet operating on a straight recoil line are stated in Equations (3.1) and (3.2). Substituting these into the last factors of Equations (3.7) and (3.8) yields:

$$\mathcal{F}_{M,Th} = \frac{\mathcal{R}_l}{\mathcal{R}_M + \mathcal{R}_l}\frac{B_r l_M}{\mu_0 \mu_r}, \tag{3.9}$$

and

$$\mathcal{R}_{M,Th} = \frac{\mathcal{R}_l}{\mathcal{R}_M + \mathcal{R}_l}\frac{l_M}{\mu_0 \mu_r A_M}. \tag{3.10}$$

Introducing the transformation

$$\boxed{\mu_{r,Th} = \left(1 + \frac{\mathcal{R}_M}{\mathcal{R}_l}\right)\mu_r}, \tag{3.11}$$

which may be known as the Thévenin equivalent recoil permeability, the Thévenin equivalents can now be written

$$\boxed{\mathcal{F}_{M,Th} = \frac{B_r l_M}{\mu_0 \mu_{r,Th}}}, \tag{3.12}$$

and

$$\boxed{\mathcal{R}_{M,Th} = \frac{l_M}{\mu_0 \mu_{r,Th} A_M}}. \tag{3.13}$$

This result is very elegant as it shows that it is possible to include the effects of a leakage reluctance by simply introducing a Thévenin equivalent recoil permeability $\mu_{r,Th}$. By using this Thévenin equivalent recoil permeability the magnetomotive force and the internal magnetic reluctance are automatically transformed into their Thévenin equivalents when using Equations (3.12) and (3.13), which have the same form as the well established Equations (3.1) and (3.3). The leakage reluctance can thus be accounted for even though it is apparently omitted from the circuit equations and any subsequent derivations. The result also has a nice physical interpretation: When the leakage reluctance $\mathcal{R}_l$ is very large compared to the internal magnetic reluctance $\mathcal{R}_M$, $\mu_{r,Th}$ reduces to μ_r and the magnetic leakage does not influence the magnetic circuit. However,

as $\mathcal{R}_l$ approaches $\mathcal{R}_M$ the "Thévenin equivalent" recoil permeability $\mu_{r,Th}$ increases and this can effectively be thought of as a reduction in the magnetomotive force and a reduction of the internal magnetomotive force. This will cause the permanent magnet to behave closer to a source of constant (although reduced) magnetomotive force. In Chapter 7 it will be shown that this effect will in fact increase the nonlinear behavior of the loudspeaker.

3.2 COMSOL Study of Magnetic Circuits

The literature is full of examples where magnetic circuits are treated as electric circuits where the magnetic flux is confined to run in the wires and through the various electrical analog components. When dealing with electric circuits this is usually a safe assumption because of the huge resistivity of air compared to typical resistor values. The ratio of electrical conductivity between copper and air is about $1 \cdot 10^{22}$ whereas the ratio of permeability between soft magnetic pole pieces and the surrounding air is usually between $1 \cdot 10^2$ and $1 \cdot 10^6$. Furthermore, as the magnetic circuits usually contain one or more air gaps with huge reluctance, it becomes attractive for the magnetic flux to leak into the air surrounding the magnetic circuit. For this reason, it is a very crude assumption to assume that the magnetic flux is confined to the permanent magnet and the soft magnetic pole pieces in any magnetic circuit that contains one or more air gaps.

In this section the numerical Finite Element Method simulation software, COMSOL is used to calculate the magnetic field throughout various magnetic circuits. This is done in order to investigate the validity of the simplified lumped element equations used in the coming sections.

3.2.1 Verification of COMSOL Simulations

In order to verify COMSOL's ability to predict magnetic DC fields correctly, a magnetic circuit with 2 variable air gaps has been constructed (see Fig. 3.4). The material used for this magnetic circuit is Hiperco® 50 Alloy. Using the measurement setup which will be described later in the thesis (sec. 4.3) the low-frequency permeability was determined to be about 5000. For the simulations it is assumed that the material has a constant DC permeability of 5000. Different permanent magnets can be inserted into one air gap while the height of the other air gap can be adjusted. A Gaussmeter fitted with a Hall effect probe with a thickness of a little less than 0.5 mm is used to measure the B-field in the air gap. This measurement is then compared to the COMSOL result. Examples of COMSOL simulations are shown in Fig. 3.5.

The NdFeB-type permanent magnets used for these experiments are all assumed to have a magnetic remanence of 1.35 T and a relative permeability of 1.05. Moreover, the magnetization is assumed to be homogeneously distributed throughout the magnet and only pointing in the direction perpendicular to the surface of the air gap area. First, it is investigated whether the permeability of the soft magnetic material significantly influences the air gap flux. As $\mu_r = 5000$ is just an estimation, it would be meaningless to compare measurements to simulations if the air gap field changes dramatically if μ_r is changed to, say, 1000 or 20000. The B-field in the middle of the air

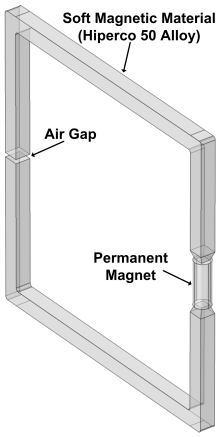

Figure 3.4: Magnetic circuit used to verify the accuracy of COMSOL's B-field simulations at DC. The height of the air gap can be adjusted independently from the height of the air gap where the permanent magnet sits.

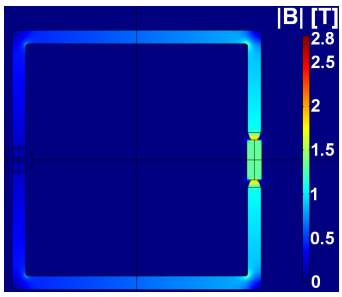

(a) B-field in the "middle" of the magnetic circuit.

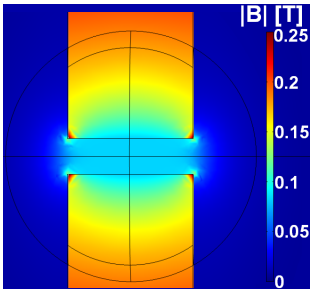

(b) B-field in the "middle" of the magnetic circuit (close-up).

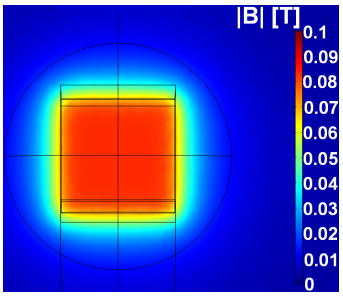

(c) B-field in the "middle" of the air gap seen from above.

Figure 3.5: COMSOL simulation showing the magnitude of the magnetic B field on different planes in space. Notice the different ranges on the figures.

gap versus permeability of the soft magnetic material is plotted in Fig. 3.6. The circuit used for this simulation is the one shown in Fig. 3.4.

It may be observed that for small permeabilities the air gap B-field varies greatly with the permeability of the soft magnetic pole pieces but when the permeability reaches a certain level the air gap B-field is largely a function of the air gap height or in fact the geometry of the magnetic circuit. At $\mu_r = 5000$ the air gap field varies relatively slowly with changes in the permeability especially for the larger air gaps. However, it is clear that the measurements and the simulations could easily vary by 10 % if the actual magnetic DC permeability is closer to 1000 or perhaps 20000. This should be kept in mind when the COMSOL simulations are compared to measurements.

In the experiment the magnetic field in the air gap is measured using a Magnetic Instrumentation Gaussmeter Model 912 fitted with a BH-209 Ultra-mini, Transverse Hall Sensor from F.W. BELL. This sensor is a little less than 0.5 mm thick so that it fits into narrow air gaps. However, the typical distance between the armature and the permanent magnets in a miniature balanced-armature loudspeaker is about 0.1 mm so the probe is still too thick to directly measure the B-field in these production models. The hall-effect probe was calibrated using 3 different calibration mag-

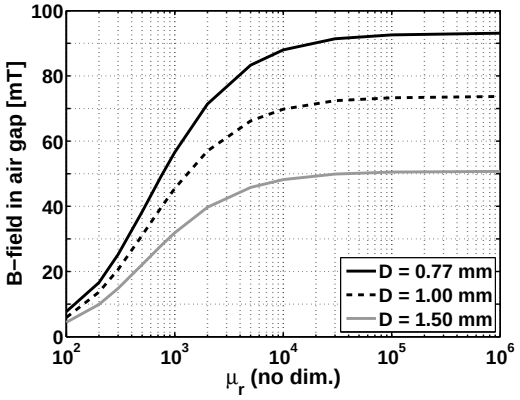

Figure 3.6: COMSOL simulation of air gap B-field vs relative magnetic permeability of the soft magnetic material for various air gap heights. The permanent magnet is a cylindrical NdFeB permanent magnet with $\mu_r = 1.05$, $B_r = 1.35$ T and a height of 8 mm and a diameter of 3 mm.

nets that produced B-fields of 0.05 T, 0.2 T and 0.5 T, respectively. It should be mentioned that the measurement of the B-field depends on where the probe is kept in the air gap as well as the angle between the B-field and the active surface of the hall-effect probe, which should be kept as perpendicular to the field as possible. Thus, it can be difficult to reproduce the measured B-field values with high precision. The values stated here are simply what appeared to be the average measured B-field. Table 3.1 shows the results obtained for a cylindrical magnet where the air gap height is adjusted. Table 3.2 shows similar results, only, this time the circuit is fitted with a smaller cylindrical magnet which is only 2 mm tall and has a diameter of 2 mm. The last row designated "Simulation error" is actually the disagreement between the COMSOL simulation and the measured B-field - it might as well be the measurement which is erroneous.

The conclusion of these experiments is that it appears that COMSOL can be trusted for predicting the air gap B-field when the meshing is done properly and the physical conditions are set up correctly. In later chapters COMSOL will be used to validate simpler lumped element circuit simulation methods.

Magnetic circuit	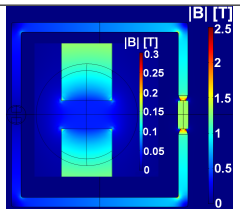	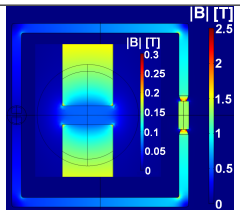	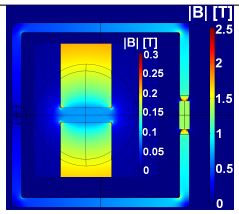
Magnet shape	Cylinder	Cylinder	Cylinder
Magnet diameter or side length	3 mm	3 mm	3 mm
Magnet height	8 mm	8 mm	8 mm
Air gap height	**1.5 mm**	**1.0 mm**	**0.77 mm**
Measured B-field	46 mT	64 mT	85 mT
Simulated B-field	45 mT	64 mT	82 mT
Simulation error	-2.2 %	0.0 %	-3.5 %

Table 3.1: Comparison between COMSOL simulations and the measured B-field in the air gaps of different magnetic circuits. The picture in the middle of each figure shows a close-up of the air gap on a different scale.

Magnetic circuit	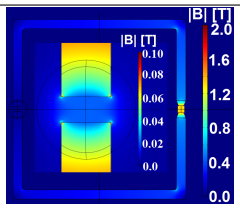	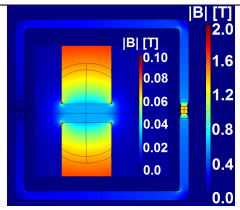
Magnet shape	Cylinder	Cylinder
Magnet diameter or side length	2 mm	2 mm
Magnet height	2 mm	2 mm
Air gap height	**1.4 mm**	**1.0 mm**
Measured B-field	25 mT	35 mT
Simulated B-field	22 mT	30 mT
Simulation error	-12 %	-14.3 %

Table 3.2: Comparison between COMSOL simulations and the measured B-field in the air gaps of different magnetic circuits. The picture in the middle of each figure shows a close-up of the air gap on a different scale.

3.2.2 Air Gap B-field for Various Ratios s_A/D

With reference to Fig. 3.2(a), in this section it is investigated how the ratio s_A/D influences the magnetic field in the air gap. s_A is the length of one side along a quadratic air gap perimeter and D is the air gap height. The relative permeability of the soft magnetic material will be fixed at $1 \cdot 10^{15}$ in order to make sure that it is only the air gaps and circuit geometry that affect the magnetic field in the circuit and not the drop in magnetomotive force due to soft magnetic material with low permeability. Consider the magnetic circuit in Fig. 3.7(a) and its equivalent circuit in Fig. 3.7(b).

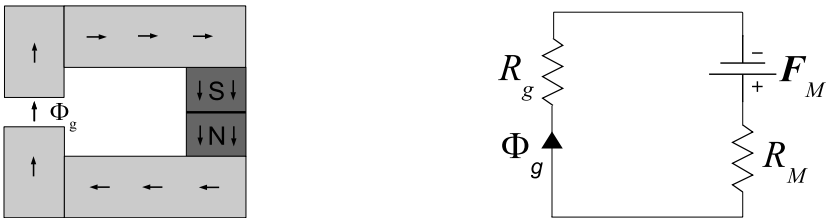

(a) Magnetic circuit. (b) Equivalent circuit.

Figure 3.7: Simple magnetic circuit with one permanent magnet and an air gap and its equivalent circuit.

Using the simple magnetic circuit analysis approach, the magnetic flux in the circuit (and the air gap) may be written

$$\Phi = \Phi_g = \frac{\mathcal{F}_M}{\mathcal{R}_M + \mathcal{R}_g} \tag{3.14}$$

assuming that the magnetic flux is confined to the well-defined magnetic circuit and does not leak into the air. Assuming that the air gap area and the magnet area are the same, the B-field in the circuit (and in the air gap) may be written

$$B = B_g = \frac{\Phi}{A} = \frac{\mathcal{F}_M}{A\left(\mathcal{R}_M + \mathcal{R}_g\right)} = \frac{\frac{B_r l_M}{\mu_0 \mu_r}}{A\left(\frac{l_M}{\mu_0 \mu_r A} + \frac{D}{\mu_0 A}\right)} \Leftrightarrow \tag{3.15}$$

$$B_g = \frac{B_r}{1 + \mu_r \frac{D}{l_M}}. \tag{3.16}$$

Thus, according to simple magnetic circuit analysis the magnetic field in the air gap does not depend on the air gap area - the only relevant geometrical parameter is the ratio between the air gap height and the magnet length. The magnetic force between two surfaces in close proximity is given as

$$F_\Phi = \frac{\Phi_g^2}{2\mu_0 A_g} = \frac{B_g^2 A_g}{2\mu_0}. \tag{3.17}$$

Substituting Eq. (3.16) into Eq. (3.17) yields

$$F_\Phi = \frac{A_g}{2\mu_0}\left(\frac{B_r}{1+\mu_r\frac{D}{l_M}}\right)^2. \tag{3.18}$$

COMSOL will be used to investigate the B-field in the air gap as well as the force between the two surfaces and this will be compared to the predictions by simple magnetic circuit theory, namely Eq. (3.16) and (3.18). The geometry of the relevant COMSOL model is shown in Fig. 3.2. For this particular circuit the remanence B_r of the permanent magnet equals 0.4 T and the relative recoil permeability is 1.15 which corresponds to the properties of a ferrite magnet. For the soft magnetic circuit the relative permeability is assumed to be $1 \cdot 10^{15}$. No real soft magnetic materials have such a high permeability but this is chosen to minimize drops in the magnetomotive force throughout the soft part of the magnetic circuit. The air gap height is always fixed at 1 mm and the magnet length at 4 mm. The ratio between the air gap height D and the length of one side of the air gap (indicated by s_A on the figure) is then adjusted by varying the thickness of the soft magnetic pole pieces. The height and width of the entire magnetic circuit is scaled by the cross-sectional area of the circuit to maintain the overall shape of the circuit. The height h_{Mc} of the magnetic circuit equals its width and it is given by the formula $h_{Mc} = 8\,(s_A/D)^{1/4}$. A simulation giving a closer look at the air gap field is shown in Fig. 3.8.

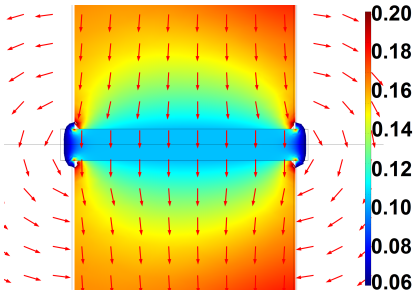

(a) Air gap field on a slice in the middle of the circuit viewed from the side.

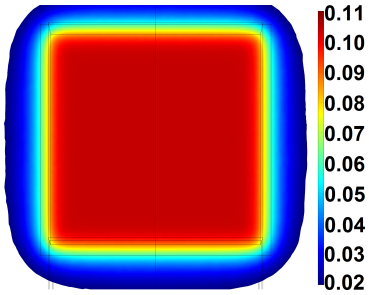

(b) Air gap field in the middle of the air gap viewed from above.

Figure 3.8: COMSOL simulation of magnetic B-field in the air gap of the magnetic circuit shown in Fig. 3.2(a). $\mu_r = 1 \cdot 10^{15}$ and $s_A/D = 7$.

The arrows in Fig. 3.8(a) indicate the direction of the B-field but they are normalized so that the length of the arrows does not reflect the magnitude of the B-field. This is done in order to observe the arrows outside the magnetic circuit that nicely visualize the fringing of the magnetic field around the air gap. Fig. 3.8(b) reveals that the magnetic field in the middle of the air gap is relatively constant over most of the area that corresponds to the surface outlined by the perimeter of the soft magnetic pole pieces. This means that the B-field in the center of the air gap reflects the average B-field well - at least for this case where the side length s_A is 7 times larger than the air gap height D. When the ratio s_A/D approaches smaller values, say 1, the air gap B field becomes

less homogeneous and it becomes more difficult to specify the field strength with just one value. Fig. 3.9(a) shows the predicted B-field in the air gap of the magnetic circuit shown in Fig. 3.2(a). Three different methods have been employed to estimate the field: COMSOL FEM simulation, simple circuit theory using Eq. (3.16) and Roters's method where various leakage permeances are taken into account (discussed in Sec. 3.1). Since Roters's method only takes the leakage paths into account that are close to the structure, the calculated leakage permeance has been increased by 10 % as a way of taking the excess leakage into account which is not included in the various considered flux paths. The increase of exactly 10 % is nothing but a qualified guess.

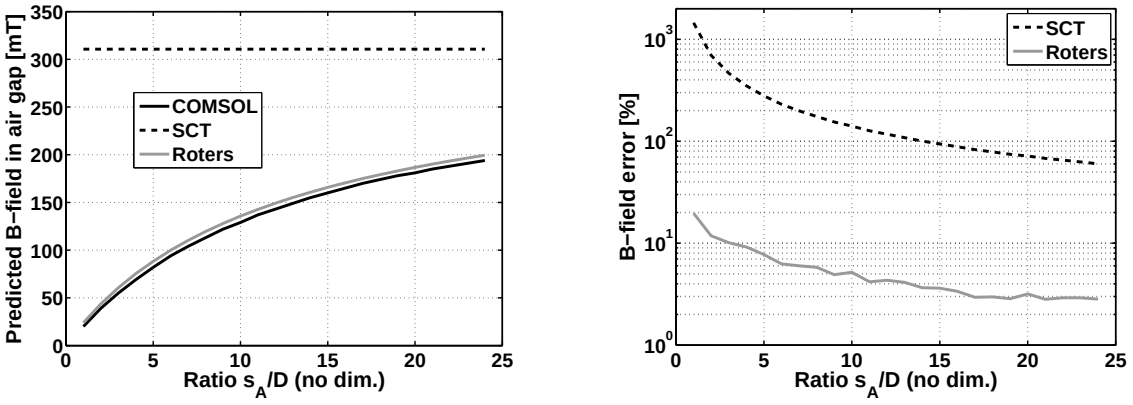

(a) Predicted air gap field.

(b) Error relative to COMSOL FEM simulation.

Figure 3.9: The predicted B-field in the air gap of the magnetic circuit shown in Fig. 3.2(a). SCT: Simple Circuit Theory. The ratio s_A/D between the edge shown in Fig. 3.2(a) and the air gap height is varied.

The B-field predicted by simple circuit theory is way off even for the largest ratios s_A/D but the predictions using Roters's method are quite close to that obtained with COMSOL. As already stated, the simple circuit theory is not sufficient to predict the circuit B-fields when there is an air gap in the circuit which introduces a huge reluctance making it attractive for the magnetic flux to leak into the air between soft pole pieces with different magnetic potential. The conclusion of this simulation experiment is that simple magnetic circuit theory without leakage reluctances should be avoided to calculate the B-field in magnetic circuits containing air gaps - especially if there is a magnetic potential difference between large surfaces, edges or corners.

Chapter 4

Electromagnetic Effects

In this chapter various electromagnetic effects are discussed. These effects are often unwanted and impossible to get rid of entirely.

4.1 Eddy Current Losses

According to Faraday's law any change in a magnetic field over time will induce an electric field. If conducting material is present inside this induced electric field, electrical current will inevitably flow and power will be dissipated due to the finite electrical resistance of the electrical conductor. Note that it is the electric field which is induced first and this causes electric current to flow. The flow of electric current depends on the conductivity of the material which implies that losses will be small if the conducting material has very high resistivity. The induced currents are often known as eddy currents. For an electrical conductor or for a conductor of magnetic flux carrying an alternating signal the effect of the eddy currents is to force the flow of the magnetic flux or electric current to occur at the surface of the conductor with the frequency-dependent skin depth being [13]:

$$\delta = \sqrt{\frac{2}{\mu_0 \mu_r \sigma \omega}} \tag{4.1}$$

where σ is the electrical conductivity of the material, μ_0 is the vacuum permeability, μ_r is the relative permeability and ω is the angular frequency of excitation. Thus, as the frequency is increased the skin depth δ is reduced. The effective magnetic reluctance or electrical resistance can be calculated assuming that the magnetic field or the electrical current flows only in the surface part of the conductor until a depth δ. The end result is that one can observe frequency-dependent eddy current losses. In a thin sheet of magnetic material, the eddy current losses per volume can be shown to be proportional to [12]:

$$p_e \propto \frac{f^2 B_m^2 t^2}{\rho}, \tag{4.2}$$

where f is the frequency of excitation, B_m is the amplitude of the B-field, t is the thickness of the sheet and ρ is the electrical resistivity of the material.

The flow of eddy currents in the balanced-armature loudspeaker may be reduced by choosing

magnetic materials with high electrical resistivity. Advances in powder metallurgy has made it possible to blend metal powders with high magnetic permeability with electrically insulating powders in order to obtain cores with nearly isotropic magnetic properties, relatively high magnetic permeabilities that are good enough for many purposes but with an electrical resistivity which can easily be 10 to 100 times that of conventional (non-powder based) soft magnetic materials [14]. On the basis of Eq. (4.2) one may (falsely) be led to believe that a reduction of the thickness of the magnetic material in the balanced-armature loudspeaker would lead to a reduction of the eddy current losses. Eq. (4.2) may be rewritten in terms of the magnetic flux Φ and the width w and thickness of the sheet:

$$p_e \propto \frac{f^2 \left(\frac{\Phi_m}{wt}\right)^2 t^2}{\rho} = \frac{f^2 \Phi_m^2}{\rho w^2}, \tag{4.3}$$

Thus if the magnetic flux Φ is largely determined by the reluctances of the air gaps and the internal reluctance of the permanent magnets, Eq. (4.3) suggests that the eddy current losses may be significantly reduced by increasing the width of the armature. An increase in the armature width will also help reduce the magnitude of the B-field, and the field will generally be less distorted with respect to the exciting H-field (see Sec. 4.3).

Eq. (4.2) is only valid for a thin sheet and even though the armature structure of a miniature balanced-armature loudspeaker is usually very thin, it hardly qualifies as a sheet. Eq. (4.2) and Eq. (4.3) in particular should therefore not be trusted fully when the considered "sheet" is in fact the armature structure of a balanced-armature loudspeaker. The eddy current losses for different armature geometries are probably best investigated using FEM simulation techniques.

4.2 Magnetic Hysteresis and Saturation

Magnetic hysteresis is a common well-described nonlinear phenomenon that takes place in soft and hard magnetic materials [12, 6, 7] and Sec. 4.3 shows examples of magnetic measurements. The area of the symmetrical hysteresis loop equals the amount of energy lost per volume for 1 magnetization cycle and the power loss associated with the hysteresis process is therefore proportional to the excitation frequency [12]. Notice that the eddy current losses are proportional to the squared frequency which means that eddy current losses will usually be the dominant ones in the audio frequency range.

With the assumption that eddy current power losses is proportional to the squared frequency and hysteresis losses being proportional to the frequency it is easy to separate power losses due to eddy currents from that due to hysteresis losses: One would only need to make a plot of the total energy loss per cycle versus frequency. The hysteresis energy loss per cycle is constant with frequency whereas the eddy current loss is proportional to the frequency so the total energy loss per cycle will be a straight line and its intersection with the vertical axis will be the hysteresis loss [12].

For a linear system the stationary output plotted against the input will form an ellipse which

is a special case of a Lissajous figure. The hysteresis curve is exactly a plot of the output (B-field) against the exciting input (H-field). If there is a linear relationship between the two the hysteresis curve will look like an ellipse where the slope of the ellipse depends on the ratio between the input and output magnitude. If the phase between the input and output is close to 0° or 180° the ellipse will look almost like a straight line and if the phase is close to 90° or 270° the ellipse will look almost like a circle. Thus, if the magnetic permeability is a constant real-valued number (with 0° phase) there will be a linear relationship between the H and the B-field and the ellipse (or hysteresis curve) will turn into a straight line and hysteresis losses will be zero. It is important to acknowledge that an elliptically shaped hysteresis curve is not an indication of a distorted B-field - it indicates a linear relationship between the H and the B-field where the phase shift merely introduces losses.

One would only need to take a look at a few textbook examples of hysteresis loops to see that the shape of hysteresis loops cannot usually be described by simple ellipses. However, the textbook examples often show the major hysteresis loop which is what can be observed when the magnetic material is fully saturated throughout the excitation cycle. If the magnetic material is not brought close to its magnetic excitation point the hysteresis curve will tend to look more like an ellipse. This statement also implies that whenever a magnetic material is brought close to its saturation point the magnetic field will be much more distorted as the response is simply compressed due to the fact that the magnetic material cannot accommodate an infinite concentration of magnetic flux. Often the saturation point will lie between 1 and 2 T.

The hysteresis loops observed for permanent magnets under recoil operation [6, 7] may come quite close to that of an ellipse and for the case of rare-earth magnets (with very low recoil permeability close to that of vacuum) the hysteresis loop will be very close to that of a straight line indicating almost no loss in the hysteresis process.

The two most popular models for modeling hysteresis are the Preisach model [15] and the Jiles-Atherton model [16, 16]. The Preisach model is not a physical model in the sense that it is not developed from any physical assumptions about how magnetic domain walls move when excited by an external H-field. Instead, it is a mathematical construction which is capable of modeling hysteresis phenomena in a lot of different fields.

The Jiles-Atherton model, on the other hand, is derived from existing ideas about how domain walls move. The original work by D. C. Jiles and D. L. Atherton was followed up by articles on how to experimentally determine the various parameters of the Jiles-Atherton model [17, 18]. The original Jiles-Atherton model is independent of the rate of change with time of the exciting H-field. However, at high frequencies, eddy currents set up in electrically conducting magnetic material will reduce the effective H-field and it will thus require a larger exciting H field to drive the B-field of the magnetic material to a given level. The net effect of this is that the hysteresis loops will appear wider as the frequency (and thereby the eddy current effect) is increased. Jiles et. al. finally extended the original model to include the effects of eddy currents [19, 20]. The eddy current losses quickly become relevant and may easily be the most significant ones in the audio frequency range and should therefore be included in any realistic B-A loudspeaker model. The original Jiles-Atherton model, unfortunately, tends to exhibit non-physical behavior for minor

loops as pointed out by Carpenter [21] and Leite et al. [22, 23]. The Ph.D. thesis by Péter Kis includes a lot of discussion and information about the Jiles-Atherton algorithm [24].

It is important to understand how the small-signal permeability, hysteresis loss, eddy current loss and saturation point of the soft magnetic material affects the performance of the balanced-armature loudspeaker. As already mentioned the magnetic reluctance tends to be dominated by that of the air gaps and the internal reluctance of the permanent magnets. This means that an increase in magnetic permeability from 10000 to 1000000 - everything else equal - will be very difficult to detect in terms of loudspeaker performance. However, for metals with high permeability the hysteresis loop tends to be more narrow and if this is the case, the hysteresis loss will be smaller for a larger permeability. As mentioned earlier, eddy current losses tend to be more significant in the audio frequency range so as long as the relative permeability of the soft magnetic material is more than a few hundred it will often be more beneficial to choose soft magnetic materials with higher resistivity. It will be shown later (see chapter 10) that the saturation point of the armature will affect the maximum output and the distortion of the balanced-armature loudspeaker tremendously. For this reason it will again be much more wise to choose a soft magnetic material with high saturation point over a material with very high permeability.

4.3 Measurement of Hysteresis

It was decided to set up a measurement system which is capable of measuring the magnetic properties of soft magnetic ring samples. This would allow to investigate how the excitation amplitude as well as frequency would affect the hysteresis loops. From the hysteresis curve it is possible to extract information about the distortion of the B-field response as well as the effective or apparent permeability. The information provided by manufacturers of magnetic materials is sometimes inadequate and with such a measurement setup the sponsoring company of this industrial Ph.D. project would have immediate access to make their own relevant measurements. A measurement system was successfully constructed and the technical report describing the setup can be found in the back of this thesis after the published papers. That report also contains examples of what kind of measurements that can be performed with the measurement setup.

4.4 Measurement Results

Acoustic Technology, DTU gained access to some magnetic steel and it was decided to measure its magnetic properties using the aforementioned measurement setup and then build a large scale B-A loudspeaker if the magnetic properties were found sufficient. The magnetic steel was cut into ring samples with an outer diameter of 10 mm, an inner diameter of 6 mm and a height (or thickness) of 1 mm. The first experiment which was carried out using this material was to compare the magnetic permeability of an untreated ring sample to that of a ring sample that had been annealed in a hydrogen atmosphere for 3 hours at 850 °C. The results of this experiment are shown in Fig. 4.1

The relative magnetic permeability is calculated as the ratio between the B-field and the ap-

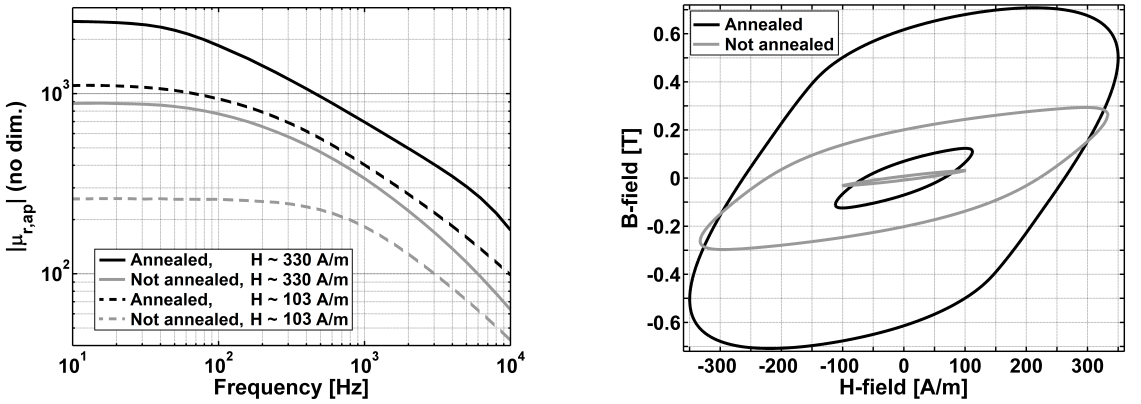

(a) Curves of relative magnetic permeability.

(b) Magnetic hysteresis curves measured at 125 Hz.

Figure 4.1: Comparison of two different ring samples of soft magnetic steel. One sample is untreated and the other one has been annealed in a hydrogen atmosphere for 3 hours at 850 °C.

plied H-field at the relevant excitation frequency i.e. the harmonics of the B-field are disregarded. The permeability curves as well as the hysteresis curves indicate an increase in the magnetic permeability for the annealed ring sample. The presented hysteresis curves are for an excitation frequency of 125 Hz. One could have chosen to show the result for a very low frequency, say, 10 Hz in order to reduce the effect of eddy current losses. However, 125 Hz was chosen as this is considered a low frequency for speech and music reproduction in hearing aids.

All the remaining measurements in this section were performed using an annealed ring sample. Fig. 4.2(b) shows hysteresis loops measured at 10 Hz at different excitation levels and Fig. 4.2(a) shows the distortion of the exciting H-field versus frequency for a range of excitation levels. The THD remains at a relatively low level in the entire range of frequencies and amplitudes.

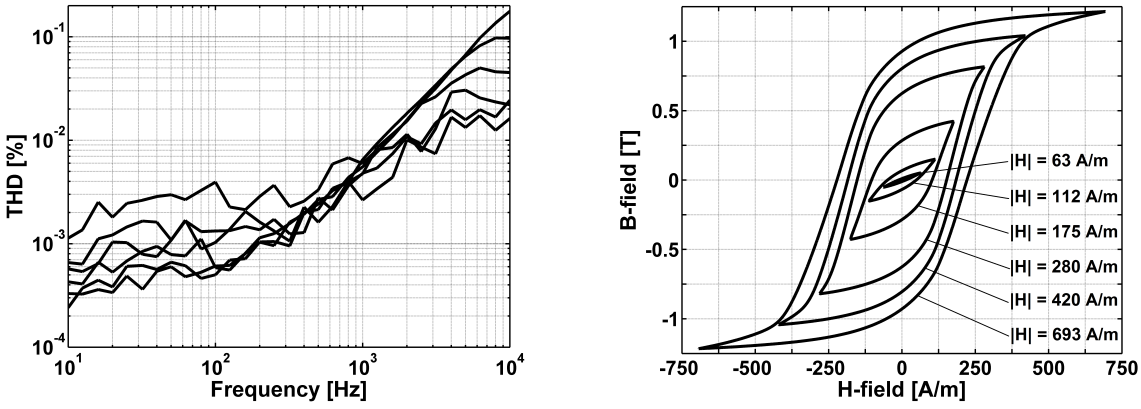

(a) H-field distortion.

(b) Magnetic hysteresis curve.

Figure 4.2: (a) shows the distortion of the exciting H-field (including 5 harmonics) measured at 6 different excitation levels between 63 A/m and 693 A/m. (b) shows hysteresis loops measured at 10 Hz with different excitation amplitudes.

Since the H-field has very low distortion it is clear that the B-field must be distorted in order to produce the hysteresis loops shown in Fig. 4.2(b). Fig. 4.3 shows the distortion of the B-field

versus frequency for a range of excitation amplitudes. The hysteresis loops shown in Fig. 4.2(b) are measured at 10 Hz and at this frequency the distortion of the B-field is between 3 % and 30 % with the distortion increasing with the excitation level.

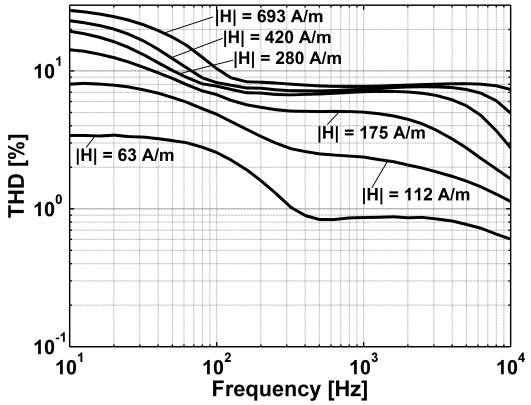

Figure 4.3: B-field distortion vs frequency measured at various excitation levels. 20 harmonics were included in the calculation of the THD

As already mentioned in Sec. 4.2 eddy currents will circulate in the ring sample trying to oppose any changes in the B-field and this causes a reduction of the effective exciting H-field. Thus, when the frequency is increased it will require a larger controllable H-field (that due to the coil) in order to set up the same B-field and the hysteresis loops will appear wider. This is shown in Fig. 4.4(a). When the frequency is increased further (Fig. 4.4(b)) the eddy current effect increases and as the B-field response becomes even smaller the hysteresis curves do not really show the effect of magnetic hysteresis anymore but are instead dominated by the eddy current losses. The hysteresis loops start to look more like ellipses indicating a lower level of distortion and this is exactly what can be observed in Fig. 4.3 where the distortion level of the B-field decreases because the eddy current losses increases with frequency.

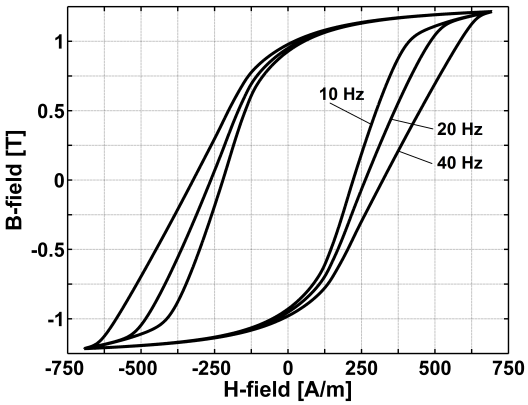

(a) H-field distortion.

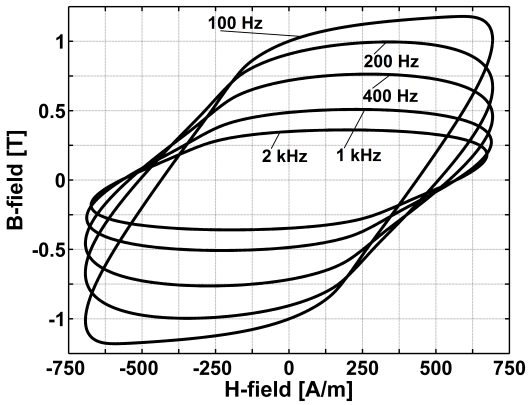

(b) Magnetic hysteresis curve.

Figure 4.4: (a) shows the distortion of the exciting H-field (including 5 harmonics) measured at 6 different excitation levels between 63 A/m and 693 A/m. (b) shows hysteresis loops measured at 10 Hz with different excitation amplitudes.

Using only the fundamental excitation frequency of the B-field it is possible to determine a

linearized apparent relative permeability response of the ring sample. The magnitude and phase of this apparent relative permeability are shown in figures 4.5 and 4.6, respectively.

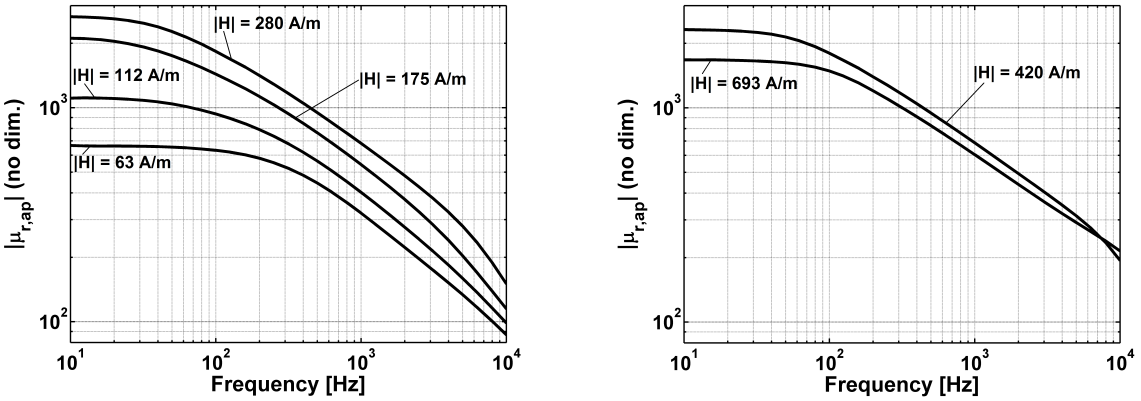

(a) Lower excitation levels.

(b) Highest excitation levels.

Figure 4.5: Apparent relative permeability (magnitude) of the material in the ring sample measured at 6 different excitation levels between 63 A/m and 693 A/m.

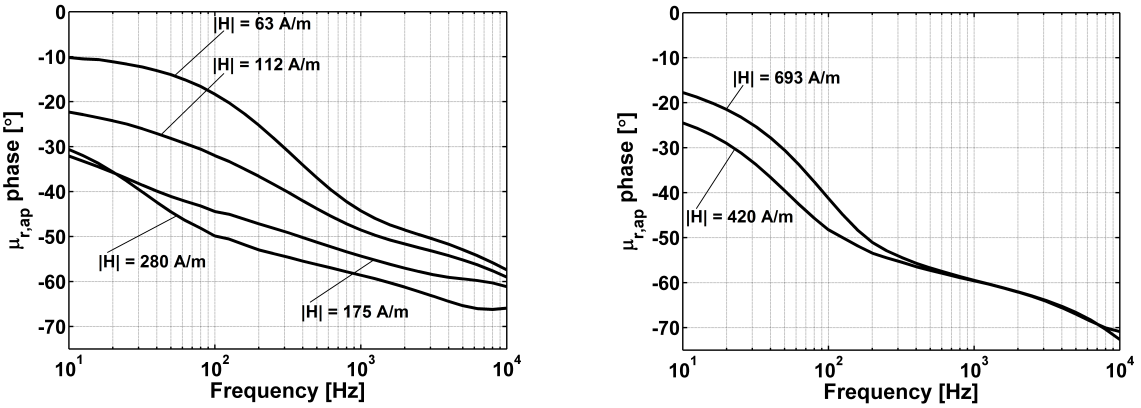

(a) Lower excitation levels.

(b) Highest excitation levels.

Figure 4.6: Apparent relative permeability (phase) of the material in the ring sample measured at 6 different excitation levels between 63 A/m and 693 A/m.

The general trend is that the apparent relative permeability decreases with frequency and this is the same trend indicated by the slope and the overall level of the B-field of the hysteresis curves in Fig. 4.4(b). As already mentioned, this is due to the effect of eddy current losses.

It can also be observed that the permeability tends to increase with excitation amplitude (see Fig. 4.5(a)) until a certain level where the material saturates i.e. when the B-field approaches the maximum B-field traced out by the major hysteresis loop: Comparing Fig. 4.5(b) to Fig. 4.5(a) one can see this phenomenon.

Figures 4.5 and 4.6 clearly show that the concept of a constant and real-valued relative magnetic permeability is a crude simplification of reality: Not only are the magnitude and the phase frequency-dependent, they are also amplitude-dependent and thus nonlinear.

Chapter 5

The Balanced-Armature Loudspeaker

In this chapter the basic elements of the balanced-armature electromechanical mechanism are described and the relevant equations are derived. Most of the chapter is written without too many interpretations of the various equations. The various equations and the significance of different parameters will be interpreted in later chapters and this chapter should most of all be viewed as a reference with regards to the derivation of the various key equations.

5.1 Analysis of Magnetic Circuit

Compared to the model developed in [25] the model presented here is improved with a simple linear model of the permanent magnets which includes the internal magnetic reluctance (see Fig. 5.1(b)). The inclusion of this reluctance influences the behavior of the loudspeaker and its optimization significantly. Using the technique described in section 3.1 it is also possible to include the effect of magnetic leakage by introducing the Thévenin equivalent recoil permeability. It is assumed that the magnets are operating along straight recoil lines. From this it follows that a magnet can be modeled as a constant magnetomotive force, $\mathcal{F}_M$, in series with an internal magnet reluctance, $\mathcal{R}_M$.

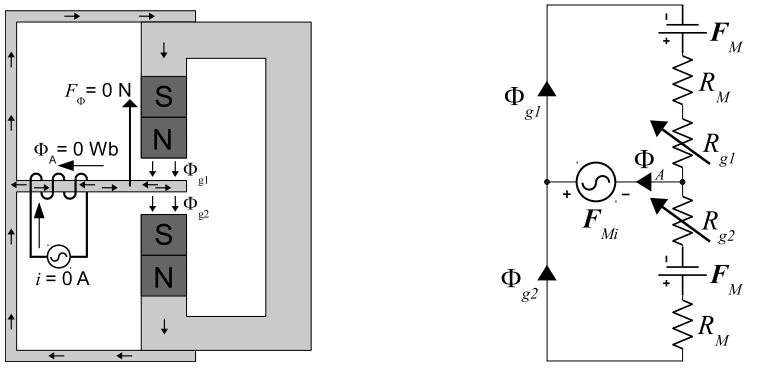

(a) Magnetic circuit.

(b) Equivalent circuit of magnetic circuit.

Figure 5.1: Simplified illustration of balanced-armature mechanism found in hearing aid receivers.

Referring to Fig. 5.1, the equations describing the balanced-armature mechanism can be written down. Assuming that the magnets are operating on a straight recoil lines the magnetomotive force can be written:

$$\mathcal{F}_M = \frac{B_r l_M}{\mu_0 \mu_r} = \frac{B_r D_M}{\mu_0}. \tag{3.1}$$

The internal magnetic reluctance of the permanent magnets is

$$\mathcal{R}_M = \frac{l_M}{\mu_0 \mu_r A_M} = \frac{D_M}{\mu_0 A_M}, \tag{3.3}$$

with D_M defined in Eq. (3.2). Assuming that the area of the magnet equals the area of the air gap:

$$A_M = A_g = A \tag{5.1}$$

it is possible to write the magnetic reluctances of the air gaps:

$$\mathcal{R}_{g1}(x) = \frac{D - x}{\mu_0 A} \tag{5.2}$$

$$\mathcal{R}_{g2}(x) = \frac{D + x}{\mu_0 A}. \tag{5.3}$$

The magnetomotive force set up by the coil is given as

$$\mathcal{F}_{Mi}(i) = Ni, \tag{3.5}$$

where N is the number of coil windings and i is the electrical current in the coil. Electrical network analysis of Fig. 5.1 leads to the following three equations:

$$\Phi_{g1} = \Phi_a + \Phi_{g2} \tag{5.4}$$

$$\mathcal{F}_M + \mathcal{F}_{Mi} = \Phi_{g1}\mathcal{R}_M + \Phi_{g1}\mathcal{R}_{g1} \tag{5.5}$$

$$\mathcal{F}_M = \mathcal{F}_{Mi} + \Phi_{g2}\mathcal{R}_M + \Phi_{g2}\mathcal{R}_{g2}, \tag{5.6}$$

where Φ_{g1} and Φ_{g2} are the magnetic fluxes in the upper and lower air gaps, respectively, and Φ_A is the armature flux. The solution to this set of equations is:

$$\Phi_a = \Phi_{g1} - \Phi_{g2} = \frac{(\mathcal{F}_M + \mathcal{F}_{Mi})(\mathcal{R}_M + \mathcal{R}_{g2}) - (\mathcal{F}_M - \mathcal{F}_{Mi})(\mathcal{R}_M + \mathcal{R}_{g1})}{(\mathcal{R}_M + \mathcal{R}_{g1})(\mathcal{R}_M + \mathcal{R}_{g2})} \tag{5.7}$$

$$\Phi_{g1} = \frac{\mathcal{F}_M + \mathcal{F}_{Mi}}{\mathcal{R}_M + \mathcal{R}_{g1}} \tag{5.8}$$

$$\Phi_{g2} = \frac{\mathcal{F}_M - \mathcal{F}_{Mi}}{\mathcal{R}_M + \mathcal{R}_{g2}}. \tag{5.9}$$

Substituting Equations (3.3), (5.2) and (5.3) into Eq. (5.7) yields the more compact expression for the armature flux

$$\boxed{\Phi_a(x,i) = 2\mu_0 A \frac{\mathcal{F}_M x + \mathcal{F}_{Mi} D_{eff}}{D_{eff}^2 - x^2}}, \tag{5.10}$$

with the introduction of the effective air gap length

$$D_{eff} \equiv D + D_M = D + \frac{l_M}{\mu_r}. \tag{5.11}$$

This armature flux can be written as a sum of the contribution from the permanent magnets $\Phi_{a,0}$ and from the coil $\Phi_{a,i}$:

$$\Phi_a(x,i) \equiv \Phi_{a,0}(x) + \Phi_{a,i}(x,i) = \frac{2\mu_0 A \mathcal{F}_M x}{D_{eff}^2 - x^2} + \frac{2\mu_0 A \mathcal{F}_{Mi} D_{eff}}{D_{eff}^2 - x^2}. \tag{5.12}$$

Substituting Equations (3.1), (3.5) and (5.11) into Eq. (5.12) yields

$$\Phi_a(x,i) = \frac{2\mu_0 A \frac{B_r D_M}{\mu_0} x}{(D + D_M)^2 - x^2} + \frac{2\mu_0 A N i (D + D_M)}{(D + D_M)^2 - x^2} \Leftrightarrow \tag{5.13}$$

$$\boxed{\Phi_a(x,i) = 2B_r \frac{A}{D} \frac{\alpha}{(\alpha+1)^2 - \left(\frac{x}{D}\right)^2} x + 2\mu_0 N \frac{A}{D} \frac{\alpha+1}{(\alpha+1)^2 - \left(\frac{x}{D}\right)^2} i}. \tag{5.14}$$

Here the ratio between the air gap length D and the equivalent air gap length of the magnet $D_M = l_M/\mu_r$ has been introduced:

$$\alpha = \frac{D_M}{D} = \frac{l_M}{\mu_r D}, \tag{5.15}$$

This ratio will turn out to be an important parameter influencing the small-signal parameters (Sec. 5.5) as well as the nonlinearity of the loudspeaker (Chapter. 7). It is useful to define the armature flux $\Phi_{a,0}$ set up only by the permanent magnets when the armature is displaced. The armature flux contribution due to coil current will depend on the frequency of excitation but $\Phi_{a,0}$ is solely determined by the properties of the magnetic circuit and the displacement of the armature:

$$\boxed{\Phi_{a,0}(x) = 2B_r \frac{A}{D} \frac{\alpha}{(\alpha+1)^2 - \left(\frac{x}{D}\right)^2} x}. \tag{5.16}$$

For small displacements ($x << D$) or for $\alpha >> 1$ the above may be linearized to

$$\boxed{\Phi_{a,0,lin}(x) = 2B_r \frac{A}{D} \frac{\alpha}{(\alpha+1)^2} x}. \tag{5.17}$$

and the nonlinear armature flux only due to the permanent magnets may be written in terms of the linearized expression

$$\Phi_{a,0}(x) = \Phi_{a,0,lin}(x) \frac{(\alpha+1)^2}{(\alpha+1)^2 - \left(\frac{x}{D}\right)^2}. \tag{5.18}$$

The armature flux solely due to coil current is

$$\boxed{\Phi_{a,i}(x,i) = 2\mu_0 N \frac{A}{D} \frac{\alpha+1}{(\alpha+1)^2 - \left(\frac{x}{D}\right)^2} i}. \tag{5.19}$$

For small displacements ($x << D$) or for $\alpha >> 1$ the above may be linearized to

$$\boxed{\Phi_{a,i,lin}(i) = 2\mu_0 N \frac{A}{D} \frac{1}{\alpha+1} i}. \tag{5.20}$$

and the nonlinear armature flux only due to coil current may be written in terms of the linearized expression

$$\Phi_{a,i}(x,i) = \Phi_{a,i,lin}(i) \frac{(\alpha+1)^2}{(\alpha+1)^2 - \left(\frac{x}{D}\right)^2}. \tag{5.21}$$

5.2 Armature Input Force

Consider a magnetic circuit with two parallel pole faces with an equal area A separated by a small air gap. The situation is depicted in Fig. 5.2 where the distance between the two pole faces is strongly exaggerated for illustration purposes.

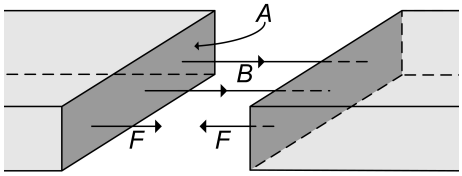

Figure 5.2: Magnetic force of attraction between opposite pole faces across air gap.

The force F_Φ between these two surfaces due to the magnetic flux Φ is [11, 7]:

$$F_\Phi = \frac{\Phi^2}{2\mu_0 A} = \frac{AB^2}{2\mu_0}, \tag{5.22}$$

where B is the average magnetic B-field over the surface area A. This force always tries to close the magnetic circuit i.e. reducing the potential magnetic energy in the system by shortening the path of magnetic flux. In the balanced-armature loudspeaker there are two permanent magnets each trying to pull the armature towards them with an equal but opposite force when the armature is located right in the middle between the two permanent magnets. The net armature input force generated by the magnetic flux in the two air gaps is the sum of the magnetic forces across the two air gaps:

$$F_\Phi = \frac{\Phi_{g1}^2}{2\mu_0 A} - \frac{\Phi_{g2}^2}{2\mu_0 A} = \frac{(\Phi_{g1} + \Phi_{g2})(\Phi_{g1} - \Phi_{g2})}{2\mu_0 A} = \frac{(\Phi_{g1} + \Phi_{g2})\Phi_a}{2\mu_0 A}. \tag{5.23}$$

Substituting Equations (5.7) to (5.9) into Eq. (5.23) first and then Equations (3.3), (3.5), (5.2) and (5.3) into this yields

$$F_\Phi(x,i) = 2\mu_0 A \frac{\mathcal{F}_M^2 D_{eff} x + \mathcal{F}_M N\left(D_{eff}^2 + x^2\right) i + N^2 D_{eff} x i^2}{\left(D_{eff}^2 - x^2\right)^2}. \tag{5.24}$$

This armature input force can be separated into a sum of three terms

$$\boxed{F_\Phi(x,i) = \frac{2\mu_0 A \mathcal{F}_M^2 D_{eff}}{\left(D_{eff}^2 - x^2\right)^2} x + \frac{2\mu_0 A \mathcal{F}_M N\left(D_{eff}^2 + x^2\right)}{\left(D_{eff}^2 - x^2\right)^2} i + \frac{2\mu_0 A D_{eff} N^2 x i}{\left(D_{eff}^2 - x^2\right)^2} i}. \tag{5.25}$$

This can be written as

$$\boxed{F_\Phi(x,i) = F_{\Phi 1}(x) + F_{\Phi 2}(x,i) + F_{\Phi 3}(x,i) = k_\Phi(x)\, x + T_{me}(x)\, i + T_{me,d}(x,i)\, i} \tag{5.26}$$

or

$$\boxed{F_\Phi(x,i) = k_\Phi(x)\, x + T_{me}(x)\, i + \frac{1}{2}\frac{dL(x)}{dx} i^2}, \tag{5.27}$$

where $k_\Phi(x)$ is the nonlinear stiffness compensation, $T_{me}(x)$ and $T_{me,d}(x,i)$ are the nonlinear transduction coefficient and the distortion transduction coefficient, respectively, from the electrical- to the mechanical domain. $L(x)$ is the nonlinear electrical inductance which will be derived in section 5.3. The three terms will be analyzed individually in the next sections. Further-

more, for small armature displacements where $x << D_{eff} \Rightarrow x << D$ the armature input force can be written

$$\boxed{F_\Phi(x,i)|_{x<<D} \approx \frac{2\mu_0 A \mathcal{F}_M^2}{D_{eff}^3} x + \frac{2\mu_0 A \mathcal{F}_M N}{D_{eff}^2} i + \frac{2\mu_0 A N^2 x i}{D_{eff}^3} i}. \tag{5.28}$$

5.2.1 Magnetic Stiffness Compensation

For zero coil current $(i = 0)$ Eq. (5.25) reduces to

$$F_\Phi(x,i)|_{i=0} = \frac{2\mu_0 A \mathcal{F}_M^2 D_{eff}}{\left(D_{eff}^2 - x^2\right)^2} x, \tag{5.29}$$

and the nonlinear (displacement-dependent) magnetic stiffness compensation may be defined as

$$\boxed{k_\Phi(x) = \frac{2\mu_0 A \mathcal{F}_M^2 D_{eff}}{\left(D_{eff}^2 - x^2\right)^2} = \frac{2B_r^2}{\mu_0}\frac{A}{D}\frac{\alpha^2(\alpha+1)}{\left[(\alpha+1)^2 - \left(\frac{x}{D}\right)^2\right]^2}}. \tag{5.30}$$

For small armature displacements where $x << D$ the small-signal magnetic stiffness compensation is

$$\boxed{k_\Phi = \frac{2\mu_0 A \mathcal{F}_M^2}{D_{eff}^3} = \frac{2B_r^2}{\mu_0}\frac{A}{D}\frac{\alpha^2}{(\alpha+1)^3}} \quad \text{, for } x << D. \tag{5.31}$$

It is also possible to write the nonlinear magnetic stiffness compensation as a product of the linear magnetic stiffness compensation and a function of α and x/D:

$$k_\Phi(x) = k_\Phi \frac{(\alpha+1)^4}{\left[(\alpha+1)^2 - \left(\frac{x}{D}\right)^2\right]^2}. \tag{5.32}$$

This makes it possible to investigate only the nonlinear part of the magnetic stiffness compensation via the second factor of Eq. (5.32). One might refer to this factor as the normalized nonlinear magnetic stiffness compensation. The same approach will be used for the remaining nonlinear parameters that are derived throughout the coming sections.

5.2.2 Transduction Coefficient T_{me}

In this section the electromechanical coupling between coil current and armature input force is investigated. We consider only the fundamental part of the armature input force:

$$F_{\Phi 2} = 2\mu_0 A \mathcal{F}_M N \frac{D_{eff}^2 + x^2}{\left(D_{eff}^2 - x^2\right)^2} i \tag{5.33}$$

From this equation the nonlinear (displacement-dependent) transduction coefficient is defined as:

$$\boxed{T_{me}(x) = 2\mu_0 A \mathcal{F}_M N \frac{D_{eff}^2 + x^2}{\left(D_{eff}^2 - x^2\right)^2} = 2B_r N \frac{A}{D} \frac{\alpha\left[(\alpha+1)^2 + \left(\frac{x}{D}\right)^2\right]}{\left[(\alpha+1)^2 - \left(\frac{x}{D}\right)^2\right]^2}} \tag{5.34}$$

For small armature displacements where $x << D$ the linearized transduction coefficient becomes

$$\boxed{T_{me} = \frac{2\mu_0 A \mathcal{F}_M N}{D_{eff}^2} = 2B_r N \frac{A}{D} \frac{\alpha}{(\alpha+1)^2}} \quad \text{, for } x << D. \tag{5.35}$$

It is also possible to write the nonlinear force factor as a product of the linear force factor and a function of α and x/D:

$$T_{me}(x) = T_{me} \frac{(\alpha+1)^2\left[(\alpha+1)^2 + \left(\frac{x}{D}\right)^2\right]}{\left[(\alpha+1)^2 - \left(\frac{x}{D}\right)^2\right]^2}. \tag{5.36}$$

5.2.3 Distortion Force Term ($F_{\Phi 3}$)

The third term of Eq . (5.25) is a distortion force which vanishes if either the electrical current or the armature displacement is zero. As this is generally not the case for a balanced-armature loudspeaker during normal operation, this distortion force is relevant to take into account. Let us define

$$\boxed{T_{me,d}(x,i) = \frac{2\mu_0 A D_{eff} N^2 x i}{\left(D_{eff}^2 - x^2\right)^2} = 2\mu_0 N^2 \frac{xi}{D^2} \frac{A}{D} \frac{\alpha+1}{\left[(\alpha+1)^2 - \left(\frac{x}{D}\right)^2\right]^2}}. \tag{5.37}$$

For small armature displacements Eq . (5.37) reduces to

$$\boxed{T_{me,d}(x,i)\big|_{x<<D} = \frac{2\mu_0 A N^2 x i}{D_{eff}^3} = 2\mu_0 N^2 \frac{xi}{D^2} \frac{A}{D} \frac{1}{(\alpha+1)^3}}. \tag{5.38}$$

It is also possible to write the nonlinear distortion force factor as a product of the linearized distortion force factor and a function of α and x/D:

$$T_{me,d}\left(x,i\right)=T_{me,d}\left(x,i\right)|_{x<<D}\,\frac{\left(\alpha+1\right)^{4}}{\left[\left(\alpha+1\right)^{2}-\left(\frac{x}{D}\right)^{2}\right]^{2}}. \tag{5.39}$$

5.3 Electrical Back-EMF

In this section the electrical back-EMF - or the electrical voltage set up in the coil due to changes in the magnetic flux - is evaluated from the relationship

$$U_{\text{back}}=N\frac{d\Phi_{a}}{dt}. \tag{5.40}$$

Using Eq . (5.10) with $\mathcal{F}_{Mi}=Ni$ and the above relationship yields

$$U_{\text{back}}=N2\mu_{0}A\frac{d}{dt}\frac{\mathcal{F}_{M}x\left(t\right)+Ni\left(t\right)D_{eff}}{D_{eff}^{2}-x\left(t\right)^{2}}\Leftrightarrow \tag{5.41}$$

$$\boxed{U_{\text{back}}=\frac{2\mu_{0}A\mathcal{F}_{M}N\left(D_{eff}^{2}+x^{2}\right)}{\left(D_{eff}^{2}-x^{2}\right)^{2}}\frac{dx}{dt}+\frac{4\mu_{0}AD_{eff}N^{2}xi}{\left(D_{eff}^{2}-x^{2}\right)^{2}}\frac{dx}{dt}+\frac{2\mu_{0}AN^{2}D_{eff}}{D_{eff}^{2}-x^{2}}\frac{di}{dt}}. \tag{5.42}$$

where it is understood that x and i are time-dependent variables. Equation (5.42) can be written as

$$\boxed{U_{\text{back}}=T_{em}\left(x\right)\frac{dx}{dt}+T_{em,d}\left(x,i\right)\frac{dx}{dt}+L\left(x\right)\frac{di}{dt}} \quad \text{or} \tag{5.43}$$

$$\boxed{U_{\text{back}}=T_{em}\left(x\right)\frac{dx}{dt}+\frac{dL\left(x\right)}{dx}i\frac{dx}{dt}+L\left(x\right)\frac{di}{dt}}, \tag{5.44}$$

where $L\left(x\right)$ is the nonlinear electrical inductance, $T_{em}\left(x\right)$ and $T_{em,d}\left(x,i\right)$ are the nonlinear transduction coefficient and the distortion transduction coefficient, respectively, from the mechanical- to the electrical domain. The three terms will be analyzed individually in the next sections. For small armature displacements where $x<<D$ the back-EMF can be written

$$\boxed{U_{\text{back}}|_{x<<D}=\frac{2\mu_{0}A\mathcal{F}_{M}N}{D_{eff}^{2}}\frac{dx}{dt}+\frac{4\mu_{0}AN^{2}xi}{D_{eff}^{3}}\frac{dx}{dt}+\frac{2\mu_{0}AN^{2}}{D_{eff}}\frac{di}{dt}}. \tag{5.45}$$

5.3.1 Electrical Inductance

For an electrical inductor the constitutive equation is

$$U_{L}=L\frac{di}{dt}. \tag{5.46}$$

Looking at Eq. (5.42) it is clear that the third term of the back-EMF has exactly that property. The idea is to divide the back-EMF into a part which is caused by changes in the electrical current di/dt and a part which is caused by armature velocity dx/dt. The inductance is

$$\boxed{L\left(x\right) = 2\mu_0 A N^2 \frac{D_{eff}}{D_{eff}^2 - x^2} = 2\mu_0 N^2 \frac{A}{D} \frac{\alpha + 1}{\left(\alpha+1\right)^2 - \left(\frac{x}{D}\right)^2}}. \tag{5.47}$$

For completeness the small-signal inductance ($x << D \Rightarrow x << D_{eff}$) is written:

$$\boxed{L = \frac{2\mu_0 A N^2}{D_{eff}} = 2\mu_0 N^2 \frac{A}{D} \frac{1}{\alpha+1}} \quad \text{, for } x << D. \tag{5.48}$$

It is also possible to write the nonlinear electrical inductance as a product of the linearized inductance and a function of α and x/D:

$$L\left(x\right) = L \frac{\left(\alpha+1\right)^2}{\left(\alpha+1\right)^2 - \left(\frac{x}{D}\right)^2}. \tag{5.49}$$

5.3.2 Transduction Coefficient T_{em}

The transduction coefficient relating mechanical velocity to electrical voltage is contained in the first term of Eq. (5.42):

$$\boxed{T_{em}\left(x\right) = 2\mu_0 A \mathcal{F}_M N \frac{D_{eff}^2 + x^2}{\left(D_{eff}^2 - x^2\right)^2} = 2B_r N \frac{A}{D} \frac{\alpha\left[\left(\alpha+1\right)^2 + \left(\frac{x}{D}\right)^2\right]}{\left[\left(\alpha+1\right)^2 - \left(\frac{x}{D}\right)^2\right]^2}} \tag{5.50}$$

For completeness the small-signal transduction coefficient ($x << D \Rightarrow x << D_{eff}$) is written:

$$\boxed{T_{em} = \frac{2\mu_0 A \mathcal{F}_M N}{D_{eff}^2} = 2B_r N \frac{A}{D} \frac{\alpha}{\left(\alpha+1\right)^2}} \quad \text{, for } x << D. \tag{5.51}$$

It is also possible to write the nonlinear force factor as a product of the linearized force factor and a function of α and x/D:

$$T_{em}\left(x\right) = T_{em} \frac{\left(\alpha+1\right)^2\left[\left(\alpha+1\right)^2 + \left(\frac{x}{D}\right)^2\right]}{\left[\left(\alpha+1\right)^2 - \left(\frac{x}{D}\right)^2\right]^2}. \tag{5.52}$$

5.3.3 Distortion Back-EMF Term

The second term of Eq . (5.42) is a distortion voltage which vanishes if either the electrical current or the armature displacement or velocity is zero. As this is generally not the case for a balanced-armature loudspeaker during normal operation this distortion voltage is relevant to take into account. Let us define

$$\boxed{T_{em,d}\left(x,i\right)=\frac{4\mu_0 A D_{eff} N^2 x i}{\left(D_{eff}^2-x^2\right)^2}=4\mu_0 N^2\frac{xi}{D^2}\frac{A}{D}\frac{\alpha+1}{\left[\left(\alpha+1\right)^2-\left(\frac{x}{D}\right)^2\right]^2}}. \tag{5.53}$$

For small armature displacements this expression reduces to

$$\boxed{T_{em,d}\left(x,i\right)\big|_{x<<D}=\frac{4\mu_0 A N^2 x i}{D_{eff}^3}=4\mu_0 N^2\frac{xi}{D^2}\frac{A}{D}\frac{1}{\left(\alpha+1\right)^3}}. \tag{5.54}$$

It is also possible to write the nonlinear distortion force factor as a product of the linearized distortion force factor and a function of α and x/D:

$$T_{em,d}\left(x,i\right)=T_{em,d}\left(x,i\right)\big|_{x<<D}\frac{\left(\alpha+1\right)^4}{\left[\left(\alpha+1\right)^2-\left(\frac{x}{D}\right)^2\right]^2}. \tag{5.55}$$

5.3.4 Loudspeaker Stiffness and the Acoustic Back Volume

The stiffness of the the balanced-armature loudspeaker - the one which is related to the displacement of the armature - comprises several elements: The armature, the diaphragm suspension, the stiffness of the acoustic back volume and the magnetic stiffness compensation. The armature stiffness and the acoustic stiffness will be discussed in more detail in sections 5.6 and 7.3, respectively. The magnetic stiffness compensation has already been touched upon and its nonlinear properties and its influence on the loudspeaker stability will be discussed in more detail in Chapters 7 and 9, respectively. The total nonlinear effective stiffness is

$$k_{eff}\left(x\right)=k_a\left(x\right)+k_s\left(x\right)+k_{mA}\left(x\right)-k_\Phi\left(x\right), \tag{5.56}$$

where $k_a\left(x\right)$ is the nonlinear stiffness of the armature, $k_s\left(x\right)$ is the nonlinear stiffness of the diaphragm suspension, $k_{mA}\left(x\right)$ is the nonlinear mechanical stiffness due to the back-volume of the loudspeaker and $k_\Phi\left(x\right)$ is the nonlinear magnetic stiffness compensation. Usually none of these stiffnesses can be disregarded. This is due to the fact that the magnetic stiffness compensation is often made, say, 60 % of the stiffness of the armature in order to reduce the system stiffness and thus increase efficiency. The stiffness due to the back volume is usually also quite large because of the small dimensions of the B-A loudspeaker. The diaphragm suspension might be the least

significant contribution to the overall stiffness. For small signals where $x << D$ the linearized expression is simply written

$$k_{eff} = k_a + k_s \ + k_{mA} - k_\Phi. \tag{5.57}$$

Sometimes k_s will not be written explicitly and it will simply be assumed that this additional stiffness due to the diaphragm suspension is contained in the stiffness of the armature k_a. It will also be useful to introduce the stiffness in the mechanical domain without the contribution from the magnetic stiffness compensation

$$k_{ma} = k_a + k_s \ + k_{mA}. \tag{5.58}$$

The stiffness ratio between the small-signal magnetic stiffness compensation and the armature stiffness is introduced here:

$$\boxed{k_r \equiv \frac{k_\Phi}{k_a}}. \tag{5.59}$$

In Chapter 9 it will become clear that this stiffness ratio has to do with the stability of the loudspeaker design.

If the back volume is very large k_{mA} becomes very small. If k_{mA} is much smaller than $k_a - k_\Phi$ and the suspension stiffness is included in k_a then Eq. (5.57) may be written

$$k_{eff} \approx k_a - k_\Phi. \tag{5.60}$$

Using Eq. (5.59) this may be written

$$k_{eff} \approx \left(\frac{1}{k_r} - 1\right) k_\Phi = (1 - k_r)\, k_a \qquad \text{for} \qquad k_{mA} << k_a - k_\Phi. \tag{5.61}$$

Eq. (5.61) provides some valuable information. It states that for zero acoustic load and for a fixed stiffness ratio k_r the effective stiffness of the loudspeaker is proportional to k_Φ which is proportional to B_r^2. Thus, increasing the force factor by using a magnetic material with higher remanence (see Eq. (5.35)) also has the unwanted indirect effect of increasing the effective stiffness. The effect is indirect in the sense that the effective stiffness is increased due to the fact that the armature stiffness has to be increased to ensure stability when the magnetic stiffness compensation increases.

5.4 Relationships Between Loudspeaker Parameters

This section provides a number of useful relationships between various loudspeaker parameters. The motivation for deriving some of these relationships might not be entirely clear to the reader at present but they will become useful in later chapters.

The nonlinear transduction coefficient from the mechanical domain to the electrical domain is the same as the one from the electrical domain to the mechanical domain so the common notation for the transduction coefficient is introduced:

$$\boxed{T\left(x\right)=T_{em}\left(x\right)=T_{me}\left(x\right)=2B_{r}N\frac{A}{D}\frac{\alpha\left[\left(\alpha+1\right)^{2}+\left(\frac{x}{D}\right)^{2}\right]}{\left[\left(\alpha+1\right)^{2}-\left(\frac{x}{D}\right)^{2}\right]^{2}}}. \tag{5.62}$$

The same notation can be used for small signals:

$$\boxed{T=T_{em}=T_{me}=2B_{r}N\frac{A}{D}\frac{\alpha}{\left(\alpha+1\right)^{2}}} \quad \text{, for } x<<D. \tag{5.63}$$

There is also a simple relationship between the distortion transduction coefficients between the two domains. Looking at Equations (5.37) and (5.53) it may be noticed that

$$\boxed{T_{em,d}\left(x,i\right)=2T_{me,d}\left(x,i\right)=4\mu_{0}N^{2}\frac{xi}{D^{2}}\frac{A}{D}\frac{\alpha+1}{\left[\left(\alpha+1\right)^{2}-\left(\frac{x}{D}\right)^{2}\right]^{2}}}. \tag{5.64}$$

The derivative of the inductance with respect to displacement is

$$\frac{dL\left(x\right)}{dx}=4\mu_{0}N^{2}\frac{A}{D^{3}}\frac{\alpha+1}{\left[\left(\alpha+1\right)^{2}-\left(\frac{x}{D}\right)^{2}\right]^{2}}x \tag{5.65}$$

and this is related to the distortion transduction coefficient:

$$\boxed{T_{em,d}\left(x,i\right)=\frac{dL\left(x\right)}{dx}i}. \tag{5.66}$$

For the small-signal parameters it turns out that

$$\frac{T}{L}=\frac{k_{\Phi}}{T}=\frac{B_{r}}{\mu_{0}N}\frac{\alpha}{\alpha+1}. \tag{5.67}$$

From this it follows that

$$\frac{k_{\Phi}}{L}=\left(\frac{B_{r}}{\mu_{0}N}\right)^{2}\left(\frac{\alpha}{\alpha+1}\right)^{2} \tag{5.68}$$

and more importantly

$$\boxed{T^2 = k_\Phi L}. \tag{5.69}$$

Eq. (5.69) expresses a very elegant relationship between the three major small-signal parameters of the balanced-armature loudspeaker. Equation (5.69) reveals that in order to increase the transduction coefficient, an increase in either the magnetic stiffness compensation or in the electrical inductance has to be accepted.

5.5 Small-Signal Parameters versus α

In this section it will be investigated how the various small-signal parameters behave as function of the ratio between the equivalent air gap length of the permanent magnet and the length of the air gap (i.e. $\alpha = D_M/D$) for a fixed air gap length D. The results from this analysis can guide the choice of the magnet length ($l_M = \mu_r \alpha D$) when a desired maximum armature displacement D has been specified. Recall that the small-signal parameters were written

$$k_\Phi = \frac{2B_r^2}{\mu_0}\frac{A}{D}\frac{\alpha^2}{(\alpha+1)^3} \tag{5.31}$$

$$T = 2B_r N \frac{A}{D}\frac{\alpha}{(\alpha+1)^2} \tag{5.35}$$

$$L = 2\mu_0 N^2 \frac{A}{D}\frac{1}{\alpha+1} \tag{5.48}$$

$$T_{me,d}\,(x,i)|_{x<<D} = 2\mu_0 N^2 \frac{xi}{D^2}\frac{A}{D}\frac{1}{(\alpha+1)^3} \tag{5.38}$$

The normalized small-signal parameters (the rightmost factors that only depend on α) are plotted together in Fig. 5.3.

5.6 The Armature

The armature of the balanced-armature loudspeaker can be considered as a beam with one end fixed and the other one free to vibrate i.e. a cantilever beam. This is a well-described structure and the bending-wave equations will not be presented here. Instead, the important features of such a cantilever beam will be presented. If the magnetic force is considered as a point force attacking the tip of the armature, the stiffness of the armature can be written:

$$k_a = \frac{3EI_a}{l_a^3} = \frac{E}{4}\left(\frac{h_a}{l_a}\right)^3 w_a, \tag{5.70}$$

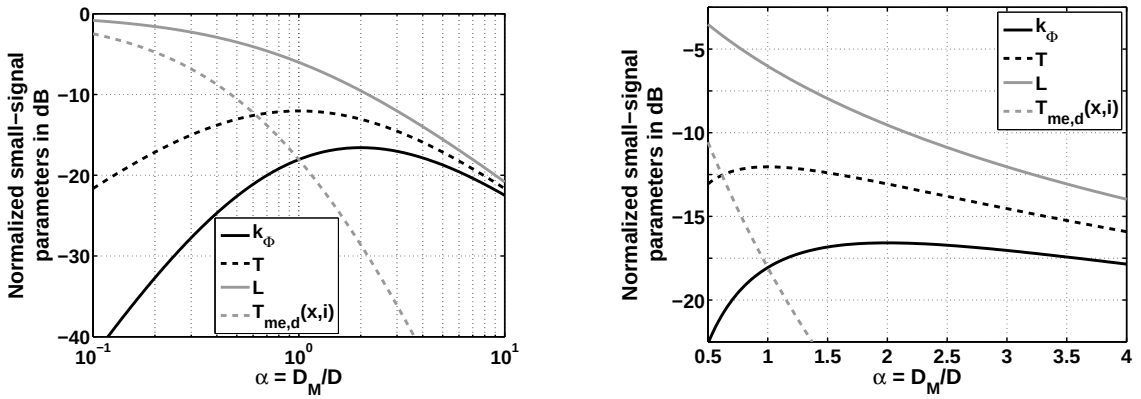

(a) Overview (logarithmic abscissa).

(b) Close-up of the most relevant α-range (linear abscissa).

Figure 5.3: Normalized small-signal parameters vs $\alpha = D_M/D$.

where E is Young's modulus (or modulus of elasticity), l_a is the length, h_a is the height (or thickness) and w_a is the width of the armature. I_a is the area moment of inertia which is

$$I_a = \frac{w_a h_a^3}{12} \tag{5.71}$$

for a simple armature geometry with constant width and height. Considering the fundamental resonance frequency of such a cantilever it is possible to extract an equivalent lumped mass that, together with the stiffness in Eq. (5.70), yields a lumped mass-spring system with the same resonance frequency as the first resonance frequency of the beam. This equivalent mass is given as

$$m_{eq} = \frac{33}{140} m_a = \frac{33}{140} \rho_a V_a = \frac{33}{140} \rho_a h_a w_a l_a, \tag{5.72}$$

where m_a is the resting mass of the armature, V_a is the armature volume and ρ_a is the armature mass density. From the definition of m_{eq} it follows that the first resonance frequency is

$$f_{n1} = \frac{1}{2\pi} \sqrt{\frac{k_a}{m_{eq}}}. \tag{5.73}$$

Finally, substituting Equations (5.70) and (5.72) into Eq. (5.73) yields the first fundamental frequency of resonance:

$$\boxed{f_{n1} = \frac{1}{2\pi} \sqrt{\frac{35}{33} \frac{E}{\rho_a}} \frac{h_a}{l_a^2}}. \tag{5.74}$$

5.7 Coil Design

In this section the properties of the coil will be studied. There is essentially two different ways to design a coil for a balanced-armature loudspeaker. One coil has the traditional circular shape and the other one is square with rounded corners. The two different types are depicted in Fig. 5.4 with the tip of the armature shown in the middle.

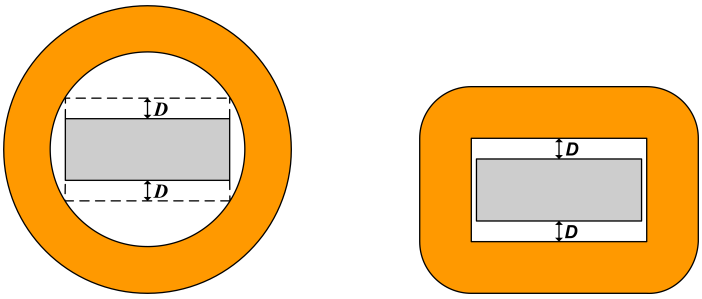

(a) Circular coil. (b) Square Coil.

Figure 5.4: Two different approaches to coil design.

The thickness of the armature and the height of the maximum armature displacement D appear exactly the same in the two figures so that it is easier to judge the amount of "wasted" space for the circular design. In section 11.1, it will become clear that the loudspeaker efficiency, in terms of the Constant Input Power response, is proportional to the ratio $N/\sqrt{R_L}$ between the number of windings N and the square root of the DC coil resistance R_L. This ratio will be referred to as the coil performance. Looking at Fig 5.4, it would seem as though - for a fixed amount of windings and wire thickness - that the length of the wire for the circular coil might be longer than that of the square coil. This implies that the electrical resistance R_L will be larger for the circular coil and that such a design would be less efficient compared to the square coil. It is important to increase the ratio $N/\sqrt{R_L}$ while maintaining a small coil volume as any volume taken up by the coil will reduce the available acoustic back volume and this will have a detrimental effect on the loudspeaker low-frequency efficiency. In the following sections, the two coil designs will be investigated and compared in details. In this section, the terms N_s and $R_{L,s}$ are introduced for the number of coil windings and DC-resistance for the square coil. Likewise, N_c and $R_{L,c}$ are used for the circular coil. Outside this section it will be understood which coil is used and the general notation N and R_L is used.

5.7.1 Circular Coil

In this section the circular coil will be investigated. The situation is depicted in Fig. 5.5.

The inner coil radius is denoted $R_{c,i}$ and the outer $R_{c,o}$. The length of the coil (along the armature) is denoted l_c and the total length of the wire l_w. The diameter of the wire is D_w. The amount of space between adjacent turns will depend on how neatly the coil is wound. If the wire is wound

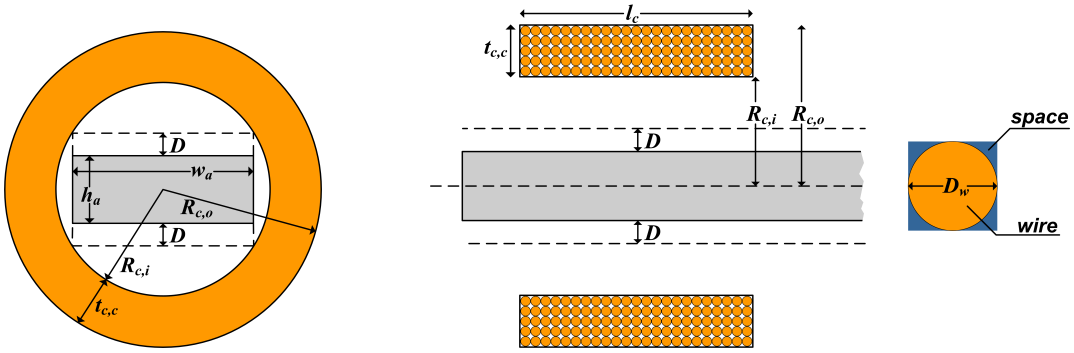

(a) Front view looking into the tip of the armature.

(b) Side view showing the cross section of the coil.

Figure 5.5: Two different approaches to coil design.

neatly so that each strand effectively occupies a total cross-sectional area of D_w^2 then the ratio between the total effective occupied area A_c and the actual total cross-sectional area A_w of the wire is given as

$$\frac{A_w}{A_c} \equiv F_f = \frac{\pi \left(\frac{D_w}{2}\right)^2}{D_w^2} = \frac{\pi}{4} \approx 0.79 \tag{5.75}$$

assuming that the coil is wound homogeneously throughout its entire volume. This ratio is often known as the filling (or fill) factor F_f. The total volume occupied by the circular coil is

$$V_{c,c} = \pi R_{c,o}^2 l_c - \pi R_{c,i}^2 l_c = \pi \left(R_{c,o}^2 - R_{c,i}^2\right) l_c \Leftrightarrow \tag{5.76}$$

$$\boxed{V_{c,c} = \pi l_c t_{c,c} \left(t_{c,c} + 2R_{c,i}\right)}, \tag{5.77}$$

where $t_{c,c}$ is simply the thickness of the coil as shown in Fig. 5.5(a). The volume of the coil windings can then easily be found using the fill factor

$$V_w = F_f V_{c,c} = F_f \pi l_c t_{c,c} \left(t_{c,c} + 2R_{c,i}\right). \tag{5.78}$$

From the total wire volume the length of the wire can be found

$$l_w = \frac{V_w}{A_w} = \frac{F_f \pi l_c t_{c,c} \left(t_{c,c} + 2R_{c,i}\right)}{\pi \left(\frac{D_w}{2}\right)^2} = \frac{4F_f l_c t_{c,c} \left(t_{c,c} + 2R_{c,i}\right)}{D_w^2} \tag{5.79}$$

The DC-resistance R_L of the circular coil is the same as that of a wire with length l_w and cross sectional area A_w:

$$R_{L,c} = \rho_w \frac{l_w}{A_w} = \rho_w \frac{4F_f l_c t_{c,c} \left(t_{c,c} + 2R_{c,i}\right)}{D_w^2} \frac{1}{\pi \left(\frac{D_w}{2}\right)^2} \Leftrightarrow \tag{5.80}$$

$$\boxed{R_{L,c} = \frac{16\rho_w}{\pi} \frac{F_f l_c t_{c,c} \left(t_{c,c} + 2R_{c,i}\right)}{D_w^4}} \tag{5.81}$$

where ρ_w is the electrical resistivity of the wire material. Now that expressions for the coil resistance and the coil volume are derived only the number of coil windings needs to be included. Looking at Fig. 5.5(b) it is clear that the coil length l_c and height $t_{c,c}$ are related to the number of windings, the diameter of the wire and the filling factor:

$$N_c = \frac{F_f l_c t_{c,c}}{\pi \left(\frac{D_w}{2}\right)^2} = \frac{4}{\pi} \frac{F_f l_c t_{c,c}}{D_w^2} \tag{5.82}$$

It is also interesting to establish a relationship between the electrical resistance and the number of coil windings:

$$\frac{R_{L,c}}{N_c} = 4\rho_w \frac{\left(t_{c,c} + 2R_{c,i}\right)}{D_w^2}. \tag{5.83}$$

As already mentioned, it will be shown that the Constant Input Power response is proportional to $N/\sqrt{R_L}$ so this is derived:

$$\boxed{\frac{N_c}{\sqrt{R_{L,c}}} = \sqrt{\frac{F_f l_c}{\pi \rho_w}} \sqrt{\frac{1}{1 + \frac{2R_{c,i}}{t_{c,c}}}}}. \tag{5.84}$$

This can also be written in terms of the coil volume $V_{c,c}$:

$$\boxed{\frac{N_c}{\sqrt{R_{L,c}}} = \sqrt{\frac{F_f}{\rho_w}} \frac{1}{\pi \left(t_{c,c} + 2R_{c,i}\right)} \sqrt{V_{c,c}}}. \tag{5.85}$$

5.7.2 Square Coil

The situation is depicted in Fig. 5.6.

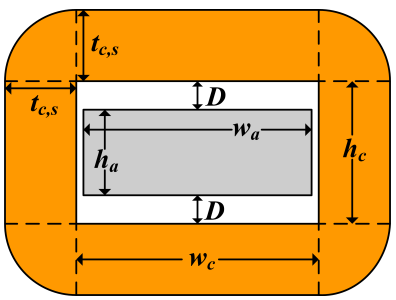

Figure 5.6: Front view looking into the tip of the armature.

The volume of the straight part of the coil is

$$V_s = 2t_{c,s}w_c l_c + 2t_{c,s}h_c l_c = l_c t_{c,s} P_{c,s}. \tag{5.86}$$

where $P_{c,s} = 2\left(w_c + h_c\right)$ is the inner perimeter of the square coil. The four corners of the coil can be viewed as a single circular coil with inner radius zero. Using the results from the previous section (Eq. (5.77)) and inserting $R_{c,i} = 0$ the total volume of the 4 corners is:

$$V_{c,c} = \pi l_c t_{c,s}^2, \tag{5.87}$$

and the total coil volume of the square coil is

$$V_{c,s} = V_s + V_{c,c} = l_c t_{c,s} P_{c,s} + \pi l_c t_{c,s}^2 \Leftrightarrow \tag{5.88}$$

$$\boxed{V_{c,s} = l_c t_{c,s}\left[P_{c,s} + \pi t_{c,s}\right]}. \tag{5.89}$$

The volume of the coil wire is

$$V_w = F_f V_c = F_f l_c t_{c,s}\left[P_{c,s} + \pi t_{c,s}\right]. \tag{5.90}$$

The length of the wire is found by dividing by the cross sectional area of the wire:

$$l_w = \frac{V_w}{A_w} = \frac{F_f l_c t_{c,s}\left[P_{c,s} + \pi t_{c,s}\right]}{\pi\left(\frac{D_w}{2}\right)^2} = \frac{4F_f l_c t_{c,s}}{\pi D_w^2}\left[P_{c,s} + \pi t_{c,s}\right]. \tag{5.91}$$

The electrical DC resistance of the square coil becomes

$$R_{L,s} = \frac{\rho_w l_w}{A_w} = \frac{\frac{4\rho_w F_f l_c t_{c,s}}{\pi D_w^2}\left[P_{c,s} + \pi t_{c,s}\right]}{\pi\left(\frac{D_w}{2}\right)^2} \Leftrightarrow \tag{5.92}$$

$$\boxed{R_{L,s} = \left(\frac{4}{\pi D_w^2}\right)^2 \rho_w F_f l_c t_{c,s}\left[P_{c,s} + \pi t_{c,s}\right]}. \tag{5.93}$$

Quite often the available coil dimensions will be given and there will be a certain desired DC-resistance of the coil. In that case the diameter of the wire should be determined by isolating D_w in Eq. 5.93:

$$D_w = \sqrt[4]{\left(\frac{4}{\pi}\right)^2 \frac{\rho_w F_f l_c t_{c,s}}{R_{L,s}}\left[P_{c,s} + \pi t_{c,s}\right]}. \tag{5.94}$$

The number of windings on the square coil is

$$N_s = \frac{F_f l_c t_{c,s}}{\pi \left(\frac{D_w}{2}\right)^2} = \frac{4F_f l_c t_{c,s}}{\pi D_w^2}. \tag{5.95}$$

The ratio between the number of windings and the coil resistance is

$$\frac{R_{L,s}}{N_s} = \frac{4\rho_w}{\pi D_w^2} \left[P_{c,s} + \pi t_{c,s}\right]. \tag{5.96}$$

It will turn out that the low-frequency CIP response is proportional to the ratio $N/\sqrt{R_L}$ so this is also evaluated for the square coil:

$$\boxed{\frac{N_s}{\sqrt{R_{L,s}}} = \sqrt{\frac{F_f l_c}{\pi \rho_w}} \sqrt{\frac{1}{1 + \frac{P_{c,s}}{\pi t_{c,s}}}} = \sqrt{\frac{F_f l_c}{\pi \rho_w}} \sqrt{\frac{1}{1 + \frac{2(w_c + h_c)}{\pi t_{c,s}}}}}. \tag{5.97}$$

This can be written in terms of the coil volume:

$$\boxed{\frac{N_s}{\sqrt{R_{L,s}}} = \sqrt{\frac{F_f}{\rho_w}} \frac{1}{2\left(w_c + h_c\right) + \pi t_{c,s}} \sqrt{V_{c,s}} = \sqrt{\frac{F_f}{\rho_w}} \frac{1}{P_{c,s} + \pi t_{c,s}} \sqrt{V_{c,s}}}. \tag{5.98}$$

5.7.3 Square Coil versus Circular Coil

For any coil design to be useful, the coil has to fit around the armature. The length of the coil is physically constrained by the armature length and the size of the magnets housing. The inner dimensions of the coil - $R_{c,i}$ for the circular coil and w_c and h_c for the square coil - are constrained by the width and the height of the armature as well as the maximum armature displacement D. The outer dimensions of the coil are constrained by the outer dimensions of the loudspeaker and the desired back volume size.

In order to compare the performance of two different coil designs it makes sense to equate the ratios $N/\sqrt{R_L}$ and then derive the ratio between the volumes of the circular coil and the square coil for a given armature geometry. The best coil design will be the one where the coil volume is smallest as this will increase the available back volume and thus the efficiency of the loudspeaker and potentially reduce the price of the coil.

$$\frac{N_c}{\sqrt{R_{L,c}}} = \frac{N_s}{\sqrt{R_{L,s}}} \Leftrightarrow \sqrt{\frac{F_f l_c}{\pi \rho_w}} \sqrt{\frac{1}{1 + \frac{2R_{c,i}}{t_{c,c}}}} = \sqrt{\frac{F_f l_c}{\pi \rho_w}} \sqrt{\frac{1}{1 + \frac{P_{c,s}}{\pi t_{c,s}}}}. \tag{5.99}$$

To make a fair comparison the electrical resistivity of the material for the two coils should be the same and the filling factor and the coil lengths should also be the same. This means that:

$$\sqrt{\frac{1}{1+\frac{2R_{c,i}}{t_{c,c}}}} = \sqrt{\frac{1}{1+\frac{P_{c,s}}{\pi t_{c,s}}}} \Leftrightarrow \frac{2R_{c,i}}{t_{c,c}} = \frac{P_{c,s}}{\pi t_{c,s}} \Leftrightarrow \tag{5.100}$$

$$t_{c,s} = \frac{P_{c,s}}{2\pi R_{c,i}} t_{c,c} \Leftrightarrow \frac{t_{c,c}}{t_{c,s}} = \frac{P_{c,c}}{P_{c,s}} \tag{5.101}$$

where $P_{c,c} = 2\pi R_{c,i}$ is the inner perimeter of the circular coil. Eq. (5.101) states the relationship between the thicknesses of the square coil and the circular coil if they are to have the same performance $N/\sqrt{R_L}$. The ratio between the volumes of the two coils with the same performance can be found using Equations (5.77) and (5.89) and substituting Eq. (5.101) into Eq. (5.89):

$$\frac{V_{c,c}}{V_{c,s}} = \frac{\pi l_c t_{c,c} \left(t_{c,c} + 2R_{c,i}\right)}{\frac{w_c+h_c}{\pi R_{c,i}} t_{c,c} l_c \left[2\left(w_c + h_c\right) + \pi \frac{w_c+h_c}{\pi R_{c,i}} t_{c,c}\right]} = \left(\frac{2\pi R_{c,i}}{2\left(w_c + h_c\right)}\right)^2. \tag{5.102}$$

The rightmost expression of Eq. (5.102) may be identified as the squared ratio between the inner perimeters of the circular and the square coil:

$$\frac{V_{c,c}}{V_{c,s}} = \left(\frac{P_{c,c}}{P_{c,s}}\right)^2 = \left(\frac{t_{c,c}}{t_{c,s}}\right)^2 = \left(\frac{2\pi R_{c,i}}{2\left(w_c + h_c\right)}\right)^2. \tag{5.103}$$

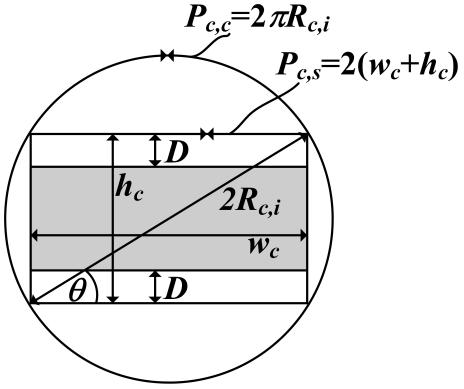

Figure 5.7: Circle representing the inner perimeter of a circular coil with a rectangle inside representing the inner perimeter of a square coil for a given armature cross sectional area and air gap height.

$P_{c,c}$ is the inner perimeter of the circular coil with radius $R_{c,i}$ and $P_{c,s}$ is the inner perimeter of the square coil with width w_c and height h_c. The inner width and height of the square coil can be written in terms of the angle θ:

$$w_c = 2R_{c,i}\cos\left(\theta\right) \tag{5.104}$$

$$h_c = 2R_{c,i}\sin\left(\theta\right) \tag{5.105}$$

and the perimeter of the square coil can then be written

$$P_{c,s} = 2\left[2R_{c,i}\cos\left(\theta\right) + 2R_{c,i}\sin\left(\theta\right)\right] = 4R_{c,i}\left[\cos\left(\theta\right) + \sin\left(\theta\right)\right]. \tag{5.106}$$

The ratio between the two perimeters can then be written

$$\frac{P_{c,c}}{P_{c,s}} = \frac{2\pi R_{c,i}}{4R_{c,i}\left[\cos\left(\theta\right) + \sin\left(\theta\right)\right]} = \frac{\pi}{2\left[\cos\left(\theta\right) + \sin\left(\theta\right)\right]} \tag{5.107}$$

and the ratio between the coil volumes with the same performance $N/\sqrt{R_L}$ becomes

$$\boxed{\frac{V_{c,c}}{V_{c,s}} = \left(\frac{P_{c,c}}{P_{c,s}}\right)^2 = \left(\frac{\pi}{2\left[\cos\left(\theta\right) + \sin\left(\theta\right)\right]}\right)^2}. \tag{5.108}$$

Eq. (5.108) is plotted in Fig. 5.8.

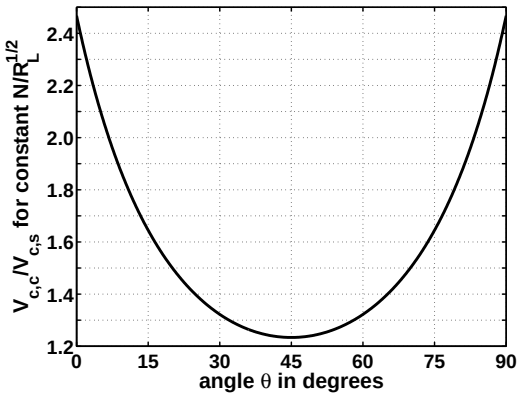

Figure 5.8: Ratio between the volume of the circular coil $V_{c,c}$ and the square coil $V_{c,s}$ for constant coil performance $N/\sqrt{R_L}$. The angle θ is defined in Fig. 5.7.

Thus, Fig. 5.8 shows how much larger the volume of the circular coil will be relative to that of the square coil for the same coil performance $N/\sqrt{R_L}$ but for different armature and air gap geometries expressed in terms of θ. The circular coil has the best performance relative to the square coil for $\theta = 45^\circ$ corresponding to the case where the cross-sectional area - constituted by the armature and air gaps - is square. For this case the volume of the circular coil will be

$$\left.\frac{V_{c,c}}{V_{c,s}}\right|_{\theta=45^\circ} = \left(\frac{\pi}{2\left[\cos\left(45^\circ\right) + \sin\left(45^\circ\right)\right]}\right)^2 = \frac{\pi^2}{8} \approx 1.23 \tag{5.109}$$

times greater than the volume of the square coil with the same performance $N/\sqrt{R_L}$. The circular coil has the worst performance relative to the square coil for θ approaching 0° corresponding to

the case where the armature is extremely wide and not very thick. For this case the volume of the circular coil will be

$$\left.\frac{V_{c,c}}{V_{c,s}}\right|_{\theta=0^\circ} = \left(\frac{\pi}{2\left[\cos\left(0^\circ\right)+\sin\left(0^\circ\right)\right]}\right)^2 = \left(\frac{\pi}{2}\right)^2 \approx 2.47 \tag{5.110}$$

times greater than the volume of the square coil with the same performance $N/\sqrt{R_L}$. From Equations (5.109), (5.110) and Fig. 5.8 it can be concluded that the circular coil will take up between 1.23 and 2.47 as much volume as the square coil for a given performance $N/\sqrt{R_L}$. Thus, by designing a square coil the saved space can be used as additional acoustic back volume which will reduce the effective stiffness and hence increase the efficiency of the loudspeaker. In the analysis in the following sections it will be assumed that a square coil is used. The coil dimensions and the armature dimensions are coupled in the sense that the inner coil dimensions should always be as close to the armature as possible while also accommodating the movement of the armature. It will prove useful to derive the coil performance $N/\sqrt{R_L}$ in terms of the armature geometry, assuming that the armature is shaped like a simple beam with constant height and width along the long direction. For the sake of the analysis it is assumed that the coil is only exactly large enough for the armature to fit for a maximum displacement of D. The dimensions of the square coil can then be written:

$$w_c = w_a \tag{5.111}$$

$$h_c = h_a + 2D \tag{5.112}$$

The coil length l_c is constrained by the length of the armature and the size of the magnets housing. It is reasonable to assume that the coil length can be written as a certain "coil length factor" $F_{cl} < 1$ times the armature length:

$$l_c = F_{cl} l_a \tag{5.113}$$

Substituting Equations (5.111) to (5.113) into Eq. (5.97) yields

$$\frac{N_s}{\sqrt{R_{L,s}}} = \sqrt{\frac{F_f F_{cl} l_a}{\pi \rho_w}} \sqrt{\frac{1}{1+\frac{2(w_a+h_a+2D)}{\pi t_{c,s}}}}. \tag{5.114}$$

Likewise, the volume of the coil can be written in terms of the armature geometry by substituting Equations (5.111) to (5.113) into Eq. (5.89):

$$V_{c,s} = F_{cl} l_a t_{c,s} \left[2\left(w_a + h_a + 2D\right) + \pi t_{c,s}\right]. \tag{5.115}$$

Some of the results presented in this section will be investigated more thoroughly in Chapter 11 where the efficiency of the balanced-armature loudspeaker is studied in greater detail.

5.8 Electrical Cut-off Frequency

The electrical cut-off frequency is defined as the frequency where the electrical current is down by 3 dB or $1/\sqrt{2}$ due to the inductance of the coil. This frequency is determined by the ratio between the electrical DC resistance and the coil inductance:

$$\boxed{\omega_{e,cut} = 2\pi f_{e,cut} \equiv \frac{R_L}{L}}. \tag{5.116}$$

Notice that the back-EMF does not influence the electrical cut-off frequency i.e. the mechanical and the acoustic domain are disregarded. The electrical $R-L$-series-circuit works as a 1$^{\text{st}}$ order low-pass filter with respect to the current. At the cut-off frequency $\omega_{e,cut}$ the amplitude of the current is reduced by 3 dB or $1/\sqrt{2}$. This cut-off frequency will greatly affect the voltage-driven pressure response of the loudspeaker and a large cut-off frequency close to the desired upper frequency range of the driver is usually preferred if the loudspeaker response is not somehow equalized. The problem is that the loudspeaker efficiency tends to go down with increasing cut-off frequency. In chapter 11 it will be shown that the efficiency is inversely proportional to $\sqrt{\omega_{e,cut}}$. This means that there is good reason - in terms of loudspeaker efficiency - not to design towards a large cut-off frequency but rather towards a low cut-off frequency.

Substituting the equations for the resistance of the square coil and the small-signal inductance (Equations (5.48) and (5.93)) into Eq. (5.116) yields

$$\omega_{e,cut} = \left(\frac{4}{\pi D_w^2}\right)^2 \rho_w F_f l_c t_c \left[P_{c,s} + \pi t_c\right] \frac{1}{2\mu_0 N^2} \frac{D}{A} \left(\alpha + 1\right). \tag{5.117}$$

Equation (5.95) may be used to express the number of coil windings N entirely in terms of the coil geometry and wire thickness. This yields

$$\boxed{\omega_{e,cut} = \frac{\rho_w}{F_f l_c t_c} \left[P_{c,s} + \pi t_c\right] \frac{1}{2\mu_0} \frac{D}{A} \left(\alpha + 1\right)}. \tag{5.118}$$

The cut-off frequency is inversely proportional to the length of the coil l_c. This is due to the fact that the electrical resistance is proportional to the coil length whereas the inductance is proportional to the squared coil length. One may also observe that the cut-off frequency becomes independent of the coil thickness when the thickness of the coil t_c becomes larger than the inner perimeter $P_{c,s}$ of the coil.

Chapter 6

Modeling the Balanced-Armature Loudspeaker

6.1 Electrical Domain

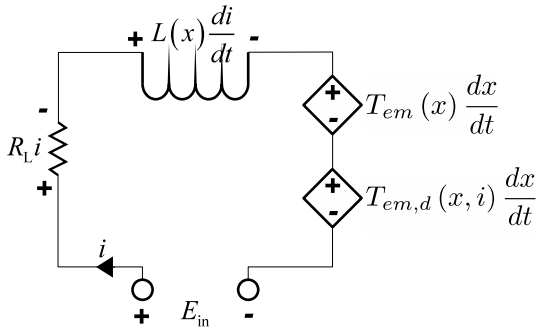

Figure 6.1: Electrical circuit of the B-A loudspeaker.

First let us consider the electrical part of the balanced-armature loudspeaker. Referring to Eq. (5.42) and by inspection of Fig. 6.1 the differential equation for the electrical circuit can be written down:

$$E_{\text{in}} = R_L i + U_{\text{back}} = R_L i + L(x)\frac{di}{dt} + T_{em}(x)\frac{dx}{dt} + T_{em,d}(x,i)\frac{dx}{dt}, \tag{6.1}$$

where E_{in} is the voltage that drives the loudspeaker and R_L is the DC-resistance of the coil. Using

$$\boxed{\frac{dx}{dt} = u}, \tag{6.2}$$

Eq. (6.1) can be rearranged into:

$$\boxed{\frac{di}{dt} = \frac{-R_L}{L(x)}i - \frac{T_{em}(x) + T_{em,d}(x,i)}{L(x)}u + \frac{E_{\text{in}}}{L(x)}}. \tag{6.3}$$

6.2 Mechanical Domain

In this section the mechanical part of the loudspeaker will be considered. This part is modeled as a linear mass-spring-damper system where the input force is given according to Eq. (5.24) or (5.25).

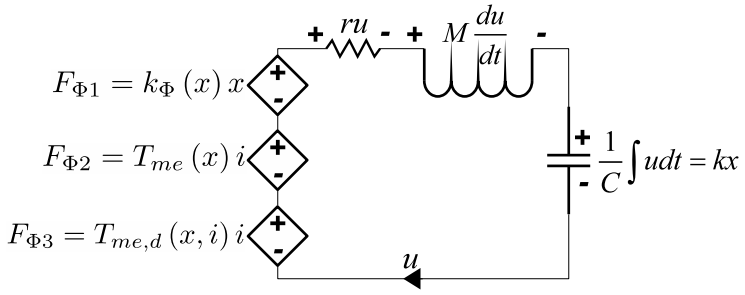

Figure 6.2: Mechanical circuit of the B-A loudspeaker.

Referring to Eq. (5.25) and by inspection of Fig. 6.2 the differential equation for the mechanical circuit can be written as

$$\mathcal{F}_\Phi(x,i) = k_\Phi(x)\,x + T_{me}(x)\,i + T_{me,d}(x,i)\,i = M\frac{du}{dt} + ru + k_a x. \tag{6.4}$$

M is the mechanical moving mass representing the armature and any other relevant contributions, k_a is the mechanical stiffness of the armature, suspension and perhaps the back volume and r is the mechanical loss factor. The mass-spring-damper system is in fact modeling a beam so a bit of explanation is necessary: k_a is the mechanical stiffness that relates the displacement of the beam tip to a point force attacking the beam at the tip. M is the mass where

$$f_{n1} = \frac{1}{2\pi}\sqrt{\frac{k_a}{M}}, \tag{6.5}$$

where f_{n1} is the first mode (or fundamental resonance frequency) of the beam. r is thus the mechanical loss factor which is related to the movement of the tip of the beam. Rearranging Eq. (6.4) yields

$$\boxed{\frac{du}{dt} = \frac{k_\Phi(x) - k_a}{M}x + \frac{T_{me}(x) + T_{me,d}(x,i)}{M}i - \frac{r}{M}u}. \tag{6.6}$$

6.3 State Space Representation

Equations (6.2), (6.3) and (6.6) compose a set of coupled first order differential equations that can be written in state space form:

$$\begin{bmatrix} \dot{i} \\ \dot{x} \\ \dot{u} \end{bmatrix} = \begin{bmatrix} \frac{-R_L}{L(x)} & 0 & -\frac{T_{em}(x)+T_{em,d}(x,i)}{L(x)} \\ 0 & 0 & 1 \\ \frac{T_{me}(x)+T_{me,d}(x,i)}{M} & \frac{k_\Phi(x)-k_a}{M} & -\frac{r}{M} \end{bmatrix} \begin{bmatrix} i \\ x \\ u \end{bmatrix} + \begin{bmatrix} \frac{1}{L(x)} \\ 0 \\ 0 \end{bmatrix} E_{\text{in}}. \tag{6.7}$$

This time domain representation of the loudspeaker may be discretized to run on a computer using e.g. the classic fourth-order Runge-Kutta method where the nonlinear parameters should be updated with the current armature displacement at each time step.

6.4 Linear Frequency Domain Model

For small signals (and even for larger signals) it makes a lot of sense to analyze the loudspeaker in the frequency domain. A frequency domain model (or frequency response) is very fast to generate if the transfer function of the loudspeaker is given. The alternative is to run the time-domain model with an input signal which is an impulse and then take the fft of the impulse response. The latter method is much slower due to the very small sampling time necessary to get reasonably exact results. For small signals the equivalent circuits for the electrical and the mechanical part of the balanced-armature loudspeaker are shown in Fig. 6.3

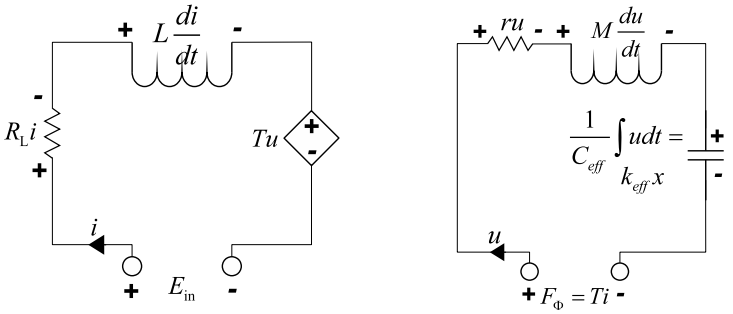

(a) Electrical circuit. (b) Mechanical circuit.

Figure 6.3: Equivalent circuits for the electrical- and the mechanical part of the linearized balanced-armature loudspeaker model.

For small signals and only considering the fundamental frequency Eq. (6.1) is written

$$E_{\text{in}} = R_L i + L\frac{di}{dt} + T\frac{dx}{dt}. \tag{6.8}$$

Transforming Eq. (6.8) into the frequency domain and using $dx/dt = u$ yields

$$E_{\text{in}}(\omega) = R_L i(\omega) + Lj\omega i(\omega) + Tu(\omega) = (R_L + Lj\omega)\, i(\omega) + Tu(\omega). \tag{6.9}$$

The linearized differential equation for the mechanical system (Eq. (6.4)) can be written

$$\mathcal{F}_\Phi(i) = Ti = M\frac{du}{dt} + ru + k_{eff}x, \tag{6.10}$$

where the magnetic input force ($k_\Phi x$) has been incorporated into the effective stiffness together with the mechanical armature stiffness, the stiffness of the back volume and the stiffness of the diaphragm suspension. Transforming Eq. (6.10) into the frequency domain and using the fact that the displacement x corresponds to the integral of the velocity u and that $C_{eff} = 1/k_{eff}$ yields

$$Ti(\omega) = Z_m(j\omega)\,u(\omega) = \left(Mj\omega + r + \frac{1}{C_{eff}j\omega}\right)u(\omega) \Leftrightarrow \tag{6.11}$$

$$i(\omega) = \frac{Z_m(j\omega)}{T}u(\omega) = \frac{1}{T}\left(Mj\omega + r + \frac{1}{C_{eff}j\omega}\right)u(\omega), \tag{6.12}$$

where the mechanical impedance is

$$Z_m(j\omega) = \frac{F_\Phi(\omega)}{u(\omega)} = Mj\omega + r + \frac{1}{C_{eff}j\omega}. \tag{6.13}$$

It is also of interest to derive the frequency response between the input current and the armature velocity which is relevant if the loudspeaker if current-driven. Rewriting Eq. (6.12) yields

$$\boxed{H_u(j\omega)|_{\text{const. } i} = \frac{u(\omega)}{i(\omega)} = \frac{T}{Z_m(j\omega)} = TY_m(j\omega) = \frac{Tj\omega}{-m\omega^2 + rj\omega + 1/C_{eff}}}, \tag{6.14}$$

where the mechanical mobility is

$$Y_m(j\omega) = \frac{1}{Z_m(j\omega)} = \frac{u(\omega)}{F_\Phi(\omega)} = \frac{j\omega}{-m\omega^2 + rj\omega + 1/C_{eff}}. \tag{6.15}$$

Substituting Eq. (6.12) into Eq. (6.9) yields

$$E_{\text{in}}(\omega) = (R_L + Lj\omega)\frac{Z_m(j\omega)}{T}u(\omega) + Tu(\omega) \Leftrightarrow \tag{6.16}$$

$$\boxed{H_u(j\omega) = \frac{u(\omega)}{E_{\text{in}}(\omega)} = \frac{T}{(R_L + Lj\omega)\,Z_m(j\omega) + T^2}}. \tag{6.17}$$

Substituting the mechanical impedance into Eq. (6.17) yields

$$\boxed{H_u(j\omega) = \frac{Tj\omega}{-LMj\omega^3 - (R_LM + Lr)\,\omega^2 + (R_Lr + L/C_{eff} + T^2)\,j\omega + R_L/C_{eff}}}. \tag{6.18}$$

Eq. (6.17) (or alternatively Eq. (6.18)) is then the frequency response for the armature velocity when the loudspeaker is voltage-driven. It is also of great interest to derive the linearized electrical input impedance. From Eq. (6.9) it follows that

$$Z_e = \frac{E_{\text{in}}(\omega)}{i(\omega)} = R_L + Lj\omega + T\frac{u(\omega)}{i(\omega)} \Leftrightarrow \tag{6.19}$$

$$\boxed{Z_e = R_L + Lj\omega + T^2 Y_m(j\omega) = R_L + Lj\omega + \frac{T^2 j\omega}{-m\omega^2 + rj\omega + 1/C_{eff}}} \tag{6.20}$$

using Eq. (6.14). Thus, using Eq. (6.18) and (6.20) it is possible to quickly simulate the electrical impedance or the armature velocity response assuming that the acoustic front load is zero and the acoustic back load acts as a pure compliance that can be incorporated into the effective stiffness.

Chapter 7

Loudspeaker Nonlinearity

In this chapter the nonlinear parameters that are inherent to the balanced-armature loudspeaker design will be discussed and the nonlinearity of small back volumes will also be discussed in some detail as this is relevant for miniature balanced-armature loudspeakers used in hearing aids. The nonlinearities discussed in this chapter are by no means the only distortion mechanisms present in the B-A loudspeaker. The nonlinear magnetic permeability and magnetic saturation are two other very important distortion mechanisms that are more difficult to deal with in the sense that the hysteresis curve of a magnetic material does not let itself describe in a simple manner. The magnetic hysteresis is discussed in Sec. 4.2.

Recall that all the nonlinear loudspeaker parameters can be written in as a product of terms of their respective small-signal parameters and a function that depends on α and the normalized displacement x/D:

$$k_\Phi(x) = k_\Phi \frac{(\alpha+1)^4}{\left[(\alpha+1)^2 - \left(\frac{x}{D}\right)^2\right]^2}. \tag{5.32}$$

$$T(x) = T \frac{(\alpha+1)^2\left[(\alpha+1)^2 + \left(\frac{x}{D}\right)^2\right]}{\left[(\alpha+1)^2 - \left(\frac{x}{D}\right)^2\right]^2}. \tag{5.36}$$

$$L(x) = L \frac{(\alpha+1)^2}{(\alpha+1)^2 - \left(\frac{x}{D}\right)^2}. \tag{5.49}$$

$$T_{me,d}(x,i) = T_{me,d}(x,i)|_{x<<D} \frac{(\alpha+1)^4}{\left[(\alpha+1)^2 - \left(\frac{x}{D}\right)^2\right]^2}. \tag{5.39}$$

Using these equations it is possible to investigate only the nonlinear part of the parameters that change with armature displacement. That is the rightmost factor of each of the four equations above. Recall that

$$\alpha = \frac{D_M}{D} = \frac{l_M}{\mu_r D}, \tag{5.15}$$

so that increasing α for a given air gap length will correspond to increasing the length of the permanent magnet or using a hard magnetic material with a lower recoil permeability. Fig. 7.1

shows how the nonlinear magnetic stiffness compensation and the nonlinear force factor vary with displacement. This figure immediately reveals that the nonlinearity of the magnetic stiffness compensation and the force factor decreases as the ratio $\alpha = D_M/D$ is increased. This corresponds to using a longer magnet for a given air gap height D. The total loudspeaker stiffness is the sum of the nonlinear stiffness compensation and the stiffness of the armature, diaphragm suspension and the back volume. The significance of the nonlinear stiffness compensation will depend on how much it influences the total stiffness. For instance, if the back volume of the loudspeaker is very small or if the armature is made very stiff the nonlinear stiffness compensation may become relatively unimportant. Furthermore, the nonlinear stiffness is only relevant in the frequency range where the mechanical impedance is dominated by stiffness i.e. below the mechanical resonance frequency. The force factor, on the other hand, influences the distortion in the entire frequency range as it is the product of the force factor and the coil current that equals the driving force of the mechanical system.

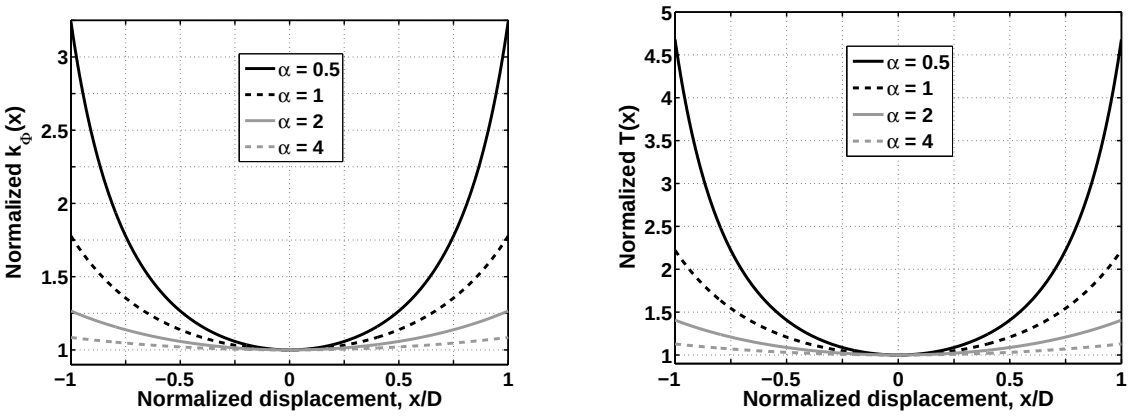

(a) $k_\Phi(x)$. (b) $T(x)$.

Figure 7.1: Normalized nonlinear parameters vs the normalized armature displacement x/D for different values of α.

Fig. 7.2 shows how the nonlinear electrical inductance and the distortion transduction coefficient vary with displacement. The nonlinearity of these parameters also decreases as the ratio $\alpha = D_M/D$ is increased. The nonlinear inductance is relevant above the frequency where the electrical impedance is not only dominated by the DC-resistance. This is above the electrical RL-cut frequency defined in Eq. (5.116). The distortion stiffness compensation is relevant in the entire frequency range (just like the nonlinear force factor) as this gives rise to an unwanted mechanical force induced by coil current and armature displacement. How significant this effect is depends on the ratio between the force factor and the distortion force factor and this is treated in more detail in Sec. 7.1.

7.1 The Ratio $T/T_{me,d}(x,i)$

Irrespective of the signal level the distortion force which is due to $T_{me,d}(x,i)\,i$ is an unwanted nonlinear effect. It has already been established that increasing α will reduce the nonlinearity of

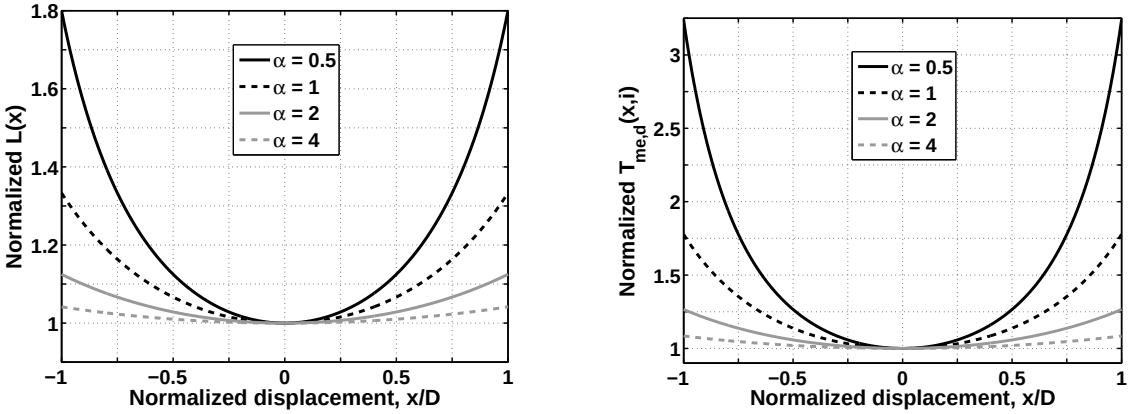

(a) $L(x)$. (b) $T_{me,d}(x)$.

Figure 7.2: Normalized nonlinear parameters vs the normalized armature displacement x/D for different values of α.

any of the loudspeaker parameters so the task is now to maximize the ratio between the force due to the small-signal force factor T and that due to the small-signal distortion force factor $T_{me,d}|_{x<<D}$. Thus, referring to Equations (5.35) and (5.38) the task is to maximize the ratio

$$T_r = \frac{Ti}{T_{me,d}(x,i)|_{x<<D}\, i} = \frac{2B_r N \frac{A}{D}\frac{\alpha}{(\alpha+1)^2}}{2\mu_0 N^2 \frac{A}{D}\frac{xi}{D^2}\frac{1}{(\alpha+1)^3}} \Leftrightarrow \tag{7.1}$$

$$\boxed{T_r = \frac{B_r}{\mu_0 N}\frac{D^2}{xi}\alpha(\alpha+1) = \frac{B_r}{\mu_0 N}\frac{D_M(D+D_M)}{xi}} \tag{7.2}$$

The armature input force which is due to the force factor is proportional to $B_r N i$ and looking at Eq. (7.2) one can conclude that most of this force should be due to $B_r i$ and not Ni. It was already demonstrated in Sec. 5.5 that $T_{me,d}|_{x<<D}$ decreases rapidly with an increase in α and this is also suggested by the squared α in the numerator of Eq. (7.2). The rightmost factor suggests that the current and the armature displacement should be as small as possible relative to the numerator $D_M(D+D_M)$. Note that it is not beneficial to increase α simply by reducing the air gap D: α should be increased by increasing the equivalent air gap length D_M of the magnet.

7.2 FEM Simulation of $k_\Phi(x)$

The COMSOL FEM simulation software was used to model the nonlinear magnetic stiffness compensation. This was done by simply shifting the armature away from its resting position by a distance x and using COMSOL to evaluate the force on the armature. The coil was omitted from the simulation setup. The simulation was run for many different magnet lengths in order to also extract the small-signal magnetic stiffness compensation as function of the magnet length or α. The geometry used for these FEM experiments is the same as the one used for the scale model discussed in Chapter 13 and shown in Fig. 13.3. The relative permeability of the soft magnetic material is set to 500.

Two of the simulation results for the magnetic force on the armature are shown in Fig. 7.3. As the armature approaches the permanent magnet the mesh used for the FEM simulation needs to be finer making the simulation task heavier. For this reason the simulations were only carried out up to about $x = 0.9D$ and the last part of the force curve is merely extrapolated using the odd powers of a 9$^{\text{th}}$ order polynomial fit.

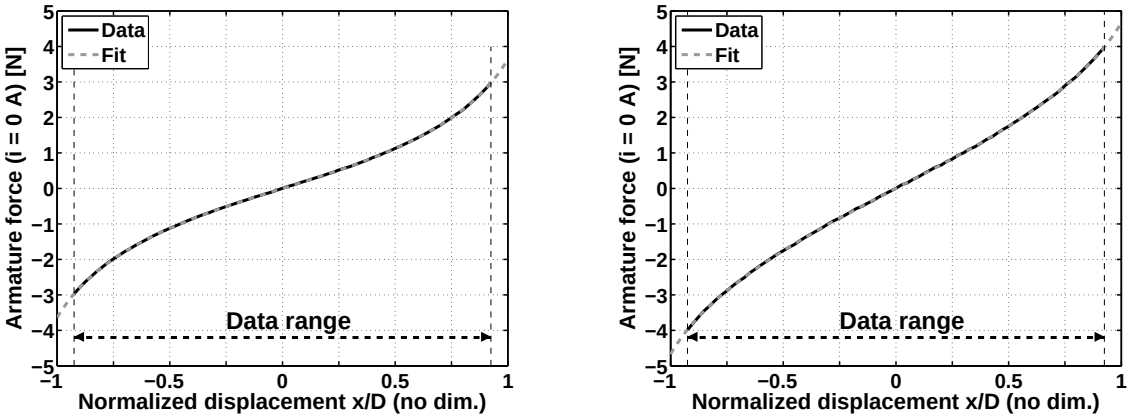

(a) $\alpha = 1$. (b) $\alpha = 4.35$.

Figure 7.3: COMSOL FEM simulation of the magnetic input force on the armature due to permanent magnets vs armature displacement.

From this data, both the nonlinear and the small-signal magnetic stiffness compensation may be extracted. Fig. 7.4(a) shows the small-signal stiffness compensation versus α and Fig. 7.4(b) shows the nonlinear stiffness compensation versus normalized displacement x/D for different values of α.

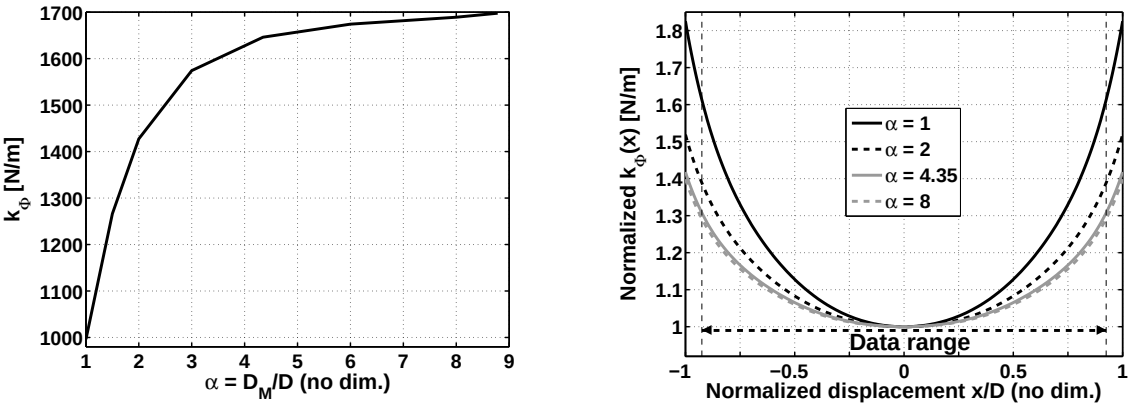

(a) Small-signal magnetic stiffness compensation k_Φ vs α.

(b) Nonlinear magnetic stiffness compensation $k_\Phi\,(x)$ vs x/D.

Figure 7.4: COMSOL FEM simulation of the both the small-signal (k_Φ) and the nonlinear ($k_\Phi\,(x)$) magnetic stiffness compensation.

The behavior of the small-signal stiffness compensation versus α looks very surprising at first

when compared to the prediction shown in Fig. 5.3 which shows that the maximum k_Φ should be reached for $\alpha = 2$. The problem is that this prediction is based on the assumption that no leakage occurs in the magnetic circuit and that the COMSOL simulation (of course) includes leakage effects. The α used on the abscissa of Fig. 7.4(a) is the ratio $\alpha = l_M/(\mu_r D)$ where l_M is the length of the permanent magnet, D is the height of the air gap when the armature is in its resting position and μ_r is the actual relative recoil permeability. Recall that the Thévenin equivalent α can be written

$$\alpha_{Th} = \frac{\mathcal{R}_l}{\mathcal{R}_M + \mathcal{R}_l}\alpha \Leftrightarrow \alpha = \left(1 + \frac{\mathcal{R}_M}{\mathcal{R}_l}\right)\alpha_{Th}. \tag{8.4}$$

Eq. (8.4) reveals that if the leakage reluctance is comparable to the magnet reluctance α_{Th} will be reduced: For instance, if $\mathcal{R}_l = 0.5\mathcal{R}_M$ an α-value of 2 will correspond to $\alpha_{Th} = 2/3$ and this is why the magnetic stiffness compensation does not reach its maximum at $\alpha = 2$ but for an even higher value. The fact that the leakage reluctance depends on the magnet height complicates things further as $\mathcal{R}_l/\mathcal{R}_M$ is generally not constant.

The nonlinear behavior of $k_\Phi\,(x)$ predicted with the FEM simulation and shown in Fig. 7.4(b) also distinguishes itself from that predicted by Fig. 7.1(a). For larger values of α the COMSOL FEM simulation indicates that the curves tends to converge and remain much more nonlinear than that suggested by Fig. 7.1(a). The leakage reluctance can also explain this tendency as the effective Thévenin equivalent α_{Th} will be reduced by the leakage reluctance causing increased nonlinear behavior.

Using the equivalent circuit shown in Fig. 3.2(a) the magnetic leakage can be taken into account. The leakage reluctance is determined for each α-value so that the nonlinear stiffness compensation matches that of Fig. 7.4(b). When this is done the leakage reluctance is that shown in Fig. 7.5(a) and the corresponding nonlinear stiffness compensation is shown in Fig. 7.5(b).

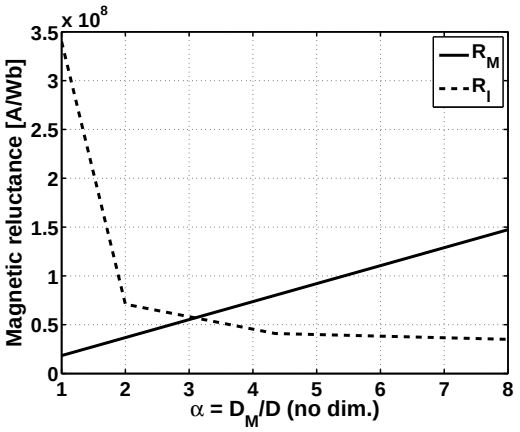

(a) Fitted leakage reluctance.

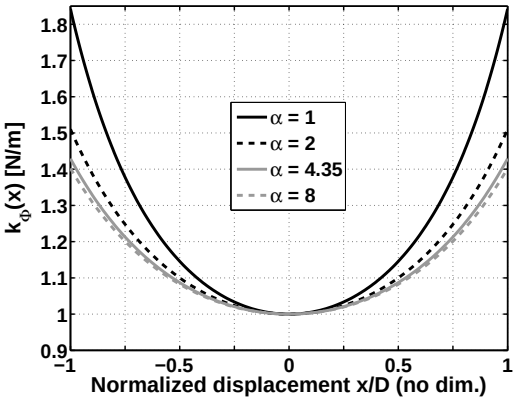

(b) Simulated nonlinear magnetic stiffness compensation $k_\Phi\,(x)$ vs x/D.

Figure 7.5: Lumped equivalent circuit simulation of the both the small-signal (k_Φ) and the nonlinear ($k_\Phi\,(x)$) magnetic stiffness compensation when leakage reluctance is fitted to give curves similar to the COMSOL simulated ones for the nonlinear magnetic stiffness compensation.

Fig. 7.6(a) shows α_{Th} versus α and one can clearly see that because of magnetic reluctance the effective Thévenin equivalent α_{Th} is only in the range between about 1 and 1.5 and this causes much more nonlinear behavior than what α in the range of 1 to 8 would suggest. Fig. 7.6(b) shows the small-signal magnetic stiffness compensation and the characteristics of this curve also fits much better with that shown in Fig. 7.4(a). The magnetic stiffness compensation reaches its maximum for an (effective) $\alpha_{Th} = 2$ (see Fig. 5.3) and as α_{Th} never reaches 2 the curve increases even for $\alpha = 8.78$. The small-signal magnetic stiffness compensation predicted by the lumped equivalent circuit model is not exactly the same as that predicted by the FEM simulation but the inclusion of the leakage reluctance still promises a much more accurate simulation of the balanced-armature loudspeaker.

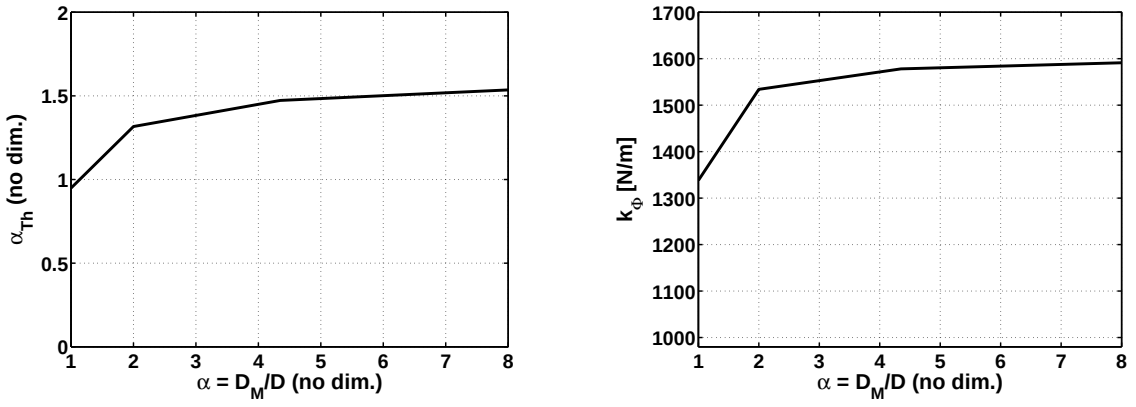

(a) Thévenin equivalent α_{Th} vs α.

(b) k_Φ vs α.

Figure 7.6: Lumped equivalent circuit simulation of the Thévenin equivalent α_{Th} vs α and the small-signal magnetic stiffness compensation k_Φ vs α. The leakage reluctance $\mathcal{R}_l$ is chosen according to Fig. 7.5(a).

The behavior of the leakage reluctance curve looks somewhat unphysical between $\alpha = 1$ and $\alpha = 2$. Nevertheless this is the leakage reluctance necessary to model the nonlinear stiffness compensation predicted by COMSOL FEM simulations.

Next it is investigated how the equivalent circuit model performs if the reluctance of the armature is included in the model and the magnetic leakage is estimated according to Roters's approach. The only leakage permeance which is calculated is that around the permanent magnet which causes the flux to leak from the north to the south pole immediately around the magnet. This value is multiplied by 1.2 in order to somehow account for the extra amount of flux which inevitably leaks between the permanent magnet pole and the armature legs and between the armature and the armature legs. This value is merely an informed guess based on the simulation results presented in Sec. 3.2.2 which suggest that Roters's method underestimate the leakage permeance by a bit more than 10 % in that specific case. The results are presented in Figures 7.7 and 7.8. The behavior of the $\mathcal{R}_l$ curve now looks more physical but the nonlinear loudspeaker parameters are not quite as nonlinear as the COMSOL FEM simulation predicts. Compared to the initial simulations with the circuit model without leakage there is, however, a clear improvement. The small-signal stiffness compensation versus α looks very much like that of the COMSOL simulation, only it is

shifted to a lower level. Again, notice that the effective Thévenin equivalent α_{Th} is never more than 2.

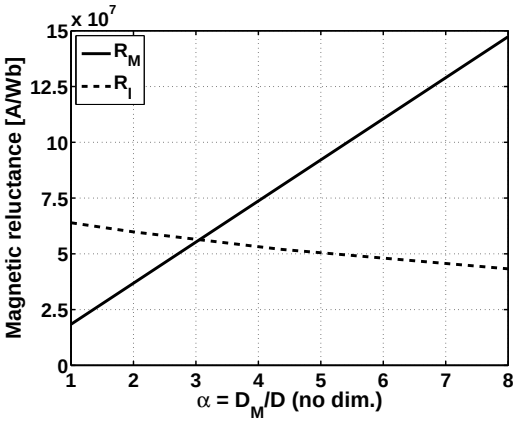

(a) Reluctance estimated using Roters's approach.

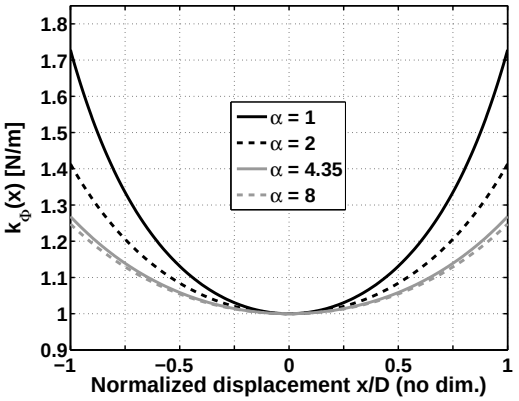

(b) Simulated nonlinear magnetic stiffness compensation $k_\Phi\,(x)$ vs x/D.

Figure 7.7: Lumped equivalent circuit simulation of the both the small-signal (k_Φ) and the nonlinear ($k_\Phi\,(x)$) magnetic stiffness compensation when armature reluctance is included and the leakage reluctance is estimated using Roters's approach.

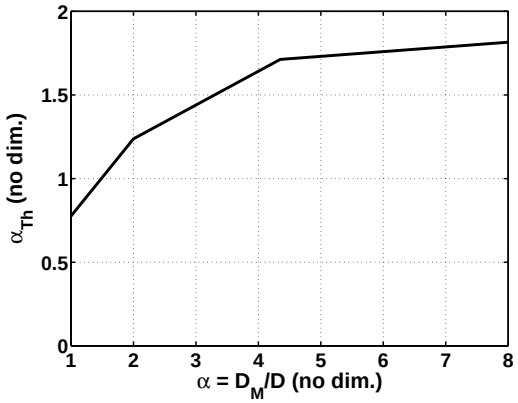

(a) Thévenin equivalent α_{Th} vs α.

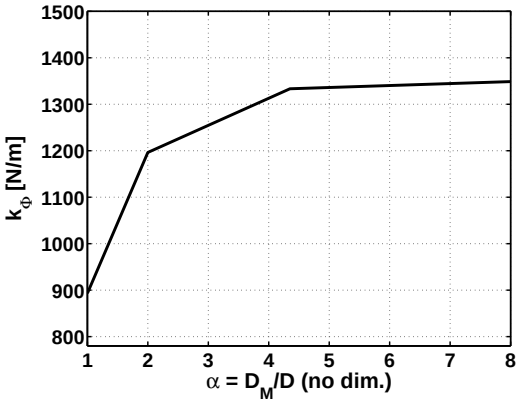

(b) k_Φ vs α.

Figure 7.8: Lumped equivalent circuit simulation of the Thévenin equivalent α_{Th} vs α and the small-signal magnetic stiffness compensation k_Φ vs α when armature reluctance is included and the leakage reluctance is estimated using Roters's approach.

7.3 Nonlinear Stiffness of Back Volume

For most loudspeakers that people have in their homes it is perfectly sufficient to model the back volume as a linear acoustic compliance because the volume displacement of the diaphragm is very small compared to the total volume of the loudspeaker box. However, for miniature balanced-armature loudspeakers the volume displacement of the diaphragm might be significant compared to the back volume and it is almost always significant for the very small front volume immediately above the diaphragm (see Fig. 1.1). When the diaphragm displacement is large compared to the volume, the acoustic compliance of the volume becomes nonlinear, i.e. dependent on the displacement of the diaphragm and this will cause distortion. The analog circuit for the acoustic domain is shown in Fig. 7.9. The acoustic compliance of the back volume C_{AB} will almost always contribute a lot to the total stiffness of the loudspeaker so any nonlinear behavior in the back volume will most likely affect the linearity of the total loudspeaker stiffness. This nonlinearity is mainly important in the low-frequency range where the loudspeaker impedance is dominated by stiffness. However, any asymmetry in the suspension may cause an offset of the diaphragm even at high frequencies and this will change the distortion patterns caused by the nonlinear parameters that are significant at higher frequencies i.e. the force factor and the inductance. The inductance and the force factor are ideally symmetrical around $x = 0$ only causing odd harmonics on the output. However, any offset of the diaphragm due to an asymmetrical suspension compliance will make the otherwise symmetrical nonlinear parameters look asymmetrical and this will produce even harmonics in the output.

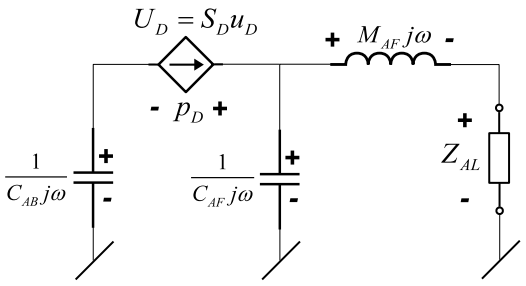

Figure 7.9: Analog circuit representing the loudspeaker diaphragm and the acoustic impedances.

The front volume is much smaller than the back volume so the acoustic compliance C_{AF} of this volume will be even more nonlinear than that of the back volume. However, as the capacitance is very small the impedance of the front volume will be very large at low frequencies and it will be the acoustic mass M_{AF} in the spout together with the external acoustic loud Z_{AL} that dominates the total acoustic front impedance: At low frequencies air will move in and out of the spout unhindered by the front volume and at very high frequencies the volume velocity will go into the front volume and the mass in the spout will block the air flow. Thus, for the relevant frequency range where the output volume velocity flow exits the loudspeaker spout, the nonlinear front volume will be less important. In order to predict the influence of the nonlinear front volume more precisely, the exact acoustic impedance at the exit of the spout needs to be well-defined. This

requires some knowledge about whether the loudspeaker will play through an acoustic tube and into an ear canal or directly into an ear canal and also how close the fit is.

As the back volume significantly affects the total stiffness of the loudspeaker the nonlinearity of the acoustic compliance of a volume will be investigated. The situation is depicted in Fig. 7.10. When air is compressed in very small volumes or slits the thickness of the viscous boundary layer and the thermal layer may be significant compared to the total volume (see [26, Sec. 6.4] and [27]). Heat flows from the air into the container walls and air molecules experience friction against the container walls. In this section the back volume will only be considered as a pure compliance where it is assumed that any viscothermal losses simply makes an otherwise perfect adiabatic process go towards an isothermal process which increases the effective compliance.

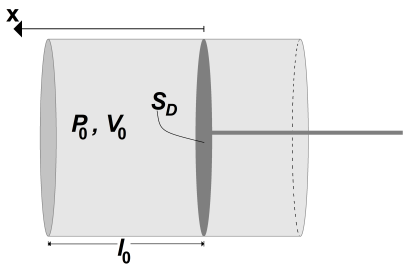

Figure 7.10: Compression of air in the back volume of a loudspeaker.

If the pressure inside the cylinder is assumed to be constant with position and the air inside the cylinder is compressed without any exchange of heat with the cylinder itself (or the air outside of the cylinder) the process is said to be adiabatic. In thermodynamical terms, the compression of air is assumed to be a reversible adiabatic process for which

$$pV^{\gamma} = \text{constant}. \tag{7.3}$$

p is the pressure inside the considered volume V and $\gamma = c_p/c_V$ is the ratio of specific heats (aka the heat capacity ratio or adiabatic index). If, on the other hand, the temperature inside the back volume remains constant γ goes towards 1 and the relationship between the pressure and the volume becomes

$$pV = \text{constant}. \tag{7.4}$$

Eq. (7.4) is relevant for the case where the gas temperature is constant because heat is exchanged with the container and maybe the surrounding media. A large amount of e.g. mineral wool in the cavity may also help provide such isothermal conditions. If the surface area of the cavity is very large compared to the size of the volume the temperature of the container walls will tend to dictate the temperature of the gas. In fact, for air at atmospheric pressure and room temperature

the thickness d_v of the viscous boundary layer and the thickness d_h of the thermal layer are [26, Eq. (6.4.31)]:

$$d_v \approx \frac{2.1}{\sqrt{f}}\,\text{mm} \tag{7.5}$$

$$d_h \approx \frac{2.5}{\sqrt{f}}\,\text{mm} \tag{7.6}$$

where f is the frequency of the sound wave. For frequencies of 100 Hz and 500 Hz the thickness of the thermal layer is 0.25 mm and 0.11 mm respectively. The dimensions of the back volume of a miniature balanced-armature loudspeaker are typically in the range of side lengths from 1.5 mm to 4.5 mm. Therefore, it is probably safe to assume that the compression process is neither entirely adiabatic nor entirely isothermal, but something in between which depends on the size of the back volume of the specific loudspeaker design. The smaller the back volume the closer the compression process is to an isothermal process with $\gamma = 1$. With the definitions

$$p_1 = p_0 + \Delta p \qquad \text{and} \qquad V_1 = V_0 - \Delta V \tag{7.7}$$

equation (7.3) can be written

$$p_0 V_0^{\gamma} = p_1 \left(V_0 - \Delta V\right)^{\gamma} \Leftrightarrow p_1 = p_0 \left(\frac{V_0}{V_0 - \Delta V}\right)^{\gamma} = \frac{p_0}{\left(1 - \frac{\Delta V}{V_0}\right)^{\gamma}}. \tag{7.8}$$

The change in pressure w.r.t. the static pressure p_0 is then

$$\frac{\Delta p}{p_0} = \frac{p_1 - p_0}{p_0} = \frac{1}{\left(1 - \frac{\Delta V}{V_0}\right)^{\gamma}} - 1. \tag{7.9}$$

The nonlinear acoustic compliance of the considered volume can be found by inserting this pressure into the definition of an acoustic compliance:

$$\boxed{C_A\left(\Delta V\right) = \frac{\Delta V}{\Delta p} = \frac{\Delta V}{p_0 \left[\frac{1}{\left(1 - \frac{\Delta V}{V_0}\right)^{\gamma}} - 1\right]} = \frac{V_0}{p_0} \frac{\frac{\Delta V}{V_0}}{\left(1 - \frac{\Delta V}{V_0}\right)^{-\gamma} - 1}}. \tag{7.10}$$

The Taylor series expansion of Eq. (7.9) is

$$\begin{aligned} \frac{\Delta p}{p_0} \approx & \gamma \frac{\Delta V}{V_0} + \frac{\gamma\left(\gamma+1\right)}{1 \cdot 2}\left(\frac{\Delta V}{V_0}\right)^2 + \frac{\gamma\left(\gamma+1\right)\left(\gamma+2\right)}{1 \cdot 2 \cdot 3}\left(\frac{\Delta V}{V_0}\right)^3 \\ & + \frac{\gamma\left(\gamma+1\right)\left(\gamma+2\right)\left(\gamma+3\right)}{1 \cdot 2 \cdot 3 \cdot 4}\left(\frac{\Delta V}{V_0}\right)^4 + \cdots . \end{aligned} \tag{7.11}$$

Thus, the first order approximation is

$$\frac{\Delta p}{p_0} \approx \gamma \frac{\Delta V}{V_0} \tag{7.12}$$

and this can be rewritten to find the linearized acoustic compliance for $\Delta V << V$:

$$C_A = \frac{\Delta V}{\Delta p} \approx \frac{V_0}{p_0} \frac{1}{\gamma}. \tag{7.13}$$

Using the fact that the speed of sound can be written

$$c = \sqrt{\frac{\gamma p_0}{\rho_0}} \Leftrightarrow \gamma p_0 = \rho_0 c^2 \tag{7.14}$$

yields the familiar linearized acoustic compliance of a cavity:

$$C_A \approx \frac{V_0}{\rho_0 c^2} \tag{7.15}$$

where ρ_0 is the air density at static pressure. One important observation can be made by studying Equation 7.13: The acoustic compliance of a volume is inversely proportional to the ratio of specific heats. Thus, as γ is reduced by the introduction of viscothermal effects the acoustic stiffness of the back volume is also reduced. Eq. 7.13 can also be used to write the nonlinear compliance in the more general form as a product of the linear compliance C_A and a function that changes with $\Delta V/V$:

$$C_A\left(\Delta V\right) = C_A \gamma \frac{\frac{\Delta V}{V_0}}{\left(1 - \frac{\Delta V}{V_0}\right)^{-\gamma} - 1}. \tag{7.16}$$

Eq. 7.16 reveals that the nonlinear part of the acoustic compliance is scaled by γ. This means that for a given volume the acoustic compliance will be more nonlinear if the thermodynamic process is adiabatic ($\gamma = 1.4$) than if the process is isothermal ($\gamma = 1$). The nonlinear part of the acoustic compliance is plotted Fig. 7.11 for different values of γ on a range corresponding to a $\pm$ 10 % displacement of the total acoustic volume. The figure reveals that the acoustic compliance can be expected to vary by about $\pm$ 10 % for volume displacements in the range of $\pm$ 10 %. Thus, to accurately model the low-frequency distortion of the balanced-armature receiver it is necessary to include the nonlinear acoustic compliance. For an accurate model it is equally important to use the correct estimation of the ratio of specific heats γ as the small-signal acoustic compliance is inversely proportional to γ. A good back volume model is particularly important if the acoustic stiffness of the back volume is significant compared to the mechanical stiffness and the magnetic stiffness compensation. This is usually the case for miniature B-A loudspeakers. Note that the

nonlinear acoustic compliance is a non-symmetrical nonlinearity which means that it cause even order distortion products to appear in the output of the loudspeaker.

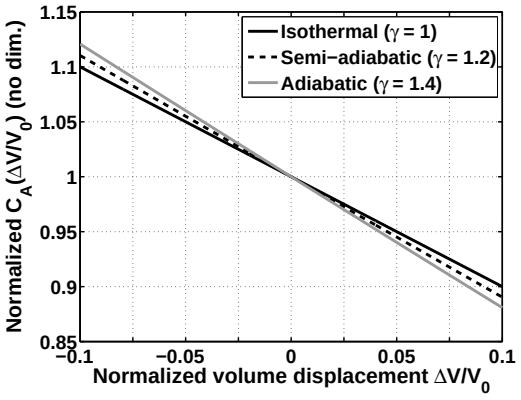

Figure 7.11: Normalized nonlinear acoustic compliance of a cavity for different thermodynamic processes.

Chapter 8

Taking Magnetic Leakage into Account

In Sec. 3.1 it was shown that the magnetic leakage could be accounted for by introducing a simple transformation of the recoil permeability which would in turn transform the magnetomotive force of the permanent magnet and its reluctance while maintaining the same equivalent circuit. Throughout this thesis the parameters D_M and α are often used to describe the various loudspeaker parameters but all the derivations are performed without taking the leakage into account. Consider Fig. 7.1(b). The designer might be appealed to make a design with $\alpha = 4$ since this will provide a much more linear force factor than, say, $\alpha = 1$. As the air gap height D and the permanent magnet material will often be determined beforehand the required magnet length l_M will be determined as

$$\alpha = \frac{D_M}{D} = \frac{l_M}{\mu_r D} \Leftrightarrow l_M = \mu_r D \alpha, \tag{8.1}$$

with the relative recoil permeability μ_r being a characteristic of the permanent magnet. However, this result is only true for the model that does not take magnetic leakage into account. For a model that does take magnetic leakage into account one should interpret the result from Fig. 7.1(b) such that it is the Thévenin equivalent α which should equal 4 in order to produce the curve with the least nonlinear force factor. This is the motivation for deriving an expression that relates α_{Th} to α: α may be used to derive the required magnet length when α_{Th} is known. The Thévenin equivalent α is

$$\alpha_{Th} = \frac{D_{M,Th}}{D} = \frac{l_M}{\mu_{r,Th} D}. \tag{8.2}$$

Substituting the Thévenin equivalent recoil permeability (Eq. (3.11)) into this yields

$$\alpha_{Th} = \frac{l_M}{\left(1 + \frac{\mathcal{R}_M}{\mathcal{R}_l}\right) \mu_r D} = \frac{1}{1 + \frac{\mathcal{R}_M}{\mathcal{R}_l}} \alpha \Leftrightarrow \tag{8.3}$$

$$\alpha_{Th} = \frac{\mathcal{R}_l}{\mathcal{R}_M + \mathcal{R}_l} \alpha \Leftrightarrow \alpha = \left(1 + \frac{\mathcal{R}_M}{\mathcal{R}_l}\right) \alpha_{Th}. \tag{8.4}$$

Thus for a design with magnetic leakage corresponding to $\mathcal{R}_l = 0.5\mathcal{R}_M$ one would obtain $\alpha = 3\alpha_{Th}$. Thus, when leakage is taken into account - referring now to Fig. 5.3 - it will not be the magnet length that corresponds to $\alpha = 1$ which will maximize the force factor T. Instead it will

be $\alpha_{Th} = 1 \Rightarrow \alpha = 3$ that maximizes the force factor (for the case $\mathcal{R}_l = 0.5\mathcal{R}_M$). Substituting Eq. (8.4) into into Eq. (8.1) the actual magnet length required in order to obtain a certain α_{Th} when taking magnetic leakage into account will be given as:

$$l_M = \mu_r D\alpha = \mu_r D \left(1 + \frac{\mathcal{R}_M}{\mathcal{R}_l}\right) \alpha_{Th}. \tag{8.5}$$

Estimating the leakage reluctance $\mathcal{R}_l$ can be done in at least 4 different ways. Referring to Fig. 3.3(a) the parameters $\mathcal{F}_M$, $\mathcal{R}_M$ and $\mathcal{R}_g$ are all well-defined. If the magnetic field in the air gap is known the leakage reluctance $\mathcal{R}_l$ may be derived writing the circuit equations. The magnetic field in the air gap can either be measured directly using a gauss meter if the air gap is large enough or alternatively it may be simulated using FEM software. The third option is to estimate the leakage reluctance using Roters's approach [12].

The most easy and practical procedure is maybe to make use of the measured or simulated armature flux for $i = 0$. This can be done using the expression for the armature flux given in Eq. (5.16) but now written in terms of the effective Thévenin equivalent α:

$$\Phi_{a,0}(x) = 2B_r \frac{A}{D} \frac{\alpha_{Th}}{(\alpha_{Th}+1)^2 - \left(\frac{x}{D}\right)^2} x. \tag{8.6}$$

If $\Phi_{a,0}$ is known it is a simple matter of solving a quadratic equation to obtain α_{Th}. When α_{Th} is known $\mu_{r,Th}$ can be determined using Eq. (8.2). When $\mu_{r,Th}$ is available it is an easy task to determine the Thévenin equivalent magnetomotive force and the Thévenin equivalent internal reluctance using Eq. (3.12) and (3.13). Finite Element simulations can be used to simulate the armature flux. For actual measurement of the armature flux it is necessary to perform a dynamic measurement by exciting the armature mechanically and use a pickup coil wrapped around the armature to measure the total flux in the armature. If the coil has a sufficient number of windings this measurement can be done at a very low frequency where the eddy current losses are small. If the displacement of the excitation is sufficiently small compared to D the problem reduces to

$$\Phi_{a,0}(x) \approx 2B_r \frac{A}{D} \frac{\alpha_{Th}}{(\alpha_{Th}+1)^2} x. \tag{8.7}$$

In the end, the reason for obtaining the Thévenin equivalent parameters is to obtain a simple and efficient lumped element model that can take magnetic leakage into account using the principles explained in Sec. 3.1.

Chapter 9

Loudspeaker Stability

The loudspeaker is considered stable when the restoring mechanical force on the armature due to its stiffness is greater than the magnetic force due to the nonlinear magnetic stiffness compensation i.e. the magnetic force only due to the permanent magnets when the coil current is zero. What this means is that it should be impossible for the armature to stick to one of the permanent magnets if the armature is displaced to the magnet either by an external mechanical force or by an electrical excitation of the coil: The armature should always return to its balanced resting position right between the two permanent magnets if left alone.

The small back volume of miniature B-A loudspeakers usually contributes significantly to the total mechanical stiffness in the audio frequency range. However, since the loudspeaker back volume is usually not 100 % air sealed it will be possible to shift the diaphragm very slowly without building up any restoring spring force in the back volume. The assumption is therefore that one can only trust the mechanical stiffness of the armature for making sure that the loudspeaker is stable. Thus, the loudspeaker is stable when

$$k_a x > \left. \mathcal{F}_\Phi(x) \right|_{i=0} = k_\phi(x)\, x \Leftrightarrow k_a > k_\phi(x). \tag{9.1}$$

Substituting Eq. (5.32) into Eq. (9.1) yields

$$k_a > k_\phi \frac{(\alpha+1)^4}{\left[(\alpha+1)^2 - \left(\frac{x}{D}\right)^2\right]^2} \Leftrightarrow k_r = \frac{k_\Phi}{k_a} < \frac{\left[(\alpha+1)^2 - \left(\frac{x}{D}\right)^2\right]^2}{(\alpha+1)^4} \Rightarrow \tag{9.2}$$

$$\boxed{\frac{x}{D} < (\alpha+1)\sqrt{1-\sqrt{k_r}}}. \tag{9.3}$$

Eq. (9.3) is plotted in Fig. 9.1 for various normalized magnet lengths.

For a magnet length corresponding to $\alpha = D_M/D = 0.5$ the receiver will be stable in the entire operating range $|x| \leq D$ only for a stiffness ratio of 0.3. If the stiffness ratio is increased to e.g. 0.7 the magnetic force will overcome the mechanical armature stiffness already when the armature is displaced to around 60 % of the air gap length. If, however, the magnet length is increased to a length corresponding to $\alpha = D_M/D = 4$, the armature can move in the entire air gap range without sticking to the permanent magnets up to a stiffness ratio of more than 0.9.

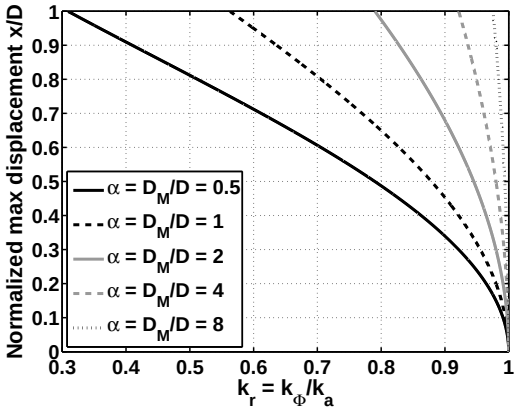

Figure 9.1: Stiffness ratio k_Φ/k_a vs maximum normalized displacement, x/D before instability. Plots are shown for various normalized magnet lengths, α.

When the right-hand side of Eq. (9.3) is larger than 1 stability is ensured in the entire operating range of the armature:

$$1 < (\alpha+1)\sqrt{1-\sqrt{k_r}} \Leftrightarrow k_r < \left(\frac{1}{(\alpha+1)^2} - 1\right)^2 \Leftrightarrow \tag{9.4}$$

$$\boxed{k_r < \frac{\alpha^2(\alpha+2)^2}{(\alpha+1)^4}} \Leftrightarrow \boxed{\alpha > \frac{1}{\sqrt{1-\sqrt{k_r}}} - 1}. \tag{9.5}$$

It will be useful to state the equation for the critically stable loudspeaker where the magnetic force exactly balances the mechanical armature force for $x = D$:

$$\boxed{k_r = \frac{\alpha^2(\alpha+2)^2}{(\alpha+1)^4}} \Leftrightarrow \boxed{\alpha = \frac{1}{\sqrt{1-\sqrt{k_r}}} - 1} \tag{9.6}$$

Eq. (9.5) and (9.6) provide constraints on the loudspeaker design that will ensure that the loudspeaker is either stable or critically stable. Eq. (9.6) is plotted in Fig. 9.2. With the aid of Fig. 9.2 one can choose an appropriate magnet length for a desired stiffness ratio.

It will prove useful to establish how the air gap area and the armature stiffness influences the stability. Substituting Eq. (5.31) into Eq. (5.59) yields

$$k_r = \frac{2B_r^2}{\mu_0}\frac{A}{D}\frac{\alpha^2}{(\alpha+1)^3}\frac{1}{k_a}. \tag{9.7}$$

Substituting Eq. (9.7) into the stability criterion (Eq. (9.5)) yields

$$\frac{2B_r^2}{\mu_0}\frac{A}{D}\frac{\alpha^2}{(\alpha+1)^3}\frac{1}{k_a} < \frac{\alpha^2(\alpha+2)^2}{(\alpha+1)^4} \Leftrightarrow \tag{9.8}$$

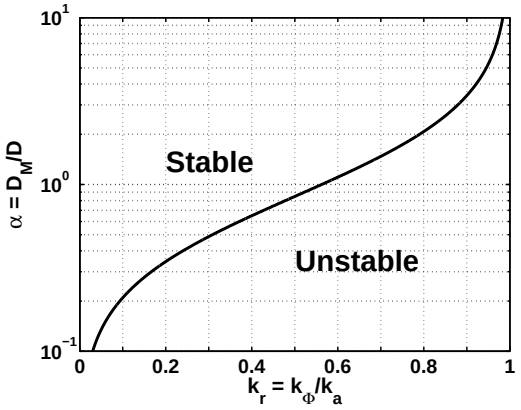

Figure 9.2: Stiffness ratio $k_r = k_\Phi/k_a$ vs minimum normalized magnet length $\alpha = D_M/D$ for ensured stability in the entire operating range, $|x| < D$.

$$\boxed{\frac{A}{D} < \frac{\mu_0}{2B_r^2}\frac{(\alpha+2)^2}{\alpha+1}k_a}. \tag{9.9}$$

It will be useful to state the limiting case as this determines the ratio A/D for the critically stable loudspeaker:

$$\boxed{\frac{A}{D} = \frac{\mu_0}{2B_r^2}\frac{(\alpha+2)^2}{\alpha+1}k_a}. \tag{9.10}$$

For the special case where the armature has a simple shape with constant width and height the armature stiffness is given by Eq. (5.70). Substituting this into Eq. (9.9) yields:

$$\frac{A}{D} < \frac{\mu_0 E}{8B_r^2}\frac{(\alpha+2)^2}{\alpha+1}\left(\frac{h_a}{l_a}\right)^3 w_a \Leftrightarrow \frac{A}{w_a} < \frac{\mu_0 ED}{8B_r^2}\frac{(\alpha+2)^2}{\alpha+1}\left(\frac{h_a}{l_a}\right)^3. \tag{9.11}$$

Pushing the receiver design close to the limit of stability means that the nonlinear magnetic stiffness compensation $k_\Phi(x)$ is approaching the mechanical stiffness of the armature k_a at $x = D$ and this again means that the mechanical armature force due to its stiffness only just balances out the magnetic force in the opposite direction towards the permanent magnet. This means that the effective armature stiffness will be quite nonlinear if the acoustic stiffness is relatively small compared to the sum of the armature stiffness and the stiffness compensation. To illustrate this, one can plot the mechanical armature stiffness, the nonlinear magnetic stiffness compensation and the effective stiffness as function of the normalized armature displacement. This is done in Fig. 9.3 for two different values of α for the critically stable design. It is clearly seen how the linearity of the effective stiffness is greater for the design with the largest α-value. Furthermore, since α is greater the stiffness ratio can also be pushed to a larger value meaning that the armature can be made less stiff and in the end the effective stiffness is much smaller for the critically stable design with $\alpha = 4$. This will make the design much more efficient. In figures 9.3 to 9.5 the small-signal

magnetic stiffness compensation is fixed to a value of 1 N/m.

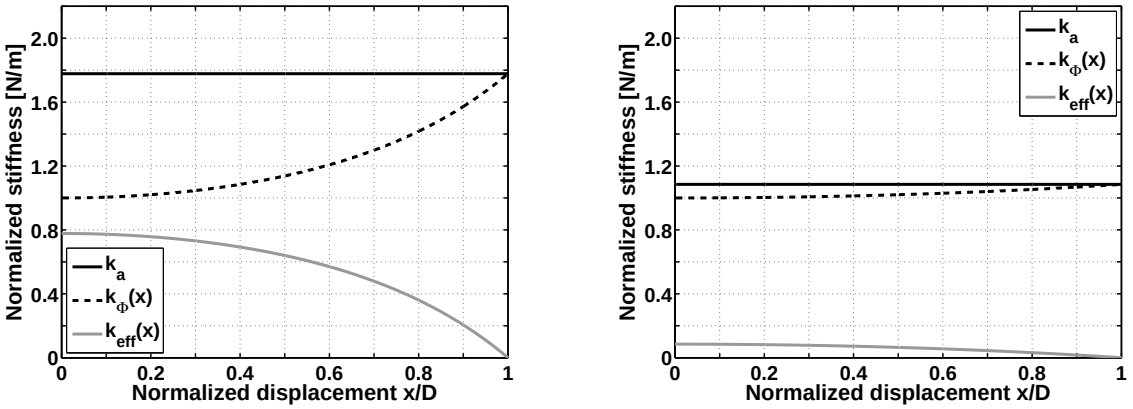

(a) $\alpha = 1$. (b) $\alpha = 4$.

Figure 9.3: Armature stiffness k_a, nonlinear magnetic stiffness compensation $k_\Phi\,(x)$ and the effective stiffness $k_{eff}\,(x)$ assuming that the acoustic stiffness is zero. The armature stiffness is chosen so that the design is critically stable. Simulations are shown for two different values of α.

If the armature stiffness is increased by 20 % relative to the critically stable case the effective stiffness will become less nonlinear and the risk of the loudspeaker being unstable is reduced. Fig. 9.4 shows the simulations of the stiffnesses for this case, again for two different values of α. The larger armature stiffness simply shifts the curve for the effective stiffness upwards towards a higher stiffness meaning that the relative change in k_{eff} becomes smaller as x/D goes from 0 to 1.

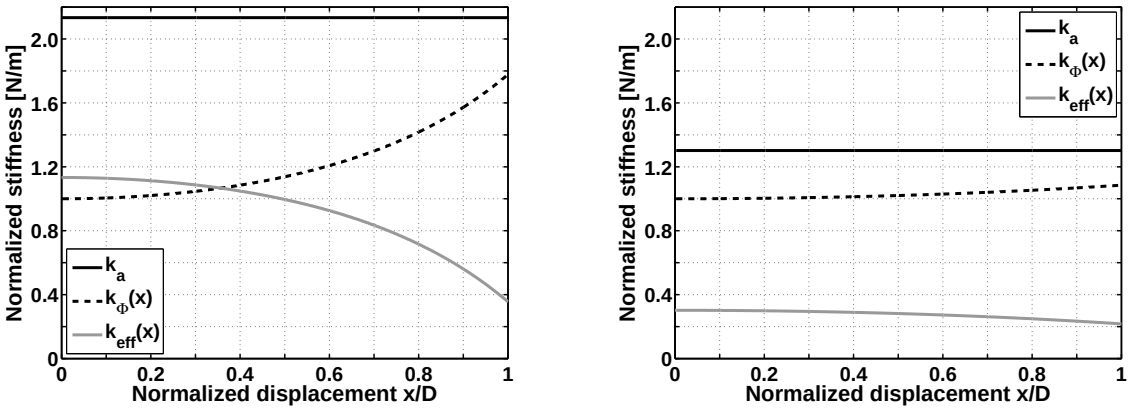

(a) $\alpha = 1$. (b) $\alpha = 4$.

Figure 9.4: Armature stiffness k_a, nonlinear magnetic stiffness compensation $k_\Phi\,(x)$ and the effective stiffness $k_{eff}\,(x)$ assuming that the acoustic stiffness is zero. The armature stiffness is 20 % greater than what is required for the design to be critically stable. Simulations are shown for two different values of α.

Finally, in Fig. 9.5 it is shown what happens if the armature stiffness is too small and the design is unstable. The armature stiffness is reduced by 10 % relative to the critically stable design and results are again shown for two different values of α. It can be seen that even though the design

with a large α-value tends to be more stable in the sense that it allows for a larger stiffness ratio k_r, it also easily becomes unstable in the entire operating range if the stiffness is reduced. The design with the smaller α-value remains stable as long as the armature displacement x is less than about 91 % of the maximum displacement D. However, it should be noted that any design that is unstable for some value of $x < D$ is a poor design.

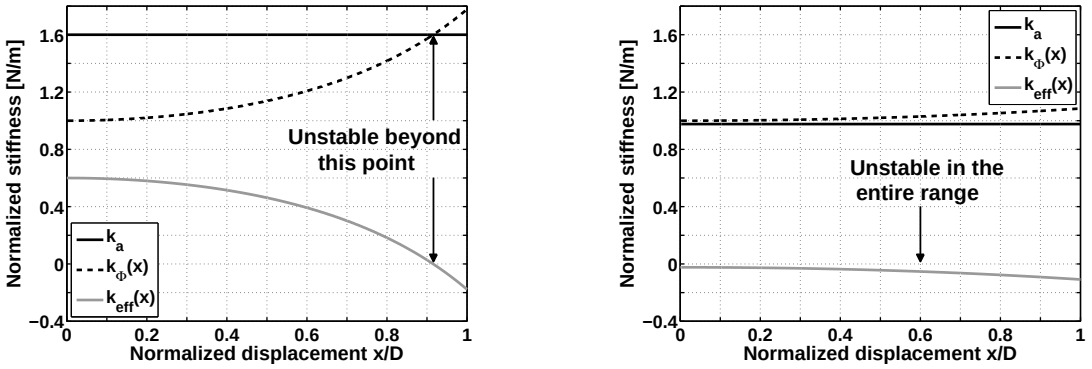

(a) $\alpha = 1$.

(b) $\alpha = 4$.

Figure 9.5: Armature stiffness k_a, nonlinear magnetic stiffness compensation $k_\Phi\,(x)$ and the effective stiffness $k_{eff}\,(x)$ assuming that the acoustic stiffness is zero. The armature stiffness is 10 % smaller than what is required for the design to be critically stable so the design is unstable. Simulations are shown for two different values of α.

9.1 Parameters for the Critically Stable Loudspeaker

In this section, the small-signal parameters and the small-signal distortion transduction coefficient will be derived for the critically stable case. This is done by substituting Eq. (9.10) into the expressions for the small-signal parameters derived in sections 5.2 and 5.3. Notice that Eq. (9.10) was derived by taking the stability criterion into account between Equations (9.7) and (9.8). In order for the stability criterion to be fulfilled, the air gap area should always be determined according to Eq. (9.10).

The derived equations are also valid for the critically saturated case (see Chapter 10). One should simply determine the armature height according to the constraint formulated in Eq. (10.33) which will ensure that the armature does not saturate until the loudspeaker has become critically stable as the air gap is increased.

Since the critically stable loudspeakers are merely a subgroup of all possible loudspeaker designs the conclusions for the general loudspeakers also hold true for the critically stable loudspeakers. This means that for the critically stable loudspeaker the nonlinear parts of the loudspeaker parameters are exactly the same as for the general case so the evaluation of the nonlinearity of the loudspeaker parameters in Chapter 7 is also valid for the critically stable case.

9.1.1 Magnetic Stiffness Compensation

Substituting Eq. (9.10) into Eq. (5.30) and using $D_M/D = \alpha$ yields

$$k_{\Phi,st}(x) = \frac{2B_r^2}{\mu_0}\frac{\mu_0}{2B_r^2}\frac{(\alpha+2)^2}{\alpha+1}k_a\frac{\alpha^2(\alpha+1)}{\left[(\alpha+1)^2-\left(\frac{x}{D}\right)^2\right]^2} \Leftrightarrow \tag{9.12}$$

$$\boxed{k_{\Phi,st}(x) = \frac{\alpha^2(\alpha+2)^2}{\left[(\alpha+1)^2-\left(\frac{x}{D}\right)^2\right]^2}k_a} \tag{9.13}$$

For small signals where $x << D$:

$$\boxed{k_{\Phi,st} = \frac{\alpha^2(\alpha+2)^2}{(\alpha+1)^4}k_a}. \tag{9.14}$$

It is also possible to write the nonlinear magnetic stiffness compensation for the critically stable case as a product of the linear critically stable magnetic stiffness compensation and a function of α and x/D:

$$k_{\Phi,st}(x) = k_{\Phi,st}\frac{(\alpha+1)^4}{\left[(\alpha+1)^2-\left(\frac{x}{D}\right)^2\right]^2}. \tag{9.15}$$

9.1.2 Transduction Coefficient

Substituting Eq. (9.10) into Eq. (5.35) and using $D_M/D = \alpha$ yields

$$T_{st}(x) = 2B_rN\frac{\mu_0}{2B_r^2}\frac{(\alpha+2)^2}{\alpha+1}k_a\frac{\alpha\left[(\alpha+1)^2+\left(\frac{x}{D}\right)^2\right]}{\left[(\alpha+1)^2-\left(\frac{x}{D}\right)^2\right]^2} \Leftrightarrow \tag{9.16}$$

$$\boxed{T_{st}(x) = \frac{\mu_0N}{B_r}\frac{\alpha(\alpha+2)^2\left[(\alpha+1)^2+\left(\frac{x}{D}\right)^2\right]}{(\alpha+1)\left[(\alpha+1)^2-\left(\frac{x}{D}\right)^2\right]^2}k_a}. \tag{9.17}$$

For small signals where $x << D$:

$$\boxed{T_{st} = \frac{\mu_0N}{B_r}\frac{\alpha(\alpha+2)^2}{(\alpha+1)^3}k_a}. \tag{9.18}$$

It is also possible to write the nonlinear force factor for the critically stable case as a product of the linear critically stable force factor and a function of α and x/D:

$$T_{st}(x) = T_{st}\frac{(\alpha+1)^2\left[(\alpha+1)^2+\left(\frac{x}{D}\right)^2\right]}{\left[(\alpha+1)^2-\left(\frac{x}{D}\right)^2\right]^2}. \tag{9.19}$$

9.1.3 Distortion Transduction Coefficient

Substituting Eq. (9.10) into Eq. (5.37) and using $D_M/D = \alpha$ yields

$$T_{me,d,st}\left(x,i\right) = 2\mu_0 N^2 \frac{xi}{D^2}\frac{\mu_0}{2B_r^2}\frac{\left(\alpha+2\right)^2}{\alpha+1}k_a\frac{\left(\alpha+1\right)}{\left[\left(\alpha+1\right)^2-\left(\frac{x}{D}\right)^2\right]^2} \Leftrightarrow \tag{9.20}$$

$$\boxed{T_{me,d,st}\left(x,i\right) = \frac{xi}{D^2}\left(\frac{\mu_0 N}{B_r}\right)^2\frac{\left(\alpha+2\right)^2}{\left[\left(\alpha+1\right)^2-\left(\frac{x}{D}\right)^2\right]^2}k_a} \tag{9.21}$$

For small signals where $x << D$:

$$\boxed{T_{me,d,st}\left(x,i\right)\big|_{x<<D} = \frac{xi}{D^2}\left(\frac{\mu_0 N}{B_r}\right)^2\frac{\left(\alpha+2\right)^2}{\left(\alpha+1\right)^4}k_a}. \tag{9.22}$$

It is also possible to write the nonlinear distortion force factor for the critically stable case as a product of the linear critically stable distortion force factor and a function of α and x/D:

$$T_{me,d,st}\left(x,i\right) = T_{me,d,st}\left(x,i\right)\big|_{x<<D}\frac{\left(\alpha+1\right)^4}{\left[\left(\alpha+1\right)^2-\left(\frac{x}{D}\right)^2\right]^2}. \tag{9.23}$$

9.1.4 Electrical Inductance

Substituting Eq. (9.10) into Eq. (5.47) and using $D_M/D = \alpha$ yields

$$L_{st}\left(x\right) = 2\mu_0 N^2\frac{\mu_0}{2B_r^2}\frac{\left(\alpha+2\right)^2}{\alpha+1}k_a\frac{\alpha+1}{\left(\alpha+1\right)^2-\left(\frac{x}{D}\right)^2} \Leftrightarrow \tag{9.24}$$

$$\boxed{L_{st}\left(x\right) = \left(\frac{\mu_0 N}{B_r}\right)^2\frac{\left(\alpha+2\right)^2}{\left(\alpha+1\right)^2-\left(\frac{x}{D}\right)^2}k_a} \tag{9.25}$$

For small signals where $x << D$:

$$\boxed{L_{st} = \left(\frac{\mu_0 N}{B_r}\right)^2\left(\frac{\alpha+2}{\alpha+1}\right)^2 k_a}. \tag{9.26}$$

It is also possible to write the nonlinear electrical inductance for the critically stable case as a product of the linear critically stable inductance and a function of α and x/D:

$$L_{st}\left(x\right) = L_{st}\frac{\left(\alpha+1\right)^2}{\left(\alpha+1\right)^2-\left(\frac{x}{D}\right)^2}. \tag{9.27}$$

9.1.5 Small-Signal Parameters versus $\alpha = DM/D$

The 3 small-signal parameters and the linearized distortion transduction coefficient for the critically stable loudspeaker were derived in the previous sections:

$$k_{\Phi,st} = \frac{\alpha^2 (\alpha+2)^2}{(\alpha+1)^4} k_a \tag{9.14}$$

$$T_{st} = \frac{\mu_0 N}{B_r} \frac{\alpha (\alpha+2)^2}{(\alpha+1)^3} k_a \tag{9.18}$$

$$L_{st} = \left(\frac{\mu_0 N}{B_r}\right)^2 \left(\frac{\alpha+2}{\alpha+1}\right)^2 k_a \tag{9.26}$$

$$T_{me,d,st}(x,i)|_{x<<D} = \frac{xi}{D^2} \left(\frac{\mu_0 N}{B_r}\right)^2 \frac{(\alpha+2)^2}{(\alpha+1)^4} k_a \tag{9.22}$$

with the air gap area A and maximum displacement D constrained by the stability criterion:

$$\frac{A}{D} = \frac{\mu_0}{2B_r^2} \frac{(\alpha+2)^2}{\alpha+1} k_a. \tag{9.11}$$

Notice that for the critically stable balanced-armature loudspeaker all the important loudspeaker parameters scale with the armature stiffness k_a. Since the critically stable loudspeakers are just a "sub group" of all possible loudspeaker designs, the equations for the potentially unstable loudspeaker also hold true for the critically stable loudspeaker e.g. the important relationship between the small-signal parameters is still valid:

$$T_{st}^2 = k_{\Phi,st} L_{st} \tag{9.28}$$

The normalized small-signal parameters (dependence of α) for the critically stable loudspeaker are plotted in Fig. 9.6

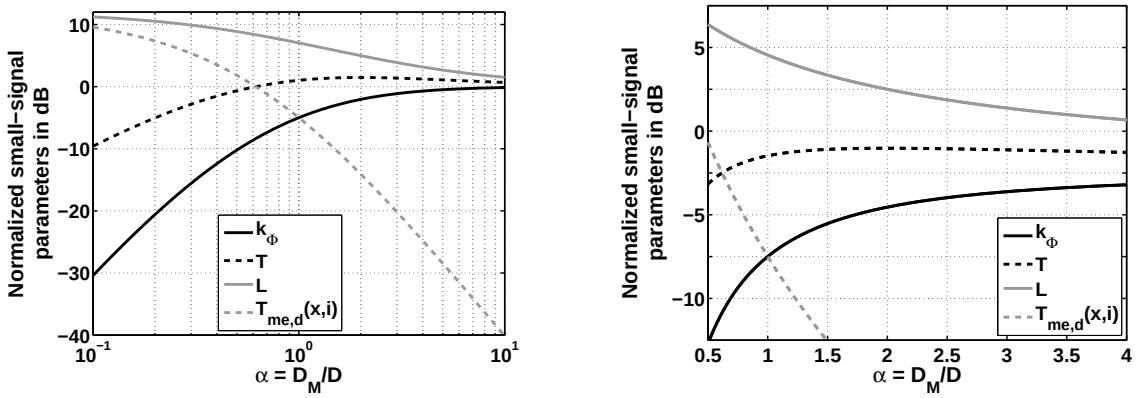

(a) Overview.

(b) Close-up of the most relevant α-range.

Figure 9.6: Normalized small-signal parameters vs $\alpha = D_M/D$ for the critically stable loudspeaker.

9.1.6 Electrical Cut-off Frequency

Substituting the stability criterion as expressed in Eq. (9.10) into Eq. (5.118) yields the electrical cut-off frequency for the critically stable loudspeaker:

$$\boxed{\omega_{e,cut,st} = \frac{R_L}{L_{st}} = \frac{\rho_w}{F_f l_c}\left[\pi + \frac{P_{c,s}}{t_c}\right]\left(\frac{B_r}{\mu_0}\right)^2\left(\frac{\alpha+1}{\alpha+2}\right)^2\frac{1}{k_a}}, \tag{9.29}$$

with

$$\frac{A}{D} = \frac{\mu_0}{2B_r^2}\frac{(\alpha+2)^2}{\alpha+1}k_a \tag{9.11}$$

ensuring that the design is critically stable. It is clear how the parameters of the first, third and fifth factors influence the electrical cut-off frequency but it is perhaps less clear how the ratio $\alpha = D_M/D$ and the ratio between the inner coil perimeter $P_{c,s}$ and the coil thickness t_c influence the cut-off frequency. Therefore, the second and the fourth factor of Eq. (9.29) are plotted in Fig. 9.7

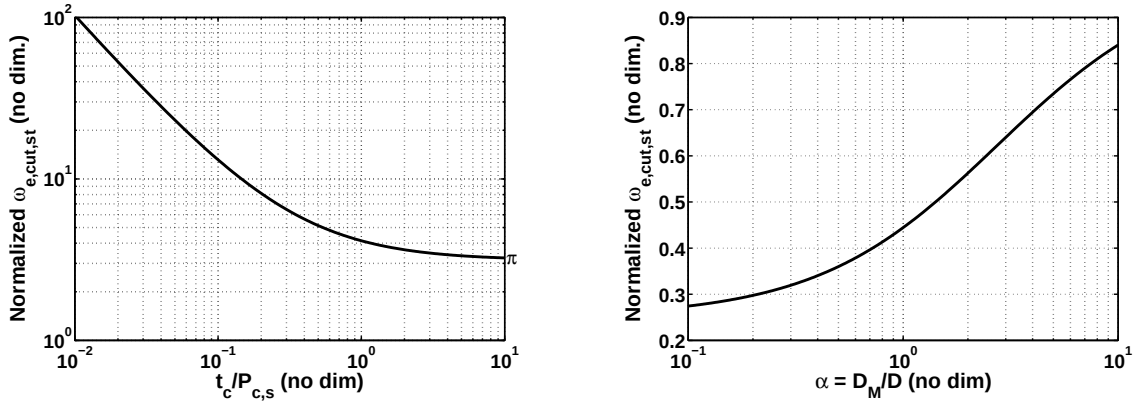

(a) $\omega_{e,cut,st}$ vs coil thickness t_c divided by the inner coil perimeter $P_{c,s}$.

(b) $\omega_{e,cut,st}$ vs $\alpha = D_M/D$.

Figure 9.7: Normalized electrical cut-off frequency $\omega_{e,cut,st}$ for the critically stable loudspeaker.

Fig. 9.7(a) reveals that when the thickness of the square coil reaches the value of the inner coil perimeter the cut-off frequency remains almost constant when the thickness is increased further. When the coil thickness is reduced below the inner coil perimeter the cut-off frequency increases as it tends to be inversely proportional to the coil thickness.

9.1.7 Effective Armature Stiffness with no Acoustic Load

For reasons of low-frequency efficiency it is interesting to see how the effective armature stiffness depends on $\alpha = D_M/D$ for the critically stable case. The case of no acoustic load will be investigated. The nonlinear effective stiffness may be expressed as

$$k_{eff}(x) = k_a - k_\Phi(x) = \frac{1}{k_r} k_\Phi(x) - k_\Phi(x) = \left(\frac{1}{k_r} - 1\right) k_\Phi(x) \tag{9.30}$$

for $k_{mA} << k_a - k_\Phi$. Substituting the nonlinear magnetic stiffness compensation for the critically stable case (Eq. (9.13)) into this equation and using the stability criterion (Eq. (9.6)) to relate k_r to α yields the effective stiffness of the critically stable loudspeaker with $k_{mA} << k_a - k_\Phi$:

$$k_{eff,st}(x) = \left(\frac{(\alpha+1)^4}{\alpha^2(\alpha+2)^2} - 1\right) \frac{\alpha^2(\alpha+2)^2}{\left[(\alpha+1)^2 - \left(\frac{x}{D}\right)^2\right]^2} k_a \Leftrightarrow \tag{9.31}$$

$$\boxed{k_{eff,st}(x) = \frac{2\alpha^2 + 4\alpha + 1}{\left[(\alpha+1)^2 - \left(\frac{x}{D}\right)^2\right]^2} k_a}. \tag{9.32}$$

For small signals where $x << D$ and $k_{mA} << k_a - k_\Phi$:

$$\boxed{k_{eff,st} = \frac{2\alpha^2 + 4\alpha + 1}{(\alpha+1)^4} k_a}. \tag{9.33}$$

It is also possible to write the nonlinear effective stiffness for the critically stable case as a product of the linear critically stable effective stiffness and a function of α and x/D:

$$k_{eff,st}(x) = k_{eff,st} \frac{(\alpha+1)^4}{\left[(\alpha+1)^2 - \left(\frac{x}{D}\right)^2\right]^2}. \tag{9.34}$$

Notice that the nonlinear part of Eq. (9.35) is exactly the same as that for the magnetic stiffness compensation so the variation of $k_{eff,st}(x)$ with armature displacement can be seen in Fig. 7.1(a).

The first factor of Eq. (9.33) is plotted in Fig. 9.8.

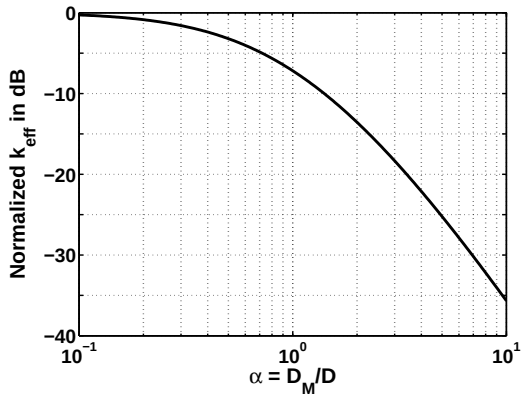

Figure 9.8: Normalized effective small-signal stiffness vs. $\alpha = D_M/D$ for critically stable operation with $k_{mA} << k_a - k_\Phi$.

According to Fig. 9.8 it is possible to significantly lower the effective stiffness for the critically stable loudspeaker by increasing the magnet length presuming that the acoustic stiffness is very small.

9.1.8 Effective Armature Stiffness for $k_{mA} \neq 0$

In order to take the stiffness of the back volume into account, this simply has to be added to the result in Eq. (9.33):

$$k_{eff,st} = \frac{2\alpha^2 + 4\alpha + 1}{(\alpha+1)^4} k_a + k_{mA} \qquad \text{for } x << D. \tag{9.35}$$

where k_{mA} is the mechanical stiffness due to the acoustic stiffness of the back volume. This is given as

$$k_{mA} = S_D^2 k_A = S_D^2 \frac{1}{C_A} = S_D^2 \frac{1}{\frac{V_A}{\rho_0 c^2}} = \frac{S_D^2 \rho_0 c^2}{V_A} \tag{9.36}$$

where k_A is the acoustic stiffness of the back volume, C_A is the acoustic compliance, V_A is the volume and S_D is the surface area of the diaphragm. The assumption is now that the acoustic volume is given as the coil volume V_c subtracted from the total volume V_T:

$$V_A = V_T - V_c. \tag{9.37}$$

Substituting Equations (9.36) and (9.37) into Eq. (9.35) yields

$$\boxed{k_{eff,st} = \frac{2\alpha^2 + 4\alpha + 1}{(\alpha+1)^4} k_a + \frac{S_D^2 \rho_0 c^2}{V_T - V_c}} \qquad \text{for } x << D. \tag{9.38}$$

Substituting the volume of the square coil (Eq. (5.115)) into Eq. (9.38) yields

$$\boxed{k_{eff,st} = \frac{2\alpha^2 + 4\alpha + 1}{(\alpha+1)^4} k_a + \frac{S_D^2 \rho_0 c^2}{V_T - F_{cl} l_a t_c \left[2\left(w_a + h_a + 2D\right) + \pi t_c\right]}}. \qquad \text{for } x << D. \tag{9.39}$$

Equation (9.39) then expresses the effective small-signal stiffness of a receiver with a square coil which is designed to be critically stable.

Chapter 10

Armature Saturation and Maximum Output

The maximum output of a balanced-armature loudspeaker is foremost determined by the maximum possible armature displacement D. Secondly, as demonstrated in this chapter, magnetic saturation of the armature is likely to limit the maximum output of the loudspeaker. This was also pointed out by Stephen Thompson in his detailed patent on a method for reducing the distortion in balanced-armature loudspeakers [28]. At low frequencies - where acoustic signals usually contain the most power - the magnetic flux in the armature due to the permanent magnets add up in phase with the magnetic flux due to the coil. Thus, the magnetic saturation might predominately occur in the armature at low frequencies and the end result is (nonlinear) compression. However, for hearing aid users with severe high-frequency hearing losses the loudspeaker input may get a large boost at high frequencies causing the drive level to be even higher at these frequencies. Fortunately, the armature displacement and the input force tends to be out of phase above the fundamental armature resonance frequency so the armature flux due to the coil and due to that of the permanent magnets do not add up in phase but may somewhat cancel each other out. Nevertheless, this analysis is carried out for low frequencies i.e. below the mechanical resonance frequency where the mechanical impedance is dominated by the stiffness. The analysis will be carried out in two steps in order to show the importance of taking the various constrains into account when analyzing the loudspeaker properties. First, the armature flux due to the permanent magnets alone will be analyzed for the general case and secondly, it will be analyzed when the stability criterion is taken into account. The armature flux due to the permanent magnets alone was stated earlier:

$$\Phi_{a,0}(x) = 2B_r \frac{A}{D} \frac{\alpha}{(\alpha+1)^2 - \left(\frac{x}{D}\right)^2} x. \tag{5.16}$$

Introducing the linear part of the armature flux

$$\Phi_{a,0,lin}(x) = 2B_r A \frac{\alpha}{(\alpha+1)^2} \frac{x}{D} \tag{5.17}$$

Eq. (5.16) could be written

$$\Phi_{a,0}(x) = \Phi_{a,0,lin}(x) \frac{(\alpha+1)^2}{(\alpha+1)^2 - \left(\frac{x}{D}\right)^2}. \tag{5.18}$$

Looking at Eq. (5.17) it is apparent that the small-signal armature flux - due to the permanent magnets alone - is proportional to the normalized armature displacement x/D and the constant factor $2B_r A\alpha/\left(\alpha+1\right)^2$. There are at least three important points of information here. First, it is the ratio x/D which is important for the armature flux and the potential saturation of the armature. Secondly, the flux is proportional to the air gap area A but as the armature width and the air gap area scale together the flux intensity (or the B-field) in the armature is constant with A. Thus, Eq. (5.17) indicates that the armature flux - due to the permanent magnets only - is independent of the size of the loudspeaker. Third, the factor that only depends on α suggests that a larger α i.e. a longer magnet or one with lower recoil permeability will result in less armature flux. The flux is also proportional to the remanence B_r. The nonlinear part of the armature flux i.e. the second factor of Eq. (5.18) is plotted in Fig. 10.1. This figure shows that the armature flux due to the permanent magnets alone can be determined with sufficient accuracy using the linearized expression Eq. (5.17) for $\alpha > 2$. In any case, the linearized prediction tends to underestimate the armature flux set up by the permanent magnets.

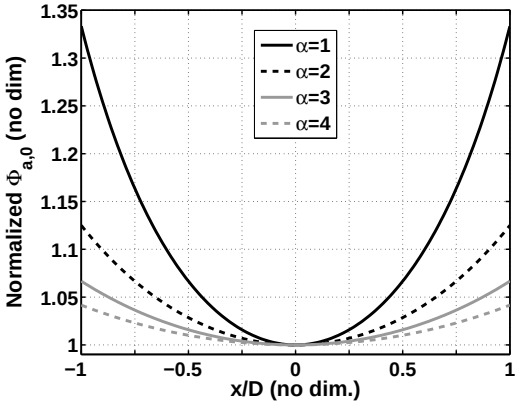

Figure 10.1: Nonlinear part of the armature flux due to the permanent magnets only i.e. the rightmost factor of Eq. (5.18) which only depends on α.

The above conclusions are valid for the general balanced-armature loudspeaker i.e. stable as well as unstable loudspeaker designs. In order to focus on stable loudspeaker designs only one may apply the stability criterion. The above analysis also completely ignores the shape of the armature which affects the stability as well as the magnetic flux intensity i.e. the B-field in the armature. Obviously, it is the strength of the B-field that determines whether the armature material saturates and it is the stiffness of the armature that determines whether the loudspeaker is stable or not. Thus, the next step is to investigate the armature flux for the critically stable loudspeaker. First, the stability of the loudspeaker is taken into account by substituting Eq. (9.10) into Eq. (5.16). This yields

$$\Phi_{a,0,st}\left(x\right) = \frac{\mu_0}{B_r}\frac{\alpha\left(\alpha+2\right)^2}{\left(\alpha+1\right)^3}\frac{\left(\alpha+1\right)^2}{\left(\alpha+1\right)^2-\left(\frac{x}{D}\right)^2}k_a x \tag{10.1}$$

with

$$\frac{A}{D} < \frac{\mu_0}{2B_r^2}\frac{(\alpha+2)^2}{\alpha+1}k_a \tag{9.9}$$

ensuring the stability. In order to also investigate the B-field and the required armature dimensions it is necessary to make an assumption about the shape of the armature. Here it is simply assumed that the armature has a constant rectangular cross-sectional area and the limiting case of Eq. (9.11) can be substituted into Eq. (5.17). This yields

$$\Phi_{a,0,st}(x) = 2B_r\frac{\mu_0 E}{8B_r^2}\frac{(\alpha+2)^2}{\alpha+1}\left(\frac{h_a}{l_a}\right)^3 w_a\frac{\alpha}{(\alpha+1)^2}x\frac{(\alpha+1)^2}{(\alpha+1)^2-\left(\frac{x}{D}\right)^2} \tag{10.2}$$

and the armature B-field becomes

$$\boxed{B_{a,0,st}(x) = \frac{\Phi_{a,0,st}(x)}{h_a w_a} = \frac{\mu_0 E}{4B_r}\frac{\alpha(\alpha+2)^2}{(\alpha+1)^3}\frac{h_a^2}{l_a^3}\frac{(\alpha+1)^2}{(\alpha+1)^2-\left(\frac{x}{D}\right)^2}x} \tag{10.3}$$

with

$$\frac{A}{w_a} < \frac{\mu_0 E}{8B_r^2}\frac{(\alpha+2)^2}{\alpha+1}\left(\frac{h_a}{l_a}\right)^3 D \tag{9.11}$$

ensuring the stability. In this derivation it was chosen to eliminate A and w_a from the expression for the armature B-field but B_r or D could have been eliminated instead by substituting the expression for the relevant parameter expressed in terms of the stability criterion (Eq. (9.11)) into Eq. (5.16). However, the maximum displacement D and the magnetic remanence of the permanent magnets will often be known beforehand and it will not be possible to adjust them freely as it is the case with the ratio A/w_a. Let us investigate each parameter of the armature B-field further. When choosing an armature material with appropriate magnetic properties the Young's modulus E might not be of primary concern but according to Eq. (10.3) it plays an important role. With the stability criterion applied it turns out that the armature B-field is in fact inversely proportional to the remanence B_r and not proportional as Eq. (5.16) suggested. This is an important observation and it has to do with the fact that the magnetic stiffness compensation k_Φ is proportional to B_r^2 and that the armature stiffness has to be increased to ensure stability whenever k_Φ is increased. The second factor that depends on α is plotted in Fig. 10.2. For very small values of α it starts out at zero and it goes towards one for large values. The transition in the relevant α-range is shown.

Next, consider the armature length l_a. By increasing the armature length the armature flux can be reduced significantly as $B_{a,0,st} \propto 1/l_a^3$. This has to do with the fact that the armature stiffness k_a is greatly reduced when the armature length is increased. The length of the armature will often be constrained by the allowed maximum size of the loudspeaker and looking at the stability criterion it can be observed that any increase in the armature length will require a much smaller air gap area A or a much larger armature width w_a. A very small air gap area may be

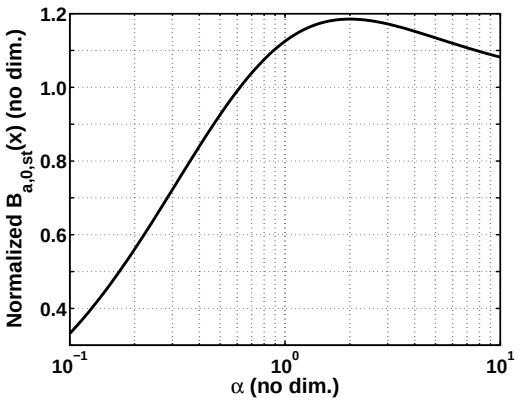

Figure 10.2: Second factor of Eq. (10.3) showing the B-field dependence on α not considering the nonlinear fourth factor.

problematic as this will increase the amount of leakage flux relative to useful air gap flux and this will effectively reduce α and thereby increase the nonlinear behavior of the force factor, inductance and the magnetic stiffness compensation. A very wide armature may also be problematic as this will reduce the coil performance as the electrical resistance is increased for each winding.

The armature B-field may also be reduced by reducing the height h_a and thereby the stiffness of the armature. However, according to the stability criterion this will put the same demands on the air gap area and the armature width as an increase in the armature length did. It is the increase in armature length that has the more profound effect on the armature B-field. Eq. (10.3) also suggests that the B-field is proportional to the armature displacement x and that the ratio A/w_a required for stability is simply scaled by the maximum displacement D. This means that larger balanced-armature loudspeakers - where larger armature displacements x are expected - will be more prone to armature saturation unless the ratio h_a^2/l_a^3 is reduced to compensate. Fortunately an increase in x by a factor of 10 will only require an increase in armature length by a factor of $\sqrt[3]{10} \approx 2.2$ to compensate. Unfortunately, the unwanted resonance frequencies of the armature will occur at lower frequencies as the armature length is increased.

The next step is to determine the armature flux due to the coil current. As we are only concerned with the armature flux at low frequencies the mechanical impedance is dominated by the stiffness. Assuming that the distortion force factor can be ignored the low-frequency mechanical differential equation Eq. (6.4) reduces to

$$\mathcal{F}_\Phi(x,i) = k_\Phi(x)\,x + T(x)\,i = k_{ma}x \Leftrightarrow \tag{10.4}$$

$$i(x) \approx \frac{[k_{ma} - k_\Phi(x)]}{T(x)}x = \frac{k_{eff}(x)}{T(x)}x. \tag{10.5}$$

where k_{ma} is the total mechanical stiffness including acoustic back volume, armature stiffness and diaphragm suspension but not including the magnetic stiffness compensation. Equation (10.5) provides a simple relationship between the coil current and the armature displacement at low

frequencies where it is assumed that the loudspeaker is largely linear or more precisely that the force $T(x)\,i$ is much larger than the force $T_{me,d}(x,i)\,i$. In sec. 7.1 the ratio between the two forces was investigated in more detail. Using Equations (5.32) and (5.36) Eq. (10.5) can be written

$$i \approx \frac{\left[k_{ma} - k_\Phi \frac{(\alpha+1)^4}{\left[(\alpha+1)^2 - \left(\frac{x}{D}\right)^2\right]^2}\right]}{T\frac{(\alpha+1)^2\left[(\alpha+1)^2 + \left(\frac{x}{D}\right)^2\right]}{\left[(\alpha+1)^2 - \left(\frac{x}{D}\right)^2\right]^2}} x. \tag{10.6}$$

Substituting the expression for the small-signal force factor (Eq. (5.35)) and rewriting yields:

$$\boxed{i \approx \frac{1}{2B_rN}\frac{D}{A}\frac{\left[(\alpha+1)^2 - \left(\frac{x}{D}\right)^2\right]^2 - \frac{k_\Phi}{k_{ma}}(\alpha+1)^4}{\alpha\left[(\alpha+1)^2 + \left(\frac{x}{D}\right)^2\right]} k_{ma}x}. \tag{10.7}$$

For small displacements where $x << D$ Eq. (10.7) may be linearized to

$$\boxed{i|_{x<<D} \approx \frac{1}{2B_rN}\frac{D}{A}\frac{(\alpha+1)^2}{\alpha}\left(1 - \frac{k_\Phi}{k_{ma}}\right)k_{ma}x}, \tag{10.8}$$

and the nonlinear expression for the coil current can then be expressed in terms of the linear one and a nonlinear function of α, x/D and k_Φ/k_{ma}:

$$i \approx i|_{x<<D}\,\frac{1}{1 - \frac{k_\Phi}{k_{ma}}}\frac{1}{(\alpha+1)^2}\frac{\left[(\alpha+1)^2 - \left(\frac{x}{D}\right)^2\right]^2 - \frac{k_\Phi}{k_{ma}}(\alpha+1)^4}{(\alpha+1)^2 + \left(\frac{x}{D}\right)^2}. \tag{10.9}$$

The relationship between current and displacement expressed in Eq. (10.7) is used in the following analysis of the armature flux due to coil current. First, it is informative to plot the normalized or nonlinear part of the coil current versus the armature displacement using the last 3 factors of Eq. (10.9). Figure 10.3 shows the relationship between the coil current and the armature displacement for a loudspeaker design where $k_\Phi/k_{ma} = 0.5$ which implies that the loudspeaker is critically stable for $\alpha \approx 0.85$ according to Eq. (9.6) and Fig. 9.2.

For the critically stable loudspeaker the magnetic force due to the permanent magnet alone exactly balances out the mechanical force due to the stiffness of the armature when the armature displacement is D and this is why no current is required to maintain this position. Any increase in the stiffness k_{ma} relative to the critically stable case will greatly increase the required current for the full armature displacement. Looking at Eq. (10.7) one may observe that an increase in k_{ma} makes the numerator in the third factor increase while i is also scaled directly with k_{ma}. Thus, it will require much less power to drive the critically stable loudspeaker to its maximum displacement. Eq. (10.7) can be rewritten into

$$i \approx \frac{k_{ma}}{2B_r N}\frac{D^2}{A}\frac{\left[(\alpha+1)^2-\left(\frac{x}{D}\right)^2\right]^2-\frac{k_\Phi}{k_{ma}}(\alpha+1)^4}{\alpha\left[(\alpha+1)^2+\left(\frac{x}{D}\right)^2\right]}\frac{x}{D}. \tag{10.10}$$

Plotting the last two factors of Eq. (10.10) will give an impression about the required coil current for a given armature displacement. This is done in Fig. 10.4. Fig. 10.4(a) shows the result for $\alpha = 1$ and Fig. 10.4(b) shows the result for $\alpha = 4$. The results are shown for different mechanical stiffnesses. The lowest mechanical stiffness corresponds to critical stability where $k_{ma} = k_{ma,st}$.

Inserting Eq. (10.7) into Eq. (5.19), the armature flux only due to current may be expressed in terms of the armature displacement:

$$\boxed{\Phi_{a,i}(x) \approx \frac{\mu_0}{B_r}\frac{\alpha+1}{\alpha}\frac{\left[(\alpha+1)^2-\left(\frac{x}{D}\right)^2\right]^2-\frac{k_\Phi}{k_{ma}}(\alpha+1)^4}{(\alpha+1)^4-\left(\frac{x}{D}\right)^4}k_{ma}x} \tag{10.11}$$

For small armature displacements where $x << D$ or for the case where $\alpha >> 1$ this can be linearized to

$$\boxed{\Phi_{a,i,lin}(x) \approx \frac{\mu_0}{B_r}\frac{\alpha+1}{\alpha}\left(1-\frac{k_\Phi}{k_{ma}}\right)k_{ma}x}. \tag{10.12}$$

and the nonlinear expression for the armature flux due to coil current can then be expressed in terms of the linear one and a nonlinear function of α, x/D and k_Φ/k_{ma}:

$$\Phi_{a,i}(x) \approx \Phi_{a,i,lin}(x)\frac{1}{1-\frac{k_\Phi}{k_{ma}}}\frac{\left[(\alpha+1)^2-\left(\frac{x}{D}\right)^2\right]^2-\frac{k_\Phi}{k_{ma}}(\alpha+1)^4}{(\alpha+1)^4-\left(\frac{x}{D}\right)^4}. \tag{10.13}$$

Notice that A/D is eliminated in Equations (10.11) to Eq. (10.13) so obviously the relationship

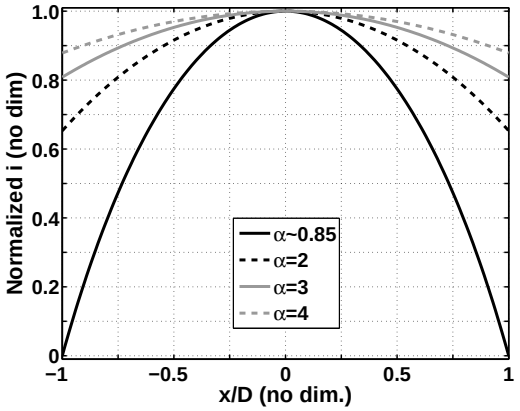

Figure 10.3: Nonlinear part of the coil current i.e. the last 3 factors of Eq. (10.9). This is plotted for various values of α with k_Φ/k_{ma} fixed at 0.5. $\alpha \approx 0.85$ is the critically stable case.

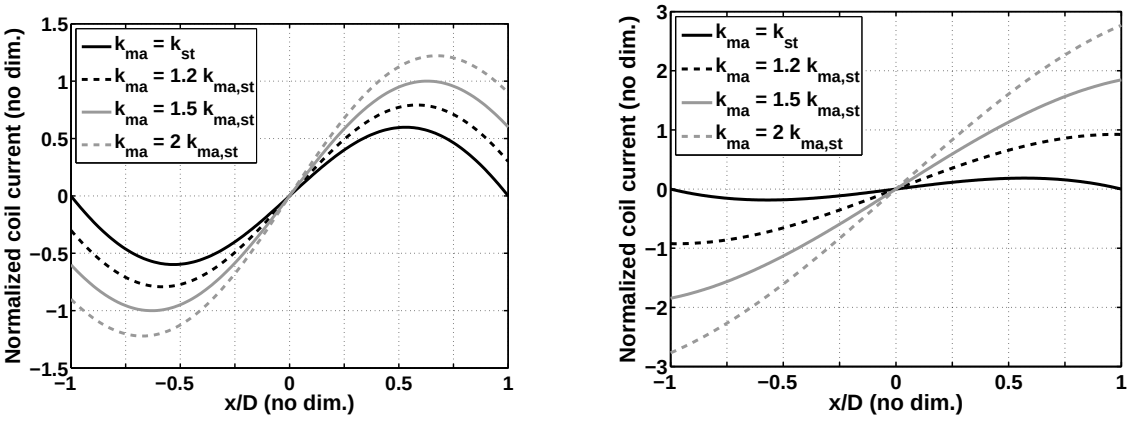

(a) $\alpha = 1$. (b) $\alpha = 4$.

Figure 10.4: Relationship between coil current and armature displacement for various mechanical stiffnesses k_{ma}. The result is valid at low frequencies where the mechanical impedance is dominated by the stiffness. Results are shown for two different values of α.

between armature flux due to current and armature displacement does not depend on the air gap area A and only the nonlinear part of the expression depends on D. As always, the ratio A/D may be chosen according to the stability criterion in Eq. (9.9).

An important lesson learned from Eq. (10.11) or Eq. (10.12) is the fact that the armature flux due to coil current is proportional to the total mechanical stiffness k_{ma} for a given ratio k_Φ/k_{ma}. Recall that for a simple shaped armature its stiffness is proportional to the cubed armature height. Thus, increasing the armature height in order to reduce the flux intensity (i.e. the B-field) is only a good solution if the armature stiffness contributes little to the total mechanical stiffness k_{ma} (i.e. if the stiffness of the back volume is quite large). Another important point is the fact that $\Phi_{a,i}$ is proportional to x meaning that larger loudspeakers designed for large displacements will be more prone to magnetic saturation in the armature. Other than that, it is clear that α should be as large as possible as this will minimize $(\alpha+1)/\alpha$ as well as maximize the possible ratio k_Φ/k_{ma} before instability occurs. B_r should be as large as possible in order to minimize $\Phi_{a,i}$. The normalized or nonlinear part of the armature flux due to coil current i.e. the last two factors of Eq. (10.13) is plotted in Fig. 10.5 for various values of α and for two different ratios of k_Φ/k_{ma}. Looking at this result it is clear that the linearized expression for the current induced armature flux should only be used for $x << D$ or for larger values of x if α is large and/or the ratio k_Φ/k_{ma} is small, otherwise the linearized expression will overestimate the flux by quite a bit.

Finally, the total armature flux due to current and displacement - expressed only in terms of the displacement - is:

$$\Phi_a(x) \approx \Phi_{a,0}(x) + \Phi_{a,i}(x) \Leftrightarrow \tag{10.14}$$

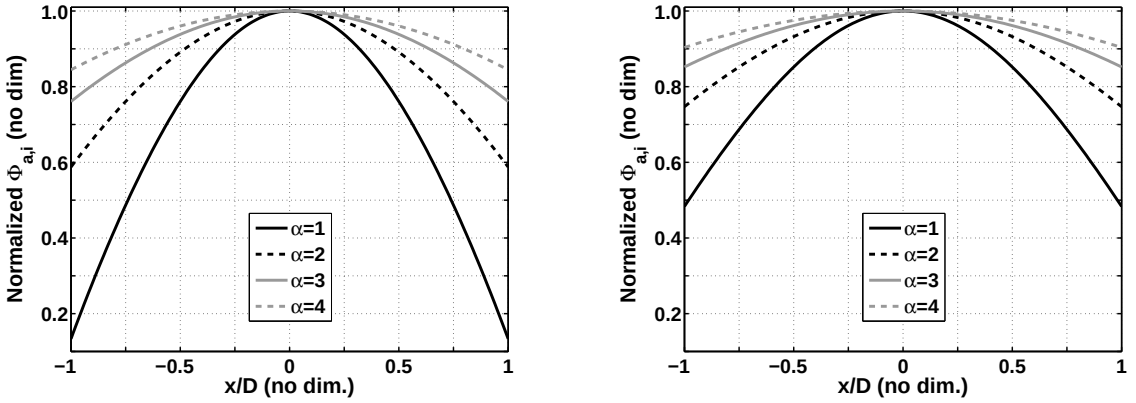

(a) $k_\Phi/k_{ma} = 0.5$. (b) $k_\Phi/k_{ma} = 0.2$.

Figure 10.5: Low-frequency relationship between the nonlinear part of the armature flux due to coil current vs the normalized armature displacement. Results are shown for two different ratios between k_Φ and k_{ma}. $k_\Phi/k_{ma} = 0.5$ corresponds to a loudspeaker where the stiffness due to the back volume and the diaphragm suspension is small compared to the armature stiffness. $k_\Phi/k_{ma} = 0.2$ corresponds to a loudspeaker where the stiffness due to the back volume and the diaphragm is maybe 1.5-3 times that of the armature stiffness.

$$\begin{aligned}\Phi_a(x) \approx & 2B_r\frac{A}{D}\frac{\alpha}{(\alpha+1)^2-\left(\frac{x}{D}\right)^2}x \\ & + \frac{\mu_0}{B_r}\frac{\alpha+1}{\alpha}\frac{\left[(\alpha+1)^2-\left(\frac{x}{D}\right)^2\right]^2-\frac{k_\Phi}{k_{ma}}(\alpha+1)^4}{(\alpha+1)^4-\left(\frac{x}{D}\right)^4}k_{ma}x.\end{aligned} \tag{10.15}$$

For small armature displacements where $x << D$ or for the case where $\alpha >> 1$ this can be linearized to

$$\boxed{\Phi_{a,lin}(x) \approx 2B_r\frac{A}{D}\frac{\alpha}{(\alpha+1)^2}x + \frac{\mu_0}{B_r}\frac{\alpha+1}{\alpha}\left(1-\frac{k_\Phi}{k_{ma}}\right)k_{ma}x} \tag{10.16}$$

with

$$k_\Phi = \frac{2B_r^2}{\mu_0}\frac{A}{D}\frac{\alpha^2}{(\alpha+1)^3}. \tag{5.31}$$

In figure 10.3 it was already shown how the coil current is zero when the armature is fully displaced for the critically stable case. This means that the armature flux due to coil current is also zero at $x = D$ for the critically stable case. It is informative to set up expressions for the armature flux due to the permanent magnets and due to that of the coil current at $x = D$. Substituting $x = D$ into Eq. (5.16) yields:

$$\boxed{\Phi_{a,0}(D) = 2AB_r\frac{1}{\alpha+2}}. \tag{10.17}$$

The stability and the stiffness of the armature may be taken into account by substituting $x = D$ into Eq. (10.1). This yields

$$\boxed{\Phi_{a,0,st}(D) = \frac{\mu_0}{B_r}\frac{\alpha+2}{\alpha+1}k_a D} \tag{10.18}$$

with

$$A < \frac{\mu_0}{2B_r^2}\frac{(\alpha+2)^2}{\alpha+1}k_a D \tag{9.9}$$

ensuring the stability. For an armature with a simple shape with constant width and height the armature B-field can be written

$$B_{a,0}(D) = \frac{\Phi_{a,0}(D)}{w_a h_a} = \frac{2AB_r}{w_a h_a}\frac{1}{\alpha+2}. \tag{10.19}$$

Now consider the armature flux due to coil current. Substituting $x = D$ into Eq. (10.11) yields:

$$\boxed{\Phi_{a,i}(D) \approx \frac{\mu_0 D}{B_r}\frac{\alpha+1}{\alpha}\frac{\left[(\alpha+1)^2-1\right]^2 - \frac{k_\Phi}{k_{ma}}(\alpha+1)^4}{(\alpha+1)^4-1}k_{ma}} \tag{10.20}$$

Using Equations (10.17) and (10.20) it is possible to determine which part of the magnetic flux is the dominant one. When this is determined one may try to minimize the most significant part in order to avoid compression due to magnetic saturation. If, for instance, $\Phi_{a,i}(D)$ is much larger than $\Phi_{a,0}(D)$ then an increase in B_r will reduce the total armature flux.

It should now be clear that for a critically stable design where the acoustic stiffness is negligible, the armature flux at $x = D$ can be predicted using Eq. (10.17). However, as the stiffness of the loudspeaker becomes greater than what is needed in order to keep the loudspeaker stable, the armature flux due to the coil current quickly increases. This is demonstrated in Fig. 10.6 where the last 3 factors of Eq. (10.20) are plotted as function of k_{ma} for various values of α and with k_Φ always fixed at 1.

Recall that the armature stiffness is proportional to the cubed armature height whereas the maximum magnetic flux before saturation is only proportional to the armature height. This means that although an increase in the armature height will increase the maximum flux capability of the armature the much increased mechanical stiffness will require a much larger coil current and armature flux (see Fig. 10.6) in order for a full armature displacement, thus reducing efficiency and most likely also the maximum displacement of the armature. Remember that one can only rely on the armature stiffness to keep the loudspeaker stable as the acoustic stiffness is close to zero for very slow diaphragm variations. For most miniature balanced-armature loudspeakers the acoustic stiffness is significant compared to the armature stiffness often making the mechanical stiffness k_{ma} more than twice as large as the armature stiffness k_a that keeps the loudspeaker

stable. This means that for miniature balanced-armature loudspeakers one will always have to consider the armature flux due to the coil current. For larger balanced-armature loudspeakers with large back volumes where the mechanical stiffness is dominated by the armature stiffness the maximum armature flux may be determined according to Eq. (10.17) assuming that the design is close enough to being critically stable.

10.1 Maximum Output

If the most narrow part of the armature has a cross-sectional area of $w_a h_a$ then the armature flux at this point is

$$\begin{aligned}\Phi_a(x) = B_a(x)\, w_a h_a \approx & 2B_r \frac{A}{D} \frac{\alpha}{(\alpha+1)^2 - \left(\frac{x}{D}\right)^2} x \\ & + \frac{\mu_0}{B_r} \frac{\alpha+1}{\alpha} \frac{\left[(\alpha+1)^2 - \left(\frac{x}{D}\right)^2\right]^2 - \frac{k_\Phi}{k_{ma}}(\alpha+1)^4}{(\alpha+1)^4 - \left(\frac{x}{D}\right)^4} k_{ma} x. \end{aligned} \tag{10.21}$$

The magnetic saturation will occur in the most narrow part of the armature. If the saturation point B_s of the armature material is known the maximum low-frequency armature displacement x_{max} can be determined numerically by solving

$$\begin{aligned} B_s w_a h_a \approx & 2B_r \frac{A}{D} \frac{\alpha}{(\alpha+1)^2 - \left(\frac{x}{D}\right)^2} x \\ & + \frac{\mu_0}{B_r} \frac{\alpha+1}{\alpha} \frac{\left[(\alpha+1)^2 - \left(\frac{x}{D}\right)^2\right]^2 - \frac{k_\Phi}{k_{ma}}(\alpha+1)^4}{(\alpha+1)^4 - \left(\frac{x}{D}\right)^4} k_{ma} x. \end{aligned} \tag{10.22}$$

with respect to x.

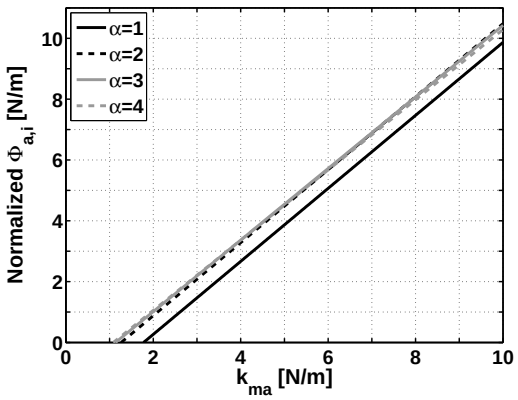

Figure 10.6: Normalized armature flux (last 3 factors of Eq. (10.20)) due to coil current at $x = D$ vs the total mechanical stiffness k_{ma} for various values of α and with the small-signal magnetic stiffness compensation k_Φ always fixed at 1.

10.2 Armature Saturation for the Critically Stable Loudspeaker

In sec. 10 it was demonstrated that the coil current and thus the armature flux due to coil current is zero for $x = D$ for the critically stable design. Consider the armature flux due to the permanent magnets:

$$\Phi_{a,0}(x) = 2B_r \frac{A}{D} \frac{\alpha}{(\alpha+1)^2 - \left(\frac{x}{D}\right)^2} x. \tag{5.16}$$

Differentiating with respect to x yields

$$\frac{d\Phi_{a,0}(x)}{dx} = 2B_r \frac{A}{D} \frac{\alpha\left[(\alpha+1)^2 + \left(\frac{x}{D}\right)^2\right]}{\left[(\alpha+1)^2 - \left(\frac{x}{D}\right)^2\right]^2}. \tag{10.23}$$

Eq. (10.23) is always positive meaning that the the armature flux increases for every increase in x. This means that the maximum armature flux due to the permanent magnets can be found - not surprisingly - when $x = D$. Thus, the maximum magnetic flux in the armature due to the permanent magnets is

$$\Phi_{a,0,max} = \Phi_{a,0}(D) = 2AB_r \frac{1}{\alpha+2}. \tag{10.17}$$

In Fig. 10.4 it was shown how the coil current is zero for $x = D$ for the critically stable loudspeaker. Assuming that the total armature flux due to coil current and the permanent magnets is at its maximum for $x = D$, the maximum armature flux for the critically stable loudspeaker can be determined using Eq. (10.17). Thus, the magnetic flux density in the simple shaped armature for maximum armature displacement is

$$\boxed{B_{a,0,max} = B_{a,0}(D) = \frac{2AB_r}{w_a h_a} \frac{1}{\alpha+2}}. \tag{10.24}$$

If the magnetic saturation level B_s is defined for the armature material the armature B-field should be kept below this level at all times:

$$B_s > B_{a,0}(D) = \frac{2AB_r}{w_a h_a} \frac{1}{\alpha+2}. \tag{10.25}$$

This may be rewritten to specify the minimum armature cross sectional area in order to avoid armature saturation:

$$\boxed{w_a h_a > \frac{2AB_r}{B_s} \frac{1}{\alpha+2}} \quad \text{avoids armature saturation.} \tag{10.26}$$

This can of course also be interpreted as a constraint to the ratio between the air gap area and the armature width:

$$\boxed{\frac{A}{w_a} < \frac{(\alpha+2)\,h_a}{2B_r}B_s} \qquad \text{avoids armature saturation.} \tag{10.27}$$

For the limiting case

$$\frac{A}{w_a} = \frac{(\alpha+2)\,h_a}{2B_r}B_s \tag{10.28}$$

we will say that the armature is critically saturated (for $x = D$). Thus, Equations (10.26) to (10.27) provide a saturation constraint to the loudspeaker design. Just as the critical stability was applied as a constraint to the loudspeaker equations, one of the above inequalities can be used to impose yet another constraint to the design. The stability criterion Eq. (9.11) constrains the ratio A/w_a if the armature stiffness is written in terms of the simple armature geometry:

$$\frac{A}{w_a} < \frac{\mu_0 ED}{8B_r^2}\frac{(\alpha+2)^2}{\alpha+1}\left(\frac{h_a}{l_a}\right)^3 = \frac{(\alpha+2)\,h_a}{2B_r}\frac{\mu_0 ED\,(\alpha+2)\,h_a^2}{4B_r\,(\alpha+1)\,l_a^3} \tag{10.29}$$

Comparing the last factors of Equations (10.27) and (10.29) it is possible to write up 3 different cases:

$$\text{Case (I):} \qquad B_s < \frac{\mu_0 ED}{4B_r}\frac{(\alpha+2)}{(\alpha+1)}\frac{h_a^2}{l_a^3}. \tag{10.30}$$

In this case the armature will be magnetically saturated before the design becomes critically stable as A is increased. This may or may not be a desirable feature. It may be possible to realize a design with a very high stiffness ratio $k_r = k_\Phi/k_a$ (and thus a very low effective stiffness) because the nonlinear magnetic force tends to be compressed due to the armature saturation. This is then a way of avoiding instability because the magnetic force does not increase beyond a certain point when saturation occurs. If the magnetic force remains constant with increasing displacement then the magnetic stiffness compensation can be thought of as having a decreasing value for large displacements under the condition that the armature saturates. On the other hand, the armature will be more prone to compressing the AC-signal set up by the coil while the armature is displaced close to one of the magnets.

$$\text{Case (II):} \qquad B_s = \frac{\mu_0 ED}{4B_r}\frac{(\alpha+2)}{(\alpha+1)}\frac{h_a^2}{l_a^3}. \tag{10.31}$$

In this case the armature will be magnetically saturated just as the design becomes critically stable as A is increased. This means that the armature is magnetically saturated under full displacement

(with i = 0 A) and that the magnetic force on the armature exactly equals out the force due to the mechanical stiffness.

$$\text{Case (III):} \qquad B_s > \frac{\mu_0 E D}{4B_r}\frac{(\alpha+2)}{(\alpha+1)}\frac{h_a^2}{l_a^3}. \tag{10.32}$$

In this case the design will become critically stable before there is a chance that the armature gets magnetically saturated as the air gap area A is increased. This may be a desirable condition as this means that it is possible to make an efficient, critically stable design without the risk of running into compression effects due to saturation in the armature.

The armature height is usually easier to adjust than the armature length or width as the two latter have more impact on the overall dimensions of the receiver. Therefore, a smart design procedure is to first define the armature length l_a, the maximum armature displacement D and an α-value where larger values in general means that a longer permanent magnet is required and that the design will be more linear. Next the armature height can be chosen according to either Eq.(10.31) or Eq.(10.32):

$$\boxed{h_a \leq \sqrt{\frac{4B_r B_s}{\mu_0 E D}\frac{(\alpha+1)}{(\alpha+2)}l_a^3}}. \tag{10.33}$$

Choosing h_a according to Eq.(10.31) will ensure that the loudspeaker design becomes critically stable before it becomes critically saturated when A is increased. After the armature height has been chosen, the ratio A/w_a can be determined using the stability criterion Eq.(9.11) which is repeated here:

$$\boxed{\frac{A}{w_a} < \frac{\mu_0 E D}{8B_r^2}\frac{(\alpha+2)^2}{\alpha+1}\left(\frac{h_a}{l_a}\right)^3} \tag{9.11}$$

This procedure will ensure that the loudspeaker design is critically stable and that it also does not saturate for $x = D$. It may seem like a surprising result that a thinner armature will ensure that the armature does not saturate before the loudspeaker becomes unstable when A is increased. This is due to the fact that A/w_a is proportional to the armature height for the saturation criterion whereas A/w_a is proportional to the cubed armature height in the stability criterion. Thus, as the armature height h_a is increased the required air gap area A that ensures a critically stable design will quickly become much greater than the air gap area that will result in armature saturation.

One may wonder whether there are any drawbacks to making the armature height smaller: The low-frequency CIP response (Eq.(11.15))) is independent of h_a except for - unsurprisingly - the part which has to do with the coil performance. The high-frequency CIP response, on the other hand, is proportional to h_a^2 (see. Eq.(11.41)). In order to avoid degrading the high-frequency efficiency, one should then choose an armature height as close to the limit as possible since an even thinner armature will quickly reduce the high-frequency efficiency. Thus, for a receiver

optimized for low-frequency use, one will be well off by choosing a thin armature as this will not affect the efficiency, the required air gap area will be reduced and the maximum armature displacement before saturation will be increased. This also means that the armature will operate at lower magnetic flux intensities and the B-field will tend to be less distorted. This is probably the opposite approach of what one would have (wrongly) taken had this analysis not been carried out: One might falsely choose a thick armature to start out with, thinking that this will help avoid magnetic saturation and thus increase the maximum displacement. However, this would be a very unwise approach according to this analysis. Since this analysis only takes the magnetic field due to the permanent magnets into account one still have to consider the magnetic field set up by the coil. In Chapter 10 it was shown that the armature flux due to coil current increases quickly with the armature stiffness. The flux capability is only proportional to the armature height whereas the armature stiffness is proportional to the cubed armature height so this also points towards a thinner armature.

Chapter 11

Efficiency of the Balanced-Armature Loudspeaker

In order to talk about the efficiency of a loudspeaker in a meaningful way, it is necessary to first establish a proper measure of loudspeaker efficiency. In [29] the Constant Input Power (CIP) response is suggested as a useful measure of loudspeaker efficiency. The CIP response is a frequency domain function that shows some relevant loudspeaker output (e.g. diaphragm velocity or sound pressure level) for 1 W of electrical input power. In other words, instead of normalizing the output to 1 V of drive voltage the output is normalized to 1 W of electrical input power. The CIP response makes it easy to compare the efficiency of different loudspeaker designs in any frequency range of interest. As the human ear is sensitive to sound pressure it will often make sense to use the sound pressure level as the relevant output parameter. For a miniature loudspeaker this sound pressure may be measured inside a small coupler and for a larger loudspeaker this may be the sound pressure in an anechoic chamber or maybe in a so-called normal listening room.

In this chapter, approximate expressions for the CIP armature velocity response will be developed in order to gain important insight into what really affects the efficiency of a balanced-armature loudspeaker. The efficiency will be considered in three different frequency ranges - low frequencies (below mechanical resonance), mid frequencies (at mechanical resonance) and for high frequencies (above mechanical resonance frequency).

The CIP armature velocity response can be written as the product of the CIP normalization function and the voltage-driven armature velocity response:

$$u_{CIP}(\omega) = f_{CIP}(\omega)\,|H_u(j\omega)|\,, \tag{11.1}$$

where the CIP normalization function is a function of the dynamic electrical input impedance only:

$$f_{CIP}(\omega) = |Z_E(j\omega)| \sqrt{\frac{1\text{ W}}{Re\{Z_E(j\omega)\}}}. \tag{11.2}$$

The armature velocity response

$$H_u(j\omega) = \frac{u(\omega)}{E_{\text{in}}(\omega)} = \frac{T}{(R_L + Lj\omega)\,Z_m(j\omega) + T^2} \tag{6.17}$$

and the electrical impedance

$$Z_E(j\omega) = R_L + Lj\omega + T^2 Y_m(j\omega) = R_L + Lj\omega + \frac{T^2 j\omega}{-m\omega^2 + rj\omega + 1/C_{eff}} \tag{6.20}$$

were derived in section 6.4 and are repeated here for clarity. The acoustic impedance $Z_A(j\omega) = Z_{AF}(j\omega) + Z_{AB}(j\omega)$ that loads the diaphragm may be reflected in the mechanical circuit (Fig. 6.3(b)) as an additional mechanical impedance $Z_{mA} = S_D^2 Z_A$ in series with the existing mechanical impedances. The significance of the acoustic impedance obviously depends on how large the acoustic impedance is compared to the mechanical one. For miniature balanced-armature loudspeakers the acoustic impedance of the back side of the diaphragm is usually important since the tiny back volume contributes significantly to the overall stiffness. Even as a first approximation this stiffness of the back volume should be taken into account.

In the next three sections, Eq. (11.1) will be investigated, and simplified expressions will be derived for each of the three frequency ranges. This is done in order to establish which loudspeaker parameters affect the efficiency in each frequency range.

11.1 Low Frequencies for $k_A = 0$

In this section the low-frequency Constant Input Power response is derived for the case where the acoustic load is zero or $k_{mA} << k_a - k_\Phi$. This result is hardly relevant for miniature balanced-armature loudspeakers since the stiffness of the back volume is usually significant. However, as the acoustic load is not directly part of the electromechanical balanced-armature transduction principle, it is still informative to investigate this simplified case. For large balanced-armature loudspeakers with larger back volumes the results of this section are also very relevant.

At low frequencies the electrical impedance will be dominated by the DC-resistance of the coil so

$$Re\{Z_E(j\omega)\} \approx R_L, \tag{11.3}$$

and the magnitude is

$$|Z_E(j\omega)| \approx R_L. \tag{11.4}$$

This implies that the CIP normalization function (Eq. (11.2)) becomes

$$f_{CIP} \approx \sqrt{R_L}\sqrt{1\ \mathrm{W}}. \tag{11.5}$$

At low frequencies the mechanical impedance is dominated by the stiffness part which is due to three different terms: The armature stiffness, the back volume stiffness and the negative magnetic stiffness compensation. Again, assuming that R_L is the significant part of the electrical impedance which is therefore much larger than $Lj\omega$ the velocity response (Eq. (6.17)) can be written

$$H_u(j\omega) \approx \frac{T}{R_L \frac{1}{C_{eff} j\omega} + T^2} = \frac{TC_{eff}}{R_L} \frac{j\omega}{1 + j\frac{\omega}{\omega_0}} \tag{11.6}$$

with

$$\omega_0 = \frac{R_L}{T^2 C_{eff}} = \frac{R_L}{T^2} k_{eff}. \tag{11.7}$$

For sufficiently small frequencies where $\omega << \omega_0$ Eq. (11.6) may be reduced to

$$H_u(j\omega) \approx \frac{TC_{eff}}{R_L} j\omega. \tag{11.8}$$

Substituting Equations (11.5) and (11.8) into Eq. (11.1) yields the CIP armature velocity response for low frequencies:

$$\boxed{u_{CIP}(\omega) \approx \frac{TC_{eff}\omega}{\sqrt{R_L}} \sqrt{1\ \mathrm{W}} = \frac{T\omega}{\sqrt{R_L} k_{eff}} \sqrt{1\ \mathrm{W}}}. \tag{11.9}$$

It is interesting, and maybe not surprising, to see that in order to maximize the loudspeaker efficiency at low frequencies one should maximize the ratio $T/\sqrt{R_L}$ as this will produce a large armature input force (Ti) for a given electrical power loss ($R_L i^2$) in the resistance. Furthermore, this force is driving a compliance (C_{eff}) at low frequencies and this should be as large as possible to create the largest displacement and thus the largest sound pressure level for a given acoustic load on the front side of the loudspeaker. If the force factor is written in terms of the electrical inductance and the magnetic stiffness compensation ($T^2 = k_\Phi L$) it is possible to write the CIP response in terms of the electrical cut-off frequency (see Eq. (5.116)):

$$u_{CIP}(\omega) \approx \frac{\sqrt{L}\sqrt{k_\Phi}\omega}{\sqrt{R_L} k_{eff}} \sqrt{1\ \mathrm{W}} = \frac{\omega}{\sqrt{\omega_{e,cut}}} \frac{\sqrt{k_\Phi}}{k_{eff}} \sqrt{1\ \mathrm{W}}. \tag{11.10}$$

Eq. (11.10) reveals that for a fixed ratio $\sqrt{k_\Phi}/k_{eff}$, low-frequency efficiency and high electrical cut-off frequency are two conflicting interests. A highly efficient transducer with low electrical cut-off frequency might therefore need to have its pressure response equalized.

Being concerned with the efficiency of stable loudspeakers only, the stability constraint can be imposed by writing $T/\sqrt{R_L}$ for the stable case using Eq. (9.18):

$$\frac{T_{st}}{\sqrt{R_L}} = \frac{\frac{\mu_0 N}{B_r}\frac{\alpha(\alpha+2)^2}{(\alpha+1)^3}k_a}{\sqrt{R_L}} = \frac{\mu_0}{B_r}\frac{N}{\sqrt{R_L}}\frac{\alpha\left(\alpha+2\right)^2}{\left(\alpha+1\right)^3}k_a. \tag{11.11}$$

Using the result from Eq. (5.97) the ratio $N/\sqrt{R_L}$ between the coil windings and the square root of the DC-resistance can be written in terms of the coil geometry and the properties of the wire:

$$\frac{T_{st}}{\sqrt{R_L}} = \frac{\mu_0}{B_r}\sqrt{\frac{F_f l_c}{\pi\rho_w}}\sqrt{\frac{1}{1+\frac{P_c}{\pi t_c}}}\frac{\alpha\left(\alpha+2\right)^2}{\left(\alpha+1\right)^3}k_a \qquad \text{for critically stable receiver.} \tag{11.12}$$

Substituting Eq. (11.12) and $k_{eff,st}$ (Eq. (9.33)) for the critically stable loudspeaker into Eq. (11.9) yields:

$$u_{CIP,st}\left(\omega\right) \approx \frac{\mu_0}{B_r}\sqrt{\frac{F_f l_c}{\pi\rho_w}}\sqrt{\frac{1}{1+\frac{P_c}{\pi t_c}}}\frac{\alpha\left(\alpha+2\right)^2}{\left(\alpha+1\right)^3}k_a\frac{\left(\alpha+1\right)^4}{2\alpha^2+4\alpha+1}\frac{1}{k_a}\omega\sqrt{1\ \mathrm{W}} \Leftrightarrow \tag{11.13}$$

$$\boxed{u_{CIP,st}\left(\omega\right) \approx \frac{\mu_0}{B_r}\sqrt{\frac{F_f l_c}{\pi\rho_w}}\sqrt{\frac{1}{1+\frac{2(w_c+h_c)}{\pi t_c}}}\frac{\alpha\left(\alpha+1\right)\left(\alpha+2\right)^2}{2\alpha^2+4\alpha+1}\omega\sqrt{1\ \mathrm{W}}} \tag{11.14}$$

with

$$\frac{A}{D} < \frac{\mu_0}{2B_r^2}\frac{\left(\alpha+2\right)^2}{\alpha+1}k_a \tag{9.9}$$

ensuring the stability of the design. If the coil dimensions are rewritten in terms of the armature geometry Eq. (11.14) becomes:

$$\boxed{u_{CIP,st}\left(\omega\right) \approx \frac{\mu_0}{B_r}\sqrt{\frac{F_f F_{cl} l_a}{\pi\rho_w}}\sqrt{\frac{1}{1+\frac{2(w_a+h_a+2D)}{\pi t_c}}}\frac{\alpha\left(\alpha+1\right)\left(\alpha+2\right)^2}{2\alpha^2+4\alpha+1}\omega\sqrt{1\ \mathrm{W}}}. \tag{11.15}$$

Keeping Eq. (5.61) i mind, it may not come as a surprise that the low-frequency efficiency is inversely proportional to the magnetic remanence B_r: k_{eff} is proportional to k_Φ which is proportional to B_r^2 whereas the force factor T is only proportional to B_r. Notice also that the efficiency is independent of the absolute value of the air gap height (except for the coil performance) - only the ratio $\alpha = D_M/D$ is important. In terms of optimizing the low-frequency efficiency the first factor of Eq. (11.14) speaks for itself but it is informative to plot the fourth factor as a function of α to see how the low-frequency efficiency is influenced by the magnet height. This is plotted in

Fig. 11.1.

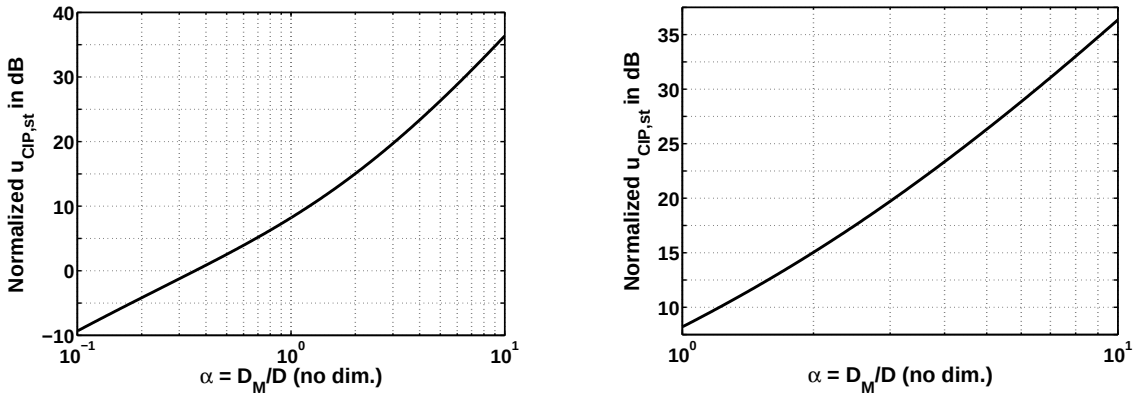

(a) Overview.

(b) Close-up.

Figure 11.1: Normalized low-frequency efficiency vs $\alpha = D_M/D$.

Fig. 11.1 clearly reveals that the low-frequency efficiency for $k_A = 0$ is strongly related to α: An increase from $\alpha = 1$ to $\alpha = 2$ will increase the low-frequency CIP response by more than 6 dB. Assuming that the efficiency of the amplifier is independent of the loudspeaker load this means that only one quarter of the power is required to produce a given armature velocity at low frequencies for the loudspeaker with $\alpha = 2$. As an example, 3 different loudspeaker designs will be compared, using different permanent magnetic materials but keeping the magnet length l_M and the air gap height D constant. It is presumed that all 3 loudspeakers are designed to be critically stable and that their coil performance are the same. Two of the materials (Alnico 8 and Ferrite) have about the same remanence B_r but different recoil permeability μ_r whereas Ferrite and NdFeB magnets have almost the same recoil permeability but quite different remanence. The values are summarized in Table 11.1.

Material:	l_M	D	B_r	μ_r	$D_M = l_M/\mu_r$	$\alpha = D_M/D$
Alnico 8	0.4 mm	0.1 mm	0.40 T	2.00	0.20 mm	2.00
NdFeB	0.4 mm	0.1 mm	1.35 T	1.05	0.38 mm	3.81
Ferrite	0.4 mm	0.1 mm	0.40 T	1.10	0.36 mm	3.64

Table 11.1: The magnetic remanence B_r and the important α-parameter for permanent magnets with the same length but made from different materials.

Going from Alnico 8 to NdFeB will result in a -10.6 dB reduction due to the increase in the magnetic remanence B_r. However, the increased α for NdFeB, due to the lower recoil permeability, will result in an increase in efficiency of about 8 dB according to Fig. 11.1(b). Thus, overall, the change from Alnico to NdFeB will cause a reduction in the low-frequency output of about 2.5 dB for the same input power assuming that the stiffness of the armature is designed so that the loudspeaker is critically stable. However, there is also a benefit related to the choice of NdFeB. The increased remanence of the NdFeB design will ensure that the armature does not saturate as easily (see Eq. (10.1), (10.3) and (10.11)) and the maximum SPL may thus be increased and the

risk of distortion due to compression is reduced. This discussion suggests that Ferrite magnets are the superior choice as these have a low recoil permeability of about 1.05 to 1.2 (depending on the grade) and at the same time a low remanence of about 0.35-0.45 T. According to Fig. 11.1 the reduced recoil permeability of Ferrite (compared to Alnico 8) will result in an increase in low-frequency efficiency of more than 6 dB. At the same time, in sec. 7 it was shown that an increased α-value (obtained with either NdFeB or Ferrite) will help reduce the nonlinear behavior of all the loudspeaker parameters and thereby reduce the distortion of the loudspeaker.

Optimizing the second and the third factor of Eq. (11.14) has to do with optimization of the coil. Eq. (5.98) has an interesting implication as it tells us that the low-frequency efficiency not only depends on the coil volume (and material resistivity) but also on the coil geometry: For a fixed coil volume the highest efficiency is obtained for a long coil as this will reduce the coil thickness t_c and the width and height (w_c and h_c) of the coil. Notice also how the wire diameter D_w and the number of windings N are irrelevant - the ratio $N/\sqrt{R_L}$ can be expressed completely in terms of the characteristic dimensions of the coil. From Eq. (11.14) it is easy to see that a doubling of the coil length l_c will result in a increase in the low-frequency efficiency of 3 dB whereas the dependence of the coil dimensions w_c, h_c and t_c is less clear. The third factor of Eq. (11.14) is plotted in Fig. 11.2 as function of $\frac{t_c}{w_c+h_c}$.

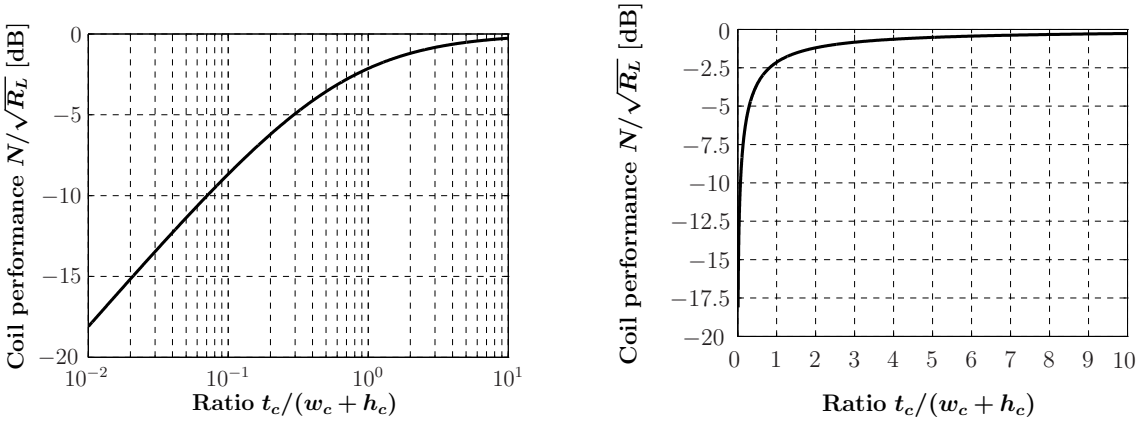

(a) Logarithmic x-axis.

(b) Linear x-axis.

Figure 11.2: Normalized low-frequency efficiency vs the ratio between coil dimensions $\frac{t_c}{w_c+h_c}$.

Fig. 11.2(b) clearly illustrates that there is a lot of efficiency to be gained in the beginning when the coil thickness is increased but after a while the gain in efficiency diminishes. This is due to the fact that the electrical resistance of one winding increases with every new layer of windings added to the coil. It appears that a ratio of about 1 will be a good compromise between coil volume and efficiency.

Thus, in the end, the low-frequency efficiency for the critically stable loudspeaker with $k_A = 0$ only depends on the coil geometry and its electrical resistivity, the ratio $\alpha = D_M/D$ and the magnetic remanence B_r. Except for the fact that the coil dimensions are restrained by the

armature dimensions the low-frequency efficiency is in fact independent of the armature geometry and therefore also its stiffness as long as the loudspeaker is designed to be critically stable.

As usual, the saturation criterion may be taken into account making sure that the armature thickness is smaller than

$$h_a \leq \sqrt{\frac{4B_r B_s}{\mu_0 E D}\frac{(\alpha+1)}{(\alpha+2)}l_a^3}. \tag{10.33}$$

Together with the stability criterion (Eq. (9.9)) this will ensure that the armature does not saturate.

11.2 Low Frequencies for $k_A \neq 0$

For most miniature balanced-armature loudspeakers the acoustic stiffness of the back volume cannot be ignored. This makes the optimization of the loudspeaker design more complicated as the volume occupied by the armature, coil and magnets influence the size of the acoustic back volume. This means that one has to find a good balanced between e.g. coil size and acoustic back volume. In fact, in this analysis, only the volume occupied by the coil is considered, as this is assumed to be the most significant limitation to the available acoustic back volume. Substituting Eq. (9.39) into Eq. (11.9) yields

$$u_{CIP,st}(\omega) \approx \frac{\frac{T\omega}{\sqrt{R_L}}}{\frac{2\alpha^2+4\alpha+1}{(\alpha+1)^4}k_a + \frac{S_D^2\rho_0 c^2}{V_T - F_{cl}l_a t_c[2(w_a+h_a+2D)+\pi t_c]}}\sqrt{1\ \mathrm{W}}. \tag{11.16}$$

Using the result from Eq. (11.12) the low frequency efficiency for the critically stable loudspeaker may be written

$$u_{CIP,st}(\omega) \approx \frac{\sqrt{\frac{F_f l_c}{\pi\rho_w}}\sqrt{\frac{1}{1+\frac{2(w_c+h_c)}{\pi t_c}}}\frac{\mu_0}{B_r}\frac{\alpha(\alpha+2)^2}{(\alpha+1)^3}k_a}{\frac{2\alpha^2+4\alpha+1}{(\alpha+1)^4}k_a + \frac{S_D^2\rho_0 c^2}{V_T - F_{cl}l_a t_c[2(w_a+h_a+2D)+\pi t_c]}}\omega\sqrt{1\ \mathrm{W}}. \tag{11.17}$$

Using $U = S_D u$ and substituting Equations (5.111) to (5.113) into Eq. (11.17) yields

$$\boxed{U_{CIP,st}(\omega) \approx S_D\frac{\mu_0}{B_r}\sqrt{\frac{F_f F_{cl} l_a}{\pi\rho_w}}\frac{\sqrt{\frac{1}{1+\frac{2(w_a+h_a+2D)}{\pi t_c}}}\frac{\alpha(\alpha+2)^2}{(\alpha+1)^3}}{\frac{2\alpha^2+4\alpha+1}{(\alpha+1)^4} + \frac{S_D^2\rho_0 c^2}{V_T - F_{cl}l_a t_c[2(w_a+h_a+2D)+\pi t_c]}\frac{1}{k_a}}\omega\sqrt{1\ \mathrm{W}}}. \tag{11.18}$$

This can also be written as

$$\boxed{U_{CIP,st}(\omega) \approx S_D \frac{\mu_0}{B_r} \sqrt{\frac{F_f F_{cl} l_a}{\pi \rho_w}} \frac{\sqrt{\frac{1}{1+\frac{2(w_a+h_a+2D)}{\pi t_c}}} \frac{\alpha(\alpha+2)^2}{(\alpha+1)^3}}{\frac{2\alpha^2+4\alpha+1}{(\alpha+1)^4} + \frac{k_{mA}}{k_a}} \omega \sqrt{1\ \mathrm{W}}}. \tag{11.19}$$

with the mechanical stiffness k_{mA} due to the back volume given as

$$k_{mA} = \frac{S_D^2 \rho_0 c^2}{V_T - F_{cl} l_a t_c \left[2\left(w_a + h_a + 2D\right) + \pi t_c\right]}. \tag{11.20}$$

Eq. (11.19) reduces to Eq. (11.15) (scaled by S_D) for $k_{mA} << k_a$. For a given design the surface area of the diaphragm S_D and the coil thickness t_c are constrained by the dimensions of the loudspeaker case. However, the coil length and the coil outer radius has to be chosen as a good compromise between maximizing the ratio $N/\sqrt{R_L}$ and not reducing the available back volume too much as this will increase the effective stiffness. The same is true for the diaphragm area: As S_D is increased the volume velocity output increases for a given armature velocity but at the same time the mechanical stiffness due to the back volume increases with S_D^2. Thus, for a given available volume V_T and a given armature geometry it is an optimization problem to choose the values of F_{cl}, t_c, S_D and α that maximizes the low-frequency efficiency. Due to the complexity of the equation it seems like a natural choice to optimize the function using a numerical method while applying proper constraints to the parameters. $\alpha = D_M/D = l_M/(\mu_r D)$ is also related to the acoustic volume since a longer magnet will reduce the available back volume but often the value of α will be chosen from other criteria such as linearity and maximum available height in the receiver construction. Also, for a given value of α the magnet volume will depend on the recoil permeability: Magnets made of material with lower recoil permeability μ_r will be smaller for a given α-value.

Consider the second (α-dependent) factor in the numerator which is plotted in Fig. 11.3. It can be observed that the gain of this factor is very close to 1 dB for α-values between 0.5 and 10. The important lesson is that the low-frequency CIP response is almost independent of α when $k_{mA} \neq 0$ and α is in the common range from 0.5 to 10.

11.3 Low Frequencies for $k_{mA} >> k_a$

For small balanced-armature receivers it may happen that the acoustic stiffness due to the back volume is larger than the stiffness of the armature alone i.e. $k_{mA} > k_a$. Already when $k_{mA}/k_a = 2$ the first (α-dependent) term in the denominator of Eq. (11.19) becomes quite insignificant for α-values larger than 1. This term is plotted in Fig. 11.4.

For $\alpha = 2$ the term has decreased to 0.21. Thus, for larger α-values and $k_{mA}/k_a > 1$ the first term in the denominator of Eq. (11.18) becomes insignificant and the low-frequency CIP response may be written

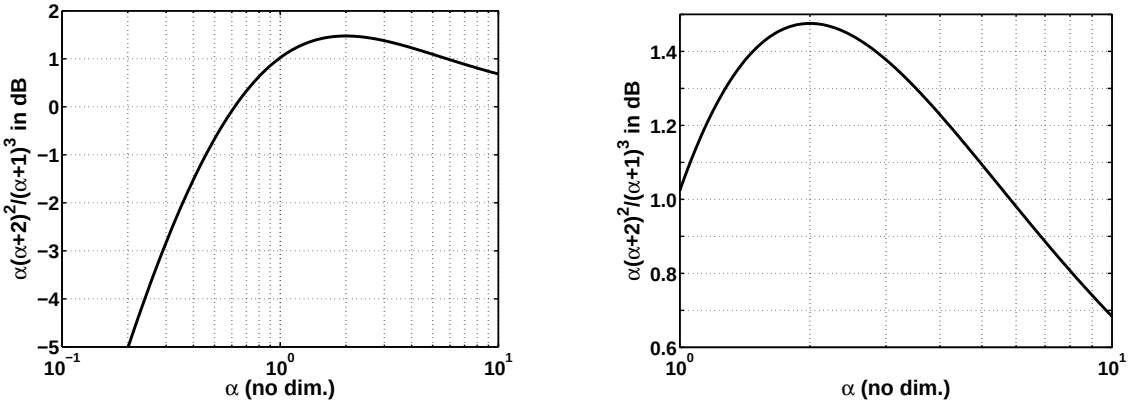

(a) Overview. (b) Close-up.

Figure 11.3: Normalized low-frequency efficiency vs $\alpha = D_M/D$.

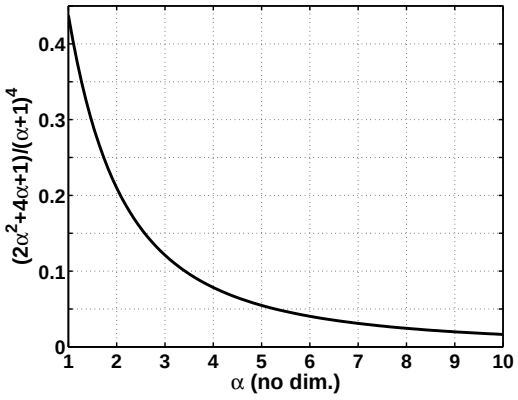

Figure 11.4: Normalized magnet length, $\alpha = D_M/D$, vs $\frac{(2\alpha^2+4\alpha+1)}{(\alpha+1)^4}$.

$$\boxed{U_{CIP,st}(\omega) \approx S_D \frac{\mu_0}{B_r}\sqrt{\frac{F_f F_{cl} l_a}{\pi\rho_w}}\frac{\sqrt{\frac{1}{1+\frac{2(w_a+h_a+2D)}{\pi t_c}}}\frac{\alpha(\alpha+2)^2}{(\alpha+1)^3}}{\frac{S_D^2\rho_0 c^2}{V_T - F_{cl} l_a t_c[2(w_a+h_a+2D)+\pi t_c]}\frac{1}{k_a}}\omega\sqrt{1\ \mathrm{W}}}. \tag{11.21}$$

or

$$U_{CIP,st}(\omega) \approx S_D \frac{\mu_0}{B_r}\sqrt{\frac{F_f F_{cl} l_a}{\pi\rho_w}}\frac{k_a}{k_{mA}}\sqrt{\frac{1}{1+\frac{2(w_a+h_a+2D)}{\pi t_c}}}\frac{\alpha(\alpha+2)^2}{(\alpha+1)^3}\omega\sqrt{1\ \mathrm{W}}. \tag{11.22}$$

The α-dependent gain factor was plotted in Fig. 11.3. Again, it can be observed that the gain of this factor is very close to 1 dB for α-values between 0.5 and 10. The low-frequency CIP response is therefore almost independent of α when $k_{mA} >> k_a$ and α is in the common range from 0.5 to 10.

11.4 Low Frequency Efficiency Simulations

In this section the low frequency efficiency for the general case, i.e. Eq. (11.18), is investigated for different loudspeaker designs. One can of course always maximize this function but this will not provide useful insight about how the efficiency depends on the various parameters. Since the loudspeaker efficiency is investigated for the critically stable case, the air gap area might differ for the different designs according to Eq. (9.9). Table 11.2 and 11.3 summarize the relevant design parameters for the investigated designs.

Design:	V_T [mm^3]	α	t_c [mm]	w_a [mm]	h_a [mm]	l_a [mm]	k_a [N/m]	k_Φ [N/m]	k_{mA} [N/m]
D#1	50.4	var.	var.	0.80	0.12	4.80	625	-	259
D#2	**84**	var.	var.	0.80	0.12	4.80	625	-	**199**
D#3	**126**	var.	var.	0.80	0.12	4.80	625	-	**134**
D#4	126	var.	var.	0.80	0.12	4.80	625	-	**534**
D#5	**50.4**	**4**	var.	0.80	0.12	4.80	625	576	-
D#6	**126**	**4**	var.	0.80	0.12	4.80	625	576	-
D#7	**var.**	**4**	1	0.80	0.12	4.80	625	576	-

Table 11.2: The relevant design parameters for different loudspeaker designs. The stated value for the stiffness k_{mA} due to the back volume is that when the coil thickness t_c is at its largest value.

Design:	B_r [T]	F_{cl}	F_f	D [mm]	E [MPa]	w_{case} [mm]	h_{case} [mm]	l_{case} [mm]	S_D [mm^2]
D#1	1.4	0.8	0.7	0.1	200	3	4	6	8.1
D#2	1.4	0.8	0.7	0.1	200	**5**	4	6	8.1
D#3	1.4	0.8	0.7	0.1	200	**6**	**5**	6	8.1
D#4	1.4	0.8	0.7	0.1	200	6	5	6	**16.2**
D#5	1.4	0.8	0.7	0.1	200	**3**	**4**	6	**var.**
D#6	1.4	0.8	0.7	0.1	200	**6**	**5**	6	**var.**
D#7	1.4	0.8	0.7	0.1	200	**var.**	4	6	**var.**

Table 11.3: The relevant design parameters for different loudspeaker designs.

It is useful to make a 3-dimensional plot of Eq. (11.18) with the CIP response as a function of the coil thickness t_c and α. Of course Eq. (11.18) could be maximized using a numerical algorithm but a 3-dimensional plot on a relevant range (say, α from 1-10 and t_c from 0.1 mm to the largest possible thickness constrained by the casing) will provide greater insight on what compromises to make. For instance, it might not be feasible to use twice as much copper for the coil to obtain a 0.1 dB increase in efficiency. Figure 11.5 shows the effect of increasing the case width from 3 mm to 5 mm and thereby increasing the total case volume V_T while the diaphragm size remains fixed. The optimal coil thickness for a ratio of $\alpha = 4$ turns out to be about 0.6 mm in the first case and about 0.8 mm in the second case. Thus the second design gains about 5 dB of low-frequency efficiency because of the increased coil size but also from the reduced stiffness of the back volume.

In the next figure (Fig. 11.6(a)) the case size is increased even further and this time there is an efficiency gain of about 4 dB for the maximum efficiency. In Fig. 11.6(b) the back volume remains the same but the diaphragm area S_D is increased by a factor of 2. Figure 11.6 has an interesting and maybe surprising implication: The loudspeaker with the smaller diaphragm area S_D is more efficient than the loudspeaker with the larger diaphragm, everything else equal geometrically-wise. This is due to the fact that the acoustic stiffness scales with S_D^2 whereas the volume velocity output

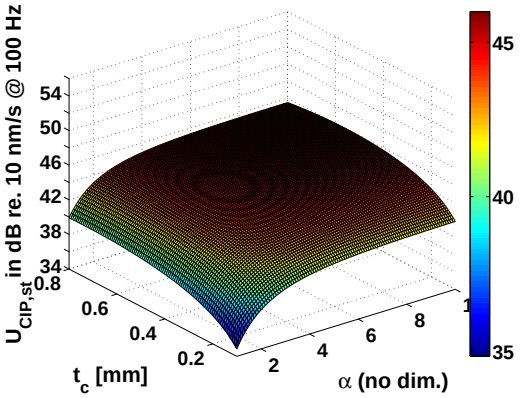

(a) D#1: $V_T = 50.4$ mm^3, $k_{mA} = 259$ N/m, $S_D = 8.1$ mm^2

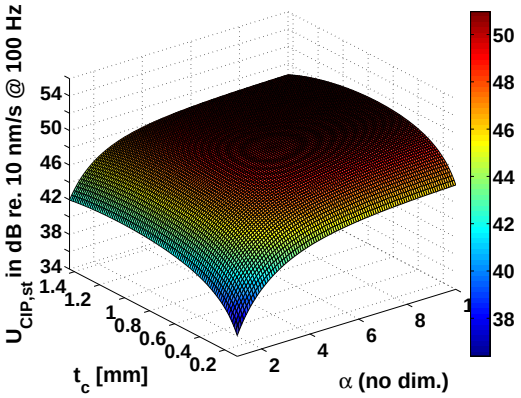

(b) D#2: $V_T = 84$ mm^3, $k_{mA} = 199$ N/m, $S_D = 8.1$ mm^2

Figure 11.5: $U_{CIP,st}$ as function of the coil thickness t_c and the ratio $\alpha = D_M/D$ for two different values of the total volume V_T.

only scales with S_D. Thus, whenever the acoustic stiffness contributes to the overall stiffness by a significant amount, it may be that a smaller diaphragm will result in a more efficient design than a larger diaphragm.

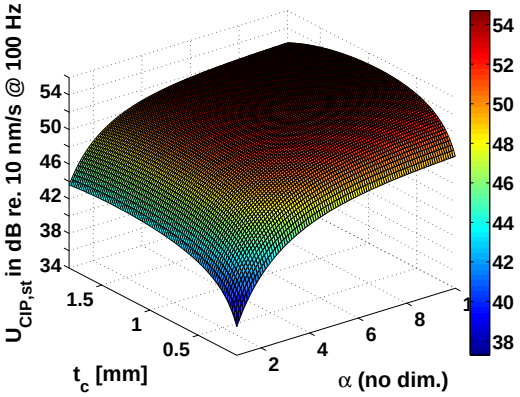

(a) D#3: $V_T = 126$ mm^3, $k_{mA} = 134$ N/m, $S_D = 8.1$ mm^2

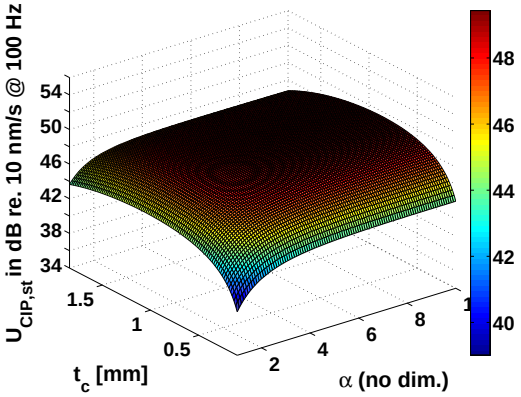

(b) D#4: $V_T = 126$ mm^3, $k_{mA} = 534$ N/m, $S_D = 16.2$ mm^2

Figure 11.6: $U_{CIP,st}$ as function of the coil thickness t_c and the ratio $\alpha = D_M/D$ for two different diaphragm sizes.

figure 11.7 shows the effect of varying diaphragm area S_D and coil thickness t_c for two different fixed volumes V_T. For the small volume (figure 11.7(a)) the optimal diaphragm area is a little less than 4 mm^2 and for the larger volume the optimal diaphragm area is a bit more than 5 mm^2.

It is interesting to vary the diaphragm area and total volume V_T for a fixed coil thickness. This essentially means that the diaphragm area S_D and the mechanical stiffness k_{mA} due to the back volume are the only variables. The CIP volume velocity response evaluated at 100 Hz and plotted as function of S_D and V_T is shown in Fig. 11.8. This figure reveals that for a fixed coil thickness the optimal surface area is small for small back volumes and larger for larger back volumes.

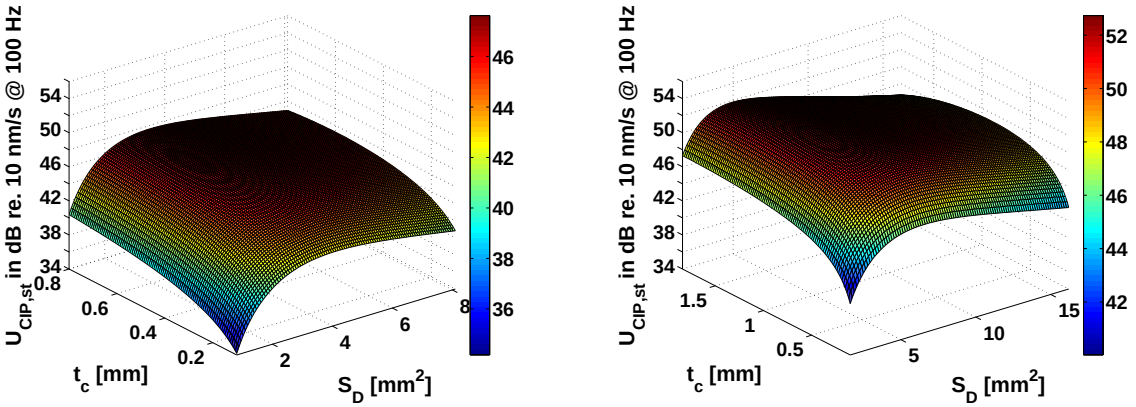

(a) D#5: $V_T = 50.4$ mm^3 (b) D#6: $V_T = 126$ mm^3

Figure 11.7: $U_{CIP,st}$ as function of coil thickness t_c and diaphragm area S_D with α fixed at 4.

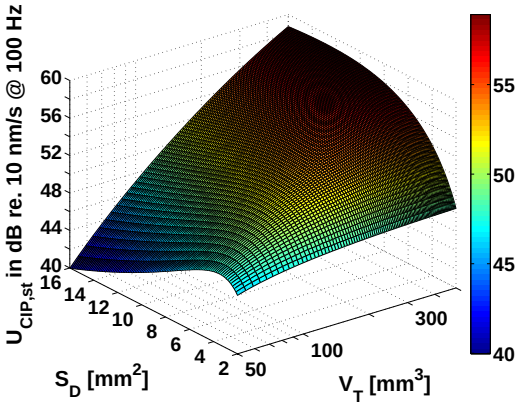

Figure 11.8: D#7: $U_{CIP,st}$ as function of the total available back volume V_T and the diaphragm area S_D. The coil thickness is fixed at 0.8 mm.

The accuracy by which the acoustic stiffness is modeled is of course important when determining the optimal diaphragm- and coil size. Thus, more work needs to be done regarding the modeling of the acoustic impedance of the back volume. However, this section does indicate that the efficiency can be improved by correctly optimizing the ratio between the coil volume and the acoustic volume and also by adjusting the diaphragm area if one can afford to compromise the maximum output.

11.5 Mid Frequencies

In this section, the efficiency in the frequency range where the loudspeaker has its effective resonance frequency $\omega_{r,eff}$ is investigated. This is the frequency where the effective stiffness due to the armature, back volume and the magnetic stiffness compensation resonates with the moving mass of the loudspeaker which consists of the armature mass but also the diaphragm mass and the mass of the drive pin and the acoustic mass which depends on the acoustic load. The me-

chanical impedance is dominated by losses at the resonance frequency so the electrical impedance (Eq. (6.20)) can be written

$$Z_E\left(j\omega\right) \approx R_L + Lj\omega_{r,eff} + \frac{T^2}{r}. \tag{11.23}$$

The real part of this impedance is

$$Re\{Z_E\left(j\omega\right)\} \approx R_L + \frac{T^2}{r} \tag{11.24}$$

and the magnitude is

$$\left|Z_E\left(j\omega\right)\right| \approx \sqrt{\left(R_L + \frac{T^2}{r}\right)^2 + \left(L\omega_{r,eff}\right)^2}. \tag{11.25}$$

Substituting Equations Eq. (11.24) and (11.25) into Eq. (11.2) yields

$$f_{CIP}\left(\omega\right) \approx \sqrt{\frac{\left(R_L + \frac{T^2}{r}\right)^2 + \left(L\omega_{r,eff}\right)^2}{R_L + \frac{T^2}{r}}}\sqrt{1\ \mathrm{W}}. \tag{11.26}$$

Using Eq. (6.17) the velocity response may be written

$$H_u\left(j\omega\right) \approx \frac{T}{\left(R_L + Lj\omega\right)r + T^2}. \tag{11.27}$$

Evaluating this at the resonance frequency $\omega = \omega_{r,eff} = \sqrt{k_{eff}/m_{tot}}$ the magnitude is

$$\left|H_u\left(j\omega\right)\right| \approx \frac{T}{\sqrt{\left(R_L r + T^2\right)^2 + \left(rL\omega_{r,eff}\right)^2}} = \frac{T}{r\sqrt{\left(R_L + \frac{T^2}{r}\right)^2 + \left(L\omega_{r,eff}\right)^2}}. \tag{11.28}$$

Substituting Equations (11.26) and (11.28) into Eq. (11.1) yields the CIP armature velocity response:

$$\boxed{u_{CIP} \approx \frac{T}{r}\sqrt{\frac{1\ \mathrm{W}}{R_L + \frac{T^2}{r}}} = \frac{\sqrt{r_0}}{r}\frac{1}{\sqrt{1 + \frac{r_0}{r}}}\sqrt{1\ \mathrm{W}}} \tag{11.29}$$

with

$$r_0 = \frac{T^2}{R_L}. \tag{11.30}$$

If the mechanical losses are small ($r << r_0$) Eq. (11.29) reduces to

$$\boxed{u_{CIP} \approx \frac{1}{\sqrt{r}}\sqrt{1\ \mathrm{W}}}. \tag{11.31}$$

Eq. (11.31) is an interesting result as it is independent of the force factor and the DC coil resistance. This result is only valid for frequencies very close to the mechanical resonance frequency.

11.6 High Frequencies

At high frequencies where the mechanical impedance is dominated by the mass ($Z_m(j\omega) \approx mj\omega$) the magnitude of the electrical impedance (Eq. (6.20)) is approximately

$$|Z_E(\omega)| \approx L\omega \tag{11.32}$$

and the real part of the impedance is approximately

$$Re\{Z_E(j\omega)\} \approx R_L. \tag{11.33}$$

Substituting Equations (11.32) and (11.33) into Eq. (11.2) yields the CIP normalization function:

$$f_{CIP}(\omega) \approx \frac{L\omega}{\sqrt{R_L}}\sqrt{1\ \mathrm{W}}. \tag{11.34}$$

The velocity response (Eq. (6.17)) can be approximated by

$$H_u(j\omega) \approx \frac{T}{Lj\omega m_{tot}j\omega + T^2} = -\frac{T}{Lm_{tot}\omega^2}\frac{1}{1-\left(\frac{\omega_0}{\omega}\right)^2}, \tag{11.35}$$

with

$$\omega_0^2 = \frac{T^2}{Lm_{tot}}. \tag{11.36}$$

For high frequencies where $\omega >> \omega_0$ Equation (11.35) becomes

$$H_u(j\omega) \approx -\frac{T}{Lm_{tot}\omega^2}, \qquad \text{for } \omega >> \omega_0. \tag{11.37}$$

Substituting Equations (11.34) and (11.37) into Eq. (11.1) yields the CIP armature velocity response:

$$\boxed{u_{CIP}\left(j\omega\right) \approx \frac{T}{\sqrt{R_L} m_{tot} \omega} \sqrt{1\ \mathrm{W}}}. \tag{11.38}$$

This result is very similar to that at low frequencies, only the mass is the dominant part of the impedance. Using Eq. (11.12) it is possible to write Eq. (11.38) for the critically stable case:

$$\boxed{u_{CIP,st}\left(j\omega\right) \approx \frac{\mu_0}{B_r} \sqrt{\frac{F_f l_c}{\pi \rho_w}} \sqrt{\frac{1}{1 + \frac{2(w_c + h_c)}{\pi t_c}}} \frac{\alpha \left(\alpha + 2\right)^2}{\left(\alpha + 1\right)^3} \frac{k_a}{m_{tot}} \frac{1}{\omega} \sqrt{1\ \mathrm{W}}}. \tag{11.39}$$

For the special case where the total mass m_{tot} is dominated by the armature mass k_a/m_{tot} may be recognized as the squared angular resonance frequency of the armature (see Eq. (5.73) and Eq. (5.74)) and Eq. (11.39) may be written:

$$\boxed{u_{CIP,st}\left(j\omega\right) \approx \frac{\mu_0}{B_r} \sqrt{\frac{F_f l_c}{\pi \rho_w}} \sqrt{\frac{1}{1 + \frac{2(w_c + h_c)}{\pi t_c}}} \frac{\alpha \left(\alpha + 2\right)^2}{\left(\alpha + 1\right)^3} \frac{35 E h_a^2}{33 \rho_a l_a^4 \omega} \sqrt{1\ \mathrm{W}}}. \tag{11.40}$$

Here it is assumed that only the armature contributes to the effective mass (i.e. $m_{tot} = m_{eq}$). Writing the coil dimensions in terms of the armature geometry finally yields

$$\boxed{u_{CIP,st}\left(j\omega\right) \approx \frac{\mu_0}{B_r} \sqrt{\frac{F_f F_{cl} l_a}{\pi \rho_w}} \sqrt{\frac{1}{1 + \frac{2(w_a + h_a + 2D)}{\pi t_c}}} \frac{\alpha \left(\alpha + 2\right)^2}{\left(\alpha + 1\right)^3} \frac{35 E h_a^2}{33 \rho_a l_a^4 \omega} \sqrt{1\ \mathrm{W}}}. \tag{11.41}$$

As it was the case for low frequencies also the high-frequency efficiency is inversely proportional to the magnetic remanence. The second factor ensures a 3 dB increase per doubling of the coil length. The effect of the third factor which depends on the armature geometry has already been shown in Fig. 11.2. The fourth (α-dependent) factor is the same as the one that went into the low-frequency efficiency expressed in Eq. (11.19) and Eq. (11.21). The effect of this factor is almost independent of α in the most common range and this was demonstrated in Fig. 11.3. However, the curve reaches its maximum for $\alpha = 2$ and the efficiency decreases for very small magnet lengths. An increase from $\alpha = 2$ to $\alpha = 4$ will increase the low-frequency efficiency, for $k_{mA} = 0$, by about 8 dB (see Fig. 11.1(b)) whereas the high-frequency efficiency is only reduced by about 0.25 dB.

The last factor of Eq. (11.41) concerns the geometry of the armature and the choice of materials. It is not surprising to see that a large Young's modulus is beneficial as this will reduce the moving mass for a given stiffness. The same is true for a small mass density ρ_a. The armature height and in particular the armature length are extremely important for the efficiency of the receiver where the total moving mass is dominated by the mass of the armature.

An important relationship is that between the coil length l_c and the armature length l_a. The

coil length cannot be larger than the armature length (unless it is placed on the armature "legs"). Also, the efficiency decreases much faster (-24 dB/oct) with l_a than it increases with l_c (+3 dB/oct). Thus, it would be unwise to increase the armature length in order to fit a longer coil. The effect of the squared armature height h_a is likewise much more significant than the effect of the h_a inside the square root.

It is possible to take the analysis even further if the saturation constraint is also applied. Inserting the limiting case of Eq. (10.33) into Eq. (11.40) yields

$$u_{CIP,st,sat}\left(j\omega\right) \approx \frac{\mu_0}{B_r}\sqrt{\frac{F_f l_c}{\pi\rho_w}}\sqrt{\frac{1}{1+\frac{2(w_c+h_c)}{\pi t_c}}} \cdot \frac{\alpha\left(\alpha+2\right)^2}{\left(\alpha+1\right)^3}\frac{35E\left(\sqrt{\frac{4B_rB_s}{\mu_0 ED}\frac{\alpha+1}{\alpha+2}l_a^3}\right)^2}{33\rho_a l_a^4\omega}\sqrt{1\ \mathrm{W}} \Leftrightarrow \tag{11.42}$$

$$\boxed{u_{CIP,st,sat}\left(j\omega\right) \approx \sqrt{\frac{F_f l_c}{\pi\rho_w}}\sqrt{\frac{1}{1+\frac{2(w_c+h_c)}{\pi t_c}}}\left(1-\frac{1}{\left(\alpha+1\right)^2}\right)\frac{140B_s}{33\rho_a l_a D\omega}\sqrt{1\ \mathrm{W}}} \tag{11.43}$$

with

$$h_a = \sqrt{\frac{4B_rB_s}{\mu_0 ED}\frac{\alpha+1}{\alpha+2}l_a^3}. \tag{11.44}$$

This result shows that - apart from the 2 first factors that have to do with the coil - the only armature dimension that influences the high-frequency efficiency of the critically stable and critically saturated loudspeaker is the armature length. The armature width and height as well as the magnetic remanence are irrelevant. The same is true for Young's modulus. On the other hand it becomes evident that the high-frequency efficiency is inversely proportional to the air gap height D.

It should be noted that the result in Eq. (11.43) does not overrule the result obtained in Equations (11.40) and (11.41). It makes perfect sense to design a loudspeaker only applying the stability constraint and not the saturation constraint. This makes it possible to design a more efficient loudspeaker where the armature is more likely to saturate i.e. the maximum output might be limited by the magnetic saturation instead of the maximum possible displacement D.

Chapter 12

Oversized Magnets

In most commercial balanced-armature loudspeakers the cross-sectional area of the permanent magnets is larger than the cross-sectional area of the air gap: The armature tip is usually slimmer than the permanent magnets. This is also the case for the B-A loudspeaker scale model which is presented in chapter 13 (see Fig. 13.1(a)). The width of the armature is 6 mm whereas the width of the permanent magnets is 12 mm. There is of course no rule saying that all B-A loudspeakers should be designed like this but as it appears that most B-A loudspeakers are indeed designed in this way, it should be investigated how that design decision influences the performance of the loudspeaker. One can construct a magnetic circuit like the one shown in Fig. 12.1(a) where the air gap area and the permanent magnet area are different but well-defined. On the other hand, Fig. 12.1(b) illustrates the case resembling that of the B-A loudspeaker scale model and many commercial miniature B-A loudspeakers. For that case it is perhaps less clear how to define an air gap area that correctly reflects the amount of flux in the magnetic circuit and also the magnetic force between the magnet and the pole piece. It is also questionable whether the internal magnet reluctance should still be inversely proportional to the full magnet cross-sectional area or an area less than that.

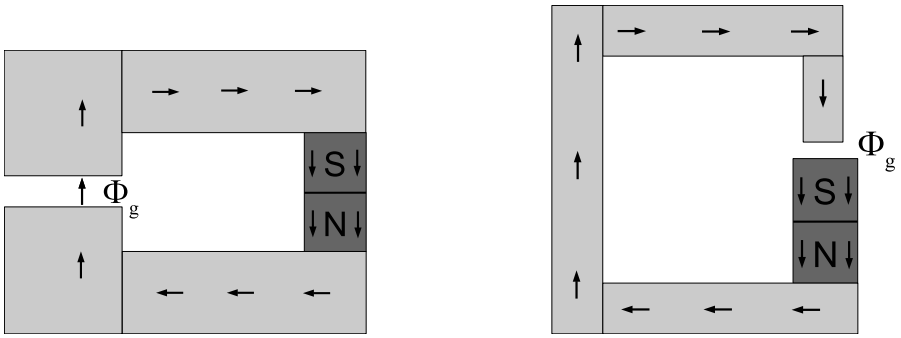

(a) $A_M \neq A_g$ but each value is well-defined.

(b) A_g is ambiguous.

Figure 12.1: Different configurations of the air gap area and the permanent magnet area.

As an increase in A_M reduces the total reluctance of the magnetic circuit but leaves the magnetomotive force of the magnets unchanged the magnetic flux in the armature and in the rest of the magnetic circuit of the loudspeaker is increased and the chance of magnetic saturation is increased. This is illustrated by the two COMSOL FEM simulations shown in Fig. 12.2 which are supposed to somehow mimic this effect. The relative permeability of the soft magnetic material is

set to $1 \cdot 10^9$ in order to reduce any effects from poor magnetic permeability. Fig. 12.2 confirms that an increase in A_M does indeed increase the magnetic B-field in the structure.

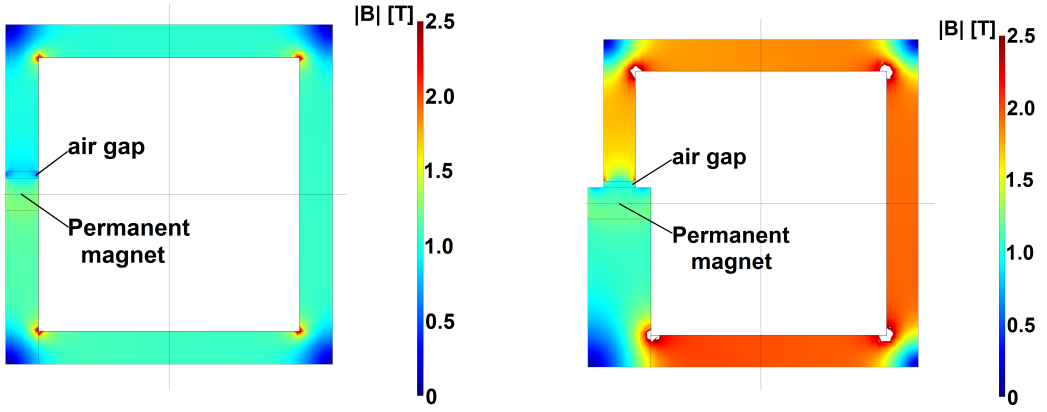

(a) $A_M = A_g$. (b) $A_M \neq A_g$.

Figure 12.2: Magnetic B-field in a simple magnetic circuit with a permanent magnet and an air gap. In (b) the width of the permanent magnet is increased by a factor of 2 compared to the upper pole piece. $\mu_r = 1 \cdot 10^9$ for the soft magnetic material and $B_r = 1.35$ and $\mu_r = 1.05$ for the permanent magnet (corresponding to a NdFeB magnet). The air gap height is 1 mm and the magnet height is 5 mm.

Fig. 12.3 reveals another problem relating to magnetic circuits where the permanent magnet has a larger cross-sectional area than the pole piece. Fig. 12.3(a) shows a COMSOL simulation of a simple circuit where the cross-sectional area of the upper pole piece is only half of that of the permanent magnet. As there is no air gap in this circuit, the permanent magnet can be said to be short circuited by a material with a relative permeability of $1 \cdot 10^9$.

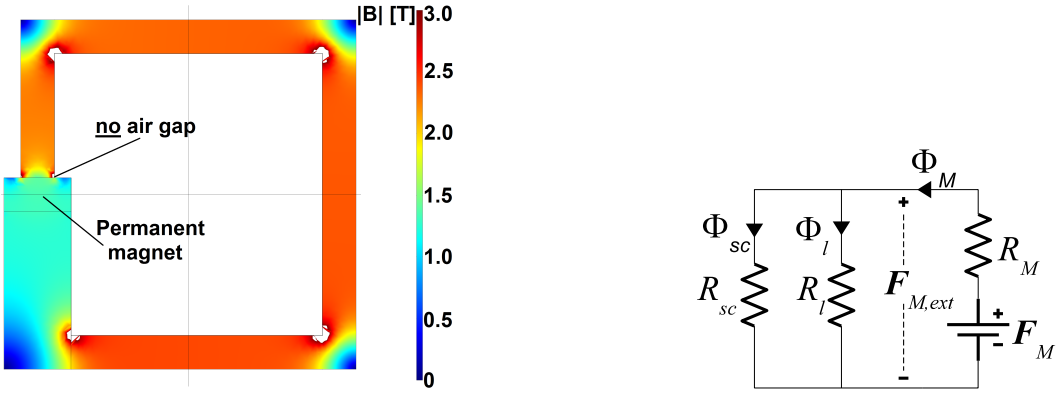

(a) COMSOL simulation. (b) Equivalent circuit where $\mathcal{R}_{sc} << \mathcal{R}_l$.

Figure 12.3: Magnetic B-field in a simple magnetic circuit with a permanent magnet and an upper pole piece with a cross-sectional area smaller than that of the magnet. $\mu_r = 1 \cdot 10^9$ for the soft magnetic material and $B_r = 1.35$ and $\mu_r = 1.05$ for the permanent magnet (corresponding to a NdFeB magnet).

Fig. 12.3(b) shows the equivalent circuit where $\mathcal{R}_l$ and Φ_l denote the leakage reluctance and leakage flux and $\mathcal{R}_{sc}$ and Φ_{sc} denote the reluctance and flux of the pole piece that short circuits the magnet. As $\mathcal{R}_{sc} << \mathcal{R}_M$ it is $\mathcal{R}_M$ that determines the flux Φ_M in the magnet and the leakage

reluctance does not have to be known. Also, as $\mathcal{R}_{sc} << \mathcal{R}_l$ all the flux that runs through $\mathcal{R}_M$ will also run through $\mathcal{R}_{sc}$. According to circuit theory:

$$\Phi_M = \frac{\mathcal{F}_M}{\mathcal{R}_M} = \frac{\frac{B_r l_M}{\mu_0 \mu_r}}{\frac{l_M}{\mu_0 \mu_r A_M}} = B_r A_M \Leftrightarrow B_M = \frac{\Phi_M}{A_M} = B_r \tag{12.1}$$

suggesting that the B-field in the magnet equals the magnetic remanence and that it is independent of the magnet cross-sectional area. However, COMSOL FEM simulations suggest otherwise. Fig. 12.4(a) shows the B-field as predicted by simple circuit theory and via COMSOL FEM simulations. Two different results are presented for COMSOL: One (B_M) is the average B-field perpendicular to the lower surface of the permanent magnet and the other (B_{sc}) is measured in the pole piece opposite of where the permanent magnet is located.

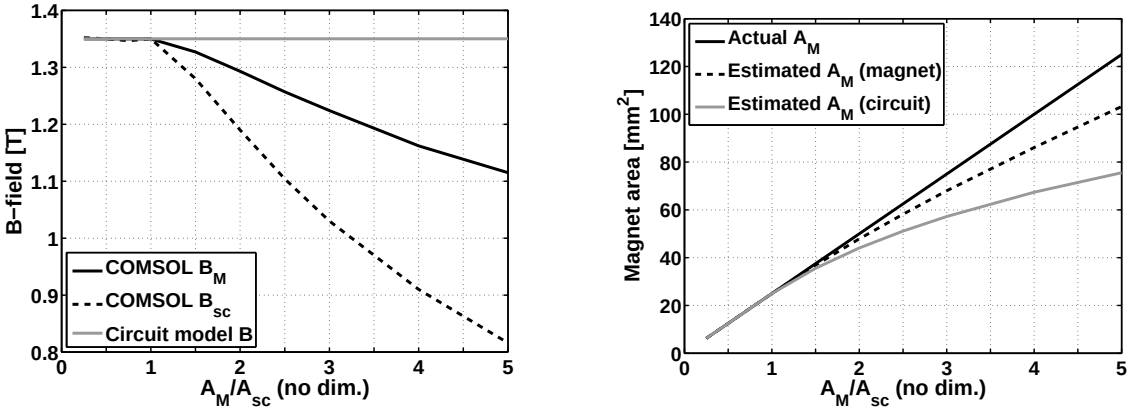

(a) B-field. (b) Effective A_M.

Figure 12.4: B-field in the magnetic circuit shown in Fig. 12.3(a). The COMSOL simulations show the B-field through the bottom surface of the permanent magnet (B_M) and through the short-circuiting pole piece opposite of where the magnet is located (B_{sc}). The lumped circuit model predicts the same (constant) B-field in the magnet and in the pole piece.

As long as the pole piece is covering the entire area of the permanent magnet ($A_M/A_{sc} < 1$), the COMSOL simulations and the simple circuit model agree. However, as the cross-sectional area of the permanent magnet becomes greater than that of the upper pole piece it is no longer possible to predict the magnetic field in the circuit using Eq. (12.1). The depth of the circuit (into the paper) is unchanged so the area of the permanent magnet is increased only by increasing the width of the magnet and its corresponding lower pole piece. The COMSOL simulations suggest that the predicted flux should be lower than what is predicted by the simple circuit model. One can make an estimate of the internal magnet reluctance using the usual equations for magnetic circuits:

$$\hat{\mathcal{R}}_M = \frac{\mathcal{F}_M}{\Phi_{M,measured}} \tag{12.2}$$

and then derive an effective magnet cross-sectional area according to the usual formula for the internal reluctance of a permanent magnet:

$$\hat{\mathcal{R}}_M = \frac{l_M}{\mu_0 \mu_r \hat{A}_M} \Leftrightarrow \hat{A}_M = \frac{l_M}{\mu_0 \mu_r \hat{\mathcal{R}}_M}. \tag{12.3}$$

Fig. 12.4(b) reveals that the measured magnetic flux can be modeled by introducing a correction factor to the magnet cross-sectional area A_M as it becomes greater than the pole piece. This investigation is done for a very specific circuit with no air gap and it is uncertain whether this result will also be true for a magnetic circuit with an air gap. What can be learnt is that it is probably necessary to introduce a correction for the internal magnet reluctance when using magnets with a large cross-sectional area. And this correction can most comfortably be introduced by correcting the magnet cross-sectional area. The investigation was performed without an air gap in order to eliminate the modeling of the air gap as a variable. However, balanced-armature loudspeakers do have an air gap between the permanent magnets and the armature and it is still necessary to investigate how to correctly model the effect of the oversized permanent magnet and the air gap with different sized pole faces. In the end, it is important to model the magnetic flux in the armature correctly as this determines the electrical back-EMF and thus also the electrical inductance (see Eq. (5.40)). Furthermore, it is important to model the magnetic flux in the air gap - and the air gap area itself - correctly in order to determine the input force to the armature correctly (see Eq. (5.22)). FEM simulations combined with actual measurements of the air gap B-field and the force between the permanent magnet and the pole piece would probably be a good approach. These simulations and measurements should uncover how the lumped elements should be defined or corrected in a simple lumped element model.

In the following, a small step towards the distinction between the area of the air gap and the permanent magnet is made. Throughout this work it has been assumed that the permanent magnet cross-sectional area A_M equals the cross sectional area of the air gap A_g and this area has simply been denoted A in the equations. In the following, it will be shown how some of the key equations are altered if the two cross-sectional areas are not the same. This is done by going back to the initial definition of the internal magnetic reluctance of a permanent magnet

$$\mathcal{R}_M = \frac{l_M}{\mu_0 \mu_r A_M} = \frac{D_M}{\mu_0 A_M}, \tag{3.3}$$

and the magnetic reluctance of an air gap between two parallel surfaces of equal surface area

$$\mathcal{R}_{g1}(x) = \frac{D - x}{\mu_0 A_g} \tag{12.4}$$

$$\mathcal{R}_{g2}(x) = \frac{D + x}{\mu_0 A_g}. \tag{12.5}$$

In the above equations, the distinction has been made between the air gap area and the magnet area. However, the Equations also imply that the air gap reluctance changes with x in a simple way. This is only true for the case where the two surfaces are parallel, have the same cross-sectional area and

are located right in front of each other i.e. as in Fig. 12.1(a). In the case of Fig. 12.1(b) the cross section of the air gap can be thought of as being shaped more like an isosceles trapezoid where the reluctance changes in a more complicated way with the distance between the pole piece and the magnet. If we would like to express the air gap reluctances in the form of Equations (12.4) and (12.5) one could introduce a displacement-dependent air gap area $A_g(x)$. As this problem is related to the above discussion about how to model the air gap correctly, for now it will simply be assumed that the air gap reluctances can be modeled according to Equations (12.4) and (12.5).

Introducing the notations

$$D_{M2} \equiv \frac{A_g}{A_M} D_M = \frac{A_g}{A_M} \frac{l_M}{\mu_r} \tag{12.6}$$

$$D_{eff2} \equiv D + D_{M2} \tag{12.7}$$

$$\alpha_2 \equiv \frac{D_{M2}}{D} = \frac{A_g}{A_M} \alpha \tag{12.8}$$

and using the same derivation procedure as in Sec. 5.1 the flux in the magnetic circuit can be written

$$\boxed{\Phi_{a2}(x,i) = 2B_r \frac{A_M}{D} \frac{\alpha_2}{(\alpha_2+1)^2 - \left(\frac{x}{D}\right)^2} x + 2\mu_0 N \frac{A_g}{D} \frac{\alpha_2+1}{(\alpha_2+1)^2 - \left(\frac{x}{D}\right)^2} i}. \tag{12.9}$$

This armature flux can again be separated into two different contributions. One due to the permanent magnets:

$$\Phi_{a2,0}(x,i) = 2B_r \frac{A_M}{D} \frac{\alpha_2}{(\alpha_2+1)^2 - \left(\frac{x}{D}\right)^2} x \tag{12.10}$$

and one due to coil current:

$$\Phi_{a2,i}(x,i) = 2\mu_0 N \frac{A_g}{D} \frac{\alpha_2+1}{(\alpha_2+1)^2 - \left(\frac{x}{D}\right)^2} i. \tag{12.11}$$

The armature input force may be evaluated as in Sec. 5.2 but using the air gap area in the expression for the force:

$$F_{\Phi 2} = \frac{\Phi_{g1}^2}{2\mu_0 A_g} - \frac{\Phi_{g2}^2}{2\mu_0 A_g} = \frac{(\Phi_{g1} + \Phi_{g2})\,\Phi_{a2}}{2\mu_0 A_g}. \tag{12.12}$$

Evaluating this expression yields loudspeaker parameters that are only slightly transformed com-

pared to the ones derived in chapter 5. The various loudspeaker parameters are summed up in the following sections.

12.1 Magnetic Stiffness Compensation for $A_M \neq A_g$

The nonlinear (displacement-dependent) magnetic stiffness compensation is

$$\boxed{k_{\Phi 2}(x) = \frac{2B_r^2}{\mu_0}\frac{A_M}{A_g}\frac{A_M}{D}\frac{\alpha_2^2(\alpha_2+1)}{\left[(\alpha_2+1)^2 - \left(\frac{x}{D}\right)^2\right]^2}}. \tag{12.13}$$

For small armature displacements where $x << D$ the small-signal magnetic stiffness compensation is

$$\boxed{k_{\Phi 2} = \frac{2B_r^2}{\mu_0}\frac{A_M}{A_g}\frac{A_M}{D}\frac{\alpha_2^2}{(\alpha_2+1)^3} = \frac{2B_r^2}{\mu_0}\frac{A_g}{D}\frac{\alpha^2}{\left(\frac{A_g}{A_M}\alpha+1\right)^3}}. \tag{12.14}$$

It is also possible to write the nonlinear magnetic stiffness compensation as a product of the linear magnetic stiffness compensation and a function of α_2 and x/D:

$$k_{\Phi 2}(x) = k_{\Phi 2}\frac{(\alpha_2+1)^4}{\left[(\alpha_2+1)^2 - \left(\frac{x}{D}\right)^2\right]^2}. \tag{12.15}$$

12.2 Transduction Coefficient for $A_M \neq A_g$

The nonlinear (displacement-dependent) transduction coefficient is:

$$\boxed{T_{me2}(x) = T_2(x) = 2B_rN\frac{A_M}{D}\frac{\alpha_2\left[(\alpha_2+1)^2 + \left(\frac{x}{D}\right)^2\right]}{\left[(\alpha_2+1)^2 - \left(\frac{x}{D}\right)^2\right]^2}}. \tag{12.16}$$

For small armature displacements where $x << D$ the linearized transduction coefficient becomes

$$\boxed{T_2 = 2B_rN\frac{A_M}{D}\frac{\alpha_2}{(\alpha_2+1)^2} = 2B_rN\frac{A_g}{D}\frac{\alpha}{\left(\frac{A_g}{A_M}\alpha+1\right)^2}}. \tag{12.17}$$

The nonlinear force factor can be written as a product of the linear force factor and a function of α_2 and x/D:

$$T_2(x) = T_2\frac{(\alpha_2+1)^2\left[(\alpha_2+1)^2 + \left(\frac{x}{D}\right)^2\right]}{\left[(\alpha_2+1)^2 - \left(\frac{x}{D}\right)^2\right]^2}. \tag{12.18}$$

12.3 Distortion Force Factor for $A_M \neq A_g$

The distortion force factor is

$$\boxed{T_{me2,d}(x,i) = 2\mu_0 N^2 \frac{xi}{D^2}\frac{A_g}{D}\frac{\alpha_2+1}{\left[(\alpha_2+1)^2-\left(\frac{x}{D}\right)^2\right]^2}}. \tag{12.19}$$

For small armature displacements Eq . (5.37) reduces to

$$\boxed{T_{me2,d}(x,i)|_{x<<D} = 2\mu_0 N^2 \frac{xi}{D^2}\frac{A_g}{D}\frac{1}{(\alpha_2+1)^3} = 2\mu_0 N^2 \frac{xi}{D^2}\frac{A_g}{D}\frac{1}{\left(\frac{A_g}{A_M}\alpha+1\right)^3}}. \tag{12.20}$$

It is also possible to write the nonlinear distortion force factor as a product of the linearized distortion force factor and a function of α_2 and x/D:

$$T_{me2,d}(x,i) = T_{me2,d}(x,i)|_{x<<D}\frac{(\alpha_2+1)^4}{\left[(\alpha_2+1)^2-\left(\frac{x}{D}\right)^2\right]^2}. \tag{12.21}$$

12.4 Electrical Inductance for $A_M \neq A_g$

Evaluating the electrical back-EMF as $U_{\text{back2}} = N\frac{d\Phi_{a2}}{dt}$ yields the loudspeaker parameters for the electrical domain:

$$\boxed{L_2(x) = 2\mu_0 N^2 \frac{A_g}{D}\frac{\alpha_2+1}{(\alpha_2+1)^2-\left(\frac{x}{D}\right)^2}}. \tag{12.22}$$

The small-signal inductance $(x << D)$ is:

$$\boxed{L_2 = 2\mu_0 N^2 \frac{A_g}{D}\frac{1}{\alpha_2+1} = 2\mu_0 N^2 \frac{A_g}{D}\frac{1}{\frac{A_g}{A_M}\alpha+1}}. \tag{12.23}$$

The nonlinear electrical inductance can be written as a product of the linearized inductance and a function of α_2 and x/D:

$$L_2(x) = L_2\frac{(\alpha_2+1)^2}{(\alpha_2+1)^2-\left(\frac{x}{D}\right)^2}. \tag{12.24}$$

12.5 Transduction Coefficient for $A_M \neq A_g$

The transduction coefficient relating mechanical velocity to electrical voltage is contained in the first term of Eq. (5.42):

$$\boxed{T_{em2}(x) = T_2(x) = 2B_r N \frac{A_M}{D} \frac{\alpha_2 \left[(\alpha_2+1)^2 + \left(\frac{x}{D}\right)^2\right]}{\left[(\alpha_2+1)^2 - \left(\frac{x}{D}\right)^2\right]^2}}. \tag{12.25}$$

The small-signal transduction coefficient ($x << D$) is written:

$$\boxed{T_2 = 2B_r N \frac{A_M}{D} \frac{\alpha_2}{(\alpha_2+1)^2} = 2B_r N \frac{A_g}{D} \frac{\alpha}{\left(\frac{A_g}{A_M}\alpha + 1\right)^2}}. \tag{12.26}$$

It is also possible to write the nonlinear force factor as a product of the linearized force factor and a function of α_2 and x/D:

$$T_2(x) = T_2 \frac{(\alpha_2+1)^2 \left[(\alpha_2+1)^2 + \left(\frac{x}{D}\right)^2\right]}{\left[(\alpha_2+1)^2 - \left(\frac{x}{D}\right)^2\right]^2}. \tag{12.27}$$

12.6 Distortion Back-EMF Term for $A_M \neq A_g$

The distortion transduction from the mechanical to the electrical domain is

$$\boxed{T_{em2,d}(x,i) = 4\mu_0 N^2 \frac{xi}{D^2} \frac{A_g}{D} \frac{\alpha_2+1}{\left[(\alpha_2+1)^2 - \left(\frac{x}{D}\right)^2\right]^2}}. \tag{12.28}$$

For small armature displacements this expression reduces to

$$\boxed{T_{em2,d}(x,i)|_{x<<D} = 4\mu_0 N^2 \frac{xi}{D^2} \frac{A_g}{D} \frac{1}{(\alpha_2+1)^3} = 4\mu_0 N^2 \frac{xi}{D^2} \frac{A_g}{D} \frac{1}{\left(\frac{A_g}{A_M}\alpha + 1\right)^3}}. \tag{12.29}$$

It is also possible to write the nonlinear distortion force factor as a product of the linearized distortion force factor and a function of α_2 and x/D:

$$T_{em2,d}(x,i) = T_{em,d}(x,i)|_{x<<D} \frac{(\alpha_2+1)^4}{\left[(\alpha_2+1)^2 - \left(\frac{x}{D}\right)^2\right]^2}. \tag{12.30}$$

12.7 The effects of oversized magnets

The equations in the previous sections of this section provide quite a bit of insight for interpreting the effect of increasing the cross-sectional area of the permanent magnet. As the magnet area is increased its magnetomotive force remains constant but its internal reluctance is reduced which in turn increases the relative change in the total magnetic reluctance caused by displacement of

the armature, thus making the loudspeaker more nonlinear. This is reflected in Eq. (12.8) which shows that α_2 is given as α (for the case where $A_M = A_g = A$) scaled by the ratio A_g/A_m. Thus, making the cross-sectional area of the magnet twice as large as the cross-sectional area of the air gap area will cut α_2 in half and thus significantly increase the nonlinear behavior and reduce the maximum stiffness ratio $k_r = k_\Phi/k_a$ that allows stable operation (see Chapter 9).

The nonlinear parts of the loudspeaker parameters are exactly the same as for the case where $A_M = A_g$; only α_2 has substituted α. This means that the nonlinearity of the loudspeaker where $A_M \neq A_g$ can be interpreted in exactly the same way as for the loudspeaker where $A_M = A_g$ remembering that α_2 as defined in Eq. (12.8) should substitute α.

The small-signal parameters are also affected by the increased A_M. First of all, the small-signal parameters vary with α_2 in the same way as the loudspeaker parameters for $A_M = A_g$ vary with α according to Fig. 5.5. However, the small-signal parameters $k_{\Phi 2}$ and T_2 also vary with A_M with $k_{\Phi 2}$ being proportional to A_M^2 and T_2 being proportional to A_M. The electrical inductance L_2 and the distortion transduction coefficients are not affected directly by A_M (only by α_2 which is inversely proportional to A_M).

Since loudspeakers for which $A_M = A_g$ are only a sub-group of all possible B-A loudspeaker designs the conclusions for these are not necessarily true for the general B-A loudspeaker where $A_M \neq A_g$. However, the important relationship for the small-signal parameters still holds true:

$$\boxed{T_2^2 = k_{\Phi 2} L_2}. \tag{12.31}$$

12.8 Armature flux for $A_M \neq A_g$

In terms of maximum output and distortion due to magnetic saturation in the armature it is interesting to observe the armature flux as expressed in Eq. (12.9). For small signals this can be written

$$\Phi_{a2}(x,i)|_{x<<D} \approx 2B_r \frac{A_M}{D} \frac{\alpha_2}{(\alpha_2+1)^2} x + 2\mu_0 N \frac{A_g}{D} \frac{1}{\alpha_2+1} i \Leftrightarrow \tag{12.32}$$

$$\Phi_{a2}(x,i)|_{x<<D} \approx 2B_r \frac{A_g}{D} \frac{\alpha}{\left(\frac{A_g}{A_M}\alpha+1\right)^2} x + 2\mu_0 N \frac{A_g}{D} \frac{1}{\frac{A_g}{A_M}\alpha+1} i, \tag{12.33}$$

where the first term expresses the flux due to the magnets and the second term expresses the flux due to the coil current. The armature flux will become smaller if the magnet area A_M is reduced but the significance of the reduction depends on the value of α_2 compared to 1. If $\alpha_2 >> 1$ an increase in A_M will reduce the armature flux much more significantly than if $\alpha_2 << 1$. As α_2 tends to be just around 1 the safest approach is to calculate $\Phi_{a2}(x,i)$ according to Eq. (12.9) and check the sensitivity to changes in the magnet area for the specific design.

12.9 Stability when $A_M \neq A_g$

With respect to loudspeaker stability, Equations (9.4), (9.5), (9.9) and (9.10) can be rewritten to take into account that $A_M \neq A_g$. The new expression for the nonlinear magnetic stiffness compensation $k_{\Phi 2}(x)$ (Eq. (12.15)) is substituted into Eq. (9.4) and the modified stability criteria follow:

$$\boxed{k_{r2} \leq \frac{\alpha_2^2 (\alpha_2 + 2)^2}{(\alpha_2 + 1)^4}} \Leftrightarrow \boxed{\alpha_2 \geq \frac{1}{\sqrt{1 - \sqrt{k_{r2}}}} - 1} \tag{12.34}$$

$$\boxed{\frac{A_M}{A_g} \frac{A_M}{D} \leq \frac{\mu_0}{2B_r^2} \frac{(\alpha_2 + 2)^2}{\alpha_2 + 1} k_a} \tag{12.35}$$

with

$$k_{r2} \equiv \frac{k_{\Phi 2}}{k_a}. \tag{12.36}$$

The balanced-armature loudspeaker becomes more prone to instability as A_M is increased relative to A_g. This is because $\alpha_2 < \alpha$ for $A_M > A_g$ and vice versa. The maximum allowed stiffness ratio k_{r2} for a given α_2 is given in Eq. (12.34) and visualized in Fig. 9.2. As α_2 is reduced by an increase in A_M the maximum allowed stiffness ratio $k_{r2} = k_{\Phi 2}/k_a$ is also reduced meaning that the magnetic stiffness compensation $k_{\Phi 2}$ has to be reduced for a given armature stiffness k_a. As $k_{\Phi 2}$ also increases with A_M (see rightmost expression in Eq. (12.14)) there is a risk of instability if the cross-sectional area of the permanent magnets are increased.

Chapter 13

A Scale Model

This Chapter describes the construction and measurements of a balanced-armature scale model. This scale model is constructed in order to directly measure the nonlinear magnetic stiffness, force factor and inductance. The scale model is shown in Fig. 13.1 and 13.2. The measured magnetic stiffness compensation will be compared to the simulations performed with a COMSOL FEM model. Fig. 13.1(a) shows the full working loudspeaker with the ferrite permanent magnets in place.

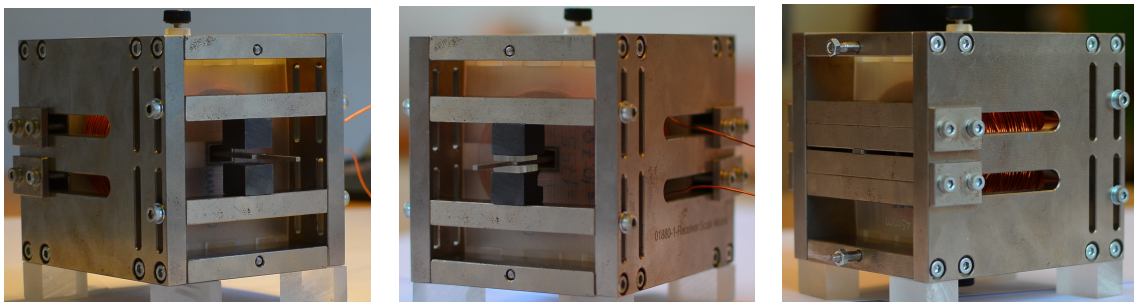

(a) Front-side view.

(b) Armature blocked.

(c) Back-side view showing the clamping mechanism for the armature.

Figure 13.1: Balanced-armature loudspeaker scale model.

The dimensions of the loudspeaker is (W x H x D) 75 mm x 80 mm x 90 mm. The horizontal bars that the magnets are attached to can be shifted in the vertical direction making it possible to experiment with different air gap and magnet heights. In Fig. 13.1(b) a couple of plastic spacers have been tightly fitted between the permanent magnets and the armature. These spacers are available in various thicknesses with 0.1 mm intervals making it possible to fix the armature in various positions and thereby measure the blocked electrical impedance from which the nonlinear displacement-dependent inductance may be derived. Fig. 13.1(c) shows the loudspeaker from the back revealing the clamping mechanism for the armature. It is possible to clamp armatures with various thicknesses and the whole clamping mechanism can be shifted in the horizontal direction towards the permanent magnets thereby reducing the effective length of the armature making the armature stiffer. Shifting the clamping mechanism forward like this will of course require a shorter coil former.

In Fig. 13.2(a) the permanent magnets have been removed. When the magnets are removed

an excitation of the coil will not cause the armature to move as the magnetic flux and therefore the magnetic force is equally strong between each horizontal bar and the armature. The armature may be fixed in various positions in order to measure the displacement dependent electrical impedance of the loudspeaker without magnets. Fig. 13.2(b) shows the coil and the aperture that makes it possible for the armature to vibrate unhindered.

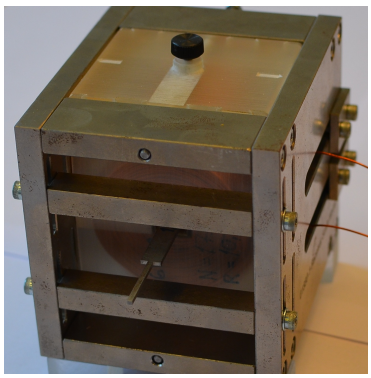

(a) Magnets removed.

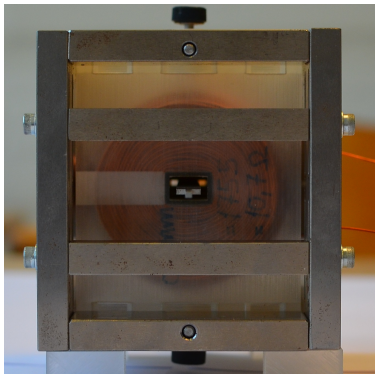

(b) Magnets removed, coil aperture exposed.

Figure 13.2: Balanced-armature loudspeaker scale model.

Soft Magnetic Material

The material used for the loudspeaker scale-model is that which was measured in Sec. 4.4. The magnetic properties of this material was measured using small ring samples with an outer diameter of 10 mm, an inner diameter of 6 mm and a height (or thickness) of 1 mm.

Armature geometry

The length of the bending part of the armature is 70 mm and the armature width and height are 6 mm and 1.35 mm, respectively corresponding to a cross-sectional area of 8.1 mm^2. There is a small protrusion at the end of the armature which sticks out beyond the permanent magnets. This makes it easy to measure the position or velocity of the armature in this point or the armature may be excited there.

Coil

The coil is wound with circular cobber wire with a diameter of 0.6 mm. The number of coil windings is 1755 and the DC resistance is about 10.7 Ω. The length of the coil (along the armature) is 45 mm and the center hole which accommodates the armature has a rectangular shape with dimensions of about 6.3 mm by 10 mm. The coil can be seen most easily in Fig. 13.1(c) and 13.2(b).

Permanent Magnets and Air Gap

The permanent magnets used in the scale model are made of Ferrite (grade Y35) with a specified remanence of 0.4-0.42 T and a recoil permeability of 1.05-1.2. The dimensions of the magnets are 12 mm x 12 mm x 10 mm and the magnetization is in the direction where the side length is

10 mm. This makes the cross-sectional area A_M = 12 mm x 12 mm = 144 mm^2. The air gap height D is about 1.9 mm and the cross-sectional area A_g of the air gap is about 12 mm x 6 mm = 72 mm^2 if the width of the armature and the side length of the magnets is used.

13.1 COMSOL Model

A simplified 3-dimensional model of the loudspeaker is constructed in COMSOL. The geometry of the model is shown in Fig. 13.3. Mechanical effects are not simulated so the magnetic force on the armature will for instance not cause the armature to bend. The magnetic affects of armature displacements are simulated by simply shifting the armature up and down i.e. not by bending. The permanent magnet material is considered isotropic with magnetization in the upward direction and the recoil permeability and the remanence is specified. The soft magnetic material is simulated using a real-valued constant relative permeability i.e. magnetic hysteresis and saturation is disregarded. Only stationary simulations are performed and the coil current is constant.

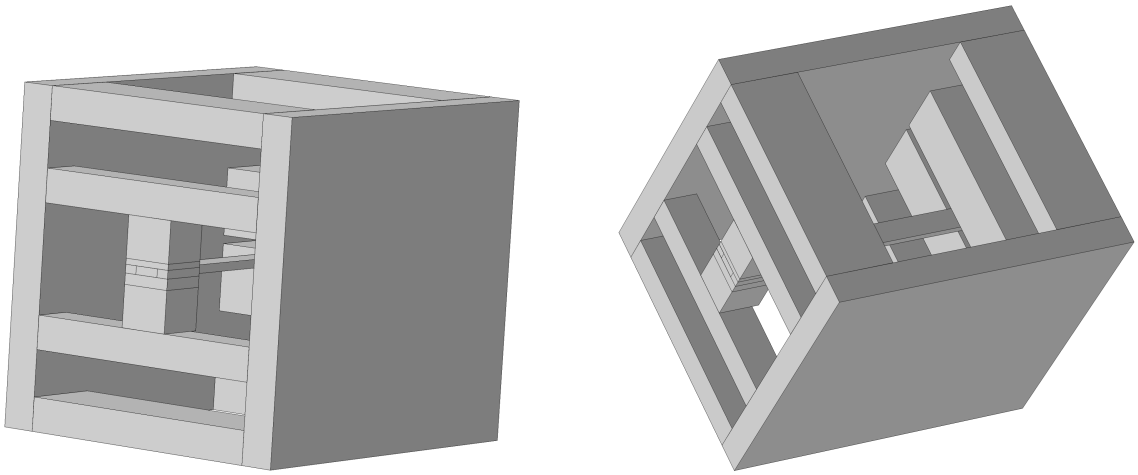

(a) Front-side view. (b) Top view.

Figure 13.3: The COMSOL scale model.

13.2 Investigation of Armature Flux using COMSOL

Magnetic flux tends to leak between surfaces of different magnetic potential and some of the magnetic flux may therefore not pass through the armature or air gaps as expected. The leakage problem is increased if the permeability of the soft magnetic material is not sufficiently large to maintain a relatively constant magnetic potential in all the connected soft magnetic parts. In the end of Chapter 3 it was mentioned that magnetic leakage could be estimated and taken into account by considering the armature flux and this is the motivation for investigating the armature flux.

Fig. 13.4 shows COMSOL simulations of the B-field throughout the length of the armature on a slice in the middle of the armature. The observed B-field is only due to the permanent magnets

as the coil current is zero. The armature is displaced by -0.5 mm. Simulations are shown for two different permeabilities plotted with the same B-field range. When the permeability of the soft magnetic structure is small (Fig. 13.4(a)) the magnetic potential tends to vary throughout the structure (including the armature) and this increases the leakage problem. The armature B-field varies by about 19 dB for $\mu_r = 100$ and the average field strength is about -25 dB. An increase in μ_r to 1000 makes the B-field much more constant throughout the armature reducing the range to about 4 dB and the average field strength is significantly increased from -25 dB to -9 dB.

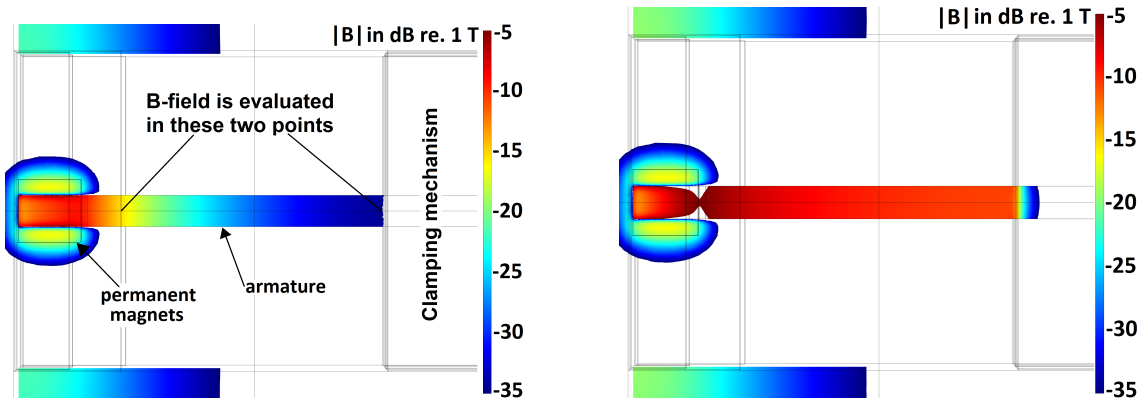

(a) $\mu_r = 100$. (b) $\mu_r = 1000$.

Figure 13.4: Simulated armature B-field along the armature on a slice in the middle of the armature (top view). The armature is displaced by -0.5 mm.

Let the average armature B-field be the average of the B-field evaluated in two different points: 2 cm away from the tip and immediately next to the armature clamping point as indicated in Fig. 13.4(a). The reason why the tip is not used is the fact that the B-field at points very close to the permanent magnets do not really reflect the armature B-field very well. Fig. 13.5(a) shows how the average B-field varies with the relative permeability μ_r of the soft magnetic material and Fig. 13.5(b) shows how the range of the armature B-field depends on μ_r. The observed B-field is only due to the permanent magnets as the coil current is zero and simulations are shown for two different armature displacements x. When the permeability of the loudspeaker structure is very large the magnetic potential of the structure tends to be at the same level - the only differences in magnetic potential exist between the north and the south pole of each of the permanent magnets and across the air gaps. For this particular geometry the magnetic performance does not really improve much beyond a magnetic permeability of 10000. The armature flux changes by $+20$ dB going from a permeability of 100 to 1 million but already at $\mu_r = 1000$ the flux has increased by about 15 dB. This indicates that there is a "sweet spot" with respect to the soft magnetic permeability beyond which almost nothing is gained in performance. As this is a simulation of a very specific case, the sweet spot cannot be expected to always be in the range between 1000 and 10000. However, one can learn that it only makes sense to improve the magnetic permeability until a certain point after which it is better to improve the circuit geometry or maybe choose a magnetic material which has lower permeability but does not tend to saturate as easily. One may

compare this result to the simulation presented in Fig. 3.6 where the performance of the magnetic circuit did not improve much beyond $\mu_r = 10000$.

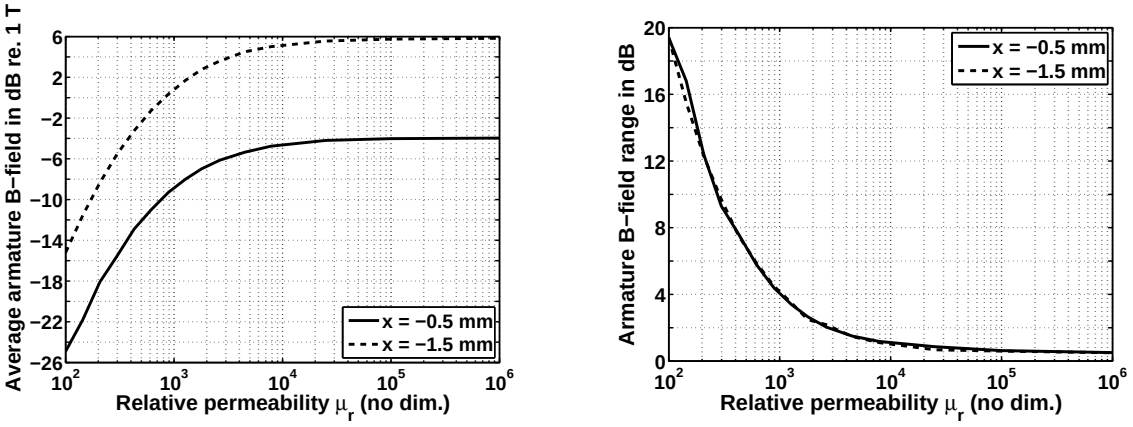

(a) Average armature B-field vs relative permeability.

(b) Armature B-field range vs relative permeability.

Figure 13.5: Simulated armature B-field vs relative permeability for two different armature displacements. The coil current is zero.

Figures 13.4 and 13.5 demonstrate the importance of FEM simulations. Roters's approach is mainly practical when estimating the leakage reluctance between surfaces with constant but different magnetic potential. If the magnetic permeability of the soft magnetic material is too low there will be a gradual drop in the magnetomotive force (or magnetic potential) throughout the geometry which greatly complicates the use of Roters's method making it impractical to use. One can argue that it does not make much sense to talk about a certain armature flux if it varies by 10 dB or more throughout the armature and this would also imply that the simple magnetic circuit models - even those taking leakage into account - are not sufficient to describe the magnetic flux flowing in the structure. However, if a material with sufficiently high μ_r is chosen the performance of the loudspeaker is better and it will be possible to describe the mechanisms with simple magnetic circuits taking leakage into account using Roters's approach or by estimation of the leakage reluctance using FEM simulations.

13.3 Estimation of Magnetic Leakage in Scale Model

COMSOL FEM simulations are used to model the magnetic flux in the armature for several armature displacements. If the circuit model is capable of capturing this behavior it should be possible to fit $\alpha_{2,Th}$ in Eq. 13.1 (adapted from Eq. 12.10) so that this equation correctly predicts the armature flux for various armature displacements x.

$$\Phi_{a2,0}(x,i) = 2B_r \frac{A_M}{D} \frac{\alpha_{2,Th}}{(\alpha_{2,Th}+1)^2 - \left(\frac{x}{D}\right)^2} x. \tag{13.1}$$

with

$$\alpha_{2,Th} = \frac{A_g}{A_M}\alpha_{Th} = \frac{A_g}{A_M}\frac{1}{1+\frac{\mathcal{R}_M}{\mathcal{R}_l}}\alpha = \frac{1}{1+\frac{\mathcal{R}_M}{\mathcal{R}_l}}\alpha_2. \tag{13.2}$$

As shown in Sec. 13.2 the armature flux can vary a great deal along the length of the armature if μ_r is not sufficiently large so it is necessary to establish a measure of the armature flux. For this purpose the average flux as explained in Sec. 13.2 is used. Based on the measurements shown in Fig. 4.1 μ_r is set to 1000 and for this permeability the average armature B-field is simulated for various armature displacements using COMSOL. Solving Eq. 13.1 with respect to $\alpha_{2,Th}$ yields the values summarized in Table 13.1 and shown in Fig. 13.6(a). Eq. 13.1 is a quadratic equation with respect to $\alpha_{2,Th}$ and it generally has two different solutions that are both viable. Therefore, $\alpha_{2,Th}$ has to be evaluated for at least two different armature displacements and the solution which is common for both displacements is the correct one. It is important to choose one small x and one large x close to D where nonlinear behavior can be observed for small α-values. As the simple lumped element model cannot be expected to model the armature flux precisely - even with the leakage effect included - the $\alpha_{2,Th}$-value determined with Eq. 13.1 cannot be expected to be exactly the same for different values of x. Looking in the last column of Table 13.1 it is clear that $\alpha_{2,Th} \approx 8.23$ is the correct value for $\alpha_{2,Th}$ which will best model the leakage effect. In Fig. 13.6 it is shown how well Eq. 13.1 can predict the armature flux with two different values for $\alpha_{2,Th}$. Notice that the small α-value is able to predict the armature flux for small armature displacements, which is also suggested by the $\alpha_{2,Th}$-column in Tab. 13.1. However, as the loudspeaker is more nonlinear for small α-values the circuit simulation predicts that the armature flux increases rapidly as the armature is displaced towards the magnets. This is not the sort of behavior which is predicted by COMSOL and it is neither the kind of behavior which is expected for a design with a permanent magnet with a relative recoil permeability close to 1 which is also more than 5 times longer than the air gap ($\Rightarrow \alpha > 4$).

x:	Average B_a	Φ_a	$\alpha_2 = (A_g/A_M)\alpha$	$\alpha_{2,Th}$	$\alpha = D_M/D$	α_{Th}
0.05 mm	36.1 mT	292.4 nWb	2.29	0.121/**8.25**	4.58	16.50
0.10 mm	72.4 mT	586.8 nWb	2.29	0.122/**8.21**	4.58	16.42
0.15 mm	108 mT	873 nWb	2.29	0.120/**8.30**	4.58	16.60
0.25 mm	180 mT	1457 nWb	2.29	0.119/**8.29**	4.58	16.58
0.35 mm	251 mT	2035 nWb	2.29	0.116/**8.31**	4.58	16.62
0.50 mm	355 mT	2874 nWb	2.29	0.110/**8.44**	4.58	16.88
0.70 mm	504 mT	4083 nWb	2.29	0.104/**8.29**	4.58	16.58
1.00 mm	724 mT	5868 nWb	2.29	0.088/**8.24**	4.58	16.48
1.25 mm	907 mT	7345 nWb	2.29	0.069/**8.25**	4.58	16.50
1.50 mm	1122 mT	9088 nWb	2.29	0.047/**7.96**	4.58	15.92
1.80 mm	1341 mT	10864 nWb	2.29	0.013/**8.04**	4.58	16.08

Table 13.1: Armature B-field for various armature displacements x. α and α_2 are the ideal values with zero magnetic leakage and α_{Th} and $\alpha_{2,Th}$ are the Thévenin equivalents that takes leakage into account. $A_M = 2A_g = 12$ mm x 12 mm, $\mu_r = 1000$ for soft magnetic material.

Magnetic leakage reduces the Thévenin equivalent α (or $\alpha_{2,Th}$) relative to α_2 according to Eq. 13.2. Therefore, it makes no physical sense that $\alpha_{2,Th}$ and α_{Th} are both determined to be larger than their counterparts α_2 and α where magnetic leakage is not taken into account. When

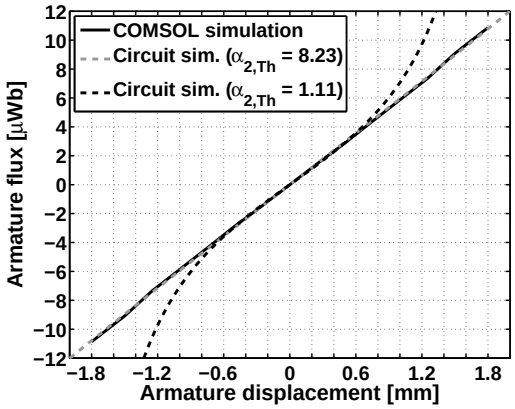

(a) $A_M = 2A_g = 12$ mm x 12 mm in the circuit model.

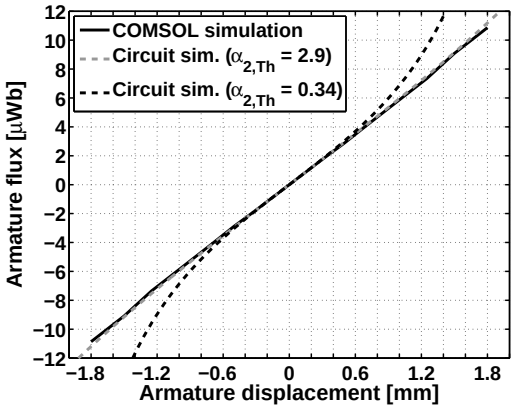

(b) $A_M = A_g = 6$ mm x 12 mm in the circuit model.

Figure 13.6: Simulated armature flux using COMSOL. COMSOL simulation is compared to circuit simulations with different estimates of α_2.

$\alpha_{2,Th}$ is determined via Eq. 13.1 it relies on the assumption that the magnetic circuit of the B-A loudspeaker can be modeled with two independent cross-sectional areas for the air gaps and for the permanent magnets. It also assumes that the leakage reluctance is independent of the armature displacement. The correct choice of A_M and A_g is somewhat unclear for the case where the permanent magnet is larger than the pole pieces as discussed in Chapter 12. The prediction of α_{Th} using Eq. 13.1 clearly suggests that the circuit model needs improvement as the large $\alpha_{2,Th}$ and α_{Th} values are unphysical. If A_M is assumed to be the same as A_g the results in table 13.2 follow. The flux curves for these α_2-values are shown in Fig. 13.6(b). With this smaller estimated A_M-value the Thévenin equivalent α is reduced by about 37 % (from 4.58 to 2.90) due to leakage and this appears to be a realistic number. However, the proposal that A_M should be reduced to equal A_g is simply an experiment with no particular physical merit: Fig. 12.4(b) suggests that A_M should be reduced by less than 15 % when A_M is twice that of A_g. However, the experiment serves to show that the estimated $\alpha_{2,Th}$ can vary a great deal depending on the choice of A_M.

x:	Average B_a	Φ_a	$\alpha_2 = \alpha = D_M/D$	$\alpha_{2,Th} = \alpha_{Th}$
0.05 mm	36.1 mT	292.4 nWb	4.58	0.353/**2.83**
0.10 mm	72.4 mT	586.8 nWb	4.58	0.355/**2.81**
0.15 mm	108 mT	873 nWb	4.58	0.347/**2.86**
0.25 mm	180 mT	1457 nWb	4.58	0.344/**2.86**
0.35 mm	251 mT	2035 nWb	4.58	0.336/**2.88**
0.50 mm	355 mT	2874 nWb	4.58	0.315/**2.96**
0.70 mm	504 mT	4083 nWb	4.58	0.298/**2.90**
1.00 mm	724 mT	5868 nWb	4.58	0.248/**2.92**
1.25 mm	907 mT	7345 nWb	4.58	0.191/**2.97**
1.50 mm	1122 mT	9088 nWb	4.58	0.131/**2.87**
1.80 mm	1341 mT	10864 nWb	4.58	0.034/**2.99**

Table 13.2: Armature B-field for various armature displacements x. α is the ideal value with zero magnetic leakage and α_{Th} is the Thévenin equivalent α which takes leakage into account. $A_M = A_g = 6$ mm x 12 mm $\Rightarrow \alpha_{2,Th} = \alpha_{Th}$, $\mu_r = 1000$ for soft magnetic material.

It is important to acknowledge that this particular $\alpha_{2,Th}$ is only correct for the specific con-

sidered geometry. Any change in the magnet height, air gap height, armature dimensions or other changes to the geometry of the magnetic circuit will affect the magnet leakage and therefore $\alpha_{2,Th}$. In the previous section it was shown how the magnetic permeability affects the magnetic flux so if the magnetic permeability is not already above, say, 1000-10000, $\alpha_{2,Th}$ will also be strongly influenced by μ_r. When $\alpha_{2,Th}$ is estimated α_{Th} can be determined according to Eq. 13.2 and the Thévenin equivalent μ_r can be determined as

$$\mu_{r,Th} = \frac{l_M}{\alpha_{Th} D}. \tag{8.2}$$

The Thévenin equivalent magnetomotive force and internal magnetic reluctance are then:

$$\mathcal{F}_{M,Th} = \frac{B_r l_M}{\mu_0 \mu_{r,Th}} \tag{3.12}$$

and

$$\mathcal{R}_{M,Th} = \frac{l_M}{\mu_0 \mu_{r,Th} A_M}. \tag{3.13}$$

Using the above transformed values (α_{Th} or $\alpha_{2,Th}$, $\mu_{r,Th}$, $\mathcal{F}_{M,Th}$ and $\mathcal{R}_{M,Th}$) will ensure that magnetic leakage is taken into account using the usual circuit equations.

13.4 Measurement of Nonlinear Parameters

In this section measurements of the nonlinear parameters are presented. The nonlinear inductance as well as the nonlinear magnetic stiffness compensation were successfully measured, although with outcomes that were different from the expected ones. The measurement of the force factor turned out to be problematic as the armature would saturate at very small displacements making it impossible to measure the force factor over the full span of the air gap. The individual measurements are described in more detail in the following sections.

13.4.1 Measurement of the Nonlinear Inductance

The nonlinear electrical inductance is given in Eq. (5.47). By fixing the armature in a certain position x the electrical back-EMF due to armature motion is eliminated and the nonlinear inductance may be derived by observing Fig. 6.3(a) with $u = 0$. The electrical impedance due to the inductance can thus be found by simply subtracting the DC-resistance of the coil. In reality, a pure nonlinear inductor is not capable of modeling the electrical impedance of the balanced-armature loudspeaker as eddy-current losses and hysteresis losses will influence the inductance. This is no different from the common moving-coil loudspeaker [30, Sec. 6.2 and 6.17] where a frequency-dependent inductor and a frequency-dependent resistor in parallel may be employed to model the lossy inductance.

In the analysis presented here the inductance is simply derived from the imaginary part of the electrical impedance assuming the relationship

$$\mathrm{im}\left\{ Z_E\left(x,\omega\right)|_{\frac{dx}{dt}=0} \right\} = L\left(x,\omega\right) j\omega. \tag{13.3}$$

In this analysis, the exact frequency dependence is not as important as the change in inductance with x for a fixed frequency. The measurement procedure was to insert a couple of small non-magnetic spacers on each side of the armature between the armature and the permanent magnets, thereby fixing the armature at a certain displacement x. The excitation signal was a 6.4 kHz wide noise signal with an rms voltage of about 500 mV applied to the loudspeaker terminals. The input current was measured by measuring the voltage across a 10 Ω resistor in series with the loudspeaker. The frequency response between the loudspeaker input voltage and current i.e. the electrical impedance was then estimated using Brüel & Kjær's Pulse hardware and software.

First, the dynamic electrical input impedance was measured. In this measurement the armature is free to move. The result is shown in Fig. 13.7. Figure 13.8 shows the same measurement results but with the DC-resistance of the coil subtracted from the measured impedance. Figure 13.8(b) indicates that for the lowest frequencies the loudspeaker load is close to being purely inductive i.e. with very small losses except, of course, for the power dissipated in the DC resistance of the coil. As the frequency is increased towards the mechanical resonance frequency the mechanical losses increase and this causes the large dip in the phase response. The velocity-induced back-EMF reaches its maximum at the mechanical resonance frequency and this causes the peak and the dip (depending on the phase) in the impedance magnitude response between 100 and 150 Hz. As the eddy current losses increase the phase starts decreasing slowly. The sudden large drop in the phase at around 2 kHz is caused by higher order mechanical modes in the armature: The resonances can barely be detected but appear to occur at around 1 kHz and 2.5 kHz. These higher order armature modes are not investigated any further and they are neither included in the model that only captures the fundamental "mass-spring" resonance.

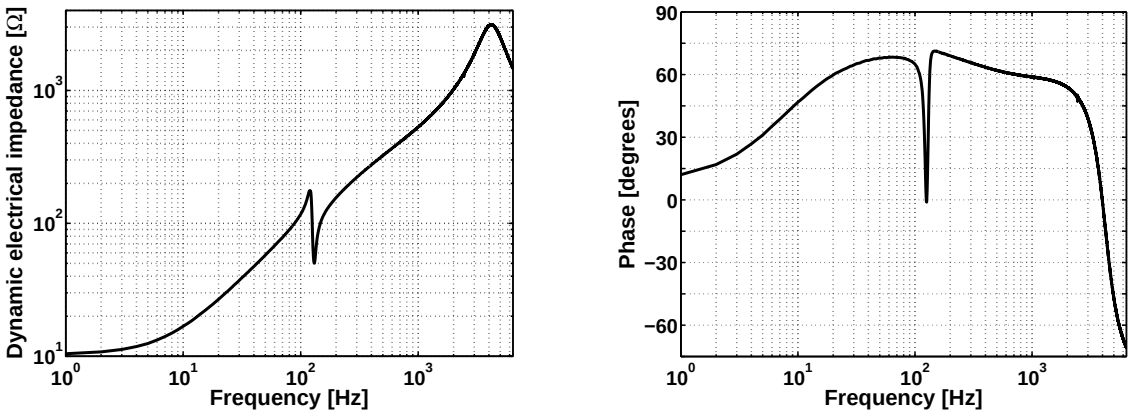

(a) Dynamic electrical impedance (magnitude).

(b) Dynamic electrical impedance (phase).

Figure 13.7: The dynamic electrical input impedance of the balanced-armature loudspeaker scale-model.

Next, the aforementioned non-magnetic spacers were put in place between the armature and

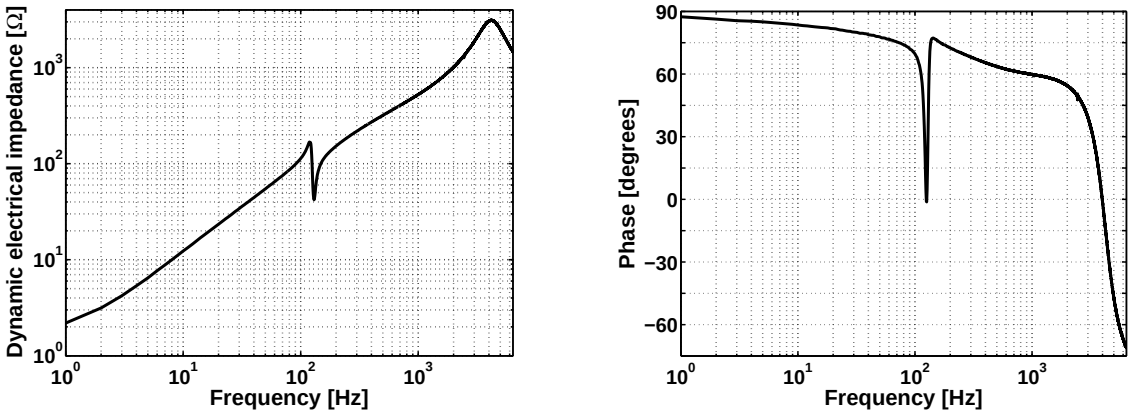

(a) Magnitude. (b) Phase.

Figure 13.8: The dynamic electrical input impedance of the balanced-armature loudspeaker scale-model after the DC-resistance of the coil has been subtracted.

the permanent magnets allowing to measure the electrical impedance without the contribution from the motional back-EMF and with the armature displaced by a certain fixed amount. Fig. 13.9 shows the blocked electrical impedance of the scale-model for 4 different armature displacements. Fig. 13.9(a) indicates that the impedance, hence the inductance decreases with x which is the exact opposite of the predicted behavior (see Fig. 7.2(a)). This motivated the measurement of the nonlinear electrical impedance with the permanent magnets removed. Removing the magnets will make it easier to identify whether the change in impedance is due to the change in geometry of the core of the coil or if it is due to the magnetic DC flux which is set up in the armature when it is displaced from its resting position. When a soft magnetic material is operated at some offset it will tend to saturate for smaller coil excitations compared to symmetrical excitation around a zero DC-flux point. Furthermore, the small-signal permeability may simply be reduced when driven at some offset due to the magnetic properties of the soft magnetic material. In the end this may cause a reduction in the effective magnetic permeability and this is exactly what is observed throughout the measurements presented in this section. When the permanent magnets are removed (Fig. 13.9(b)) the impedance only shows a very weak dependence on the armature displacement. The reason for that will be discussed at the end of this section, for now, let it be accepted that the electrical impedance is almost independent of the armature displacement when the permanent magnets are removed. For comparison reasons measurements with and without the permanent magnets mounted will be shown in pairs throughout this section.

Fig. 13.10 shows the phase of the electrical impedance. With the permanent magnets removed the phase of the electrical impedance is only affected very little by the displacement of the armature. However, with the permanent magnets mounted the phase is clearly affected.

As the DC-resistance of the coil in the loudspeaker is about 10.65 Ω it is interesting to subtract this resistance from the electrical impedance to better observe the behavior of the lossy inductance. Fig. 13.11 and 13.12 show the magnitude and the phase of the electrical impedance when the DC-resistance of the coil has been subtracted. Results are shown for the case where the permanent magnets are in place and when they are removed. It may be observed that for low frequencies

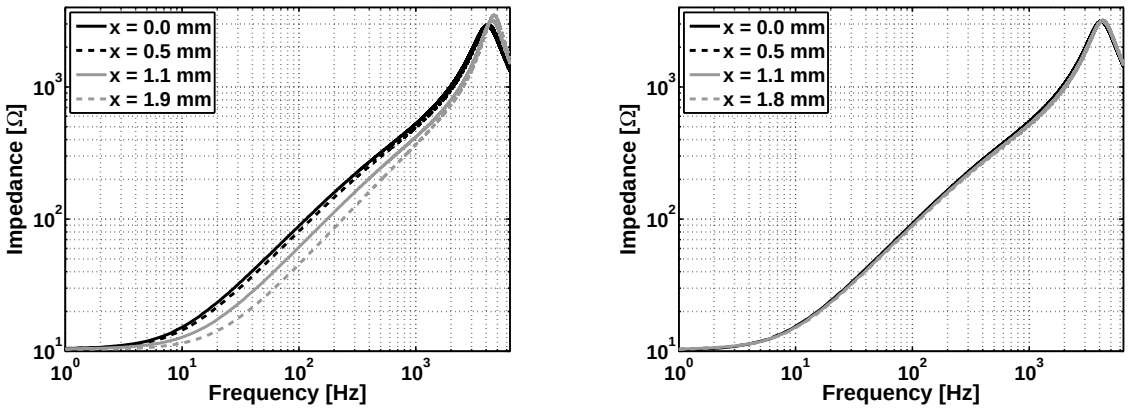

(a) With permanent magnets.

(b) Permanent magnets removed.

Figure 13.9: The blocked electrical input impedance of the balanced-armature loudspeaker scale-model for 4 different armature displacements.

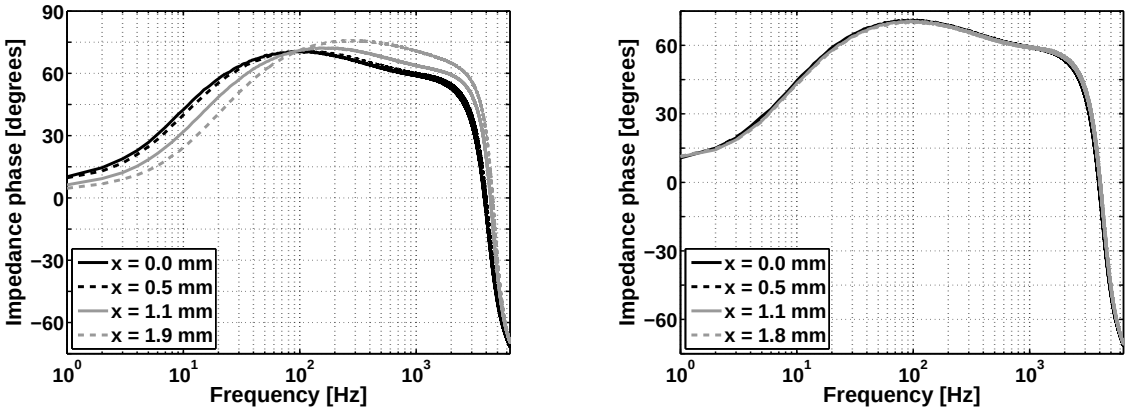

(a) With permanent magnets.

(b) Permanent magnets removed.

Figure 13.10: The phase of the blocked electrical input impedance of the balanced-armature loudspeaker scale-model. Results are shown for 4 different armature displacements

where the eddy current losses are relatively small the phase of the impedance is very close to 90° indicating that the core of the coil has very little losses and that the loudspeaker impedance therefore behaves almost as a pure inductor when the DC-resistance of the coil is neglected. Comparing Figures 13.11(a) and 13.12(a) at 1 kHz one can make a curious observation: For $x = 0$ the magnitude of the impedance is largest indicating that the magnitude of the magnetic permeance and hence the permeability is largest here whereas the phase of the impedance is at a minimum here indicating that the loss in the magnetic core is at its maximum here. So how can the magnetic losses be at their maximum when the magnetic permeability appears to be at its maximum also? Looking at the measured hysteresis curves in Sec. 4.4 it is perfectly possible to imagine a hysteresis loop or a perfect elliptical Lissajous curve which has a larger slope than an other hysteresis loop while at the same time spanning a larger area indicating larger hysteresis losses.

In order to observe the nonlinear behavior of the electrical inductance the inductance is plotted as function of the armature displacement for a certain frequency. The inductance is derived using

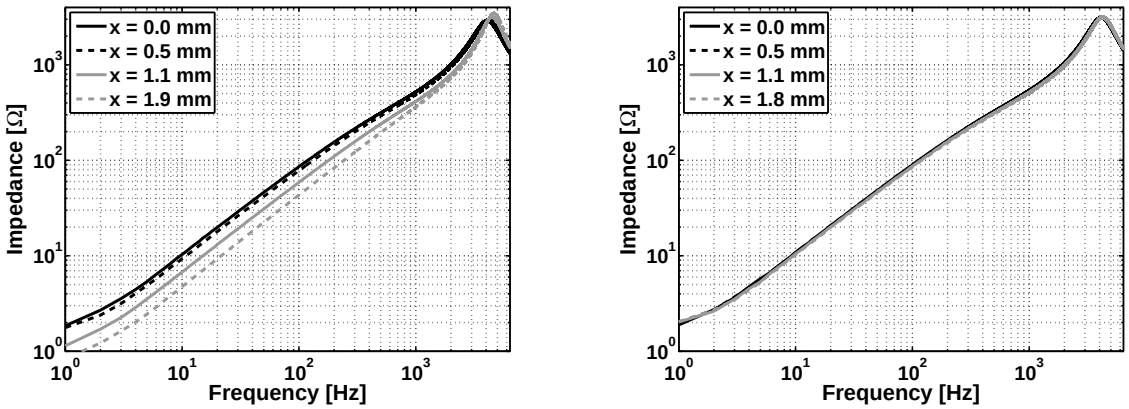

(a) With permanent magnets.

(b) Permanent magnets removed.

Figure 13.11: The blocked electrical input impedance of the balanced-armature loudspeaker scale-model after the DC-resistance of the coil has been subtracted. Results are shown for 4 different armature displacements.

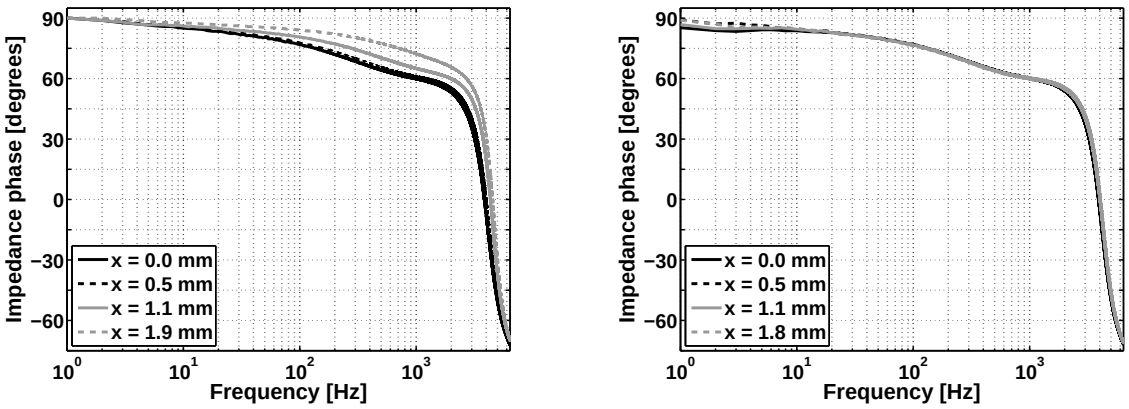

(a) With permanent magnets.

(b) Permanent magnets removed.

Figure 13.12: The phase of the blocked electrical input impedance of the balanced-armature loudspeaker scale-model after the DC-resistance of the coil has been subtracted. Results are shown for 4 different armature displacements

Eq. (13.3). The nonlinear inductance with and without the permanent magnets mounted are shown in Fig. 13.13 and Fig. 13.14 shows the normalized nonlinear inductance. Clearly, the measured nonlinear inductance does not behave as expected (see Fig. 7.2(a)). The inductance was expected to increase with the displacement of the armature as this ought to improve the flux path through the coil. It is possible to explain the observed behavior by comparing Fig. 13.13(a) to Fig. 13.13(b): It is clear that the armature displacement affects the inductance much more significantly when the permanent magnets are in place. This confirms that the most significant reduction of the induction is indeed caused by the DC-flux set up in the armature by the permanent magnets as the armature is displaced. Even though this phenomenon will generally occur in any balanced-armature loudspeaker it is also a phenomenon which is very much related to the specific choice of soft magnetic material. Comparing the same two figures one can observe a good agreement between the inductance when the magnets are removed to that of the small-signal inductance

when the permanent magnets are in place. This is expected as the DC-offset in armature flux is small for small displacements.

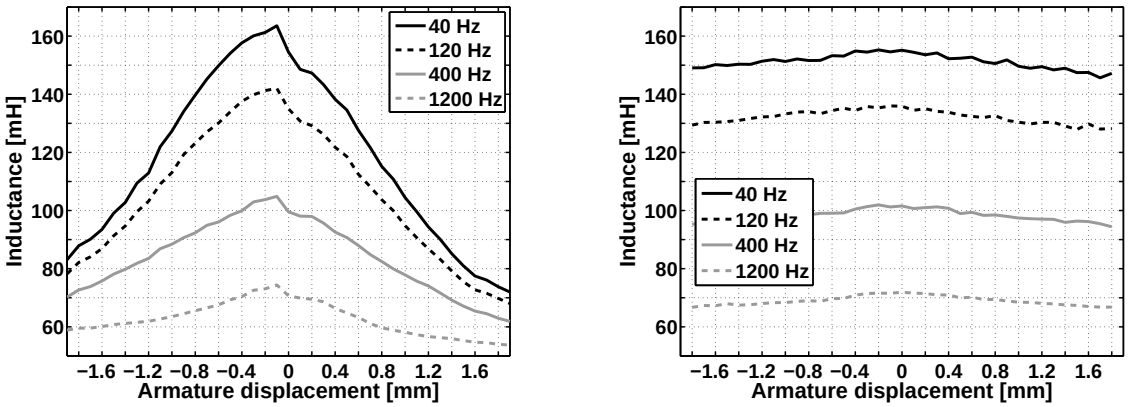

(a) With permanent magnets.

(b) Permanent magnets removed.

Figure 13.13: The nonlinear inductance of the balanced-armature loudspeaker scale-model shown with and without the permanent magnets mounted. Results are shown for 4 different frequencies.

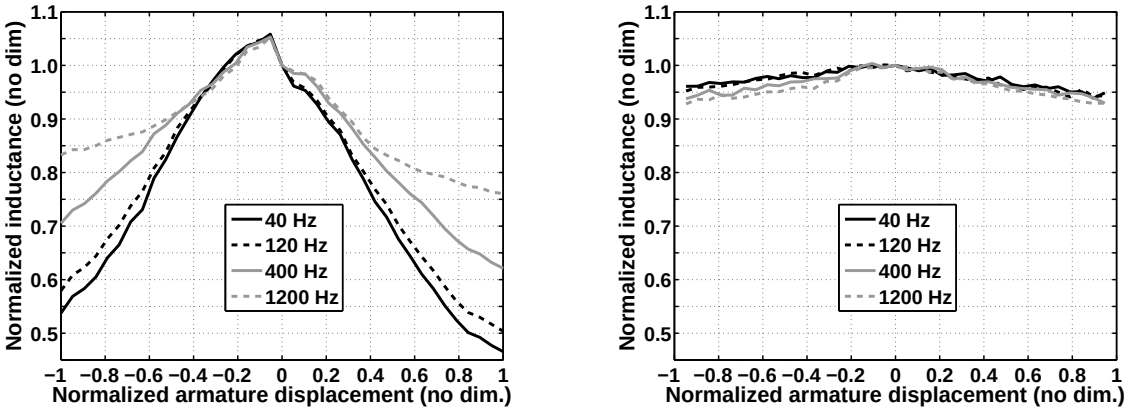

(a) With permanent magnets.

(b) Permanent magnets removed.

Figure 13.14: The normalized nonlinear inductance of the balanced-armature loudspeaker scale-model with and without the permanent magnets mounted. Results are shown for 4 different frequencies.

The displacement-dependent inductance when the permanent magnets are removed still needs to be explained. The obvious explanation to the observed reduction of the inductance is to argue that the effective core permeance is reduced as the armature is displaced. However, a reduction in the core permeance may either be ascribed to reduced material permeability or to a deterioration of the core geometry. COMSOL finite element simulations of the loudspeaker without the permanent magnets suggest that the armature flux due to coil current increases by less than 0.4% with the armature displaced by 2 mm. This indicates that the flux path of the coil core, hence the inductance, is improved, although only very little, when the armature displaced. This tiny increase in electrical inductance is nowhere near the predicted (see Fig. 7.2(a)). These simulations use a constant real-valued permeability so this simulation is not capable of capturing any magnetic effects imposed on the soft magnetic material due to an offset in the DC flux level. Thus, there is good reason

to believe that the observed (small) decrease in inductance with x - for the loudspeaker without permanent magnets - is indeed due to a reduction in the magnetic permeability as the armature is displaced. The permeability could be reduced for the following reason: As the permanent magnets are removed from the loudspeaker DC-flux remains in the soft magnetic material of the armature and the loudspeaker structure due to magnetic hysteresis. As the flux path is improved slightly when the armature is displaced a buildup of DC-flux may occur. This magnetic flux DC-offset in the soft magnetic material will likely reduce its permeability and thus the observed inductance will be reduced if the effect of the reduced armature permeability is more significant than the improved flux path due to the change in geometry caused by the armature displacement.

It is of some interest to observe the relative deviations of the normalized inductance shown in Fig. 13.14(a). At 40 Hz the deviation is more than -45 % for a full armature excursion. In comparison, the predicted inductance should vary by less than +35 % for a full armature excursion for $\alpha = 1$ (see Fig. 7.2(a)).

In conclusion it may be observed that for this specific loudspeaker design the nonlinear electrical inductance is influenced much more by the magnetic properties of the soft magnetic material than by the geometrical change on its own. Looking at Fig. 13.5(a) this should be no surprise as the COMSOL simulations suggest that the B-field (due to the permanent magnets only) is more than 1 T for an armature displacement of 1.5 mm for a permeability of 1000. FEM simulations suggest that the coil alone adds another 0.7-1 T when a steady current of 50 mA is injected into the coil corresponding to a drive voltage of about 0.5 V_{rms}. This suggests that there is good reason to believe that the armature gets magnetically saturated during this measurement of the nonlinear inductance as the armature is displaced further away from its resting position.

13.4.2 Measurement of the Nonlinear Magnetic Stiffness Compensation

The nonlinear magnetic stiffness compensation $k_\Phi(x)$ is deduced via the relation

$$k_{a,tot}(x) = k_a(x) - k_\Phi(x) \Leftrightarrow k_\Phi(x) = k_a(x) - k_{a,tot}(x). \tag{13.4}$$

where $k_{a,tot}(x)$ is the total displacement-dependent armature stiffness when the mechanical armature stiffness $k_a(x)$ and the magnetic stiffness compensation are taken into account. For the scale-model there is no acoustic stiffness nor any suspension that can affect the total stiffness. Thus, the total stiffness experienced by a constant force attacking the tip of the armature is only affected by the mechanical stiffness of the armature and the magnetic force due to the nonlinear magnetic stiffness compensation. Measurements were carried out by statically loading the tip of the armature while measuring the displacement of the armature. This was done using an Instron 3343 load frame mounted with an Instron 2519-103 force transducer. The interaction between the force transducer and the armature was via a pointy, non-magnetic rod which would push down on the tip of the armature right in front of the permanent magnets. The stiffness of the rod is much greater than that of the armature. The force measurements for the downward direction are shown in Fig. 13.15(a). $F_a(x)$ denotes the force that the armature tip exerts on the force transducer when

the permanent magnets are removed from the loudspeaker. $F_{a,tot}\,(x)$ denotes the force which is exerted on the force transducer when the permanent magnets are in place so that the experienced force is the sum of the magnetic force and the armature force due to its stiffness. The magnetic force is derived as the difference between those two force measurements. The sudden increase in force at about -1.9 mm is due to the armature hitting the lower permanent magnet. Due to magnetic hysteresis the force curves do not cut through (0,0): With the magnets mounted, a full displacement of the armature in the upward direction will cause the armature to settle a little bit higher than the center between the magnets when released. The legend indicates that for the force measurements in the downward direction the armature was initialized by pushing it up against the upper magnet and then left to rest a little bit above the center. It can be observed that the total required force that displaces the armature all the way down to the permanent magnet is significantly reduced from about 3.5 N to less than 1 N by the magnetic stiffness compensation.

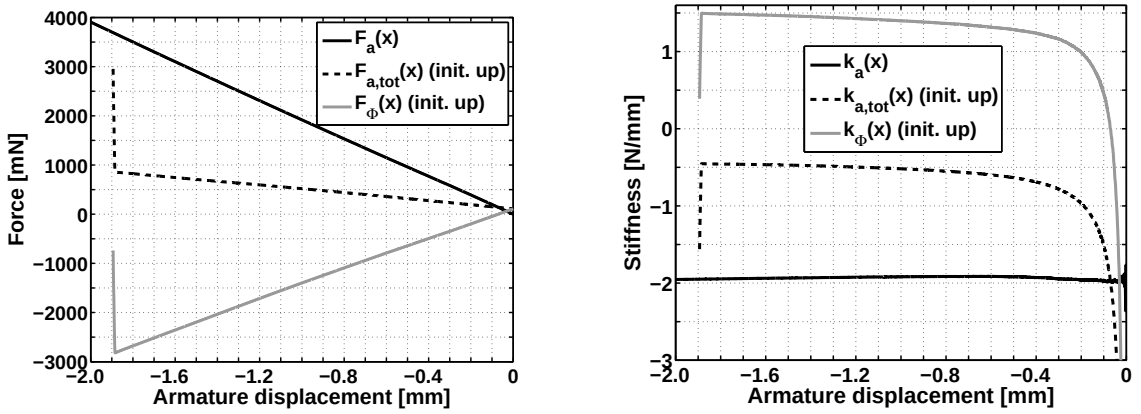

(a) Forces. (b) Stiffnesses.

Figure 13.15: The armature force due to mechanical stiffness, the magnetic force and the sum of the two (a). (b) shows the corresponding stiffnesses obtained by dividing the forces by the armature displacement.

One may associate a nonlinear stiffness to each of these force measurements. This is defined as the force divided by the armature displacement and this is shown in Fig. 13.15(b). The strange behavior below about $x = 0.5$ mm can mainly be attributed to magnetic hysteresis which puts an offset on the total force curve so that the force is not zero for zero armature displacement. This can be observed for the $F_{a,tot}$ curve in Fig. 13.15(a): The force starts out being greater than zero because the armature has been initialized by pushing it towards the upper magnet which leaves the armature in a resting position above $x = 0$ due to magnetic hysteresis. This suggests that it would be beneficial to use a soft magnetic material with higher initial permeability and smaller coercivity.

The small force offset at $x = 0$ for the total force shown in can give a false impression of how the stiffness changes with displacement due to the definition of the stiffness. Imagine that a force versus displacement curve can be described by the equation

$$F\,(x) = ax + b. \tag{13.5}$$

The local stiffness is the slope of this curve $dF\left(x\right)/dx$ but the stiffness $k\left(x\right)$ of interest in this work is the one that provides the relationship between the force and the displacement through the relationship $F\left(x\right) = k\left(x\right)x$. This means that the stiffness associated with the force defined in Eq. (13.5) is

$$k\left(x\right) = \frac{F\left(x\right)}{x} = a + \frac{b}{x}. \tag{13.6}$$

The nonlinear stiffness provided in Eq. (13.6) does indeed provide the relationship between force and displacement but it does not reflect how the stiffness changes locally. However, if the offset force b at $x = 0$ is subtracted before dividing by x one would simply get the parameter a which provides more useful information regarding how the stiffness changes locally. This idea is applied to the force measurements shown in Fig. 13.15: The small force offset is subtracted from $F_{a,tot}\left(x\right)$. This will also remove the offset from the magnetic force which is derived as the difference between the total force and the armature force with the permanent magnets removed. The force curves with the offset removed and the associated stiffness curves are shown in Fig. 13.16.

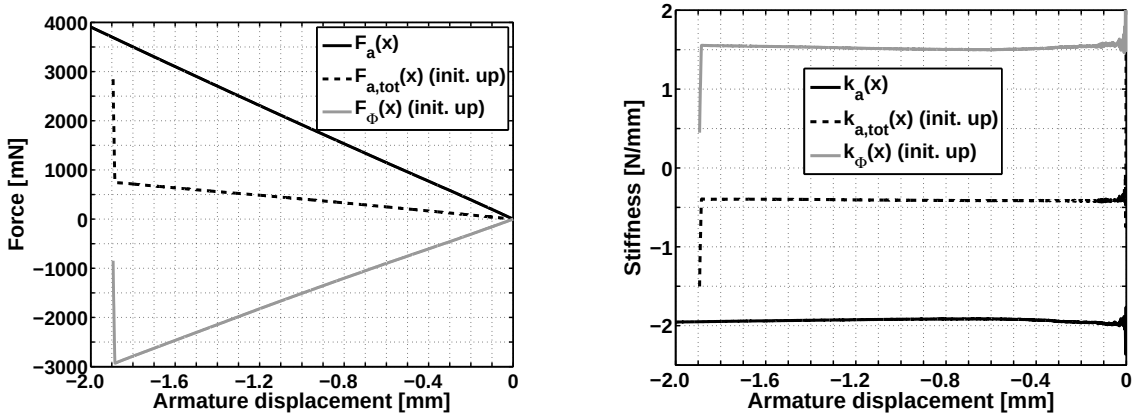

(a) Forces with offset removed.

(b) Stiffnesses with force offset removed.

Figure 13.16: The armature force due to mechanical stiffness, the magnetic force with offset removed and the sum of the two (a). (b) shows the corresponding stiffnesses obtained by dividing the forces by the armature displacement.

This figure reveals that, aside from the offset, the forces appear to be almost linearly related to the armature displacement. If the stiffnesses are normalized to ± 1 and shifted it is easier to see any nonlinear behavior. This is shown in Fig. 13.17. It may be observed that the magnetic stiffness compensation $k_{\Phi}\left(x\right)$ increases by less than 5 % which corresponds to what can expected for $\alpha > 4$ according to Fig. 7.1(a). Including leakage effects the α of this scale-model loudspeaker is expected to be lower than that.

Fig. 13.17(b) shows that the magnetic stiffness compensation is only a bit nonlinear but that it does increase with armature displacement as predicted in Fig. 7.1(a). The COMSOL simulations of $k_{\Phi}\left(x\right)$ presented in Sec. 7.2 revealed that the magnetic stiffness compensation was more

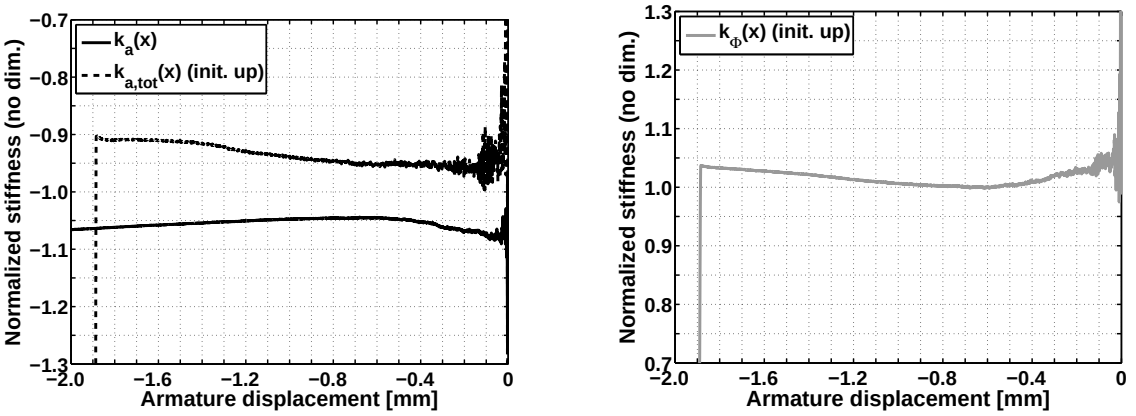

(a) Normalized and shifted $k_{a,tot}\left(x\right)$ and $k_a\left(x\right)$.

(b) Normalized $k_\Phi\left(x\right)$.

Figure 13.17: (a): Normalized magnetic stiffness compensation $k_\Phi\left(x\right)$ and (b):normalized and shifted total stiffness $k_{a,tot}\left(x\right)$ and armature stiffness with permanent magnets removed.

nonlinear than expected and this was explained by the effect of magnetic leakage reducing the effective Thévenin equivalent α. The author believes that had it not been for magnetic saturation in the armature the measured $k_\Phi\left(x\right)$ would have been more nonlinear: The magnetic saturation tends to compress $k_\Phi\left(x\right)$ for large displacements which is the exact opposite effect of that ascribed to the geometrical changes (see Fig. 7.1(a)).

13.4.3 Measurement of the Nonlinear Transduction Coefficient

In order to avoid eddy current effects it was decided to attempt to measure the transduction coefficient under static conditions. The total force versus armature displacement under static conditions was measured in the previous section. This means that the static input force to the armature can be determined if the armature displacement is known. This input force is that due to the coil current which generates the two forces $T\left(x\right)i$ and $T_{me,d}\left(x,i\right)i$. Assuming that the latter distortion force is much smaller than the force that follows the input current it is possible to equate the force $F_{a,tot}\left(x\right)$ required to displace the armature by a certain distance with the input force set up by the coil current:

$$F_{a,tot}\left(x\right) = T\left(x\right)i \Leftrightarrow \tag{13.7}$$

$$T\left(x\right) = \frac{F_{a,tot}\left(x\right)}{i}. \tag{13.8}$$

When the force factor is estimated this way it will provide the ratio ratio between coil current and armature input force applied to the tip of the armature. For instance, a small non-magnetic spacer of, say, 0.5 mm was put on top of the lower permanent magnet and the coil current was increased until the armature would touch the spacer. In this fashion Fig. 13.18(a) was produced, showing the measured coil current versus the armature displacement. Optimally there should be a linear

relationship between the two with the displacement growing linearly with the excitation current. However, the curve shows strong signs of compression which is due to magnetic saturation in the armature. Notice that 150 mA displaces the armature by 0.8 mm and a further increase to 500 mA only increases the total armature displacement to 0.9 mm. Using the $F_{a,tot}(x)$ curve from Fig. 13.16(a) it is possible to relate the armature displacement to the force which is required for that given displacement. That force divided by the coil current is the nonlinear force factor and is plotted in Fig. 13.18(b). Again, it may be observed that there is a lot of compression in the system with the force factor starting at more than 11 N/A and dropping to a little less than 1 N/A for a displacement of only 0.9 mm. The reason why there is no data for very small displacements is because of magnetic hysteresis in the soft magnetic material of the loudspeaker - the armature is already offset by a small amount before any current is applied. The data for larger armature displacements are missing since it would require very large currents to displace the armature any further.

It is interesting to observe that it is (again) the magnetic saturation in the armature that determines the nonlinearity of the force factor and not so much the changes in the loudspeaker geometry. For a loudspeaker without armature saturation problems the force factor is expected to look like that shown in Fig. 7.1(b) which predicts a completely different behavior.

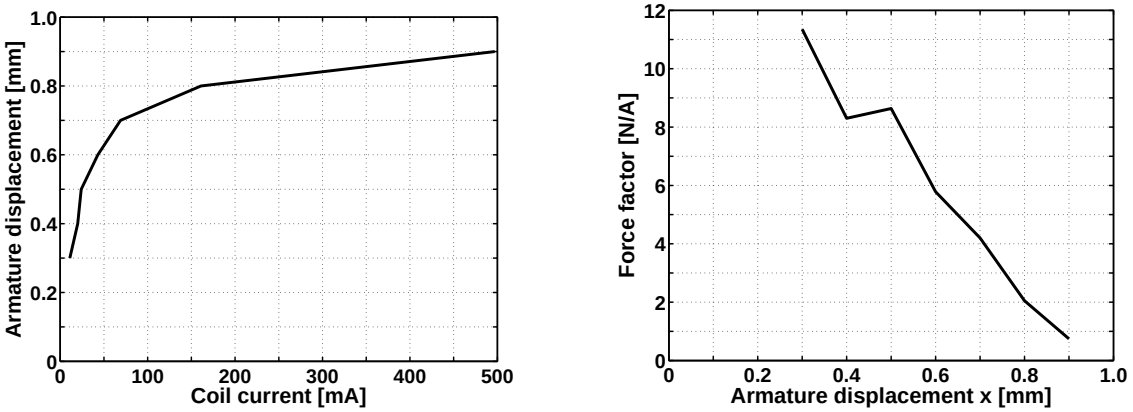

(a) Measured coil current vs armature displacement.

(b) Measured nonlinear force factor.

Figure 13.18: (a) Coil current vs armature displacement for a steady (DC) current applied to the coil. (b) Nonlinear force factor (or transduction coefficient) as function of armature displacement under static conditions.

13.4.4 Discussion

The largest obstacle in terms of measuring the nonlinear parameters due to geometrical changes is believed to be that of the saturation of the armature. Using the findings in Chapter 10 regarding the magnetic saturation of the armature and the adjustment possibilities of the B-A loudspeaker scale model a different design less prone to saturation should be made.

The measured loudspeaker scale-model configuration was designed to exhibit linear behavior in terms of the geometrical changes: This was done by the choice of a permanent magnet with a length more than 5 times that of the air gap height and with a low recoil permeability resulting

in $\alpha \approx 4.5$. In order to better measure the expected nonlinearities due to geometrical changes it would be beneficial to choose a design with smaller α.

The techniques used for the measurement of the nonlinear inductance and the nonlinear stiffness compensation appear to be working quite well. However, the method used to measure the nonlinear force factor is rather inaccurate: It is difficult to evaluate when the armature is actually touching the spacer. This measurement could easily be improved by measuring the armature displacement with a laser at the tip of the armature. However, this technique still relies on the force measurement of the armature performed in Sec. 13.4.2. A more direct way to measure the force factor dynamically would be to use a mechanical exciter on the armature and measure the armature velocity (with a laser) and the open-loop coil voltage for various armature offsets. The relationship between the coil voltage and the armature velocity is given in Eq. (5.43). If the voltage is measured in open-loop mode the electrical current is zero and the voltage due to the inductance can be assumed to be zero. The distortion force factor is proportional to the current so this will also be zero and $U_{\text{back}} = T(x)\, dx/dt$ is all that is left. Thus, when the induced voltage and the armature velocity dx/dt are known the nonlinear force factor $T(x)$ can be calculated.

Chapter 14

Discussion and Future Work

The usefulness of simple lumped element models has been stressed several times. Electrical, mechanical and acoustic lumped element models have proven themselves useful in many engineering applications as long as the considered frequencies are not too high. However, the use of lumped elements for magnetic modeling pose a problem due to magnetic leakage, hysteresis and eddy current effects. The fundamental "building blocks" of the balanced-armature loudspeaker magnetic circuit should be investigated in greater detail. Some of the questions that might be investigated are:

- How does the magnetomotive force set up by a coil depend on coil geometry for a fixed number of windings and a fixed electrical current?
- How should the air gap area and the corresponding magnetic flux between the armature and the magnets be determined in order to best predict the magnetic force between them?
- How should the armature flux be determined in order to best reflect the induced coil voltage?

One major deficit of the modeling approach presented in this thesis is the lack of a proper way to model eddy current losses and magnetic hysteresis. It is necessary to find an efficient way to model these phenomena with sufficient accuracy in order to predict the behavior of the balanced-armature loudspeaker. In order to implement a nonlinear model in the time domain, it is necessary to utilize physical time domain differential equations to model the eddy current losses and the hysteresis. One approach for capturing the effects of eddy currents might be to use a low-pass filter between the well-defined apparent H-field H_{ap} and the effective magnetizing H-field H_{eff} which is reduced at high frequencies due to eddy currents. The magnetic permeability could then be defined as a nonlinear parameter depending on H_{eff} so that the magnetic B-field could be determined as $B = \mu_0 \mu_r \left(H_{eff}\right) H_{eff}$. The nonlinear permeability could be described by the hyperbolic tangent or similar "S" shape sigmoid functions. As the overall goal of the proposed model is not very high accuracy but rather to gain insight, such a simple magnetic model might be well suited for capturing the general behavior of the balanced-armature loudspeaker.

It would be great to supplement the measurements of the scale model with measurements of the magnetic flux in the air gaps. This would help verify and refine the lumped element model. Hall-effect probes for measuring steady magnetic B-fields are available at thicknesses down to about 0.5 mm. With such a probe it is possible to measure the air gap B-field as function of the armature displacement for a scale model with an air gap height of 2 mm.

In this work, the back volume of the balanced-armature receiver is simply assumed to act as a pure lossless compliance. However, the back volume of the balanced-armature loudspeaker (see Fig. 1.1) contains narrow slits and openings between the armature and coil and the armature and the magnets housing. This means that a simple acoustic compliance may be insufficient to model the acoustic impedance at the back of the diaphragm. Also, since the surface area inside the back volume is rather large compared to the volume, viscothermal losses are probably relevant to include in an accurate model. It has already been discussed that the isothermal process near the thermal boundary layer yields an increased compliance but the increased acoustic losses due to viscous effects might also be necessary to include in order to accurately model the back volume. These are linear effects but the nonlinearity of the small front and back volume can also be included in the model to capture these distortion mechanisms if they are expected to be significant. In any case, the task of modeling the acoustic impedance at the back of the diaphragm is certainly a topic that deserves further investigations.

It has been shown (Chapter 7) that the various nonlinear loudspeaker parameters i.e. the magnetic stiffness compensation, the force factor, and the inductance increase due to the geometrical changes caused by the displacement of the armature. It is worth keeping in mind that some of these effects can counteract each other. In [25] it is demonstrated how an armature with increasing stiffness for increasing armature displacement may counteract the effect of the nonlinear stiffness compensation. It might be possible to obtain similar effects by balancing the effects of the nonlinear force factor, the nonlinear inductance and the magnetic saturation of the armature. Recall that an increase in the magnetic stiffness compensation for large x will reduce the effective stiffness for large x. At high frequencies where the inductance is significant the increased inductance for large x will reduce the input current and this may counteract the increase of the force factor factor. It has been demonstrated that magnetic saturation of the armature is a likely effect if the balanced-armature loudspeaker is not designed correctly. However, a small amount of compression may help counteract the effect of increasing force factor and reduced effective stiffness for large x.

Depending on the required frequency range of the loudspeaker and the geometry and material of the armature it will often be necessary to include a model of the armature which is capable of capturing the higher order modes of vibration. The same may be true for the diaphragm and the thin drive pin that connects the armature to the diaphragm.

Chapter 15

Conclusions

The three main goals of this work was to gain a better understanding of the distortion mechanisms, the efficiency and the limitations of the maximum output of the balanced-armature loudspeaker. Important steps have been taken in all three areas and the most important ones are summarized below. A few unexpected but important results that are not directly related to any of the above mentioned areas are also pointed out at the end of this chapter.

Nonlinear Parameters and Distortion

It has been shown how the various nonlinear loudspeaker parameters $k_\Phi(x)$, $T(x)$, $L(x)$ and the distortion force factors $T_{me,d}(x,i)$ and $T_{em,d}(x,i)$ are all affected by geometrical changes caused by armature movement. More important, it has been demonstrated that an increase in the ratio $\alpha = D_M/D$ will reduce the nonlinearity of all these parameters. An increase in α will also help reduce the unwanted distortion force factor and the distortion back-EMF.

Analytical expressions for the magnetic armature flux were derived, showing that unless the loudspeaker is carefully designed, there is a risk of saturating the armature with magnetic flux, and this was confirmed with measurements on a large scale model. Magnetic saturation of the armature causes compression of the loudspeaker signal and this compression has the potential to impact the behavior of the various nonlinear loudspeaker parameters more than the geometrical changes caused by armature movement. However, in order to model this type of distortion the loudspeaker model should be supplemented with a hysteresis model of sufficient accuracy i.e. one that captures frequency effects, saturation and minor hysteresis loops correctly.

It has been demonstrated how the acoustic compliance of the small volumes in the balanced-armature loudspeaker may easily be nonlinear for the relevant volumes and diaphragm displacements. In general, the nonlinearity of the back volume will affect the behavior of the loudspeaker more than the nonlinearity of the small front volume, but this depends on the specific front load. The asymmetrical nonlinear compliance of the back volume will cause even order distortion products in the acoustic output.

Efficiency

It is shown that the efficiency of the balanced-armature loudspeaker is largely related to the produced armature input force Ti for a given power dissipation $R_L i^2$ in the coil. Besides this, at low frequencies the effective armature stiffness, including the stiffness of the back volume and the diaphragm suspension, should be small. At high frequencies the total moving mass consisting

of armature, diaphragm, drive pin and any acoustic mass should be as small as possible. It is shown that an increase in α significantly increases the low frequency efficiency if the back volume stiffness is not dominant.

It has been shown that the performance of the coil, in terms of Constant Input Power efficiency, is related to its geometry with increasing efficiency for increasing coil dimensions. However, as more layers of windings are added to the coil, the increase in efficiency becomes very small beyond a certain point. This implies that there is a "sweet spot" in terms of coil size. Increasing the coil thickness beyond this point will only increase the coil performance very little but it will increase the coil price a lot and it will also reduce the available back volume. As the back volume is reduced the acoustic compliance decreases and this will cause a drop in the low-frequency efficiency.

The above observation implies that there is an optimal ratio between coil size and back volume for low frequency efficiency. Simulations show that at least a few dB of sound pressure may be gained by carefully adjusting this ratio. When the stiffness of the back volume has a large effect on the overall loudspeaker stiffness, the efficiency may also be improved by reducing the diaphragm area. This, however, will reduce the maximum possible output pressure.

Maximum Output

Through theoretical considerations of the equations derived from simple lumped-element models and through COMSOL FEM simulations and measurements performed on a large scale B-A loudspeaker it has been shown that magnetic saturation of the armature is the main limitation of the maximum output.

Equations based on the lumped element model show that the magnetic armature flux increases with the maximum possible displacement D. This suggests that the balanced-armature topology is ill-suited for large loudspeaker designs.

Leakage

It has been shown how the effect of magnetic flux leaking between the magnetic south and north pole can be taken into account using a simple transformation of the recoil permeability of the permanent magnets. It is also shown that by taking leakage into account the effective α is reduced causing an increase in the nonlinearity of the various loudspeaker parameters.

Loudspeaker Stability

Throughout this work, it is demonstrated that a certain criterion in terms of the armature stiffness has to be met, otherwise the loudspeaker will be unstable i.e. the armature will spontaneously flip away from its balanced position and cling to one of the permanent magnets. It has been demonstrated how the stability constraint can be imposed to the general loudspeaker equations. When this is done, only stable loudspeaker designs are considered and the various equations can be simplified and further insight may be gained. Taking the stability constraint into account sometimes result in counterintuitive results.

Other Findings

It has been shown that the 3 major small-signal loudspeaker parameters T, k_Φ and L are related via the relationship $T^2 = k_\Phi L$. This is a very fundamental result which reveals a lot about the properties of the B-A loudspeaker and the necessary compromises.

Finally, a measurement setup for the characterization of soft magnetic materials was built. With this setup it is possible to measure the magnetic hysteresis of small ring samples of soft magnetic material. The hysteresis can be measured in the entire audio range for different excitation amplitudes and an offset in the H-field may be applied. The associated MATLAB scripts makes it possible to generate curves showing the apparent magnetic permeability and the distortion of the B-field for the tested material.

Bibliography

[1] W. J. Cunningham. Non-linear distortion in dynamic loudspeakers due to magnetic effects. *J. Acoust. Soc. Am.*, 21(3):202–207, May 1949.

[2] Harry F. Olson. *Elements of Acoustical Engineering*. D. VAN NOSTRAND COMPANY, INC., 2nd edition, 1957.

[3] Wolfgang Klippel. Dynamic measurements and interpretation of the nonlinear parameters of electrodynamic loudspeakers. *J. Audio Eng. Soc.*, 38(12):944–955, Dec. 1990.

[4] Wolfgang Klippel. The mirror filter - a new basis for reducing nonlinear distortion and equalizing response in woofer systems. *J. Audio Eng. Soc.*, 40(9):675–691, September 1992.

[5] Hans Schurer, Alex G.J. Nijmeijer, Mark A. Boer, Cornelis H. Slump, and Otto E. Herrmann. Identification and compensation of the electrodynamic transducer nonlinearities. *1997 IEEE International Conference On Acoustics, Speech, And Signal Processing*, 3:2381–2384, April 1997.

[6] Malcolm McCaig and Alan G. Clegg. *Permanent magnets in theory and practice*. John Wiley & Sons, 2nd edition, 1987.

[7] Peter Campbell. *Permanent Magnet Materials and Their Application*. Cambridge University Press, reprint edition, July 1996.

[8] Edward P. Furlani. *Permanent Magnet and Electromechanical Devices*. Academic Press, 2001.

[9] David C. Hamill. Gyrator-capacitor modeling: A better way of understanding magnetic components. *IEEE Transactions on Power Electronics*, 8(2):297–103, April 1993.

[10] David C. Hamill. Gyrator-capacitor modeling: A better way of understanding magnetic components. In *Applied Power Electronics Conference and Exposition, 1994. APEC '94. Conference Proceedings 1994., Ninth Annual*, volume 1, pages 326–332. IEEE Conference Publications, September 1994.

[11] Frederick V. Hunt. *Electroacoustics - The Analysis of Transduction and Its Historical Background*. Published by the American Institute of Physics for the Acoustical Society of America, Printed in the United States of America, 1954, 1982.

[12] Herbert Christopher Roters. *Electromagnetic Devices*. John Wiley & Sons, January 1941.

[13] B. I. Bleaney and B. Bleaney. *Electricity and Magnetism*. Oxford University Press, 3rd edition, 1989, reprint 1991.

[14] L. P. Lefebvre, S. Pelletier, and C. Gélinas. Effect of electrical resistivity on core losses in soft magnetic iron powder materials'. *Journal of Magnetism and Magnetic Materials*, 176(2):93–96, December 1997.

[15] Von F. Preisach. Über die magnetische nachwirkung. *Zeitschrift für Physik*, 94(5-6):277–302, May 1935.

[16] D. C. Jiles and D. L. Atherton. Theory of ferromagnetic hysteresis. *Journal of Magnetism and Magnetic Materials*, 61:48–60, September 1986.

[17] D. C. Jiles and J. B. Thoelke. Theory of ferromagnetic hysteresis: Determination of model parameters from experimental hysteresis loops. *IEEE Transactions on Magnetics*, 25(5):3928–3930, September 1989.

[18] David C. Jiles, J. B. Thoelke, and M. K. Devine. Numerical determination of hysteresis parameters for the modeling of magnetic properties using the theory of ferromagnetic hysteresis. *IEEE Transactions on Magnetics*, 28(1):27–35, January 1992.

[19] D. C. Jiles. Frequency dependence of hysteresis curves in conducting magnetic materials. *J. Appl. Phys.*, 76(10):5849–5855, November 1994.

[20] D. C. Jiles. Modelling the effects of eddy current losses on frequency dependent hysteresis in electrically conducting media. *IEEE Transactions on Magnetics*, 30(6):4326–4328, November 1994.

[21] Kenneth H. Carpenter. A differential equation approach to minor loops in the jiles-atherton hysteresis model. *IEEE Transactions on Magnetics*, 27(6):4404–4406, November 1991.

[22] Jean V. Leite, Abdelkader Benabou, and Nelson Sadowski. Accurate minor loops calculation with a modified jiles-atherton hysteresis model. *COMPEL: The International Journal for Computation and Mathematics in Electrical and Electronic Engineering*, 28(3):741–749, 2009.

[23] Jean V. Leite, N. Sadowski, Patrick Kuo-Peng, and Abdelkader Benabou. Minor loops calculation with a modified jiles-atherton hysteresis model. *Journal of Microwaves, Optoelectronics and Electromagnetic Applications*, 8(1):49–55, June 2009.

[24] Péter Kis. *Jiles-Atherton Model Implementation to Edge Finite Element Method*. PhD thesis, Budapest University of Technology and Economics, August 2006.

[25] Joe Jensen, Finn Agerkvist, and James Harte. Nonlinear time-domain modeling of balanced-armature receivers. *Journal of Audio Engineering Society*, 59(3):91–101, March 2011.

[26] Philip M. Morse and K. Uno Ingard. *Theoretical Acoustics*. Princeton University Press, 41 William Street, Princeton, New Jersey 08540, 1st edition, 1986.

[27] R. Christensen, P. Juhl, and V. Cutanda Henriquez. Practical modeling of acoustic losses in air due to heat conduction and viscosity. *Acoustics '08, conference in Paris, June 29 - July 4 2008.*, June-July 2008.

[28] Stephen C. Thompson for The Penn State Research Foundation. Patent: WO 2010/025351 A2. Methods and Apparatus for Reduced Distortion Balanced Armature Devices, March 2010.

[29] Joe Jensen. A new method for evaluating loudspeaker efficiency in the frequency domain. In *Audio Engineering Society Convention 131*, New York, USA, October 2011.

[30] Jr. W. Marshall Leach. *Introduction to Electroacoustics & Audio Amplifier Design*. Kendall-Hunt Publishing Company, 3rd edition, 2003.

Paper A

Nonlinear Time-Domain Modeling of Balanced-Armature Receivers*

JOE JENSEN AND FINN T. AGERKVIST, *AES Member*

(joejens@gmail.com) (fa@elektro.dtu.dk)

Institute of Acoustic Technology, Technical University of Denmark, Lyngby, DK-2800, Denmark

AND

JAMES M. HARTE**

(J.Harte@warwick.ac.uk)

Centre for Applied Hearing Research (CAHR), Technical University of Denmark, Lyngby, DK-2800, Denmark

Nonlinear distortion added by the loudspeaker in a hearing aid lowers the signal-to-noise ratio and may degrade the hearing aid user's ability to understand speech. The balanced-armature-type loudspeakers, predominantly used in hearing aids, are inherently nonlinear devices, as any displacement of the loudspeaker diaphragm inevitably changes the magnetic and electrical characteristics of the loudspeaker. A numerical time-domain model capable of describing these nonlinearities is presented. By simulation it is demonstrated how the output distortion could potentially be reduced significantly through careful design of the mechanical properties of the armature.

0 INTRODUCTION

The tiny loudspeakers (commonly known as receivers) used in the construction of modern hearing aids produce unwanted distortion at high sound pressure levels. This distortion reduces the signal-to-noise ratio experienced by the hearing aid users and may degrade their ability to understand speech. The loudspeakers used in hearing aids are almost exclusively of the balanced-armature type due to their high efficiency. However, the balanced-armature loudspeaker is nonlinear by design in the sense that any displacement of the diaphragm inevitably changes the magnetic and electrical characteristics of the loudspeaker.

There are few historical studies of the operating principles of balanced-armature loudspeakers available, compared to those of the "regular" moving-coil loudspeaker. Descriptions of balanced-armature transducers were given by Bauer [1], [2] and Hunt [3], but these historical studies are limited to the linear operation of the transducer. To the authors' knowledge no published studies are available regarding the most recent incarnations of the balanced-armature transducer. An accurate, nonlinear model can help clarify how the linear range of the balanced-armature loudspeaker may be extended or how the efficiency may be increased by design. An accurate nonlinear model may also make it possible to actively compensate for the nonlinearities with a control scheme based on an inverted loudspeaker model. This has been demonstrated for moving-coil loudspeakers by Klippel [4] and Schurer et al. [5].

A numerical discrete-time balanced-armature loudspeaker model capable of modeling the key inherent nonlinearities is presented. The magnetic circuit is simplified to increase the transparency of the model in the present study. However, by employing the principles demonstrated in this paper, more details of the transducer's magnetic circuit can be incorporated to increase the accuracy of the model. Finally an example of how the model can be used is presented. It is demonstrated that the distortion of the armature output may be reduced significantly through careful design of the armature mechanical stiffness. No attempt at modeling the acoustical radiation impedance has been made and it is simply assumed to be zero.

1 GLOSSARY OF SYMBOLS

A_g Cross-sectional area of air gap, m^2
B_g Magnitude of magnetic B field in air gap, Wb/m^2 or T
D Length of air gap between armature and permanent magnet when armature is in its resting position, m
E_{in} Electric input voltage on loudspeaker terminals, V
E_L Voltage across inductor due to alternating current, V
E_u Electric back-EMF due to part of armature flux change related to armature velocity, V

*Manuscript received 2010 July 13; revised 2011 January 11.

**Now with Institute of Digital Healthcare, WMG University of Warwick, Coventry, CV4 7AL, UK.

F_Φ Armature input force due to magnetic flux in air gaps, N
$F_{\Phi 1}$, $F_{\Phi 2}$ Armature input force due to magnetic flux in air gaps 1 and 2, N
$\boldsymbol{F}_M$ Magnetomotive force of permanent magnet, A·turns or simply A
$\boldsymbol{F}_{Mi}$ Magnetomotive force due to current in coil, A·turns or simply A
i Electric current, A
k_m Mechanical stiffness of armature alone, N/m
k_Φ Flux stiffness for small armature displacements, N/m
k_{eff} Effective mechanical stiffness of armature when magnetic flux stiffness is taken into account, N/m
L Electric inductance, H
M Moving mass of armature, kg
N Number of wire turns (no dimension)
Q_{eff} Effective quality factor of mechanical system when magnetic flux stiffness is taken into account (no dimension)
Q_m Quality factor of mechanical system (no dimension)
r Mechanical resistance, N · s/m or kg/s
R_A Reluctance of armature, A/Wb
R_g Reluctance of air gap, A/Wb
R_H Reluctance of permanent magnets housing, A/Wb
R_i Reluctance of "arms" of armature structure, A/Wb
R_L DC resistance of coil, Ω
R_M Internal reluctance of permanent magnet, A/Wb
RL_{cut} 3-dB cutoff frequency for RL series circuit, Hz
T_{em} Transduction coefficient relating electric potential E_u to armature velocity u, V · s/m
u Armature velocity, m/s
x Armature displacement relative to resting position, m. (Upward direction in Fig. 1 is positive.)
ρ_g Permeance of air gap, Wb/A
Φ_A Magnetic flux in armature, Wb
Φ_g Magnetic flux in air gap, Wb
μ_0 Permeability of air or free space, $4\pi \cdot 10^{-7}$, N/A^2 or H/m

2 BALANCED-ARMATURE LOUDSPEAKER

The balanced-armature transducer has been rendered in a variety of shapes and structural modifications over the years. An illustration of the typical underlying principle of the modern balanced-armature transducer is shown in Fig. 1.

The coil that surrounds the armature does not touch or move along with the armature, so changing the number of windings of the coil does not influence the armature's moving mass. The armature is balanced between two permanent magnets, which exert an equal but opposite magnetic force on it when the electric current in the coil is zero. The mechanical stiffness of the armature ensures that it does not flip away from its balanced resting position and then cling to one of the permanent magnets. The armature is surrounded by a coil that magnetizes it when an electric current flows through the coil. A positive current will increase the magnetic flux in the upper part of the magnetic circuit, leading to an increased attractive force between the upper permanent magnet and the armature. Conversely, the flux in the lower part of the magnetic circuit will decrease, leading to a reduced attractive force between the lower permanent magnet and the armature. This gives rise to a net external force on the armature causing it to move upward, as illustrated in Fig. 1(b).

The armature itself is not a very efficient radiator of sound, so it is connected rigidly to a thin and light diaphragm, of which the front and back are acoustically isolated. The diaphragm and the casing of the balanced-armature mechanism are omitted from Fig. 1 for clarity. Fig. 2 gives a better impression of how the typical balanced-armature loudspeaker is constructed as a whole.

3 NONLINEAR MODEL

In the following sections a time-domain model will be developed accounting for the electrical, mechanical, and magnetic effects suggested in Fig. 1.

3.1 Magnetic Circuit

Magnetic circuits have been modeled extensively using the approach of equivalent electric circuits (see [6], for example). Magnetic reluctance can be used as the equivalent of electric resistance, magnetomotive force corresponds to electric potential or electromotive force, and magnetic flux then corresponds to electric current. However, when using the magnetic reluctance approach one should be careful since the usual electric circuit relations for power and energy do not hold. For instance, despite the reluctance of an air gap in a magnetic circuit, no power is dissipated and only magnetic energy is stored. The magnetic reluctance approach does, however, represent the fluxes faithfully and is chosen here for its simplicity and sufficiency for the modeling task at hand. Fig. 3 shows the lumped electrical equivalent of the magnetic circuit.

The air gap reluctance R_g is assumed to be much larger than any other reluctance in the circuit, and the permanent magnets are assumed to have the same magnetomotive force $\boldsymbol{F}_M$. These assumptions lead to the simplified magnetic circuit shown in Fig. 3(b). Electric network analysis of Fig. 3(b) leads to the equations for the magnetic flux,

$$\begin{bmatrix} \Phi_{g1} \\ \Phi_{g2} \\ \Phi_A \end{bmatrix} = \begin{bmatrix} \rho_{g1}(\boldsymbol{F}_M + \boldsymbol{F}_{Mi}) \\ \rho_{g2}(\boldsymbol{F}_M - \boldsymbol{F}_{Mi}) \\ \boldsymbol{F}_M(\rho_{g1} - \rho_{g2}) + \boldsymbol{F}_{Mi}(\rho_{g1} + \rho_{g2}) \end{bmatrix} \quad (1)$$

where the magnetic permeances ρ_{g1} and ρ_{g2} of the air gaps and the magnetomotive force $\boldsymbol{F}_{Mi}$ due to the coil are given as

$$\rho_{g1}(x) = \frac{1}{R_{g1}(x)} = \frac{\mu_0 A_g}{D - x},$$
$$\rho_{g2}(x) = \frac{1}{R_{g2}(x)} = \frac{\mu_0 A_g}{D + x} \quad (2)$$

$$\boldsymbol{F}_{Mi} = Ni. \quad (3)$$

Here N is the number of windings on the coil that surrounds the armature, i is the electric current that flows in it, D is the distance between a permanent magnet and the armature when at rest, x is the displacement of the armature, A_g is the effective air-gap area between the armature and one permanent magnet, and μ_0 is the permeability of free space. The magnetic reluctance of the air gap is thus proportional to the length of the air gap and inversely proportional to the air gap area, similar to the electric resistance of a typical homogeneous material.

3.2 Armature Input Force

The magnetic force of attraction between the two opposite pole faces across an air gap is [7, eq. (4.47)]

$$F = \frac{A_g B_g^2}{2\mu_0} = \frac{\Phi_g^2}{2\mu_0 A_g} \tag{4}$$

where B_g is the magnetic B field across the air gap and A_g is its cross-sectional area. This is illustrated in Fig. 4. The force between the two surfaces is attractive, regardless of the direction of the magnetic field.

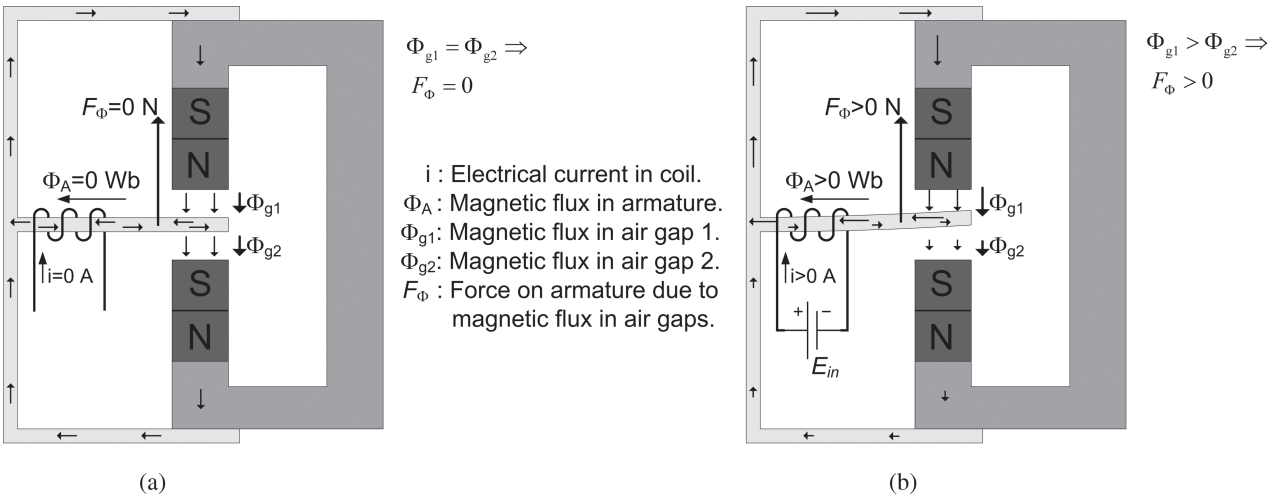

(a) (b)

Fig. 1. Balanced-armature mechanism. (a) With zero coil current armature is in its resting position, balanced between two permanent magnets. (b) When positive current flows in coil, armature is displaced from its resting position. Magnitude and direction of magnetic flux in meshes of magnetic circuit are indicated by arrows.

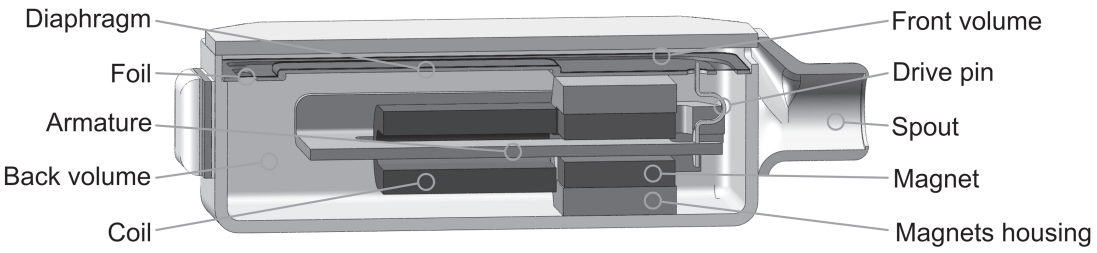

Fig. 2. Cross-sectional view of typical balanced-armature loudspeaker. (Courtesy of Sonion A/S.)

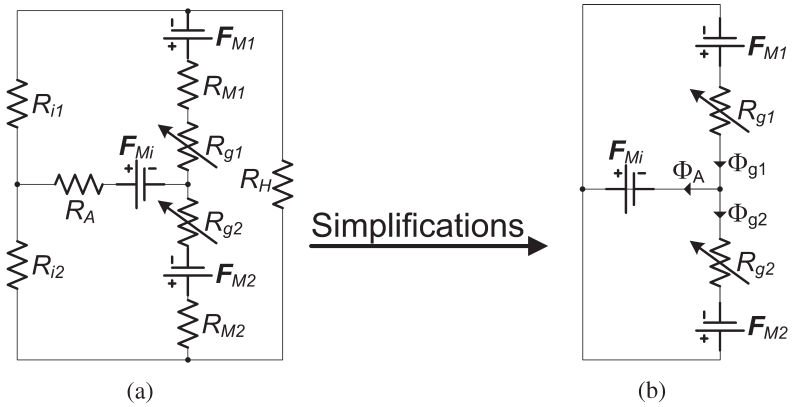

(a) (b)

Fig. 3. (a) Magnetic circuit of balanced-armature transducer. (b) Simplified magnetic circuit.

The input force on the armature due to the magnetic flux in air gaps 1 and 2 can then be written as

$$F_{\Phi 1} = \frac{\Phi_{g1}^2}{2\mu_0 A_g}, \qquad F_{\Phi 2} = -\frac{\Phi_{g2}^2}{2\mu_0 A_g}. \tag{5}$$

The total input force on the armature due to flux in the two gaps then becomes

$$F_\Phi = F_{\Phi 1} + F_{\Phi 2} = \frac{\Phi_{g1}^2 - \Phi_{g2}^2}{2\mu_0 A_g} = \frac{(\Phi_{g1} + \Phi_{g2})\Phi_A}{2\mu_0 A_g}. \tag{6}$$

Expressing the magnetic flux in terms of armature displacement, coil current, and the various constants of the magnetic circuit yields

$$F_\Phi(x,i) = 2\mu_0 A_g \frac{\boldsymbol{F}_M^2 Dx + N\boldsymbol{F}_M(D^2 + x^2)i + N^2 Dxi^2}{(D^2 - x^2)^2}. \tag{7}$$

Eq. (7) reveals the nonlinear relationship between the coil current and the armature input force. The first term in the numerator represents the steady pull from the magnets as soon as the armature moves away from its balanced resting position. The second term represents the (nonlinear) displacement-dependent relationship between the coil current and the input force to the mechanical system. The third term can be regarded as an unwanted distortion force. For small armature displacements ($x \ll D$) this term will be small compared to the second term provided that Ni is smaller than $\boldsymbol{F}_M$. It is informative to analyze Eq. (7) for $x \ll D$ and zero coil current,

$$F_\Phi(x,i)|_{i=0} \approx \frac{2\mu_0 A_g \boldsymbol{F}_M^2}{D^3} x. \tag{8}$$

Thus for small armature displacements and open loop electric circuit, the steady pull from the permanent magnets acts as a negative mechanical armature stiffness trying to pull the armature away from its resting position. The factor

$$k_\Phi = \frac{2\mu_0 A_g \boldsymbol{F}_M^2}{D^3} \tag{9}$$

can then be interpreted as a magnetic flux stiffness that subtracts from the mechanical armature stiffness. The effective small-signal stiffness of the transducer becomes

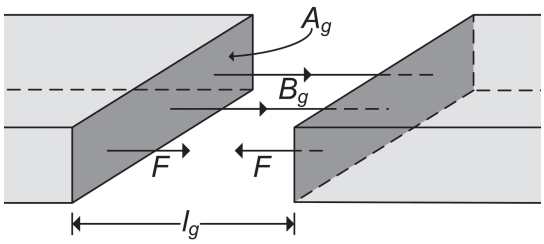

Fig. 4. Magnetic force of attraction between opposite pole faces across air gap.

$$k_{\text{eff}} = k_m - k_\Phi = k_m - \frac{2\mu_0 A_g \boldsymbol{F}_M^2}{D^3} \tag{10}$$

where k_m is the (positive) mechanical armature stiffness. The permanent magnets thus have the effect of reducing the stiffness and hence the resonance frequency of the armature. The additional magnetic flux stiffness should thus always be considered when choosing the loudspeaker design parameters. The distance D between armature and permanent magnets has a particularly large effect on the resonance frequency, since the flux stiffness is inversely proportional to D^3. In the case where k_Φ is larger than k_m the loudspeaker will be unstable, and the armature will spontaneously flip away from its resting position and cling to one of the permanent magnets.

3.3 Mechanical Part of Loudspeaker

The mechanical part of the loudspeaker can be treated as a linear second-order system consisting of armature mass M, armature stiffness k_m, and a viscous damping coefficient r. The equation of motion then becomes

$$M\frac{d^2x(t)}{dt^2} = F_\Phi(t) - r\frac{dx(t)}{dt} - k_m x(t) \tag{11}$$

with r and k_m being positive real numbers.

3.4 Electrical Part of Loudspeaker

According to Faraday's law the induced electromotive force in a conducting loop of N turns is given by

$$\varepsilon = -N\frac{d\Phi}{dt} \tag{12}$$

where $d\Phi/dt$ is the rate of change of magnetic flux (in Wb/s) through the N loops. The magnetic flux through the cross-sectional area of the loop is given by the surface integral

$$\Phi = \int_S \overline{B} \cdot \, d\overline{A}. \tag{13}$$

For a regular inductor this change of flux is due to the varying magnetic field produced by the alternating current in the coil. However, the change in flux could also be due to a change in the magnetic circuit that constitutes the core of the coil. This is exactly what happens in the balanced-armature loudspeaker. When the armature moves toward one permanent magnet the flux path of the coil core changes, and the flux through the coil (set up by the permanent magnets) will vary. This, in addition to the alternating current, gives rise to a time-varying flux through the coil. The electric circuit is shown in Fig. 5.

The resistor R_L simulates the electric resistance of the coil and E_L simulates the voltage across the coil due to the variations in electric current alone. This voltage is given by the regular inductor equation

$$E_L = L\frac{di}{dt}. \tag{14}$$

The voltage E_u, on the other hand, simulates the back-EMF

across the inductor due to the armature velocity. E_u can be observed in the electric open-loop circuit where the current is zero; E_L can be observed when a current runs in the electric circuit while the armature velocity is zero, which implies that the mechanical circuit is open loop.

The inductor voltage E_L is evaluated first. The task is to find the inductance L, so the inductor equation is written in terms of the electric current i and the magnetic flux Φ through the wire turns,

$$L = N\frac{\Phi}{i} \Leftrightarrow N\Phi = Li. \tag{15}$$

Differentiating with respect to time on both sides in general yields

$$N\frac{d\Phi}{dt} = L\frac{di}{dt} + i\frac{dL}{dt}. \tag{16}$$

Since the inductor voltage is observed for zero armature velocity, the inductance change over time dL/dt is zero. The inductance is a function of the number of wire turns and the geometry of the magnetic circuit. Therefore Eq. (16) can be rearranged and reduced to

$$L = N\frac{d\Phi_i}{di} = N\frac{d\Phi_A}{di}\bigg|_{dx/dt=0} \tag{17}$$

where Φ_i is the flux in the armature due to the electric current alone. $d\Phi_i/di$ can be evaluated using the expressions for the armature flux [Eqs. (1) and (3)],

$$\frac{d\Phi_i}{di} = N(\rho_{g1} + \rho_{g2}). \tag{18}$$

Combining Eqs. (17) and (18) the inductance finally becomes

$$L(x) = N^2(\rho_{g1} + \rho_{g2}) = N^2\frac{2\mu_0 A_g D}{D^2 - x^2}. \tag{19}$$

The nonlinear behavior of the electrical inductance is clearly observed by studying this equation. A ratio of around 0.3 between the armature displacement x and the air-gap distance D will increase the inductance by 10%.

Next E_u, the back-EMF due to the armature velocity, needs to be evaluated with the coil current being zero,

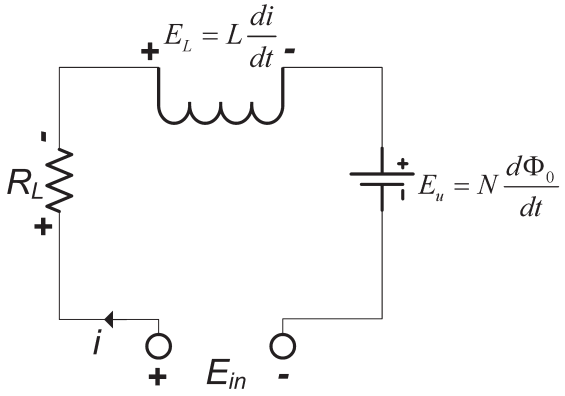

Fig. 5. Electric circuit of balanced-armature transducer.

$$E_u = N\frac{d\Phi_0}{dt} = N\frac{d\Phi_0}{dx}\frac{dx}{dt} = T_{em}\frac{dx}{dt} \tag{20}$$

with

$$T_{em} = N\frac{d\Phi_0}{dx} = N\frac{d\Phi_A}{dx}\bigg|_{i=0} \tag{21}$$

where Φ_0 is the flux in the armature due to the permanent magnets alone since $i = 0$, and T_{em} is the transduction coefficient that relates the armature velocity dx/dt to E_u, the electric back-EMF. The transduction coefficient can be found by evaluating Eqs. (1)–(3) with $i = 0$,

$$T_{em}(x) = 2\mu_0 N A_g \boldsymbol{F}_M \frac{x^2 + D^2}{(D^2 - x^2)^2}. \tag{22}$$

The transduction coefficient is clearly also a nonlinear parameter. The transduction coefficient is always positive, meaning that a positive armature velocity (directed upward in Fig. 1) will result in a positive voltage E_u as defined in the electric circuit of Fig. 5. Finally the equation for E_u and the complete electric circuit can be expressed as

$$E_u = T_{em}(x)\frac{dx}{dt} \tag{23}$$

$$E_{in} = R_L i + L(x)\frac{di}{dt} + T_{em}(x)\frac{dx}{dt}. \tag{24}$$

4 MODEL IMPLEMENTATION

All the governing equations have been derived in Section 3. In order to create a numerical time-domain model, these need to be discretized. This can be accomplished using the simple forward-Euler method, where the time derivative of a discrete-time signal $x(n)$ is estimated as

$$\frac{dx_n}{dt} = u_n \approx \frac{x_{n+1} - x_n}{T_s}. \tag{25}$$

The sample period $T_s = 1/f_s$ should be much smaller than the period of any signal present in the system. The double derivative of x with respect to t is then

$$\frac{d^2x_n}{dt^2} = \frac{du_n}{dt} \approx \frac{u_{n+1} - u_n}{T_s} \approx \frac{x_{n+2} - 2x_{n+1} + x_n}{T_s^2}. \tag{26}$$

Using Eqs. (25) and (26) the continuous-time differential equation for the mechanical system [Eq. (11)] along with the expression for the magnetic input force [Eq. (7)] can be written as a recursive formula,

$$u_{n+1} = \frac{2T_s\mu_0 A_g N}{M(D^2 - x_n^2)^2}\left[\boldsymbol{F}_M(D^2 + x_n^2) + NDx_n i_n\right] i_n + \frac{T_s}{M}\left[\frac{2\mu_0 A_g \boldsymbol{F}_M^2 D}{(D^2 - x_n^2)^2} - k_m\right] x_n + \left(1 - \frac{rT_s}{M}\right) u_n. \tag{27}$$

From Eq. (25) it follows directly that the displacement can be written

$$x_{n+1} = x_n + T_s u_n. \tag{28}$$

Using Eq. (24) the recursive formula for the coil current can be written as

$$i_{n+1} = \left[1 - \frac{R_L T_s}{L(x_n)}\right] i_n - \frac{T_s T_{em}(x_n)}{L(x_n)} u_n + \frac{T_s}{L(x_n)} E_{in,n}. \tag{29}$$

Using Eqs. (27)–(29) the recursive formula for coil current, armature displacement, and armature velocity can be written as

$$\overline{X}_{n+1} = \begin{bmatrix} i_{n+1} \\ x_{n+1} \\ u_{n+1} \end{bmatrix} = \overline{\overline{F}}_n \overline{X}_n + \overline{G}_n E_{in,n} \tag{30}$$

with the state space equations

$$\overline{\overline{F}}_n = \begin{bmatrix} 1 - \dfrac{R_L T_s}{L(x_n)} & 0 & \dfrac{-T_s T_{em}(x_n)}{L(x_n)} \\ 0 & 1 & T_s \\ \dfrac{2T_s \mu_0 A_g N}{M(D^2 - x_n^2)^2}\left[\boldsymbol{F}_M(D^2 + x_n^2) + NDx_n i_n\right] & \dfrac{T_s}{M}\left[\dfrac{2\mu_0 A_g \boldsymbol{F}_M^2 D}{(D^2 - x_n^2)^2} - k_m\right] & 1 - \dfrac{rT_s}{M} \end{bmatrix} \tag{31}$$

$$\overline{G}_n = \begin{bmatrix} \dfrac{T_s}{L(x_n)} \\ 0 \\ 0 \end{bmatrix}. \tag{32}$$

Here $E_{in,n}$ is the input voltage at the loudspeaker terminals. Finally the pseudo code for the simulation model can be expressed as

```
% Initialization of algorithm:
I1 = 0, x1 = 0, u1 = 0;
K = number of samples in input signal;

% Algorithm:
for n=1 to K-1
  Calculate inductance, Ln;
  Calculate transduction coeffi-
    cient, Tem,n;
  Calculate Fn;
  Calculate Gn;
  Xn+1 = FnXn + GnEin,n;
end
```

5 SIMULATIONS

The simulations presented in this section are based on a balanced-armature loudspeaker with realistic parameters summarized in Table 1.

Using these loudspeaker parameters yields the small-signal ($x << D$) parameters summarized in Table 2. RL_{cut} is the −3-dB low-pass cutoff frequency of the current in the electric RL circuit when the back-EMF is not taken into account. The stiffness, quality factor, and undamped natural frequency of the mechanical system with and without the flux stiffness taken into acount are also shown.

A sampling frequency of 1 MHz was used to produce the frequency-domain and distortion simulations presented in Section 5.1. In Section 6 distortion simulations (intermodulation and pure tone) with a 3-kHz input tone are presented. A sampling frequency of 20 MHz was used. Note that the maximum armature displacement during steady state for the pure-tone and intermodulation distortion simulations is referred to as armature amplitude and is denoted by $|x|$.

5.1 Frequency Response and Distortion Simulations

In order to investigate the behavior of the loudspeaker in the frequency domain, it is useful to make use of a voltage impulse and take the fast Fourier transform (FFT) of the various system signals. For instance, taking the FFT of the coil current impulse response yields the frequency response $i(j\omega)/E_{in}(j\omega) = 1/Z_e$, and the electric impedance Z_e can thus be found in this manner. Before making such investigations one should make sure that the armature displacement is small enough, such that the loudspeaker can be assumed to be operating in its linear range. A simulation of the electric impedance is shown in Fig. 6. Notice that the magnitude of the electric impedance is much higher than for typical moving-coil loudspeakers. This is due to the much larger dc resistance and coil

Table 1. Reference loudspeaker parameters used throughout simulations.

Mechanical parameters	
D	125×10^{-6} m
N	310 turns
A_g	5.1×10^{-6} m^2
M	80×10^{-6} kg
r	0.146 N • s/m
k_m	19×10^3 N/m
Magnetic parameters	
μ_0	$4\pi \times 10^{-7}$ N/A^2
$\boldsymbol{F}_M$	35 A • turns
Electrical parameters	
R_L	50 Ω

inductance in the balanced-armature receivers. Fig. 7 shows the armature displacement frequency response when the loudspeaker is current driven to eliminate the effect of the inductance and the back-EMF. This simulation demonstrates the reduced mechanical resonance frequency due to the magnetic flux stiffness. The peak of this response is located at 1855 Hz, which is only a bit less than the predicted effective undamped mechanical resonance frequency $f_{n,\mathrm{eff}}$ of 1863 Hz stated in Table 2. Fig. 8 shows the armature displacement response when the loudspeaker is voltage driven. The response rolls off at a lower frequency than the mechanical resonance because of the low-pass characteristics of the electric circuit.

When the armature distortion is investigated for pure-tone voltage inputs, a time window is applied to the armature displacement signal so that the first transient part of the signal does not influence the spectrum, that is, only the steady-state portion is considered. The armature displacement distortion patterns are shown in Fig. 9 for various input voltages at a frequency of 200 Hz. The level of the third-order harmonic is indicated in the figure. It is observed how the relative magnitude of the harmonics increase with the input voltage and armature displacement as the various nonlinear loudspeaker parameters deviate from their respective small-signal values.

Table 2. Derived loudspeaker parameters using physical parameters of Table 1.

$L_{\mathrm{small}} = 9.85 \times 10^{-3}$ H
$T_{\mathrm{em,\ small}} = 8.9$ V • s/m
$RL_{\mathrm{cut}} = 808$ Hz
$k_{\mathrm{m}} = 19000$ N/m
$k_{\mathrm{eff}} = 10961$ N/m
$f_n = 2453$ Hz
$f_{n,\mathrm{eff}} = 1863$ Hz
$Q_m = 8.44$
$Q_{eff} = 6.41$

6 APPLICATION EXAMPLE OF MODEL

The magnetic force on the armature for zero coil current follows from Eq. (7),

$$F_{\Phi}(x,i)|_{i=0} = \frac{2\mu_0 A_{\mathrm{g}} F_{\mathrm{M}}^2 D}{\left(D^2 - x^2\right)^2} x. \tag{33}$$

As was mentioned, this relationship between magnetic force and armature displacement is approximately linear for small x, effectively lowering the mechanical small-signal resonance frequency. For large displacements this relationship is no longer linear, and the displacement dependency of the armature input force contributes to the output distortion. The magnetic force on the armature for zero coil current is plotted in Fig. 10.

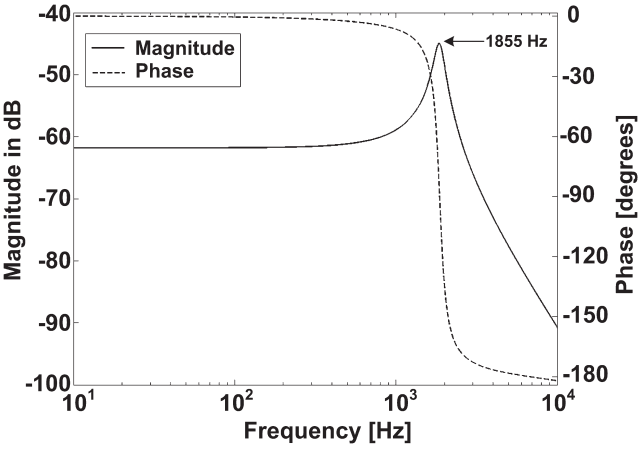

Fig. 7. Armature displacement frequency response; loudspeaker is current driven.

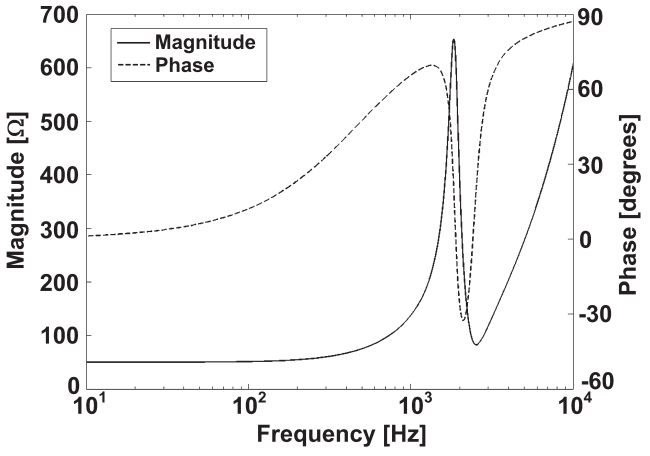

Fig. 6. Electric impedance.

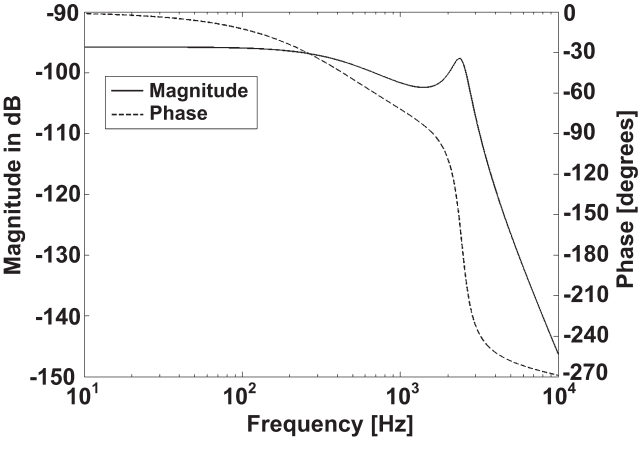

Fig. 8. Armature displacement frequency response; loudspeaker is voltage driven.

For small displacements x the magnetic force of attraction is almost straight and acts like a negative linear mechanical spring trying to drive the armature away from its resting position. As the armature moves toward either of the permanent magnets, the magnetic force increases rapidly and may overcome the mechanical spring force that tries to hold the armature in its resting position. If the mechanical armature spring force were nonlinear, that is, increasing with displacement in a fashion somewhat similar to the magnetic force, then the operating range of the armature would be extended and the distortion reduced. The force profile of such a theoretical nonlinear armature spring is shown in Fig. 10 by a dashed curve. The two force curves sum up to a straight curve with a slope that corresponds to the negative effective mechanical stiffness k_{eff}. The force–displacement relationship of the nonlinear mechanical spring is

$$F_{\text{nonlin,spring}} = -\left[k_{\text{eff}} + \frac{2\mu_0 A_g F_M^2 D}{(D^2 - x^2)^2}\right] x. \tag{34}$$

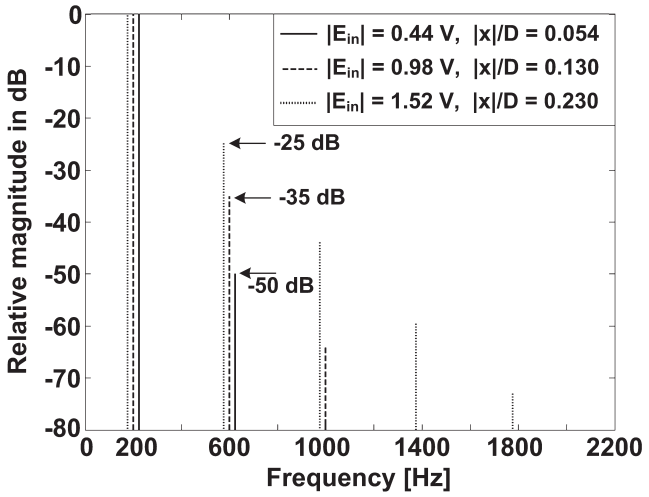

Fig. 9. Armature displacement spectrum for 200-Hz pure-tone input at three different levels. Input voltage amplitude and ratio between armature displacement amplitude $|x|$ and air-gap length D are indicated in legend.

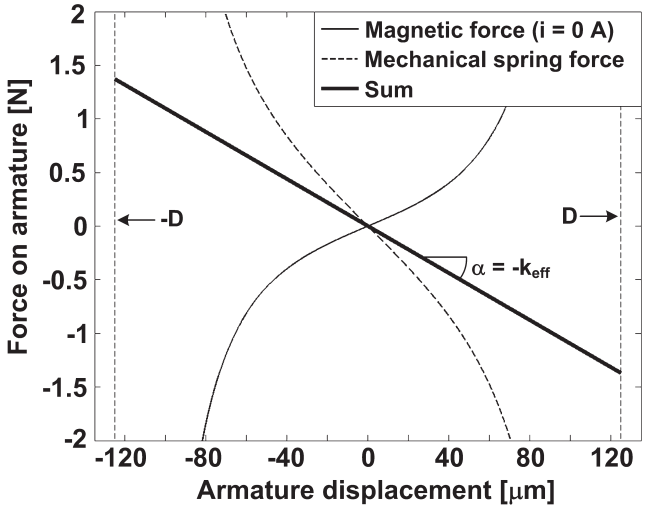

Fig. 10. Armature force due to magnetic field set up by permanent magnets ($i = 0$ A) and restoring (nonlinear) spring force of a theoretical armature spring.

Fig. 11 shows the armature displacement harmonic distortion for the reference loudspeaker with linear spring compared to that of an otherwise identical loudspeaker but with the nonlinear armature spring force, as depicted in Fig. 10. Since the loudspeaker with the nonlinear spring has a different voltage sensitivity, the input voltage is adjusted to a level where the displacement amplitude is equal to that of the loudspeaker with the linear spring. The nonlinear force profile of the theoretical spring has reduced the output distortion significantly for a 200-Hz input tone.

An important implication of these considerations is that the driving force generated by the electric current cannot tell the difference between the mechanical armature stiffness and the flux stiffness generated by the permanent magnets. The effective (nonlinear) stiffness k_{eff} can thus be viewed as a nonlinear stiffness that dominates the mechanical impedance below resonance frequency. As the frequency is increased well above the effective resonance frequency the mass becomes the dominating part of the mechanical impedance and the contribution from the nonlinear effective stiffness becomes insignificant. A simulation with a 5-kHz pure tone verifies this as the level difference between the third-order distortion products of loudspeakers with linear and nonlinear springs, respectively, is merely 0.3 dB for a displacement of $|x|/D = 0.1$. At 200 Hz, where the mechanical impedance is dominated by the (nonlinear) stiffness, this difference is a much more significant 2.8 dB for a similar displacement of $|x|/D = 0.1$. For balanced-armature loudspeakers the stiffness-dominated frequency range is

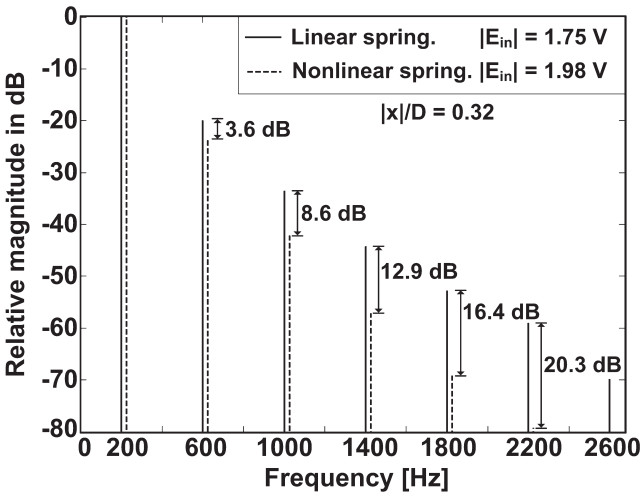

Fig. 11. Armature displacement spectrum for 200-Hz pure-tone input with linear and nonlinear armature stiffness. Input voltage amplitude is indicated in legend. Ratio between armature displacement amplitude $|x|$ and air-gap length D is 0.32.

large, as the effective resonance frequency is typically above 1 kHz.

A simulation similar to that in Fig. 11 was done with a 3-kHz input, and the result is shown in Fig. 12. This time the distortion was higher for the nonlinear spring than for the linear one as the mechanical impedance is no longer dominated by the stiffness. In general the third-order distortion of a tone with a frequency above, say, 1 kHz is lower than that of a 200-Hz tone due to the slope in the frequency response above around 3 kHz (see Fig. 8).

Fig. 13 shows a simulation of the intermodulation distortion for an input signal consisting of the sum of a 200-Hz tone and a 3-kHz tone, with the amplitude of the 200-Hz tone being four times that of the 3-kHz tone in order to somewhat reflect a real-life audio signal. The nonlinear spring has reduced the overall distortion, but the intermodulation distortion products above 2 kHz have increased.

It was possible to reduce the low-frequency distortion further (below resonance) by employing a mechanical nonlinear force profile that had a larger slope than the one already proposed. This is because the compressive effect of the nonlinear spring can compensate for the inverse effect of the force generated by the coil current, which tends to increase for large displacements [see second and third terms in Eq. (7)]. However, this technique affects the high-frequency distortion and the low-frequency sensitivity severely, in negative ways. Such a transducer could be tuned for low-frequency purposes such as in a high-end multiway headphone system.

7 DISCUSSION

Currently the proposed model does not take magnetic hysteresis or eddy currents into account. In order to predict the distortion patterns as well as the small-signal frequency response accurately, these effects need to be included in an improved model. The magnetic circuit can easily be extended to include leakage flux paths and/or magnetic reluctances of permanent magnets or armature structure, as demonstrated in Section 3.1.

It is known that for the widespread moving-coil loudspeaker the stiffness of the suspension is not linear, that is, it generally increases with the displacement of the diaphragm and, maybe more importantly, the stiffness tends to drift with the average displacement amplitude and/or temperature [8], [9]. The stiffness of these transducers is dominated by the spider and the outer suspension, which typically are made of textile and rubber, respectively. The stiffness of the balanced-armature loudspeaker is predominantly determined by the armature stiffness and the flux stiffness, so it is expected that the stiffness of the balanced-armature loudspeaker has less tendency to drift, as is the case for moving-coil loudspeakers. If all loudspeaker nonlinearities remained constant during operation it might be possible to reduce output distortion dramatically by actively compensating for the nonlinearities with an open-loop control scheme, as discussed in [10]. For systems where parameter drift is expected, the adaptive feedforward methods discussed in [4], [5], [10] may still be useful. Both methods rely on a simulation model that contains enough details to model the nonlinear behavior of a real loudspeaker accurately.

The reluctance of the air gap, which was stated in Eq. (2), is valid for parallel surfaces only. This is not entirely the case for the balanced-armature loudspeaker since any displacement of the armature will result in its angular displacement. This angular displacement can usually be safely ignored since the displacement x is very small compared to the length of the armature. Another

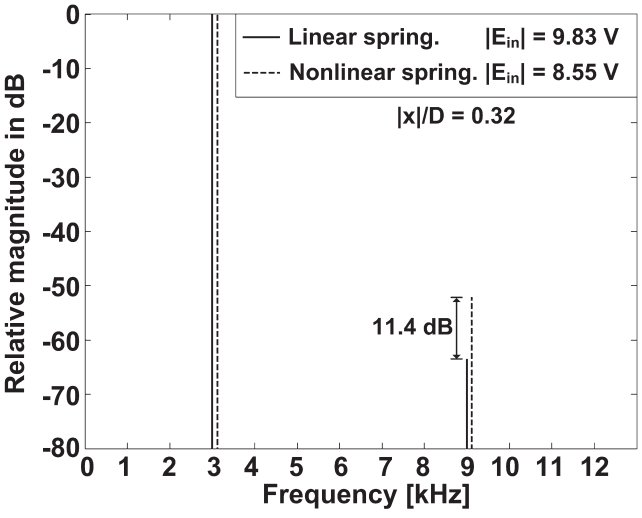

Fig. 12. Armature displacement spectrum for 3-kHz pure-tone input with linear and nonlinear armature stiffness. Input voltage amplitude is indicated in legend. Ratio between armature displacement amplitude $|x|$ and air-gap length D is 0.32.

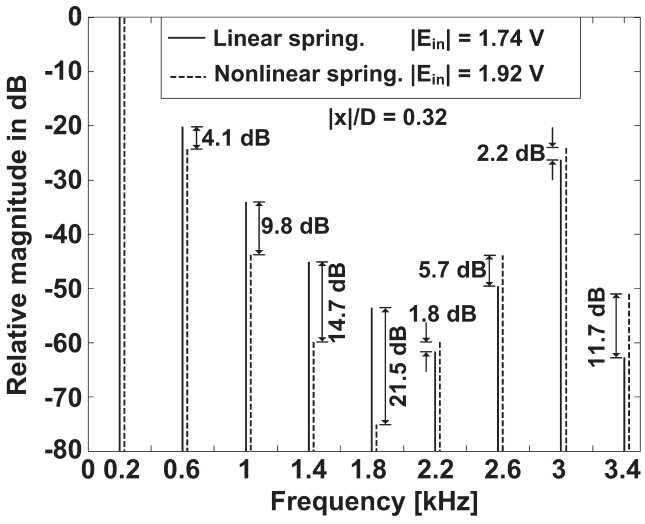

Fig. 13. Armature displacement spectrum showing intermodulation distortion. Input is sum of a 200-Hz tone and a 3-kHz tone with a magnitude of 12 dB below that of the 200-Hz tone. Input voltage amplitude of 200-Hz tone is indicated in legend. Ratio between armature displacement amplitude $|x|$ and air-gap length D is 0.32.

phenomenon related to the air gap that should not be ignored is the fringing field outside the air-gap area, which increases the air-gap area effectively as the pole surfaces move further apart. This effect will reduce the air gap reluctance for a given distance between the pole surfaces. This fringing field is due to the relatively small ratio of permeability between air and magnetic materials compared to such factors as the ratio of conductivity for copper and air when dealing with electric circuits. Furlani [6, fig. 3.24b] provides an equation to calculate the reluctance of an air gap where the distance D between the surfaces is taken into account,

$$R_g = \frac{D}{\mu_0(w+D)(t+D)} \tag{35}$$

with w and t being the width and thickness of the rectangular pole faces of equal dimensions. Using this expression instead of Eq. (2) reduces the calculated air-gap reluctance by a significant 20% when the armature displacement of the reference loudspeaker is at its maximum (125 μm). The magnetic pole faces (armature and magnet) can hardly be considered as having equal surface areas because of the oblong shape of the armature. However, the effective air-gap area still increases with the distance between armature and magnets. A displacement-dependent air-gap area can easily be implemented in the proposed numerical model as was done with the nonlinear mechanical stiffness. The effective air-gap area is simply updated for each time step.

8 CONCLUSION

A framework for numerical modeling of the inherent nonlinearities of the balanced-armature loudspeaker has been presented, and various improvements have been proposed. It has been demonstrated how the model may be used to simulate loudspeaker "modifications" such as the nonlinear armature stiffness, which reduced the low-frequency distortion. As stated in the discussion section, the model still needs to be improved by incorporating various magnetic effects to more accurately model the distortion patterns as well as the small-signal frequency response.

[1] B. B. Bauer, "Magnetic Translating Device," U.S. patent 2,454,425 (1948 Nov. 23).

[2] B. B. Bauer, "A Miniature Microphone for Transistorized Amplifiers," *J. Acoust. Soc. Am.*, vol. 25, pp. 867–869 (1953 Sept.).

[3] F. V. Hunt, Electroacoustics—The Analysis of Transduction and Its Historical Background." (Acoustical Society of America, New York, 1954, 1982).

[4] W. Klippel, "The Mirror Filter—A New Basis for Reducing Nonlinear Distortion and Equalizing Response in Woofer Systems," *J. Audio Eng. Soc.*, vol. 40, pp. 675–691 (1992 Sept.).

[5] H. Schurer, A. G. J. Nijmeijer, M. A. Boer, C. H. Slump, and O. E. Herrmann, "Identification and Compensation of the Electrodynamic Transducer Nonlinearities," in Proc. *IEEE Int. Conf. on Acoustics, Speech, and Signal Processing* (ICASSP '97), (1997 Apr.), pp. 2381–2384.

[6] E. P. Furlani, *Permanent Magnet and Electromechanical Devices* (Academic Press, San Diego, CA, 2001).

[7] P. Campbell, *Permanent Magnet Materials and Their Application* (Cambridge University Press, Cambridge, MA, 1994).

[8] F. T. Agerkvist and B. R. Pedersen, "Time Variance of the Suspension Nonlinearity," presented at the 125th Convention of the Audio Engineering Society, *(Abstracts)* www.aes.org/events/125/125thWrapUp.pdf, (2008 Oct.), convention paper 7560.

[9] F. T. Agerkvist and B. R. Pedersen, "Time Varying Behavior of the Loudspeaker Suspension: Displacement Level Dependency," presented at the 127th Convention of the Audio Engineering Society, *(Abstracts)* www.aes.org/events/127/127thWrapUp.pdf, (2009 Oct.), convention paper 7902.

[10] A. Bright, "Active Control of Loudspeakers: An Investigation of Practical Applications," Ph.D thesis, Technical University of Denmark, Lyngby, Denmark (2002).

THE AUTHORS

J. Jensen

F. Agerkvist

J. Harte

Joe Jensen received a B.Sc. degree in electronics and computer engineering from the Copenhagen University College of Engineering, Denmark, in 2007. In 2010 he received an M.Sc. degree in acoustics from the Technical University of Denmark (DTU). Later that year he started an industrial Ph.D. collaboration with Sonion A/S studying the nonlinear behavior of balanced-armature receivers used in hearing aids.

●

Finn T. Agerkvist received an M.Sc. degree in electrical engineering in 1991 and a Ph.D. degree in 1994, both from the Technical University of Denmark, Lyngby.

From 1994 to 1997 he was assistant professor in the Department of Acoustic Technology, Technical University of Denmark. From 1997 to 2001 he worked as a senior scientist at the Danish Defence Research Establishment. Since 2002 he has been associate professor of the Acoustic Technology Group at DTU-Elektro, Technical University of Denmark. His research interests include signal processing, electroacoustics, and nonlinear systems.

●

James Harte received a Ph.D. degree in nonlinear identification of the human auditory system in 2004 from the University of Southampton, UK.

He is a biomedical engineer, who originally specialized in acoustics and vibration. His research now focuses on objective correlates of the normal and impaired auditory system, neuroimaging, and biomedical signal processing. Before joining the University of Warwick, where he is currently an assistant professor, he was an associate professor of physiological acoustics and technical audiology at the Technical University of Denmark.

Paper B

Audio Engineering Society

Convention e-Brief

Presented at the 131st Convention
2011 October 20–23 New York, NY, USA

A new Method for evaluating Loudspeaker Efficiency in the Frequency Domain

Joe Jensen[1]

[1] Institute of Acoustic Technology, Technical University of Denmark, Kgs. Lyngby, DK-2800, Denmark
joejens@gmail.com

ABSTRACT

The Constant Input Power (CIP) frequency response is proposed as a new method to evaluate loudspeaker efficiency in the frequency domain. Through a simulation study it is demonstrated how the CIP response can be a valuable tool when designing loudspeakers for which high efficiency is a priority.

1. INTRODUCTION

Energy efficiency is an increasingly important parameter for evaluating the performance of electronic equipment. Software algorithms are tuned to reduce power consumption and switching power supplies, and amplifiers are often marketed with claims about high efficiency. For products such as hand-held electronic devices and hearing aids, which both employ miniature loudspeakers, the power efficiency of every single component of the system needs to be considered.

It is, however, not always easy to interpret the efficiency or sensitivity figures that loudspeaker manufacturers provide. Some manufacturers state the sensitivity as the on-axis sound pressure level produced at a distance of 1 m for an input voltage of 1 V. Other manufacturers use 2.83 V which has to do with the fact that this corresponds to an electrical input power of 1 W for an 8 Ohm voice coil resistance [1]. Yet, other manufacturers scale the input voltage according to the voice coil resistance in order to input 1 W of electrical power into what would be the "rated impedance" of the loudspeaker [2]. However, it is not always clear how this rated impedance is defined so this technique is clearly problematic as the electrical impedance of a loudspeaker usually varies a lot with frequency. Also, the efficiency measurement specified in [2] involves a more or less complicated measurement of the radiated acoustic power.

In this paper, the Constant Input Power (CIP) frequency response is proposed as a method to estimate loudspeaker efficiency in the frequency domain. A great advantage of the CIP frequency response is that it can be obtained without the need to perform additional measurements besides the regular pressure frequency response and the complex electrical input impedance. The CIP frequency response makes it easy to compare the power efficiency of two different loudspeaker designs in the relevant frequency range. Also, the CIP frequency response is backward compatible in the sense that it can be produced from any old loudspeaker pressure response and complex electrical impedance measurement.

2. METHOD

The CIP frequency response can be obtained from the complex electrical input impedance and e.g. the free-field on-axis pressure frequency response when the loudspeaker is voltage-driven. The CIP pressure frequency response then shows the RMS pressure as a function of frequency for a constant input power of exactly 1 W at each frequency. Such a curve provides valuable, easy-to-interpret information about the efficiency characteristics of a loudspeaker - not only at a few discrete frequencies, as it is common practice, but over its entire operating frequency range.

The time-averaged input power to an electrical circuit at frequency ω is

$$P_{in}(\omega) = I_{RMS}^2(\omega)\mathrm{Re}\{Z_E(j\omega)\}, \quad (1)$$

where $I_{RMS}(\omega)$ is the RMS value of the input current, and $Z_E(j\omega)$ is the complex, frequency dependent, electrical input impedance. Substituting

$$I_{RMS}(\omega) = \frac{U_{RMS}(\omega)}{|Z_E(j\omega)|}, \quad (2)$$

into Eq. (1) yields

$$P_{in}(\omega) = \mathrm{Re}\{Z_E(j\omega)\}\frac{U_{RMS}^2(\omega)}{|Z_E(j\omega)|^2}, \quad (3)$$

where $U_{RMS}(\omega)$ is the RMS value of the input voltage at the frequency ω. Equating the electrical input power to 1 W and rearranging yields

$$U_{RMS}(\omega) = |Z_E(j\omega)|\sqrt{\frac{1\,W}{\mathrm{Re}\{Z_E(j\omega)\}}}. \quad (4)$$

Thus, driving the electrical circuit with the frequency dependent voltage, $U_{RMS}(\omega)$, as given by Eq. (4), the time-averaged input power will constantly be 1 W at all frequencies. Assuming linearity, the voltage driven loudspeaker magnitude response simply needs to be scaled by Eq. (4) in order to obtain a curve that shows the RMS pressure (or diaphragm displacement or velocity) while the loudspeaker is driven at a constant input power of 1 W at all frequencies. For instance, for a voltage driven loudspeaker with the diaphragm displacement frequency response

$$H(j\omega) = \frac{X(j\omega)}{U(j\omega)}, \quad (5)$$

and electrical impedance $Z_E(j\omega)$, the CIP displacement frequency response would be

$$X_{CIP}(j\omega) = |Z_E(j\omega)|\sqrt{\frac{1\,W}{\mathrm{Re}\{Z_E(j\omega)\}}}|H(j\omega)|. \quad (6)$$

It is useful to introduce the (real) CIP normalization function

$$f_{CIP}(j\omega) = |Z_E(j\omega)|\sqrt{\frac{1\,W}{\mathrm{Re}\{Z_E(j\omega)\}}}, \quad (7)$$

such that the CIP frequency response can be written as a product of two frequency dependent functions that can be evaluated separately:

$$X_{CIP}(j\omega) = f_{CIP}(j\omega)|H(j\omega)|. \quad (8)$$

It should be noted that the CIP frequency response is not a measure of physical efficiency, which would be defined as the ratio of the acoustical output power to the electrical input power. Rather, the CIP frequency response shows how efficiently a given loudspeaker produces diaphragm displacement, diaphragm velocity or sound pressure under specified acoustic conditions. The pressure could be the free-field on-axis pressure or it could be the pressure in a small coupler in the case of miniature loudspeakers. Notice that the concept of radiated acoustic power is meaningless for a small rigid coupler which essentially acts as a capacitive load where no acoustic power is dissipated. The human ear is sensitive to acoustic pressure (and not power), and the pressure that a miniature loudspeaker can produce inside a, say, 2 cm^3 coupler can be extremely high. This justifies the measurement of acoustic pressure in many situations instead of radiated acoustic power.

The CIP frequency response is a virtual frequency response in the sense that a loudspeaker is not usually driven with a constant electrical input power. Thus, the CIP frequency response does not provide any

information about how the loudspeaker will sound when driven by an ordinary constant-voltage amplifier.

3. APPLICATION EXAMPLE

The following example is a simulation study of two different 3rd-order loudspeaker designs; a reference design and a design with reduced electrical DC resistance R and reduced electromechanical transduction coefficient T (often referred to as the *force factor*). The diaphragm displacement frequency responses are presented in Fig. 1. The response is more flat for the modified loudspeaker and the loudspeaker generally has a higher voltage sensitivity than the reference design. The electrical input impedances, which should be measured under the same conditions as the displacement frequency responses, are shown in Fig. 2. This plot reveals the reduced DC impedance of the modified loudspeaker. The CIP normalization functions in Fig. 3 indicate that the efficiency of the modified loudspeaker is reduced. This is fully demonstrated by the CIP frequency responses shown in Fig. 4. This diaphragm CIP displacement frequency response is generated according to Eq. (6). $X_{CIP}(j\omega)$ is thus the RMS-value of the diaphragm displacement at a certain frequency for a time-averaged electrical input power of 1 W.

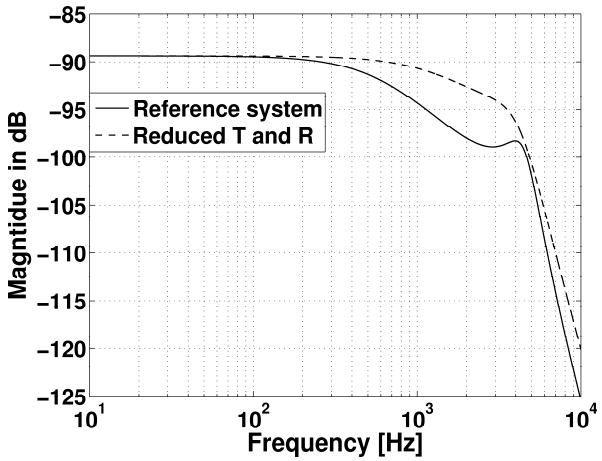

Figure 1 Diaphragm displacement frequency response (magnitude) for reference loudspeaker and for loudspeaker with reduced force factor and electrical DC-resitance.

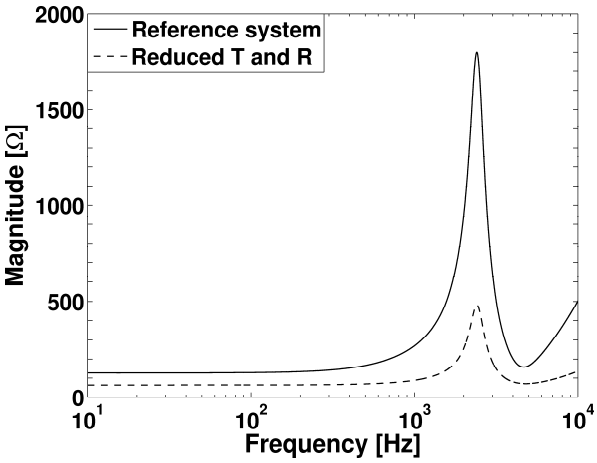

Figure 2 Electrical impedance (magnitude) for reference loudspeaker and for loudspeaker with reduced force factor and electrical DC resistance.

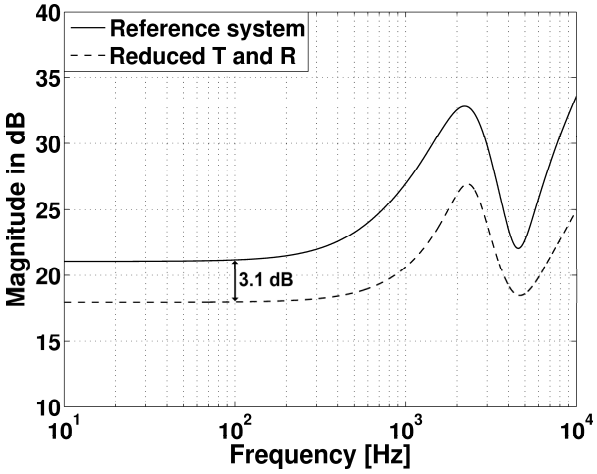

Figure 3 CIP normalization function for reference loudspeaker and for loudspeaker with reduced force factor and electrical DC resistance.

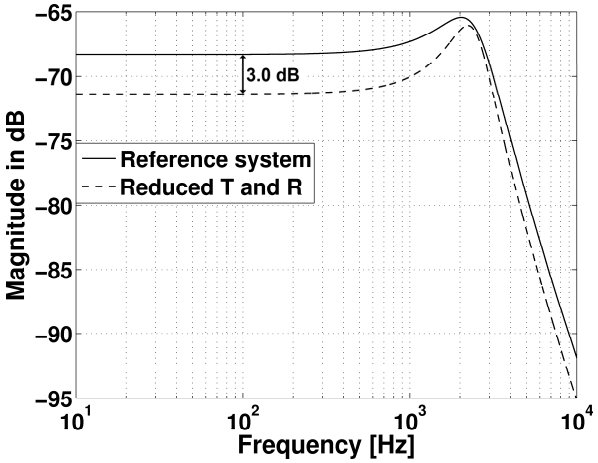

Figure 4 Diaphragm CIP displacement frequency response for reference loudspeaker and for loudspeaker with reduced force factor and electrical DC resistance.

4. DISCUSSION

As the trend towards digital audio signal processing increases, the need for a good (e.g. flat) loudspeaker frequency response becomes less important since the response can often be corrected by digital filters. Therefore a loudspeaker with high efficiency but poor (e.g. not flat) frequency response may be the superior choice. In this case, the CIP frequency response is a much more relevant performance parameter than the ordinary pressure- or displacement frequency response. Figures 1 and 4 illustrate this point: The CIP frequency responses (Fig. 4) give the opposite impression of what one might falsely be led to believe when looking at the frequency responses for the voltage-driven case (Fig. 1). In order to compensate for the difference of around 3 dB between the two responses below 1 kHz the amplifier in use would have to drive twice the electrical power into the modified loudspeaker to produce a certain desired sound pressure level. Thus, a lot of power can be saved by choosing the most efficient loudspeaker design.

5. CONCLUSION

The CIP frequency response, if used as a standard loudspeaker performance parameter, could help drive the development of more efficient loudspeakers. As an addition to the standard electrical impedance and pressure frequency response measurements the CIP frequency response provides a more detailed picture of a loudspeaker's properties, and it may help eliminate some of the confusion that surrounds loudspeaker voltage sensitivity and actual loudspeaker efficiency. The CIP frequency response could thus be a valuable tool in the loudspeaker designer's toolbox, and it could have the potential to substantially influence the way loudspeakers are engineered.

Finally it should be noted that the proposed method is not restricted for use in connection with loudspeakers. The method can be used with advantage for assessment of efficiency of various electromechanical devices.

6. REFERENCES

[1] W. Marshall Leach, Jr. Introduction to Electroacoustics and Audio Amplifier Design. Kendall/Hunt Publishing, 3rd Edition, 2003.

[2] IEC standard 60268-5. Sound system equipment – Part 5: Loudspeakers, 2003.

Technical Report on the Measurement of Magnetic Properties of Soft Magnetic Ring Samples

Description of Measurement Setup and Procedures for the Measurement of Soft magnetic Properties using Ring Samples

A report written by:
Joe Jensen, Sonion A/S
March 14, 2012

Contents

1 Introduction

This report describes a setup developed for the measurement of the magnetic properties of soft magnetic materials. The measurement setup uses a soft magnetic ring sample with 2 separate coils wound around it - one to excite the magnetic material and a second one to measure the magnetic response. The exciting signal and the magnetic response are measured as voltages with a data acquisition unit with 16 bit precision and a sampling rate up to 1.25 MHz. The high sampling frequency is necessary in order to capture the important harmonics in the magnetic response when the exciting signal is in the audio range up to 10 kHz.

The setup is able to produce hysteresis curves at various excitation frequencies in one go. Separate measurements have to be made for different excitation amplitudes. The measured data is processed with MATLAB where magnetic permeability responses and a THD curves are also generated.

2 Theory

2.1 Terminology on H-Field and Permeability in a soft magnetic Ring Sample

Ampere's law in integral form is:

$$\oint_C \vec{H} \cdot d\vec{l}_{Fe} = i_{free,enc.} = i_{coil} + i_{eddy} \tag{1}$$

i.e. the free enclosed current can be viewed as the sum of the coil current and the eddy currents. For a closed magnetic ring sample of average length, l_{Fe}, with an N-winding coil wrapped tightly around it (see Fig. 1) Eq. (1) reduces to

$$Hl_{Fe} = Ni_{coil} + i_{eddy} \Leftrightarrow H = \frac{Ni_{coil}}{l_{Fe}} + \frac{i_{eddy}}{l_{Fe}}. \tag{2}$$

No assumptions are made about what parameters i_{eddy} depends on such as the frequency or the geometry of the ring sample. Defining

$$H_{coil} = \frac{Ni_{coil}}{l_{Fe}} \qquad \text{and} \qquad H_{eddy} = \frac{i_{eddy}}{l_{Fe}}, \tag{3}$$

the applied H-field can be written as a sum of the directly controllable H-field, H_{coil}, and the unknown H-field, H_{eddy}, which is due to eddy currents:

$$H = H_{coil} + H_{eddy} = \frac{Ni_{coil}}{l_{Fe}} + \frac{i_{eddy}}{l_{Fe}}, \tag{4}$$

Per definition the small-signal relationship between the H-field, $H = H_{coil} + H_{eddy}$ and the magnetic B-field inside the ring sample:

$$B = \mu_0 \mu_r H = \mu_0 \mu_r \left(H_{coil} + H_{eddy} \right). \tag{5}$$

Substituting the expression for H_{eddy} from Eq. (3) into Eq. (5) yields

$$B = \mu_0 \mu_r \left(H_{coil} + \frac{i_{eddy}}{l_{Fe}} \right) \Leftrightarrow \tag{6}$$

$$\mu_{r,ap} \equiv \frac{B}{\mu_0 H_{coil}} = \mu_r \left(1 + \frac{i_{eddy}}{H_{coil} l_{Fe}} \right), \tag{7}$$

where the apparent relative permeability, $\mu_{r,ap}$, has been introduced. Using Eq. (3) this can be rewritten into

$$\boxed{\mu_{r,ap} \equiv \frac{B}{\mu_0 H_{coil}} = \mu_r \left(1 + \frac{H_{eddy}}{H_{coil}}\right) = \mu_r \left(1 + \frac{i_{eddy}}{N i_{coil}}\right)}. \tag{8}$$

Notice that the apparent relative permeability reduces to the relative permeability for $i_{eddy} << i_{coil}$ as expected. At first look it might seem like a good idea to increase the number of coil windings, N, in order to reduce the effects of eddy currents but note that the eddy currents can be expected to be proportional to N.

In conclusion, it is possible to measure an apparent relative permeability, $\mu_{r,ap}$,which incorporates the effects of eddy currents. For small AC excitations we introduce the linearized relationship between the directly measurable complex H-field, $\hat{H}_{coil}(\omega)$ and the complex B-field, $\hat{B}(\omega)$ set up inside the coil (and ring sample) and measurable as an induced voltage across the inductor:

$$\boxed{\hat{\mu}_{r,ap}(\omega) \equiv \frac{\hat{B}(\omega)}{\mu_0 \hat{H}_{coil}(\omega)}}. \tag{9}$$

The voltage across an inductor is given by Faraday's law:

$$U_{ind.} = N\frac{d\Phi}{dt} = NA_{Fe}\frac{dB}{dt}. \tag{10}$$

Assuming a linear relationship between $U_{ind.}$ and B (for small changes in B) Eq. (10) can be written in the frequency domain as

$$\hat{U}_{ind.}(\omega) = NA_{Fe} j\omega \hat{B}(\omega) \Leftrightarrow \tag{11}$$

$$\hat{B}(\omega) = \frac{\hat{U}_{ind.}(\omega)}{NA_{Fe} j\omega}. \tag{12}$$

The complex H-field set up by the coil only can be written directly from Eq. (3):

$$\hat{H}_{coil}(\omega) = \frac{N\hat{i}_{coil}(\omega)}{l_{Fe}}. \tag{13}$$

Substituting Equations (12) and (13) into (9) yields the general result

$$\boxed{\hat{\mu}_{r,ap}(\omega) = \frac{l_{Fe}}{A_{Fe}} \frac{1}{N^2 \mu_0 j\omega} \frac{\hat{U}_{ind.}(\omega)}{\hat{i}_{coil}(\omega)} = \frac{l_{Fe}}{A_{Fe}} \frac{1}{N^2 \mu_0 j\omega} \hat{Z}_{ind.}(\omega)}. \tag{14}$$

Notice that Eq. (14) is in agreement with the fact that the inductance of a coil is given as the core permeance $\mathcal{P}(\omega)$ multiplied with the squared number of windings. This can be seen by rewriting Eq. (14):

$$\hat{Z}_{ind.}(\omega) = N^2 \frac{\mu_0 \hat{\mu}_{r,ap}(\omega) A_{Fe}}{l_{Fe}} j\omega = N^2 \mathcal{P}(\omega) j\omega = Lj\omega. \tag{15}$$

2.2 Using a primary Coil to set up the H-Field and a secondary Coil to pick up the B-Field

There are numerous advantages to the method depicted in Fig. 1 compared to the method of using only one coil. First of all, by making the number of windings for setting up the H-field and for picking up the B-field independent, it is possible to apply a small H-field (few windings,

small current/high resistance) without affecting the precision by which it is possible to pick up the B-field since the secondary coil may have plenty of windings. Also, since the induced voltage on the secondary coil is measured in open-loop condition the DC-resistance, R_s, of the secondary coil does not influence the measurement. One disadvantage of this method is that it complicates the measurement setup and increases the time it takes to prepare a sample for characterization.

Again, the apparent relative permeability is given by Eq. (9). The B-field can be written similarly to Eq. (12) but this time it is the number of secondary windings and the voltage picked up by the secondary coil that goes into the equation:

$$\hat{B}(\omega) = \frac{\hat{U}_s(\omega)}{N_s A_{Fe} j\omega}. \tag{16}$$

The secondary voltage is measured with a high-impedance instrument so the voltage drop across R_s is negligible. The H-field set up by the current in the primary coil is given by

$$\hat{H}_{coil}(\omega) = \frac{N_p \hat{i}_p(\omega)}{l_{Fe}}. \tag{17}$$

Substituting Equations (16) and (17) into (9) yields

$$\hat{\mu}_{r,ap}(\omega) = \frac{l_{Fe}}{A_{Fe}} \frac{1}{N_p N_s \mu_0 j\omega} \frac{\hat{U}_s(\omega)}{\hat{i}_p(\omega)}. \tag{18}$$

Substituting $\hat{i}_p(\omega) = \frac{\hat{U}_{Ri}(\omega)}{R_i}$ into Eq. (18) finally yields:

$$\boxed{\hat{\mu}_{r,ap}(\omega) = \frac{l_{Fe}}{A_{Fe}} \frac{R_i}{N_p N_s \mu_0 j\omega} \frac{\hat{U}_s(\omega)}{\hat{U}_{Ri}(\omega)}}. \tag{19}$$

Notice that any uncertainties in the measurement of R_i only influences the gain (and not the phase) of the measured permeability.

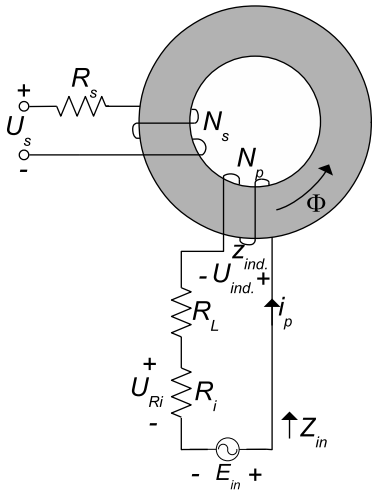

Figure 1: Experiment setup for permeability measurement using a primary coil to set up the H-field and a secondary coil to pick up the B-field.

3 Hardware Setup

The measurement setup is depicted in Fig. 2. A pure-tone current signal is ensured by using the V_{sense} input on the amplifier as illustrated in Fig. 3. The individual components in the setup are described in the following sections.

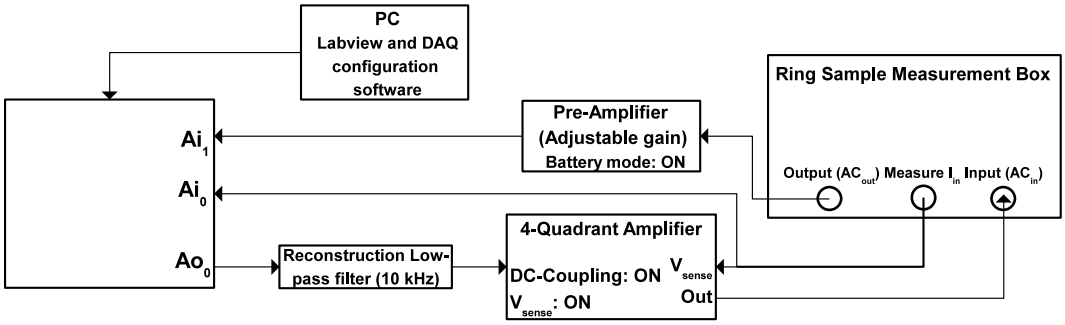

Figure 2: Experiment setup for permeability measurement using a constant-voltage source.

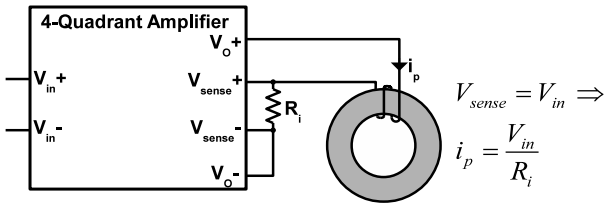

Figure 3: Using the amplifier's V_{sense} input to ensure an undistorted excitation current through the primary ring sample winding.

3.1 Equipment

- PC with LabVIEW software and DAQ configuration software from National Instruments.
- National Instruments NI USB-6259 BNC. USB High-Speed M series Multifunction DAQ.
- Toellner TOE 7610-10. 4-Quadrant Amplifier, DC to 100 kHz, 150 W source and sink power.
- Low-pass (3^{rd} order) Reconstruction Filter with 10 kHz cut-off frequency.
- Ring Sample Measurement Box. Magnetically shielded Box with BNC inputs and outputs.
- Stanford Research Systems SR560 Low-Noise Voltage Preamplifier with battery power supply and variable gain from 1 to 50,000.

3.2 Data Acquisition System

The Data Acquisition System is based on a 16 channel USB device from National Instruments (NI 6259). This device has 16 analog input channels. However, internally the DAQ only has 1 A/D converter so the performance of the device is influenced by how many channels are used and the sampling frequency. When only 1 channel is used the maximum sampling rate is 1.25 MHz with a precision of 16 bit. When more channels are used the maximum scanning frequency is 1 MHz (i.e. 2 channels can be sampled at 0.5 MHz each or 4 channels can be sampled at 0.25 MHz each). The input range of each channel can be set to the levels ±10 V, ±5 V, ±2 V, ±1 V, ±0.5 V, ±0.2 V, ±0.1 V. Due to the nature of this construction, the sampling precision depends on the sampling frequency and the voltage level difference between two successive measurements, the input range chosen for the successive inputs and the output impedance of the signal sources. Read more about this issue in Section "4.7 - Multichannel Scanning Considerations" in [1].

Due to this issue it has been decided to measure the input signal and the output signal in two independent runs - or sequentially instead of in parallel. Thus, a very reasonable assumption is made; that the system is non-chaotic and behaves the same way in the two independent measurement runs. In the first run the input signal is measured and in the second run the output signal is measured. When this method is used there appears to be no delay between two different input channels whereas when measurements are performed in parallel, a delay of 1 μs was measured

between two channels when sampling at 500 kHz on each channel. This is due to the fact that the measurements are not really sampled in parallel but that the single internal A/D converter has to switch between the two different inputs and this causes the delay.

The device also has 4 analog outputs with a DAC resolution of 16 bit in the interval ±10 V or ±5 V. The maximum update rate is 2.86 MHz when using 1 output and 1.25 MHz for 4 outputs. This output is used to generate the analog excitation signal from a wave file.

3.3 Excitation Signal

The excitation signal is a wave file which is created in MATLAB. It consists of a series of appended pure-tone signals. The frequency starts out at 10 Hz and increases with $1/3^{\text{rd}}$ octave spacing as default. Each sinusoid starts out by increasing to its full amplitude through a 5 ms (default) Hann window. This is done to avoid high-frequency spectral artifacts from the box window which creates disturbing peaks in output response. Then the signal continues at full amplitude for 5 ms (default) for any transients to die out and then follows 1 full period (default) of excitation to make sure that the magnetic state of the sample under test is well defined before the actual steady-state piece of the signal is taken out for analysis. The piece of the sinusoid which is taken out for analysis will typically be 1 or 2 periods long depending on the chosen excitation frequency. An integer number of periods is always taken out so that the excitation frequency is always a multiple of the fft frequency resolution, $df = fs/N$. This approach eliminates leakage and any need for windowing before frequency analysis. The composition of the excitation signal is illustrated in Fig. 4 and 5.

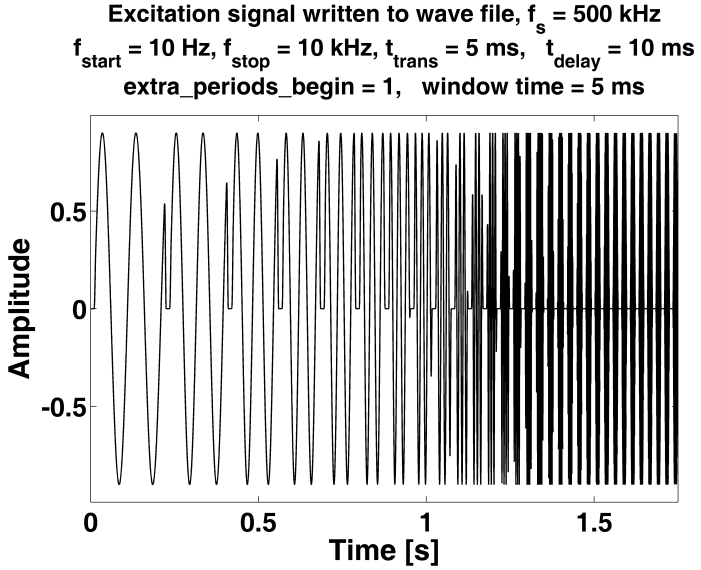

Figure 4: Complete stepped-sine excitation signal starting at 10 Hz and ending at 10 kHz.

There is a delay (t_{delay}) of 10 ms (default) between each sinusoid where the signal is simply zero. Then, the windowed sinusoid is applied for 5 ms (t_{window}) where the amplitude grows to the final level. Then the sinusoid runs for another 5 ms (t_{trans}) which is assumed to be the time it takes for any transients to die out in the system. Then the sinusoid continues 1 period more to ensure that the magnetic sample under test has already been fully excited at this amplitude before the actual steady-state piece is taken out for frequency analysis. Finally the sinusoid is decreased reducing its amplitude through a 5 ms (default) *Hann window*.

Another important side-effect of the windowing is that it helps bring the magnetic ring sample to a well defined magnetic state so that the two sequential runs do not produce different results because the initial magnetization level is different in the second run. This is particularly true for the high frequencies where several rounds on the hysteresis curve is traced out with decreasing amplitude. For the low frequencies the 5 ms is not enough for the excitation signal to trace out

several rounds on the hysteresis curve so this is why there is always at least 1 extra period before the actual measurement.

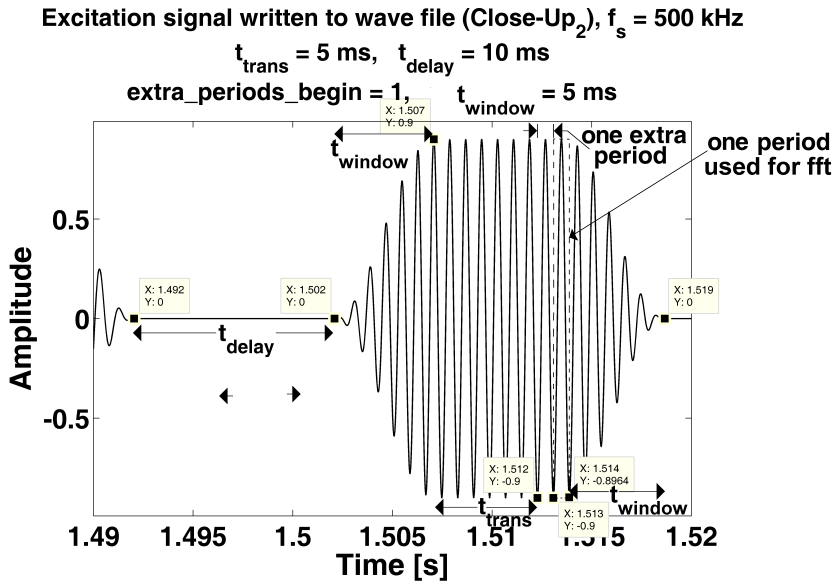

Figure 5: Close-up of one sinusoid in the stepped-sine signal, illustrating the composition of each sine.

The signal is created at a sampling frequency of 500 kHz with 16 bit precision as default.

3.4 Reconstruction Filter

The spectral replication and the aliasing phenomena can both be explained in the following useful way: Sampling a continuous-time signal, $x_c(t)$, can be interpreted as a multiplication of $x_c(t)$ with the Dirac comb function, $\Delta_T(t)$. Multiplication in the time domain corresponds to convolution in the frequency domain, and this is a straightforward process in the case of a Dirac comb function. The procedure is illustrated in Fig. 6.

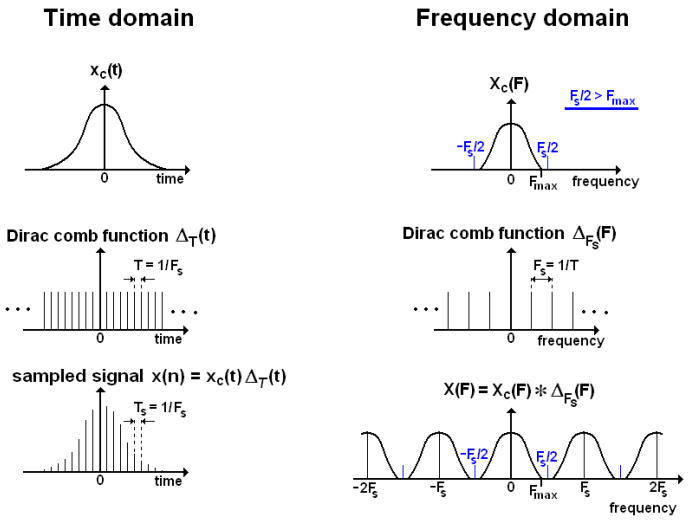

Figure 6: Spectral replication due to sampling.

It is necessary to somehow deal with the spectral replicas during the reconstruction of the analog continuous-time signal. This leads us to the reconstruction process. Reconstruction is the process of converting a discrete digital signal into an analog continuous-time signal. This process can be

realized in many different ways, but what they all have in common is usually the need to remove the spectral replicas above half the sampling frequency, $F_s/2$. One simple way of realizing the digital-to-analog conversion is the sample-and-hold method where the input sample value is held constant on the output until a new sample arrives at the input. This process is illustrated in Fig. 7a. This sample-and-hold interpolation function corresponds to convolving the discrete time signal with a square pulse of duration T_s. The time domain convolution corresponds to multiplication in the frequency domain where the square pulse becomes a sinc-function. The magnitude spectrum of the sample-and-hold box-function is shown in Fig. 7b. Thus the sample-and-hold process has the effect that it low-pass filters the signal. As the magnitude response is only down by 4 dB at $F_s/2$ this is not really a significant effect at 10 kHz for a 500 kHz sampling rate.

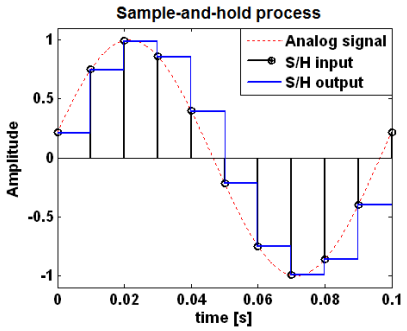

(a) Sample-and-hold process.

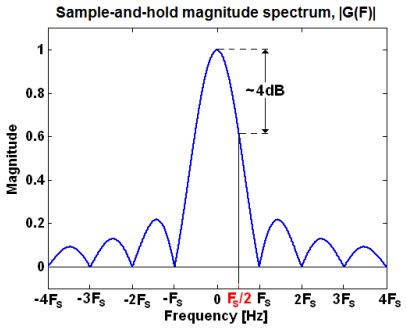

(b) Magnitude spectrum of the Sample-and-hold interpolation function.

Figure 7: Reconstruction process without dedicated low-pass filtering.

Two things should be noted from the frequency spectrum in Fig. 7b. Firstly, the amplitude of the highest frequency within the Nyquist rate ($F_s/2$) is attenuated by 4 dB. Secondly, the spectral replicas of the signal above $F_s/2$ are far from removed by the sample-and-hold low-pass function alone. The signal can be distorted particularly by the frequencies corresponding to the peaks of the side lobes. Since the spectrum of a discrete signal is repeated every integer multiple of F_s (see Fig. 6) the frequencies corresponding to the peaks of the side lobes are the replicas of the high frequencies in the Nyquist interval between 0 and $F_s/2$ Hz. Thus, when reconstructing a signal, one should make sure to low-pass filter the signal after the sample-and-hold (or other) interpolation in order to remove any unwanted frequencies. Notice that these replicas occur independently of the sampling frequency. The spectral replication has nothing to do with aliasing but is rather a phenomenon inherent to the process of sampling a continuous-time signal. This is the reason why the Reconstruction Low-pass filter is placed after the analog output of the Data Acquisition System. Else the ring sample would also be excited by the spectral replicas of the intended pure-tones that are located in the audio range.

The sampling frequency of 500 kHz used for the construction of the wave file, together with the frequency range up to 10 kHz means that the first spectral replica will be located at 500 kHz $\pm$ 10 kHz and attenuated according to Fig. 7b where F_s now corresponds to 500 kHz. The lowest frequency content of the replica will be located at the frequency 490 kHz. The inputs of the A/D converter has a built-in low-pass filter which is fixed at a -3 dB cut-off frequency of around 1.5 MHz (-4 dB at 2 MHz). This means that one cannot rely on this filter for the removal of the first spectral replicas! A signal at 490 kHz will be interpreted (aliased) as a 10 kHz signal at a measurement sampling frequency of 500 kHz and a signal at 495 kHz will be interpreted as a 5 kHz signal at a sampling frequency of 500 kHz. Therefore it is important to suppress the spectral replicas and this is what the 10 kHz low-pass reconstruction filter is for. The 10 kHz 3$^{\text{rd}}$ order low-pass reconstruction filter will dampen a signal at 495 kHz by around:
$3 \cdot 1$ decade $\cdot$ 20 dB/dec $+ 3 \cdot 2$ octaves $\cdot$ 6 dB/oct $= 96$ dB.

3.5 Amplifier

The 4-Quadrant amplifier is there to deliver the sort of electrical current which is required to set up the desired H-field in the ring sample. The second function of the amplifier is to function as a constant-current source by using the V_{sense} input as illustrated in Fig. 3. The amplifier is DC-coupled so it can be used to add a DC H-field to see how this influences the permeability.

3.6 Ring Sample

The ring samples that are currently used have the convenient dimensions: Inner diameter of 6 mm, outer diameter of 10 mm and a thickness of 0.3 mm or more. The ring sample under test should be large enough to accommodate around 50 windings to pick up the magnetic flux changes. It should also be thick enough so that it does not bend when the windings are wound as this may influence the magnetic properties of the sample.

3.7 Number of Windings for primary Coil

So far, a very small number of windings (4) has been chosen for the primary excitation coil in order to reduce the influence of the induced back-EMF on the driving current, i_p. As the experiment developed it was realized that the Voltage Amplifier could be used as a constant-current source and this makes it possible to use more windings if necessary. Reasons to increase the number of primary windings are to keep the input current down, reach higher H-field excitation levels and to have less relative uncertainty on the number of windings (e.g. 10 $\pm$0.5 windings instead of 4 $\pm$0.5 windings). Reasons to keep the number of windings down is primarily to reduce the time it takes to prepare a ring sample for measurement. For ring samples with higher saturation flux density, B_s, larger coercivity, H_c, smaller permeance, ρ (either due to reduced permeability or maybe reduced cross sectional area or increased diameter) it may be necessary to increase the number of windings a bit to be able to saturate the material without running into the output voltage limitation of the amplifier. It is recommended to use about 10 windings.

3.8 Number of Windings for secondary Coil

So far, 50 windings have been used in order to retrieve a signal without too much noise for the chosen ring sample dimensions and to be able to measure all the way down to 10 Hz. Satisfactory results may be obtained with less windings, especially for ring samples with larger cross sectional area as they can sustain a larger amount of flux at a given flux density and this will increase the induced voltage signal on the secondary coil. The fact that great results can be obtained all the way down to 1 Hz with a Supra 50 sample (0.32 mm thick, inner and outer diameter of 6 and 10 mm) using 50 windings, indicate that for a measurement signal between 10 Hz and 10 kHz one could do with only 5 secondary windings. It is therefore recommended to use 10-20 windings if the lowest excitation frequency is 10 Hz or greater as the induced field will tend to be smaller for materials with a lower permeability than Supra 50.

3.9 Ring Sample Box

A box with BNC connectors has been made to interconnect with the ring sample i.e. to measure the input current to the primary winding that excites the sample and the output voltage on the secondary coil which reflects the magnetic flux changes. The box is made out of iron (soft magnetic material) so this helps shield the ring sample against 50 Hz noise signals from the power system. Referring to Fig. 3, the box also contains the resistor, R_i, which is able to handle a power dissipation of 10 W.

3.10 Pre-Amplifier

The preamplifier with adjustable gain is there to get a good match between the output of the ring sample and the dynamic range of the Data Acquisition System. Unfortunately the output

DC-offset has to be adjusted for every gain setting. It is no problem to remove the DC through post processing of the measured signal but the preamplifier may clip if the DC level is too large. The preamplifier should be used with the power chord removed as this will force it into battery operation and this eliminates 50 Hz noise. An abnormal behavior was observed: When the pre-amplifier had been re-charging and was used afterwards (in battery-mode) there would be a large DC-drift on the output. It was observed that the power supply/battery got very warm during the re-charging process so it is believed that the slow temperature reduction that follows after a recharge is causing the output DC drift.

4 Software

The excitation signal is generated in MATLAB and the measured time-series signals are analyzed with MATLAB scripts. The DAQ is configured with dedicated National Instruments software and the data communication between the PC and the DAQ happens through LabVIEW.

4.1 LabVIEW

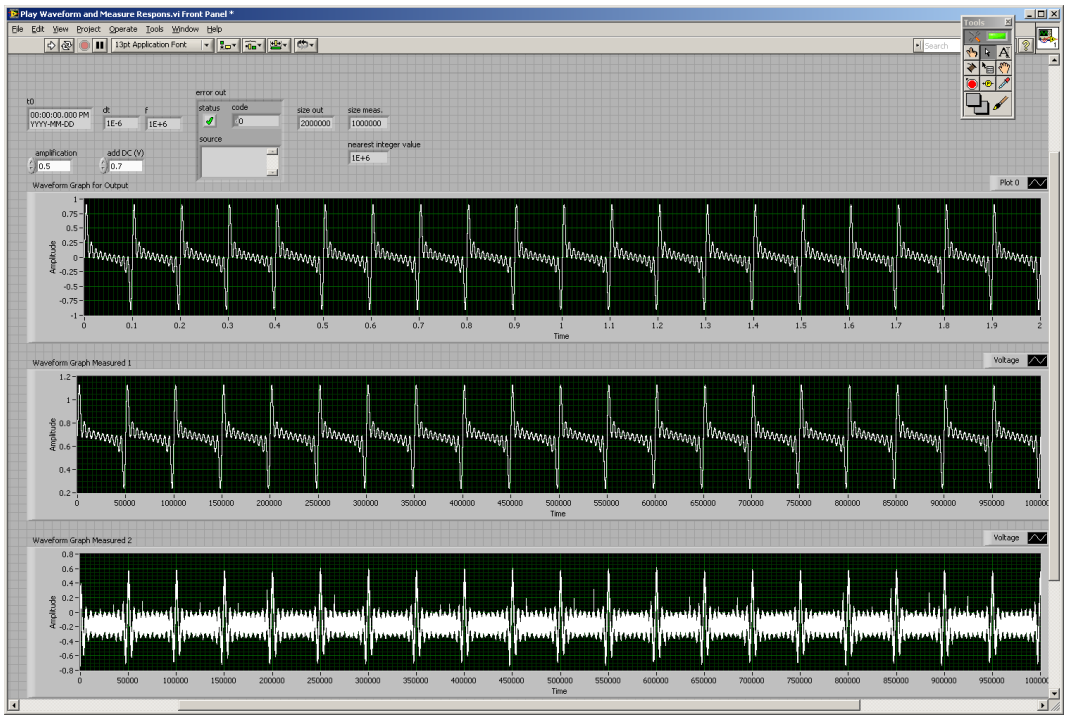

Figure 8: LabVIEW program interface.

4.2 Analysis Approach and Graphs

The excitation signal is composed of a series of appended pure-tone sinusoids - a so-called stepped-sine signal which starts at the low end of the frequency spectrum and ends in the high. The input current to the primary excitation coil is measured and the induced voltage on the secondary coil is measured. The B-field is obtained through numerical integration of the U_s signal (see Eq. (10)). Any DC is removed from U_s before integration to ensure that the B-field signal does not have a constant positive or negative slope. When a signal with zero DC has been integrated using a running cumulative integration method the integral will in general have a DC-offset so this is also removed after the integration. The input excitation signal, H_{coil}, is obtained directly through the relation $H_{coil} = Ni_{coil}/l_{Fe} = Ni_p/l_{Fe}$ as stated in Eq. (3).

From the time-series data it is possible to construct hysteresis curves by plotting the applied H-field against the B-field for every excitation frequency. An example of measurements of the H-field and the B-field and a hysteresis curve are shown in Figures 9 and 10. The hysteresis curve is generated simply by plotting the H-field and the B-field against each other. The area of the hysteresis loop is indicated in the title of the hysteresis loop figures. This is a measure of the energy loss per cubic meter per excitation cycle. This is, however, only true for very low frequencies where the eddy current effects are vanishingly small. Then one can be certain that the entire supplied magnetic H-field goes into the magnetization process and that it it not "eaten up" by energy losses due to eddy currents.

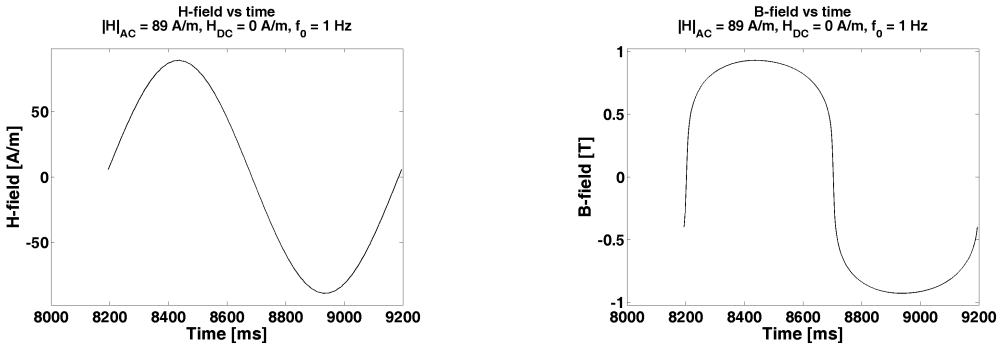

(a) H-field.

(b) B-field generated by numerical integration of the measured voltage, U_s.

Figure 9: Time series signals.

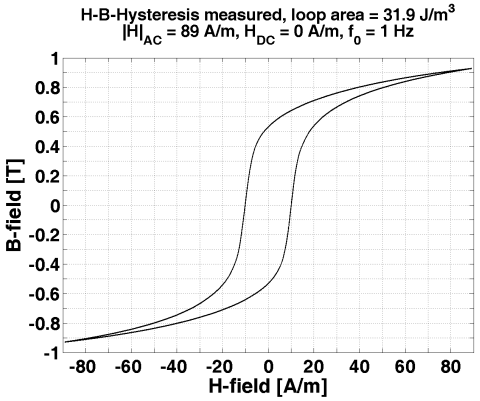

Figure 10: Hysteresis curve.

As the frequency content of the excitation signal is well-defined, the harmonics in the *fft* of the output signal can be picked out. These can be used to generate a THD response (THD vs excitation frequency). A permeability frequency response is also generated for which only the fundamental frequency in the output is used to determine the permeability according to Eq. (19). Note that the harmonics are disregarded in this process. Examples of a permeability response and THD responses are shown in Figures 11 and 12, respectively. Note that the distortion of the picked up voltage, U_s is NOT the same as the distortion of the B-field which is obtained by integration of U_s. The integration process, which corresponds to division by $j\omega$ in the frequency domain, will reduce the amplitude of the high frequencies relative to the low frequencies (think of integration as a low-pass-filter with -20 dB/dec slope in the entire frequency range). Also keep in mind that the wave file (and the Data Acquisition System) only have 16 bit precision so this introduces some quantization noise which puts a natural limit to how low the distortion can get. This is particularly relevant for the H-field where the measured distortion is very low.

The permeability response, THD response and hysteresis curves can be measured for different

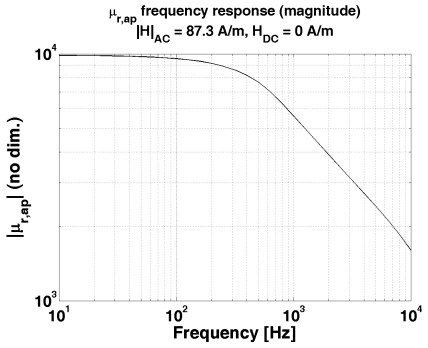

(a) Magnitude.

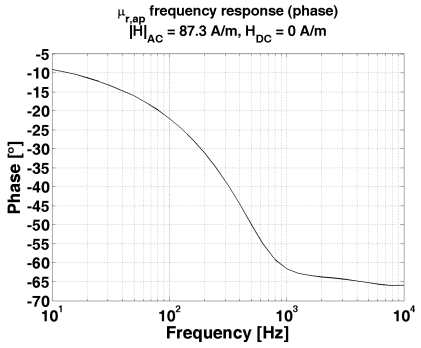

(b) Phase.

Figure 11: Apparent magnetic permeability $\mu_{r,ap}(\omega)$.

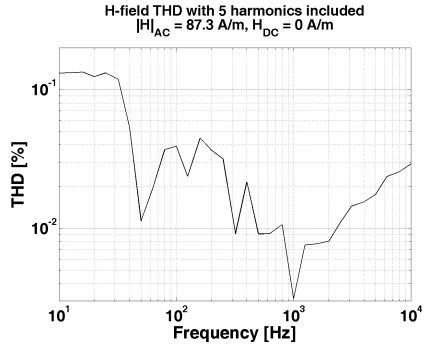

(a) THD of input current, i_p.

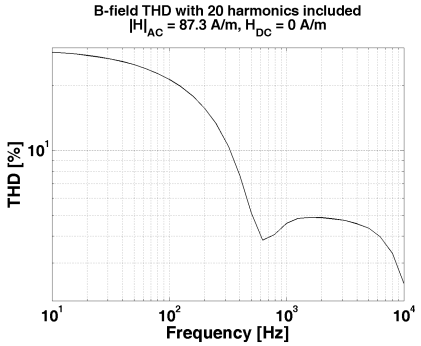

(b) THD of B-field.

Figure 12: Total harmonic distortion of input- and output signal.

excitation amplitudes by simply scaling the input in the LabVIEW interface. From this interface it is also possible to apply a DC level to the exciting field (see Fig. 8).

Notice that (for an ordinary hard disk drive based system) about 80 % of the processing time is spent generating figures (actually producing the *.PNG files and saving them to the disk). The time this takes also depends on the chosen figure resolution. Therefore it is important to disable the figures that are not of interest in order to speed up the processing time.

5 Performing a Measurement and processing the Data

In order to perform a basic measurement, first a measurement wave file needs to be generated. This is done using the MATLAB package *MagMeas_1*. Open the main file and follow the following steps (and always read the messages in the Command Window for help):

1. Locate the variable `output_folder` and specify the path to the location where you would like your measurement wave file (and ultimately the processed data) to go.

2. Locate the variable `process_measurements` in the main MATLAB file and set the value to "`false`".

3. Locate the variables `f_start` and `f_stop` in the MATLAB main file and specify the frequency range you would like to analyze.

4. Locate the variable `extra_periods_begin_list` and specify how many extra excitation periods you would like to run before the actual measurement starts. This is done in order to put the magnetic ring sample in a well-defined state of magnetization. Try with just 1 period and increase if the hysteresis loops look strange.

5. Run the MATLAB main script and notice the information given in the MATLAB Command Window.
6. Copy the generated measurement wave file to the LabVIEW computer which is part of the magnetic measurement setup and start the program "Perform Magnetic Measurement" (or whatever todo).
7. In LabVIEW, set the desired gain of the excitation signal (with 1 corresponding to about 900 mV).
8. In LabVIEW, set the desired DC-offset of the H-field.
9. Adjust the gain of the pre-amplifier and choose the dynamic range of the DAQ inputs so that the largest amplitudes of the excitation- and response signals utilize as much of the DAQ's dynamic range as possible.
10. Name the measured input current data files according to the standard: "`i_p_XXXXmV_U_R_YY_Ohm_N_p_Z_DC_AAAAmV.txt`", where `XXXX` is the voltage of the excitation signal in millivolts (as specified in the LabVIEW interface), `YY` is the resistance of the resistor R_i in Ohm, `Z` is the number of primary coil windings and `AAAA` is the DC voltage offset of the excitation signal in millivolts.
11. Name the measured output voltage data files according to the standard: "`V_s_XXXXmV_U_R_YY_Ohm_gain_GGGG_N_p_Z_DC_AAAAmV.txt`", where the variables are the same as above and `GGGG` is the gain setting of the pre-amplifier in amplitude (NOT in dB).
12. Copy the measurement files to some desired location on the MATLAB computer.
13. The location chosen above is specified in the variable `input_folder` in the main file.
14. Create two text files in the folder specified in 13. Name these text files something like: "`Supra50_input_1.txt`" and "`Supra50_input_2.txt`". Type in a list of the measurement files in each of these files. For instance, in "`Supra50_input_1.txt`" type: "`i_p_0300mV_U_R_15_Ohm_N_p_4_DC_0000mV.txt`" on the first line and: "`i_p_0600mV_U_R_15_Ohm_N_p_4_DC_0000mV.txt`" on the second line until all the measurement files for input 1 are specified. Now open "`Supra50_input_2.txt`" and specify the measurements for input 2 like "`V_s_0300mV_U_R_15_Ohm_gain_0100_N_p_4_DC_0000mV.txt`" on the first line and "`V_s_0600mV_U_R_15_Ohm_gain_0050_N_p_4_DC_0000mV.txt`" on the second line and so forth.
15. Locate the variables `U_R_i_measurements` and `U_s_measurements` and specify the names of the two files that were just created in 14.
16. Locate the variable `process_measurements` in the main MATLAB file and set the value to "`true`".
17. Specify the physical characteristics of the ring sample and the number of windings of the coils in the variables `l_Fe`, `t_Fe`, `w_Fe`, `N_p` and `N_s` in the MATLAB main file.
18. Choose which figures you would like to generate in the section "`Choose which figures to generate (choose true or false)`" in the MATLAB main file.
19. Locate the variable `figure_visible` and choose "`on`" if you would like to see the figures on screen as well as saving the figures to disk. It is usually more convenient to set this to "`off`" as this will only save the figures to disk. Then the figures can be inspected with a picture viewer afterwards.
20. Locate the variable `figres` in the main MATLAB file and set the desired resolution of the produced figures.
21. Run the MATLAB script and follow the information given in the Command Window and find the generated figures in the output folder specified in 1.

6 Discussion

Recall that it was discussed that the the sampling of one input could affect the next sample read from a different input. It was later discovered that a workaround for this problem was to read a short circuited input between the two actual readings. This, on the other hand, means that 4 different inputs needs to be read in each cycle and the maximum sampling frequency per channel is thus reduced to 250 kHz which is enough to reconstruct frequencies up to 125 kHz corresponding to 12 harmonics at 10 kHz. One also has to take the delay between the 2 readings into account.

References

[1] National Instruments. Daq m series user manual, 2008.

www.elektro.dtu.dk

Department of Electrical Engineering
Acoustic Technology
Technical University of Denmark
Ørsteds Plads
Building 348
DK-2800 Kgs. Lyngby
Denmark
Tel: (+45) 45 25 38 00
Fax: (+45) 45 93 16 34
Email: info@elektro.dtu.dk

ISBN 978-87-92465-48-1